Osteological Correlates of Cephalic Skin Structures in Amniota: Documenting the Evolution of Display and Feeding Structures with Fossil Data

A dissertation presented to

the faculty of

the College of Arts and Sciences of Ohio University

In partial fulfillment

of the requirements for the degree

Doctor of Philosophy

Tobin L. Hieronymus

March 2009

This dissertation titled

Osteological Correlates of Cephalic Skin Structures in Amniota: Documenting the Evolution of Display and Feeding Structures with Fossil Data

by

TOBIN L. HIERONYMUS

has been approved for

the Department of Biological Sciences

and the College of Arts and Sciences by

Lawrence M. Witmer

Chang Ying-Chien Professor of Paleontology

Benjamin M. Ogles

Dean, College of Arts and Sciences

ABSTRACT

HIERONYMUS, TOBIN L., Ph.D., March 2009, Biological Sciences

Osteological Correlates of Cephalic Skin Structures in Amniota: Documenting the Evolution of Display and Feeding Structures with Fossil Data (254 pp.)

Director of Dissertation: Lawrence M. Witmer

The research presented here is an examination of the morphology and histology of several broad categories of skin structures in living amniotes, together with analyses of the osteological correlates associated with each skin category. The epidermal horn and armor-like dermis of extant rhinoceros are examined in detail, and the evolution of both of these skin structures is reconstructed in phylogenetic context from fossil evidence. The evolution of rhinoceros dermal armor is strongly associated with the evolution of shearing tusks used in fighting behaviors, and precedes the evolution of epidermal horns by ~20 Ma. The distribution and morphology of cephalic scales, rhamphothecal plates, and feathers in Sauropsida is then examined in an analysis of evolutionary modularity. Two distinct regions of skin, one around the mouth and another on the skull roof, show independent patterns of morphological evolution, suggesting that skin features in these regions are interconnected as modules. Rhamphotheca in neornithine birds are one possible expression of this modularity. In a separate analysis, plates of compound rhamphotheca (e.g., in albatross) are shown to be homologous with regions of simple rhamphotheca. Rhamphotheca occupy a topographically similar area of skin in nearly all neornithine birds, and the variable expression of softer grooves leads to several homoplastic occurrences of compound rhamphotheca. Several adaptive scenarios have

been proposed for novel skin structures in non-avian dinosaurs, but the lack of direct fossil evidence for skin in these animals and the ambiguity in available reconstructions has made it difficult to evaluate these scenarios. Detailed reconstructions for cephalic skin structures drawing on gross morphology and paleohistology are presented for the lineage of centrosaurine dinosaurs leading to *Pachyrhinosaurus* and for the abelisaurid theropod *Majungasaurus*. The transition from tall horn cores to gnarled pachyostotic bosses in centrosaurine dinosaurs closely resembles the morphology and evolution of the frontal boss in muskox. The rugose bone on *Majungasaurus* skulls closely resembles the attachment of dermal armor in rhinoceros. In both cases, agonistic behaviors associated with similar skin structures in extant animals cast doubt on the idea that they functioned only in visual display. The evolution of these novel structures was most likely driven by social selection.

Approved: _____

Lawrence M. Witmer

Chang Ying-Chien Professor of Paleontology

DEDICATION

This work is dedicated to my mother,

Barbara Lee Hieronymus

Because of all the outstanding teachers I have had, she was the first,

from my place in her preschool class to the present day, to show me how learning comes

alive when the connections between people are genuine and attentive;

and to my father,

Fred Randall Hieronymus

because much of my childhood reads like a chapter from Between Pacific Tides*;*

I now understand how beautiful a gift it was as to learn with him, and also how precious

it was for him to teach me, as I hope to teach others in turn.

ACKNOWLEDGMENTS

Discussion and correspondence with Lorenzo Alibardi, Audrone Biknevicius, Lisa Noelle Cooper, Philip Currie, Joseph Daniel, David Dufeau, Andew Farke, Cynthia Marshall Faux, Mark Goodwin, Sue Herring, Robert Hill, Casey Holliday, Dominique Homberger, Angela Horner, Jack Horner, John Hutchinson, Andrew Lee, Gerald Mayer, Eric McElroy, Hillary Maddin, Paul Maderson, Matt Milbachler, Donald Miles, Molly Morris, Patrick O'Connor, Chris Organ, Kevin Padian, Erin Rasmusson, Steve Reilly, Margaret Rubega, Michael Ryan, Natalia Rybczinski, Torsten Scheyer, Nancy Stevens, Alycia Stigall, Darren Tanke, Takanobu Tsuihiji, Matt Vickaryous, Susan Williams, and Larry Witmer have all greatly aided this research. For access to histology and microscopy equipment I wish to thank Dan Hembree, David Kidder, Greg Nadon, Patrick O'Connor, Gar Rothwell, and Susan Williams. David Dufeau and Ryan Ridgely at OUμCT provided invaluable assistance with CT scanning. For access to osteological and paleontological specimens, I wish to thank James Gardner at the Royal Tyrrell Museum; Jack Horner, Pat Lieggi, Carrie Ancell, Bob Harmon, David Varrichio, Ellen-Thérèse Lamm, and Susan Winking at the Museum of the Rockies; Kevin Seymour and Mark Peck at the Royal Ontario Museum; Greg Schneider and Janet Hinshaw at the University of Michigan Museum of Zoology; Mark Goodwin, Pat Holroyd, and Kevin Padian at the University of California Museum of Paleontology; Steve Rogers and Suzanne Mclaren at the Carnegie Museum of Natural History; Linda Gordon, Robert Purdy, and Matt Carrano at the National Museum of Natural History; Eileen Westwig, Paul Sweet, Susan Bell, Carl Mehling, and Mark Norell at the American Museum of Natural History; Christine

Lefèvre and Alexis Martin at the Muséum national d'Histoire naturelle; Gerald Mayer at the Naturmuseum Senckenberg; Link Olson at the University of Alaska Museum; and Scott Sampson, Mike Getty, Mark Loewen, and Eric Lund at the University of Utah Museum of Paleontology. This research was funded by the Jurassic Foundation (TLH), the National Science Foundation (NSF IBN-0343744 & IOB-0517257; LMW), and Ohio University (TLH).

TABLE OF CONTENTS

Page

LIST OF TABLES

Page

LIST OF FIGURES

Page

CHAPTER 1: THE STRUCTURE OF WHITE RHINOCEROS (*CERATOTHERIUM SIMUM*) HORN INVESTIGATED BY X-RAY COMPUTED TOMOGRAPHY AND HISTOLOGY WITH IMPLICATIONS FOR GROWTH AND EXTERNAL FORM

Abstract

The nasal and frontal horns of two individuals of *Ceratotherium simum* were examined by x-ray computed tomography (CT scanning), gross observation of sectioned horn, and light microscopy of histological sections of the horn tissue. CT scans of both sets of horns reveal a periodic banding pattern that is evident upon gross observation of sections as darker bands of tissue. The overlap of these bands in both histological and CT slices suggests the presence of both a photoabsorbent component (melanin) and a radiodense component (calcium phosphate salts, most likely hydroxyapatite or octocalcium phosphate). The distribution of these two components in the horns is hypothesized to contribute to the differential wear patterns that produce the characteristic sweeping conical shape of rhinoceros horn from what otherwise (in the absence of wear and UV exposure) would be cylindrical blocks of constantly growing cornified papillary epidermis. Although extant rhinocerotids are unique in possessing a massive entirely keratinous horn that approximates the functions of keratin-and-bone horns such as those of bovid artiodactyls, the tissue structures that make up the horn are strikingly convergent with other examples of papillary cornified epidermis found in horses, artiodactyls, cetaceans, and birds.

Introduction

Rhinoceros horns are unusual among the horns of ungulates in that they lack a bony horn core. Instead, the horns are anchored to the dermis covering the frontal and nasal bones, and are associated with pronounced bony rugosities in most individuals (Hieronymus and Witmer, 2004). The true 'horny' part of rhinoceros horn is an epidermal derivative, consisting of keratinized tubules of cells set in an amorphous keratinized matrix. The tubules comprise approximately 40 lamellae of squamous cells and range from 300 to 500 μm in diameter (Ryder, 1962). The amorphous matrix is made up of keratinized fusiform interstitial cells (Lynch, 1973). Each tubule grows from a generative layer of epidermis (stratum germinativum) covering a dermal papilla. The amorphous matrix is grown from the stratum germinativum of the epidermis between dermal papillae. As the epithelial cells of the horn are dead upon the completion of keratinization, all growth in rhinoceros horn takes place at the base.

Rhinoceros horns, as structures formed of cornified papillary epidermis, are part of a phylogenetically diverse assemblage of convergent cornified epidermal appendages, including the cornified sheaths of pecoran artiodactyl horns, bird beaks, turtle beaks, amniote claws and hooves, and baleen (Homberger, 2001). The independent origin of each of these examples provides a basis for identifying convergent morphologies, which in turn may shed light on functional aspects of cornified papillary epidermis (e.g., resistance of tubules to bending, preferential tearing directions). Here we report on previously undescribed aspects of melanization and calcification in the horns of white

rhinoceros *Ceratotherium simum*, and discuss the impact these that features may have on the growth and shape of the horn.

Materials and Methods

The horns examined in this study came from two individuals, a 32-year-old female (Ohio University Vertebrate Collection [OUVC] 9541) formerly housed at The Wilds (Cumberland, Ohio) and a 41-year-old male (OUVC 9754) formerly housed at the Phoenix Zoo (Phoenix, Arizona). Both animals died for reasons unrelated to this study.

The nasal and frontal horns of OUVC 9541 (Fig. 1-1A) and the frontal horn of OUVC 9754 were bisected in the midsagittal plane for gross anatomical observation. A longwave ultraviolet lamp (Ultra Violet Products UVL-26P, Upland) was used to examine fluorescence in the epidermal horn (Fig. 1-1A). The right half of the nasal horn of OUVC 9541 and the entire frontal horn of OUVC 9754 were scanned on a GE HiSpeed FX/i Helical CT scanner at O'Bleness Memorial Hospital in Athens, Ohio. Slice thickness and spacing was 1mm. Scanning parameters for OUVC 9541 were 120kV and 150mA, whereas those for OUVC 9754 were 120kV and 120mA. Field of reconstruction was 278mm for OUVC 9541 and 282mm for OUVC 9754 for 512 x 512 pixels using a bone algorithm. CT data were compiled in the Amira 3.1.1 (Mercury-TGS, San Diego) and eFilm 2.0 (Merge-eFilm, Toronto) software packages for analysis and three-dimensional reconstruction.

Portions along a medial parasagittal section of the horn of OUVC 9541 (Fig. 1-1A) were embedded in EpoThin epoxy (Buehler, Lake Bluff), mounted on plastic slides, and ground to approximately 2 mm thickness. This set of unstained sections was

examined by transmitted light microscopy to determine melanin distribution within the horn.

Results

Horn is deposited dorsoventrally in successive sheets (here termed horn laminae) with irregular layers of approximately 1.0 – 2.0 mm. Each lamina represents a presumably coeval period of growth of horn tubules and intertubular matrix. In sagittal or transverse section, horn laminae appear as bands (Fig. 1-1B, C). The horn laminae fluoresce under UV light, aiding in their delineation. The color value of each lamina varies across its lateral extent, such that the central part of each lamina is darker in color than the periphery. This central dark patch is not uniform along the length of the horn, but rather shows pulses of darker horn interspersed with lighter horn. These dark patches alternate at an approximately 6 cm interval (Fig. 1-1A). The pattern of dark patches is also visible in CT as alternating radiolucent and radiodense bands (Fig. 1-1D). Gross examination of the frontal horn shows a similar pattern of periodic dark patches, at an approximately 2 cm interval (Fig. 1-1A), and horn laminae that alternate irregularly at approximately 0.5 – 2.0 mm (Fig. 1-1B).

Histological examination of thick sections shows that within dark patches, more heavily pigmented cornified epidermal tissue is restricted to the intertubular matrix (Fig. 1-2). The horn tubules themselves retain a similar light color from the edge of the horn to its center. Rhinoceros horn can thus be viewed as a composite material, with tubules of keratinocytes forming 'fibers' that are embedded in a matrix of varying composition (Fig. 1-3).

Discussion

Periodic banding and annual growth

The 6 cm periodicity of the radiodense dark patches in the nasal horn corresponds very well with annual growth rates of white rhinoceros nasal horn in wild populations (~5 cm/yr per Pienaar et al., 1991; 5–6 cm/yr per Rachlow and Berger, 1997; both rates were measured from internal landmarks in the horns and represent tissue turnover rather than whole-horn elongation). The 2 cm periodicity of the frontal horn reflects its relatively slower growth, which is also consistent with the findings of Rachlow and Berger (1997). The periodicity of the horn laminae is much more irregular. Color value changes between adjacent horn laminae may be more akin to fault bars in feathers, which are caused by changes in keratinization due to external factors (mechanical damage, diet, etc.) during feather growth (Prum and Williamson, 2001).

Seasonal variation in the growth rates of other keratinized tissues such as the claws of sheep and cattle have been variously linked to changes in photoperiod and changes in temperature (Clark and Rakes, 1982; Hahn et al., 1986). OUVC 9541 spent the entirety of its life outside of the climate and historical latitudinal range of naturally occurring white rhinoceros populations (~40° N in Ohio, U.S.A., compared to a probable historical range in Africa of ~33° N to 33° S as per Groves, 1972). OUVC 9754, however, lived in an environment (Arizona, U.S.A.) that is quite similar to the northern- and southern-most extent of the African range. As both of these specimens show similar periodic structures in their horns, we are confident that this horn morphology is not simply an artifact of unusual environments.

Co-occurrence of radiodense features and dark periodic bands

The intensity of the dark patches suggests that there are differences in the rate of melanin deposition during the process of horn growth. Although this satisfactorily explains the gross observation results, melanin itself is not radiodense enough to produce similar patterns in a radiograph. The difference in contrast in radiography can be attributed to higher concentrations of calcium salts accompanying melanin deposition in the dark patches. Co-occurrence of melanin and calcium (as octocalcium phosphate) has been noted in the horns of saiga (*Saiga tatarica*) (Hashiguchi et al., 2001). The presence of higher concentrations of calcium can be interpreted as a primary mechanism and not a pathological finding, as several other forms of horny tissue aside from rhino and saiga horn also contain appreciable portions of hydroxyapatite or octocalcium phosphate (Arnott and Pautard, 1968; Pautard, 1970; Hashiguchi et al., 1995).

Horn growth and shape

The generalities of rhinoceros horn morphology have been fairly well understood for quite some time (Boas, 1931), but the mechanism by which horns maintain this morphology has received little attention. The variations in melanin content and calcification described here provide a mechanistic basis for controlling horn shape by differential wear.

Melanin has been variously implicated in increasing the hardness and strength (Bonser and Witter, 1993; Bonser, 1996b) as well as the long term resistance to wear (Averill, 1923; Bonser, 1996a) of cornified epidermal structures at a gross level. However, a number of studies have shown no quantifiable increase in work-to-fracture or

hardness (stiffness) associated with melanin in cornified epidermal tissues such as horse hoof wall and feather barb (Bertram and Gosline, 1986; Douglas et al., 1996; Butler and Johnson, 2004), thus refuting a mechanically significant role for melanin in these systems. However, keratins are substantially weakened by prolonged exposure to UV light (Marshall, 1986), and melanin may act to reduce the degree of wear by absorbing light entering the tissue (Jimbow et al., 1986). Although melanin itself does not appear to contribute to increased work-to-fracture or hardness, it is highly probable that calcification accompanying melanization (as shown by Hashiguchi et al. [2001] and this study) changes the hardness or compressional modulus of these tissues. The co-occurrence of calcification in melanized cornified epidermis may be responsible for the equation of hardness and melanization reported in other systems (Bonser and Witter, 1993; Bonser, 1996a).

The higher concentration of melanin and calcium salts in the center of white rhinoceros horn is likely to play a role in determining the overall conical shape of the horn. Healthy horn grows at a nearly constant rate throughout its areal extent. In the absence of any wear or keratin degradation, growing rhinoceros horn would form a gently curving cylinder. Three major factors combine to remove material from the horns by abrasion and wear: (1) UV-induced keratin degradation (Marshall, 1986); (2) reduced work-to-fracture as the horn tissue desiccates (Bertram and Gosline, 1987; Kitchener, 1987); and perhaps most importantly (3) stereotypical behavioral use patterns, such as scraping and 'horn-wiping' on the ground, vegetation, or bars in an enclosure, and horn-clashing between individuals (Bigalke, 1946; Kingdon, 1979; Owen-Smith, 1988;

Dinerstein, 2003). Progressive wear on older (i.e., more distal, dehydrated, and UV-damaged) portions of the horn produces the characteristic conical horn shape. The fact that mature males engage in more frequent bouts of scraping and horn-clashing than females may thus explain their slightly shorter horns (Kingdon, 1979).

The horns of many rhinos are not uniformly conical, but rather show a marked change in slope, such that the base forms a squat cone and the distal part continues as a more tapered cone. This change reflects the rate at which softer outer horn is worn away to expose more resistant material in the center. The change occurs near the point where the more heavily melanized and calcified tissue nears the external wear surface (arrow in Fig. 1-1A). The difference between the concentration of melanin and calcium salts in the intertubular matrix of the horn and the tubules themselves suggests that the intertubular matrix is responsible for these differences in hardness.

Conclusions

Rhinoceros horn provides an independently derived example of a cornified papillary epidermal appendage. The concentration of melanin and calcium salts in the core of rhinoceros horn varies annually, and appears to play a role in maintaining characteristic horn morphology. Local differences in melanin content and calcium salts reflect changes in the composition of the intertubular matrix, without necessarily involving the tubules of the papillary dermis.

Although the specific disposition of melanin and calcium salts in rhinoceros horn is perhaps unique among cornified papillary epidermis, the general tissue structure that forms rhinoceros horn is strongly convergent with many similar tissues, such as ungulate

hoof wall (Nickel, 1938), bovid artiodactyl horns (Trautmann and Fiebiger, 1952:368), baleen plates (Lambertsen et al., 1989), and the papillary horn of cockatoo bills (Homberger, 2001). Comparative studies that take advantage of this convergence may shed light on phylogenetic and functional controls on cornified epidermis morphology.

Literature Cited

Arnott HJ, Pautard FGE. 1968. The inorganic phase of bone: A re-appraisal. Calcified Tissue Reseach 2(suppl.):2.

Averill CK. 1923. Black wing tips. Condor 25:57–59.

Boas, JEV. 1931. In: Bolk L, Göppert E, Kallius E, Lubosch W, editors. Handbuch der Vergleichenden Anatomie der Wirbeltiere.

Bertram JEA, Gosline JM. 1986. Fracture toughness design in horse hoof keratin. Journal of Experimental Biology 125:29–47.

Bertram JEA, Gosline JM. 1987. Functional design of horse hoof keratin: the modulation of mechanical properties through hydration effects. Journal of Experimental Biology 130:121–136.

Bigalke R. 1946. The regeneration of the anterior horn of the black rhinoceros, *Diceros bicornis* (Linn.). Proceedings of the Zoological Society of London 115:323–326.

Bonser RHC. 1996a. Comparative mechanics of bill, claw, and feather keratin in the Common Starling, *Sturnus vulgaris*. Journal of Avian Biology 27: 175–177.

Bonser RHC. 1996b. The mechanical properties of feather keratin. Journal of Zoology (London) 239: 477–484.

Bonser RHC, Witter MS. 1993. Indentation hardness of the bill keratin of the European Starling. Condor 95: 736–738.

Butler M, Johnson A. 2004. Are melanized feather barbs stronger? Journal of Experimental Biology 207:285–293.

Clark AK, Rakes AH. 1982. Effects of methionine hydroxy analog supplementation on dairy cattle hoof growth and composition. Journal of Dairy Science 65:1439–1502.

Dinerstein E. 2003. The return of the unicorns: the natural history and conservation of the greater one-horned rhinoceros. New York: Columbia University Press.

Douglas JE, Mittal C, Thomason JJ, Jofriet JC. 1996. The modulus of elasticity of equine hoof wall: Implications for the mechanical function of the hoof. Journal of Experimental Biology 199:1829–1836.

Groves CP. 1972. *Ceratotherium simum*. Mammal Species 8:1–6.

Hahn MV, McDaniel BT, Wilk JC. 1986. Rates of hoof growth and wear in Holstein cattle. Journal of Dairy Science 69:2148–2156.

Hashiguchi K, Hashimoto K. 1995. The mineralization of crystalline inorganic components in Japanese serow horn. Okajimas Folia Anatomica Japan 72:235–244.

Hashiguchi K, Hashimoto K, Akao M. 2001. Morphological character of crystalline components present in saiga horn. Okajimas Folia Anatomica Japan 78:43–48.

Hieronymus TL, Witmer LM. 2004. Rhinoceros horn attachment: Anatomy and histology of a dermally influenced bone rugosity. Journal of Morphology 260:298.

Homberger DG. 2001. The case of the cockatoo bill, horse hoof, rhinoceros horn, whale baleen, and turkey beard: The integument as a model system to explore the concepts of homology and non-homology. In: Dutta HM, Datta Munshi JS, editors. Vertebrate functional morphology: Horizon of research in the 21st century. Enfield: Science Publishers Inc. p 317-343.

Jimbow K, Fitzpatrick TB, Quevedo WC Jr. 1986. Formation, chemical composition and function of melanin pigments. In: Bereiter-Hahn J, Matoltsy AG, Sylvia Richards K, editors. Biology of the integument, vol. 2: Vertebrates. Berlin: Springer. p 278–292.

Kingdon J. 1979. East African mammals, vol IIIB. Chicago: University of Chicago Press. 436 p.

Kitchener A. 1987. Fracture toughness of horns and a reinterpretation of the horning behaviour of bovids. Journal of Zooloy (London) 213:621–639.

Lambertsen RH, Hintz RJ, Lancaster WC, Hirons A, Kreiton KJ, Moor C. 1989. Characterization of the functional morphology of the mouth of the Bowhead Whale, *Balaena mysticetus*, with special emphasis on feeding and filtration mechanisms. Report to the Department of Wildlife Management, North Slope Borough, Box 69, Barrow, AK from Ecosystems, Inc., Institute for Environmental Medicine, University of Pennsylvania Medical Center, Philadelphia, PA 19104. 134 pp.

Lynch LJ, Robinson V, Anderson CA. 1973. A scanning electron microscope study of the morphology of rhinoceros horn. Australian Journal of Biological Sciences 26:395–399.

Marshall RC. 1986. Nail, claw, hoof, and horn keratin. In: Bereiter-Hahn J, Matoltsy AG, Richards SK, editors. Biology of the integument, vol. 2: Vertebrates. Berlin: Springer. p 722–738.

Nickel R. 1938. Uber den Bau der Hufrorchen und seine Bedeutung fur den Mechanismus des Pferdhufes. Deutsche Tierarztliche Wochenschrifte (Hannover) 46:449–552.

Owen-Smith RN. 1988. Megaherbivores. Cambridge: Cambridge University Press. 369 p.

Pautard FGE. 1970. The mineral phase of calcified cartilage, bone, and baleen. Calc Tiss Res 4(suppl.):34–36.

Pienaar DJ, Hall-Martin AJ, Hitchins PM. 1991. Horn growth rates of free-ranging white and black rhinoceros. Koedoe 34:97–105.

Prum RO, Williamson S. 2001. Theory of the growth and evolution of feather shape. Journal of Experimental Zoology 291:30–57.

Rachlow JL, Berger J. 1997. Conservation implications of patterns of horn regeneration in dehorned white rhinos. Conservation Biology 11:84–91.

Ryder ML. 1962. Structure of rhinoceros horn. Nature 193:1199–1201.

Trautmann A, Fiebiger J. 1952. Fundamentals of the histology of domestic animals. Ithaca: Comstock Publishing Associates. 426 p.

CHAPTER 2: ADAPTATION, EXAPTATION, AND CONVERGENCE IN RHINOCEROTID HORN EVOLUTION

Abstract

All living rhinoceros possess both (a) elaboration of the dermis as body armor and (b) derived dermal support of their characteristic epidermal horns. Here we show that two separate bony indicators for these traits can be seen in fossil taxa, revealing two independent evolutionary events leading to the appearance of rhinoceros horns. Rhinoceros dermal armor first appeared in the late Eocene (39–42 Ma) as an adaptive response to the use of shearing tusks in intraspecific agonistic behavior. The stiff collagenous tissue of dermal armor was then exapted to support solid epidermal horns in the early Miocene (16–20 Ma). The separation of these two events suggests that rhinoceros horns did not arise as a single novel adaptation, but rather as a sequence of discrete responses to different selection regimes.

Introduction

Rhinoceros horn evolution has acquired iconic status as an example of evolutionary novelty and adaptation (Lewontin 1978; Coddington 1990), but the adaptive explanations and evolutionary scenarios proposed for the appearance of rhinoceros horns have proved to be more problematic than similar events in other taxa, such as horn and antler evolution in artiodactyls. Like other ungulate horns, rhinoceros horns have been hypothesized to function as organs of antipredator defense (Lewontin 1978) or intraspecific display (Berger and Cunningham 1998; Rachlow et al. 1998). Whereas most amniote horns are composed of a thin keratin sheath covering a large bony process,

rhinoceros horn is a unique arrangement of massive epidermal tissue (Ryder 1962) lacking a bony core and supported only by dense dermis (Fig. 2-1). This dense and highly organized structure, in fact, characterizes the dermis across most of the body, and appears to function as dermal armor (Shadwick et l. 1992), particularly in the neck and flanks. Similar arrangements of dermis have arisen independently in such distantly related mammals as hippopotamids, suids, hyrax, and pinnipeds (Schumacher 1931; Sokolov 1982).

Existing reconstructions of extinct rhinocerotids typically point to any form of rugosity on the nasal bones as evidence of horns (Cerdeño 1995; Antoine 2002). Moreover, a typological conception of rhinoceros (the name literally means 'nose horn') has no doubt also played some role, to the point of nasal horn reconstructions made even in the absence of any attachment rugosity. Such broadly defined interpretations place the first occurrence of horns at *Diceratherium* in the latest early Oligocene at approximately 30 Ma, and portray most subsequent rhinocerotids as horned.

Examining the evolutionary history of these soft-tissue features requires an assessment of the causal relationship between skin morphology and any bony elements that may be preserved in fossil taxa. By studying extant taxa with similar skin morphologies, the osteological correlates or bony signatures of specific skin attributes can be directly established, and fossil taxa can then be surveyed for more informative bony indicators. Distinguishing the bony indicators of dermal armor from those of horns in extant rhinocerotids allows a reassessment of the evolutionary history of these skin-related characters in extinct taxa.

Results & Discussion

Osteological correlates of dermal armor

In extant rhinoceros, the presence of dermal armor on the skull is marked by several patches of rugose bone (Fig. 2-2C). This rugose surface is the result of the direct formation of bone from dermal tissue (metaplastic ossification; Fig. 2-2B). Similar patches of rugose bone are also found on skulls of hippopotamus (Fig. 2-3) and the African suids *Hylochoerus* and *Potamochoerus*, all of which are hornless, suggesting that rugosity alone is not a sufficient signature of horn attachment in extinct rhinocerotids.

Osteological correlates of integumentary horns

Ossification features associated with horns can be distinguished from those associated only with dermal armor by the presence of an annular (ring-shaped) distribution of rugose bone (Fig. 2-2A), presumably the result of epigenetically-controlled bone growth in response to stress concentrations at the edges of heavily keratinized horns. Similar patterns, albeit at a much smaller scale, can be seen in other taxa with prominent rigid skin appendages, such as the comb duck *Sarkidiornis* and the American white pelican *Pelecanus erythrorhynchos* (Fig. 2-4). This distinction allows two separate skin-related characters to be scored for fossil taxa: (a) presence or absence of homogeneous patches of rugose bone (the bony signature for dermal armor), and (b) presence or absence of annular rugosities (the signature for epidermal horns).

Osteological correlates of dermal armor in fossil taxa

Homogeneous patches of rugose bone on other regions of the skull appear more basally than nasal rugosities, with faint expression on the squamosal bones of *Trigonias*

osborni (39–42 Ma) and well-developed squamosal rugosity in *Subhyracodon* spp. (Fig. 2-5). Squamosal rugosity (Fig. 2-3D) is in fact the most widespread evidence of dermal armor in extinct rhinocerotids, and is the most pronounced cranial rugosity in the elasmotherine lineage (Deng 2005; *Diceratherium – Huaqintherium* in Fig. 2-5), even persisting after nasal rugosities have been secondarily lost in more derived taxa such as *Procoelodonta*.

Osteological correlates of epidermal horns in fossil taxa

The nasal rugosities of basal rhinocerotids such as *Diceratherium* and *Menoceras* do not form annular patterns (Figs. 2-6 & 2-7), and thus do not provide any positive evidence for the presence of horns. In fact, we found such evidence only in the crown group of living rhinocerotids, which includes the extinct taxa *Coelodonta* (the 'woolly rhino') and *Ceratotherium neumayri*. Similar annular rugosities have been described and figured for *Punjabitherium* (Khan 1971) and the stem taxon *Gaindatherium* (Colbert 1934), placing the first occurrence of horns at 16–20 Ma, approximately 20 Ma after the first evidence of dermal body armor (Fig. 2-5). This timing rules out the possibility that rhinoceros dermal armor is an adaptive response to horn use in agonistic behavior (Larson and Losos 1996).

Evolutionary history of rhinocerotid dermal armor

The use of sharpened tusks in intraspecific agonistic behaviors has been cited as a possible selection pressure driving the evolution of dermal body armor (Shadwick et al. 1992), and shearing tusks occur convergently in many of the extant mammalian taxa that possess this derived dermal morphology (Schumacher 1931; Sokolov 1982). We present

the results of two phylogenetic comparative tests that address the premise and support for adaptive explanations, respectively: (a) a lineage test that maps the relative positions of the putative selection regime and adaptation on a phylogeny (selection regime must closely precede adaptation to be a valid adaptive explanation (Larson and Losos 1996); and (b) a convergence test that examines whether independent occurrences of the selection regime are accompanied by the putative adaptation more often than would be expected by chance (Pagel 1994).

A lineage test for adaptive relationship between shearing tusks and the bony indicator for dermal armor in rhinocerotids (Cerdeño 1995; Antoine 2002; Antoine et al. 2003; Maddison and Maddison 2006a, b) shows that the two traits are closely related, with dermal armor appearing in *Trigonias* spp. approximately 4 Ma after the first evidence of shearing tusks in their immediate basal outgroup *Teletaceras* (Fig. 2-5), indicating that an adaptive relationship is plausible. A convergence test of this same relationship among extant mammals (Sokolov 1982; Nowak and Paradiso 1983; Pagel 1994; Arnason and Janke 2002; Fernández and Vrba 2005; Kriegs et al. 2006) shows significant character correlation ($p = 0.005$; Fig. 2-8), indicating a degree of convergence best explained by adaptation. Tusks and dermal armor both initially develop as sexually dimorphic characters in basal rhinocerotids, and tusks, not horns, remain the primary offensive weapons of the three basal extant rhinoceros species (Dinerstein 1991; Prothero and Schoch 2002), further supporting the relationship of shearing tusks as the selection pressure and dermal armor as the adaptive response. The evolution of these two traits in rhinocerotids is thus convergent with the evolution of analogous sexually dimorphic traits

in other mammals with highly territorial males such as swine, hippopotamus, and elephant seals.

Evolutionary history of rhinoceros horns

This finding falsifies a part of the previously held adaptive hypothesis for rhinoceros horn evolution in that the intrasexual selection pressures previously used to explain this event (Janis 1982) are in place by the late Eocene, that is, well in advance of the appearance of horns. Nevertheless, an early Miocene date for horn evolution in rhinoceros is highly congruent with the timing of horn and antler evolution in other ungulates. The first appearance of rhinocerotid horns (as marked by *Gaindatherium* at 16–20 Ma) coincides closely with the independent appearance of horn-like cranial appendages in six other ungulate lineages, and all of these events occur within 5 Ma of the onset of regional increases in the prominence of grassland habitat (Fig. 2-5; Janis and Scott 1987; Jacobs et al. 1999). Although it is currently unclear what mechanism drives the evolution of horns in ungulates, and indeed whether or not the same mechanism is acting on all seven convergent lineages, the similarity in timing and degree of convergence between these lineages suggests a common cause, perhaps relating to enhanced visual communication in their newly more open habitats. The temporal relationship between the appearance of horns and the spread of more open savannah habitats is further corroborated by the timing of increased cheek tooth crown height (mesodonty–hypsodonty) in many ungulate lineages, including several rhinocerotid taxa. Hypsodonty is strongly correlated with grass-rich diet in extant mammals (Janis 1988)—the independent increases in crown height in rhinocerotid lineages tracks their transition

from closed and mixed habitats to more open, grass-rich habitats during the early and middle Miocene (Fig. 2-9).

Conclusions

The architecture of the dermis that first evolved as an adaptation to produce body armor was later co-opted (exaptation) in the region covering the nasal and frontal bones in rhinocerotids to produce a support for massive keratinous horns (Fig. 2-5). Although the internal structure and dermal support of rhinocerotid horns are novel features, their external form and the ecological context of their first appearance are convergent with primitive horns and antlers in other ungulate lineages. The novel features of rhinoceros horns are thus not the result of a single novel selection pressure, but instead arise from a sequential combination of two commonly occurring selection pressures. Both the adaptive and the exaptive events in this scenario are convergent on adaptive responses in other large mammal groups. Thus, a more detailed view of rhinoceros skin evolution adds another layer to the iconic one- or two-horn adaptation model (Lewontin 1978; Coddington 1990), emphasizing the importance of combinatorial processes in the origin of novelty.

Materials and Methods

Anatomy and histology of horn attachment

No detailed descriptions of rhinoceros horn attachment are available in the anatomical literature. Bony characters pertaining to skin and horns were examined in skeletal specimens representing all five extant rhinoceros taxa, all four extant tapir taxa, and four extant equid taxa (together composing an ingroup sample of 116 individuals;

Appendix A), as well as a number of extant mammalian taxa with similar bony characters and their sister taxa (outgroup sample, 71 individuals in 11 taxa; Appendix A), to separate skin-related bone morphology from individual and/or phylogenetically controlled variation. We then examined the nasal and frontal horn bosses and adjacent skin and bone of one specimen of *Ceratotherium simum* (OUVC 9541) by dissection, histology, and x-ray computed tomography (CT scanning) to document the pattern of soft-tissue elaboration and ossification that produces the characteristic rugose bone surfaces of rhinoceros skulls.

Analysis of fossil material

Twenty-five extinct ceratomorph taxa (63 individuals; Appendix A) were examined for skin-related characters identified from extant specimens. Presence/absence and homogeneity/annularity of rugose bone patches were scored as binary categorical characters in Mesquite v1.12 (Maddison and Maddison 2006a) with asymmetrical two-parameter models of character state change. We generated a matrix representation with parsimony (MRP; Ragan 1992) supertree of rhinocerotids (Swofford 2001; Maddison and Maddison 2006a) from existing morphological and molecular phylogenies (Morales and Melnick 1994; Cerdeño 1995; Tougard et al. 2001; Antoine 2002; Antoine et al. 2003; Orlando et al. 2003), and trimmed this tree to encompass the 24 extant and extinct rhinocerotid taxa of our sample. Taxon appearance times were fixed using locality data from specimens in our sample as well as occurrence data downloaded from the Paleobiology Database. Confidence intervals around taxon first appearances were calculated using the method of Strauss and Sadler (1989). Internal branches nearest to

terminal taxa were set at 1 Ma, placing internal nodes close to documented fossil occurrences. We then reconstructed ancestral character states with a maximum likelihood criterion onto this phylogeny (Maddion and Maddison 2006b), both with branch lengths in Ma and with all branch lengths set to one (no substantive difference exists between these reconstructions). First appearances of traits reported here correspond to the more conservative indicator of a confidence interval around the first fossil evidence for a trait, not the reconstruction of the trait at a node.

Lineage test for adaptation

For the lineage test, we imported mesial dentition characters (an organismal proxy for the putative selection regime) from published sources (Cerdeño 1995; Antoine 2002; Antoine et al. 2003) into Mesquite v1.12 as binary categorical characters with asymmetrical two-parameter models of character state change and reconstructed ancestral character states with a maximum likelihood criterion. We then compared the order of appearance and temporal separation of shearing tusks (selection regime) and dermal armor (adaptation). The appearance of dermal armor more basal than shearing tusks would falsify a hypothesis of dermal armor as an adaptive response (Larson and Losos 1996). No strict criteria for interpreting temporal separation between selection regime and adaptive response exist, beyond the conceptual model that adaptation should accompany selection regime in 'short order.' Spans of 5 Ma between selection regime and adaptation in the Miocene record have been discussed as problematic (Strömberg 2006), although interpretations depend upon the temporal resolution of fossil occurrences and the degree of uncertainty that surrounds the first appearance of a trait in a fossil taxon.

Convergence test for adaptation

For the convergence test, we imported data on mesial dentition (Nowak and Paradiso 1983) and dermal morphology (Sokolov 1982) in representative mammalian species from published sources into Mesquite v1.12, and placed these taxa in a composite higher-level phylogeny of mammals (Arnason and Janke 2002; Fernández and Vrba 205; Kriegs et al. 2006) with all branch lengths set to one to reflect uncertainty in rates of morphological change. Correlation between shearing tusks and dermal armor was tested in this phylogenetic framework using Pagel's Omnibus test with 10 likelihood searches and 1000 Markov chain Monte Carlo replicates (Pagel 1994; Maddison and Maddison 2006a).

Assessing temporal congruence

We examined congruence in the timing of horn evolution between artiodactyl and rhinocerotid lineages by comparing the interval for the first appearance of horns in *Gaindatherium* with Strauss and Sadler (1989) confidence intervals for the earliest representative taxon for each occurrence of horns or antlers in artiodactyls (Janis 1982; Janis and Scott 1987) . We then compared the dates of these intervals with published dates for the spread of grassland habitat by continent (Jacobs et al. 1999). Ancestral states for a composite cheek tooth height character (Cerdeño 1995; Antoine 2002; Antoine et al. 2003) were calculated on the complete rhinocerotid supertree using a symmetrical one-parameter character model and a likelihood criterion, and likelihood ratios for low vs. high cheek teeth were mapped onto nodes of the trimmed supertree to determine independent occurrences of mesodonty or hypsodonty.

Literature Cited

Antoine P-O 2002. *Phylogénie et évolution des Elasmotheriina (Mammalia, Rhinocerotidae.)* Paris: Publications scientifiques du Muséum.

Antoine P-O, Duranthon F, Wellcome J-L. 2003. *Alicornops* (Mammalia, Rhinocerotidae) dans le Miocene superieur des Collines Bugti (Balouchistan, Pakistan): implications phylogenetiques. GEODIVERSITAS 25:575–603.

Arnason U, Janke A. 2002. Mitogenomic analyses of eutherian relationships. Cytogenetic and Genome Research 96:20.

Berger J, Cunningham C. 1998. Natural variation in horn size and social dominance and their importance to the conservation of black rhinoceros. Conservation Biology 12:708–711.

Cerdeño E. 1995. Cladistic analysis of the family Rhinocerotidae (Perissodactyla). American Museum Novitates 3143:1–25.

Coddington JA. 1990. Bridges between evolutionary pattern and process. Cladistics 6:379–386.

Colbert EH. 1934. A new rhinoceros from the Siwalik beds of India. American Museum Novitates 749:1–13.

Deng T. 2005. New discovery of *Iranotherium morgani* (Perissodactyla, Rhinocerotidae) from the late Miocene of the Linxia Basin in Gansu, China, and its sexual dimorphism. Journal of Vertebrate Paleontology 25:442–450.

Dinerstein E. 1991. Sexual dimorphism in the greater one-horned rhinoceros (*Rhinoceros unicornis*). Journal of Mammalogy 72:450–457.

Fernández MH, Vrba ES. 2005. A complete estimate of the phylogenetic relationships in Ruminantia: a dated species-level supertree of the extant ruminants. Biological Reviews 80:269–302.

Hieronymus TL, Witmer LM, Ridgely RC. 2006. Structure of white rhinoceros (*Ceratotherium simum*) horn investigated by X-ray computed tomography and histology with implications for growth and external form. Journal of Morphology 267:1172–1176.

Jacobs BF, Kingston JD, Jacobs LL. 1999. The origin of grass-dominated ecosystems. Annals of the Missouri Botanical Garden 86:590–643.

Janis CM. 1982. Evolution of horns in ungulates: ecoogy and paleoecology. Biological Reviews 57:261–318.

Janis CM. 1988. An estimation of tooth volume hypsodonty indices in ungulate mammals, and the correlation of these factors with dietary preference. In: Russell DE, Santoro J-P, Sigogneau-Russell D, editors. Teeth Revisited, Proceedings of the VIIth International Symposium on Dental Morphology. Paris: Mémoires du Muséum d'Histoire Naturelle Séries C. p. 367–387.

Janis CM, Scott KM. 1987. The interrelationships of higher ruminant families, with special emphasis on the members of the Cervoidea. American Museum Novitates 2893:1–85.

Khan E. 1971. *Punjabitherium* gen. nov.: An extinct rhinocerotid of the Siwaliks (Punjab, India). Proceedings of the Indian Natural Sciences Academy 37A:105–109.

Kingdon J. 1979. East African mammals: An atlas of evolution in Africa. Vol.3. Part B, Large mammals London: Academic Press.

Kriegs JO, Churakov G, Kiefmann M, Jordan U, Brosius J, Schmitz J. 2006. Retroposed elements as archives for the evolutionary history of placental mammals. PLoS Biology 4:e91.

Larson A, Losos JB. 1996.Phylogenetic systematic of adaptation. In: Rose MR, Lauder GV, editors. Adaptation. San Diego: Academic Press. p. 187–220.

Lewontin RC. 1978. Adaptation. Scientific American 239:212–222.

Maddison WP, Maddison DR. 2006a. Mesquite: a modular system for evolutionary analysis, v1.12 (http://mesquiteproject.org).

Maddison WP, Maddison DR. 2006b. StochChar: a package of Mesquite modules for stochastic models of character evolution, v1.1 (http://mesquiteproject.org).

Morales JC, Melnick DJ. 1994. Molecular systematics of the living rhinoceros. Molecular Phylogenetics and Evolution 3:128–134.

Nowak RM, Paradiso JL. 1983. Walker's mammals of the world. Baltimore: Johns Hopkins University Press.

Orlando L, Leonard JA, Thenot A, Laudet V, Guerin C, Hänni C. 2003. Ancient DNA analysis reveals woolly rhino evolutionary relationships. Molecular Phylogenetics and Evolution 28:485–499.

Pagel M. 1994. Detecting correlated evolution on phylogenies: A general method for the comparative analysis of discrete characters. Proceedings of The Royal Society B Biological Sciences 255:37.

Prothero DR, Schoch RM. 2002. Horns, tusks, and flippers: The evolution of hoofed mammals. Baltimore: Johns Hopkins University Press.

Rachlow JL, Berkeley EV, Berger J. 1998. Correlates of male mating strategies in white rhinos (*Ceratotherium simum*). Journal of Mammalogy 79:1317–1324.

Ragan MA. 1992. Phylogenetic inference based on matrix representation of trees. Molecular Phylogenetics and Evolution 1:53–58.

Ryder ML. 1962. Structure of rhinoceros horn. Nature 193:1199–1201.

Schumacher Sv. 1931. Integument der Mammalier. In: Bolk L, Goppert E, Kallius E, Lubosch W, editors. Handbuch der Vergleichenden Anatomie der Wirbeltiere. Berlin: Urban und Schwarzenburg. p. 449–504.

Shadwick RE, Russell AP, Lauff RF. 1992. The structure and mechanical design of rhinoceros dermal armour. Philosophical Transactions of the Royal Society of London. Series B, Biological sciences 337:419–428.

Sokolov VE. 1982. Mammal skin. Berkeley: University of California Press.

Strauss D, Sadler PM. 1989. Classical confidence intervals and Bayesian probability estimates for ends of local taxon ranges. Mathematical Geology 21:411–427.

Strömberg CAE. 2006. Evolution of hypsodonty in equids: testing a hypothesis of adaptation. Paleobiology 32:236–258.

Swofford DL. 2001. PAUP*: phylogenetic analysis using parsimony (*and other methods), v4.10b. Sunderland: Sinauer Associates.

Tougard C, Delefosse T, Hänni C, Montelgard C. 2001. Phylogenetic relationships of the five extant rhinoceros species (Rhinocerotidae, Perissodactyla) based on

mitochondrial cytochrome b and 12S rRNA genes. Molecular Phylogenetics & Evolution 19:34–44.

CHAPTER 3: EVOLUTIONARY MODULARITY IN SAUROPSID CEPHALIC SKIN

Abstract

The skin on the heads of sauropsids (lizards, turtles, crocodylians, and birds) displays a striking variety of integumentary features. Classical topographic anatomical regions have been separately proposed for 'reptiles' and birds, based on the distribution of scales, feathers, or other structures on the head. In many cases, the shapes and placements of the resulting anatomical regions show strong similarities, which has led to hypotheses that corresponding skin features are homologous across Sauropsida (e.g., squamate labial scales are transformational homologs of avian beak plates). This similarity does not always pass the standard tests of homology, but it does present a pattern that can be assessed with phylogenetic comparative methods, specifically a test for modularity. Here we show that two areas of cephalic skin in Sauropsida form discrete interdependent units, or evolutionary modules: (1) skin directly surrounding the oral margin; and (2) skin covering the skull roof and adjacent parts of the face, including the ventral border of the mandible. Data on integumentary features from a sample of 83 sauropsid taxa were used to generate maximum parsimony ancestral character state reconstructions of skin morphology in discrete cephalic regions. The resulting regional histories of change in skin morphology were compared using standard multivariate tests of association. The evolutionary modularity shown by these comparative tests is most likely the result of a conserved reaction-diffusion mechanism of embryonic skin development, in which the spacing of integumentary features is originally determined by two or three separate centers on the head. Because these centers define the morphological

pattern of later-differentiating skin, development of morphology within the resulting regions fits the definition of modularity in being strongly integrated and relatively insensitive to external conditions. The phylogenetic pattern shown in this study, when combined with published information on the development of cephalic skin, suggests that the recurring similarities in topographic anatomy within sauropsids is caused by the retention of two major skin modules, not by homology between topographic regions or their component parts.

Introduction

Sauropsids, the group comprising lizards, snakes, turtles, crocodiles, and birds, show a diverse set of cephalic skin features. Examples of this diversity include scaly armor in many lizards (e.g., *Cordylus*), the soft cephalic skin of soft-shelled turtles (*Trionyx*), and the plumes and combs seen in many birds (*Gallus*). Because cephalic skin is so variable, it has historically been an important source of taxonomic characters. As such, several classification schemes have been devised for grouping and naming the integumentary features present on the head. Some of these groupings include the plates of avian compound beaks (Coues 1866; Boetticher 1928), feathers of the capital pterylae (i.e., feather tracts; Fig. 3-1A, B; Lucas and Stettenheim 1972) and scales and cephalic shields of squamates and crocodylians (Fig. 3-1C, D; Cope 1900).

Different classification systems often outline topographically similar areas of skin, even in comparisons between distantly related groups. The degree of similarity between, for example, labial scales in lizards and compound rhamphotheca in birds has been pointed to as evidence of homology by some authors (Lönnberg 1904). Although

the skin features described in such broad hypotheses (i.e., Cope 1900; Lönnberg 1904) do not meet current criteria for tests of homology (Patterson 1982; Wagner 1989), the similarity in topographic anatomy within Sauropsida is still compelling.

The persistent topographic similarity of sauropsid cephalic skin regions suggests some form of modularity or morphological constraint. Evolutionary constraints on morphology often arise within systems where the development and morphology of separate parts are internally interdependent but externally independent, forming a developmental module (Schlosser and Wagner 2004). In this paper, we address the question of whether the phylogenetic pattern of morphological change in any one cephalic skin region is independent from change in adjacent regions.

To assess evolutionary independence in this system, this study reconstructs the phylogenetic patterns of change in cephalic skin features on a region-by-region basis, and tests those patterns for non-random associations between regions. Because many cephalic skin features of sauropsids are morphologically divergent, ancestral character state reconstruction (change in character state over time) may only capture major evolutionary changes, such as the first appearance of beaks in birds and in turtles. Instead, this study considers the rate of coincident change (i.e., change on the same branch of a phylogenetic tree) in many character states over time, which allows direct comparisons of change between unrelated character states (e.g., comparing change from cephalic shields to large scales in one skin region to change from large scales to small scales in another skin region; both character state changes involve an increase in the number of integumentary features in a given skin region, regardless of the morphology of the individual features).

This study examines rates of coincident change to assess whether morphological change in adjacent skin regions co-occurs more often than would be expected by random chance. Non-random coincident change matches the phylogenetic pattern expected for developmental modules (Schlosser 2004; Fig. 3-2), and the presence of similar phylogenetic patterns of morphological change in sauropsid cephalic skin may shed light on the persistent topographic similarity seen in these systems.

Materials and Methods

Skin regions

Sauropsid cephalic skin was subdivided into 15 regions based largely on published descriptions (Coues 1866; Cope 1900; Lönnberg 1904; Boetticher 1928; Lucas and Stettenheim 1972) to provide a common scheme for scoring morphological characters (Fig. 3-3). Previous definitions of regional borders were often based on underlying skeletal elements, but such a method of classification is limited in areas where reference points are obscured by the fusion of bony elements (e.g., rhamphotheca over the fused bony rostrum in birds). In these cases, the edges of discrete epidermal elements such as beak plates were used as regional boundaries. The topographic anatomy used here lumps together some of the regions of previous authors (e.g., avian malar pterylae and the temporal region) and subdivides other regions (e.g., the most lateral parietal scale groups in lepidosaurs, crocodylians, and turtles are considered to form a separate squamosal skin region).

Character states

A sample of 83 extant sauropsid taxa (Appendix B) was used to document the predominant integumentary morphology present in each region. Sources of morphological data included alcohol-preserved specimens, osteological specimens, and images from the California Academy of Sciences online image database (http://calphotos.berkeley.edu). Skin covering each region was scored as showing one of six character states: (1) a single scale or plate per region; (2) a single scale or plate continuing into an adjacent region; (3) multiple irregular scales; (4) multiple hexagonal scales; (5) scaleless soft skin (including cere and apteria); and (6) feathered skin (pteryla). Character states are illustrated in Figure 3-4. Scores for each taxon are listed in Appendix B.

Ancestral character state reconstruction

A maximum parsimony ancestral character state reconstruction was performed in Mesquite 2.01 (Maddison and Maddison 2007) for each region, using a composite phylogenetic hypothesis derived from current literature (Shaffer 1997; Brochu 2003; Cracraft et al. 2004; Lee et al. 2004; Appendix B). Classically accepted hypotheses of evolution between character states were modeled using a step-matrix of character state transition costs (Table 3-1). Costs in the step-matrix represent a simplified version of hypotheses for the evolution of sauropsid integumentary features from basal amniote integument, shown in Figure 3-5 (Maderson 1965; Lucas and Stettenheim 1972; Sengel 1976; Harris et al. 2002; Prum and Brush 2002; Alibardi 2004; Wu et al. 2004; Sawyer et al. 2005).

Table 3-1. Step-matrix of character state transition costs used for maximum parsimony ancestral character state reconstructions.

	Single	Continuous	Multiple	Hexagonal	Scaleless	Feathered
Single	-	1	1	2	1	2
Continuous	1	-	2	3	1	3
Multiple	1	2	-	1	2	1
Hexagonal	2	3	1	-	2	1
Scaleless	1	1	2	2	-	2
Feathered	2	3	1	1	2	-

Coincident change in separate skin regions

To examine interdependence of morphological change between skin regions, a matrix of regions by change along branches was constructed. For every region, each branch of the composite phylogeny was scored for change or stasis, defined as any difference between the ancestral character state reconstruction of the parent and daughter node for that branch (Fig. 3-6). Change and stasis scores for all skin regions in this matrix were analyzed using Jaccard, Hamming, and Raup-Crick multivariate similarity indices in the PAST statistical package (Hammer et al. 2001). Jaccard similarity scores coincident change but not coincident stasis, whereas Hamming similarity accounts for both coincident change and coincident stasis. Raup-Crick similarity is a probabilistic measure that compares frequency of coincident changes to a distribution generated by a 200-replicate bootstrap. Raup-Crick similarity scores that fall in the tails of the bootstrapped distribution (greater than 0.975 or less than 0.025 for $p = 0.05$) can be

considered significantly non-random, both in terms of similarity (non-random associated change, or interdependence) and dissimilarity (non-random dissociated change, or independence).

Relationships between similarity scores for each region were visualized using non-metric multidimensional scaling (NMDS), unweighted paired-group average (UPGMA) cluster analysis, and neighbor-joining (NJ) cluster analysis in PAST. Clusters from UPGMA and NJ analyses were evaluated using 1,000 replicate bootstraps. This method of examining patterns of change is similar in construction to the Concentrated Changes test (Maddison 1990), although its treatment of phylogenetically structured data is exploratory rather than probabilistic, and only changes that co-occur on the same branch are counted. Like Concentrated Changes, the outcome of this analysis depends heavily upon the accuracy of the initial ancestral character state reconstructions.

Results

Perioral skin regions show high rates of coincident change

Skin regions directly surrounding the oral margin (including rostral, symphyseal, supralabial, and infralabial regions) form a robust group on the basis of frequent coincident changes (Fig. 3-7; UPGMA and NJ bootstrap values of ≥ 79 for all similarity indices, Raup-Crick similarities ≥ 0.965). This grouping does not show coincident changes with other skin regions on the head more often than would be expected by chance (Table 3-2), and indeed often shows positive evidence of independence from change in adjacent regions (all Raup-Crick similarities between perioral regions and other adjacent regions ≤ 0.185). Thus, even though character state may be similar between

perioral skin and adjacent skin regions (e.g., the presence of multiple irregular scales in both the supralabial and loreal regions of scincoid lizards), changes in character state in perioral skin occur as a unit, disjunct from morphological change in other regions of the head.

Table 3-2. Raup-Crick similarity scores for adjacent topographic regions that show non-random coincident change at $p \leq 0.2$. Asterisks denote non-random coincident change at $p \leq 0.05$.

Regions	Raup-Crick similarity
Perioral module associations	
Rostral—Supralabial	1.0*
Symphyseal—Infralabial	0.9975*
Symphyseal—Gular	0.93
Perioral module dissociations	
Symphyseal—Sublabial	0.0325
Rostral—Internasal	0.0325
Rostral—Nasal	0.0375
Supralabial—Nasal	0.04
Supralabial—Loreal	0.0475
Cranial module associations	
Prefrontal—Frontal	1.0*
Prefrontal—Supraocular	1.0*
Frontal—Supraocular	1.0*

Frontal—Parietal	1.0*
Parietal—Squamosal	1.0*
Frontal—Squamosal	0.985*
Squamosal—Temporal	0.975*
Squamosal—Supraocular	0.945
Internasal—Prefrontal	0.93

Skin regions across the skull roof show consistent coincident change

Morphological change in skin regions of the skull roof (prefrontal, frontal, supraocular, parietal, squamosal, and temporal regions) generally show strong Raup-Crick similarity indices (Table 3-2), but clusters formed by character state change in these regions show low bootstrap values and variable topologies (Fig. 3-7). Thus these skin regions form a unit in the same manner as the perioral skin regions, but interdependence between the regions of the skull roof is less tightly coordinated. The most consistent linked change in these skin regions involves the frontal, prefrontal, and supraocular regions. These regions form an exclusive cluster with Jaccard and Hamming similarity indices in both UPGMA and NJ cluster analyses (bootstrap values ≥ 67), indicating a region of interdependent morphological change on the rostral skull roof that is variably linked to the remaining caudal cephalic skin regions.

Skin regions of the face show some interdependence with skin of the skull roof

Internasal, nasal, loreal, sublabial, and gular skin regions show patterns of change that are relatively independent from other regions of the head (Fig. 3-7). With the exception of the gular region, these skin regions all show strong independence from the

perioral skin group (Table 3-2). Thus, their closest associations are with skin regions of the skull roof.

Discussion

General patterns of change in cephalic skin

Despite the apparent similarity in topographic anatomy of cephalic skin in sauropsids, strongly linked change across the skin of the skull roof and the skin of the oral margin suggests that cephalic skin comprises two evolutionary modules (hereafter referred to as cranial and perioral modules, respectively), not several independent smaller regions. Thus the subdivisions within these two modules in systems of topographic anatomy may be effectively arbitrary, referring to convenient features for demarcation rather than pointing out evolutionarily or developmentally independent areas. A degree of morphological independence or individuality has been suggested as one of the biological bases for homology (Wagner 1989). Because the fifteen regions of topographic anatomy identified in this study do not show strong individuality, the biological basis for any homologous arrangement of integumentary features they contain across all of Sauropsida is questionable. This result supports Boetticher's (1928) broad conclusion of non-homology between arrangements of integumentary features on the skulls of widely divergent sauropsids (e.g., lizards and birds), while still allowing for homology between individual skin features within a module (such as rhamphothecal plates) within more restricted clades (see Chapter 4).

Patterns of change in the perioral module

A majority of the linked change that drives the robust grouping of perioral skin regions in this analysis occurs within Lepidosauria and Neornithes. Each of these groups shows a slightly different mode of character state change. Morphological change in the perioral module within Lepidosauria occurs as a number of convergent transitions and reversals from the basal arrangement (single rostral and symphyseal scales, multiple irregular supralabial and infralabial scales) to a derived 'small scale' arrangement (multiple irregular rostral and symphyseal scales, multiple hexagonal supralabial and infralabial scales). The 'small scale' arrangement generally occurs as part of a trend toward reduced scale size in both modules, for example leading to the small cephalic scales of varanids and acrodont iguanians, but the perioral module lags behind the cranial module in this trend.

In contrast, change in perioral skin within Neornithes follows two general trends. The first, seen across Neornithes as a whole, involves several transitions and reversals from the basal arrangement of compound rhamphotheca (single plates in all perioral regions) to a derived arrangement of simple rhamphotheca (plates continuous with adjacent regions in all perioral regions; see Chapter 4). A second, less widespread trend within galloanserine birds involves convergent transitions of the infralabial region from a single or continuous plate to an area of soft skin similar to cere. These changes do not occur as part of any noticeable trend in other regions of neornithine cephalic integument.

Patterns of change in the cranial module and the face

Changes in skin morphology across the skull roof also show phylogenetic trends. Most of the coincident change in the cranial module seen here is documented within Lepidosauria, where the character states used in this study are able to discriminate relatively small differences in morphology (e.g., transitions between a single prefrontal shield and two prefrontal scales). In contrast, most Neornithes show a feathered skull roof, and are thus all scored as showing the same character state regardless of differences in the number of feathers present across the skull roof, leading to little or no resolution of coincident change among skull roof regions. A quantitative treatment of differences in pterylosis would no doubt uncover patterns of change that are not visible in this analysis, as even within galloanserine birds there are marked differences in the number of feathers within each section of the capital tracts (Eames and Schneider 2005).

Evolutionary modules and skin development

The phylogenetic patterns of coincident change in cephalic skin seen in this study constitute evolutionary modules, which are not necessarily linked to modularity in development (Schlosser 2004). However, published accounts of cephalic skin development in sauropsids support the idea that developmental modules are responsible for the evolutionary patterns described above. The regular hexagonal distribution of some tracts of scales and feathers matches the pattern expected from a morphogenetic model known as the reaction-diffusion model (Turing 1952). In this model, antagonistic morphogens (an activator and an inhibitor) of different sizes are expressed in the extracellular space of developing tissues. Small perturbations to this system result in an

alternating spatial pattern of activator and inhibitor concentrations that radiates from the site of the perturbation, specifying the positions of later-differentiating dermal and epidermal contributions to skin features.

Reaction-diffusion mechanisms have been demonstrated to play a role in the patterning of feather tracts (Jung et al 1998; Noramly and Morgan 1998; Patel et al 1999; Jiang et al 2004), and have been inferred to play the same role in squamate scales based on similarity in other developmental processes (Alibardi 2004). As a result, the arrangement of these integumentary features is dependent upon the initial location of a small number of perturbations or initiating centers. In this system, individuality *sensu* Wagner (1989) can only be assigned to a field or area of integumentary features that radiates from a single initiating center. The resulting fields are internally interdependent (or integrated), and externally independent (or context-insensitive), matching process criteria proposed for developmental modules (Schlosser 2004).

Although information on the morphology of embryonic feather tracts (pterylosis) and scale tracts (squamation) is somewhat scarce, the general pattern observed in sauropsids includes separate initiating centers on the skull roof and the oral margin (Dufaure and Hubert 1961; Koecke and Kuhn 1962). The mechanism that specifies the development of a horny beak in the perioral region in birds is unclear, but keratinization in the horny beak begins in the area immediately surrounding the caruncles or egg teeth and proceeds caudally (Kingsbury et al. 1953; Clark 1961; Fig. 3-8A). In lepidosaurs, the rostral ends of the oral margin form the first centers for initiating squamation on the head (Dufaure and Hubert 1961), with perioral scale pattern spreading caudally from these

centers (Fig. 3-8B). Birds show multiple skull roof initiating centers: a paired set on the dorsal surface of the orbit (the *Scheitelfeld* of Koecke and Kuhn 1962; Fig. 3-8A), a median center in some taxa (Eames and Schneider 2005), and another paired set dorsal to the external auditory meatus (the *Kopfseitenfeld* of Koecke and Kuhn 1962). Embryonic squamation has not been described in detail for lepidosaurs, but at least one separate center appears on the skull roof (Dufaure and Hubert 1961; Fig. 3-8B). The presence of a center that initiates squamation on the skull roof is also found in many teleosts (Sire and Arnulf 1990), and may be a plesiomorphic feature of vertebrate cephalic skin development. The separation of perioral skin differentiation from skull roof skin differentiation as developmental modules may be responsible for the patterns of coincident morphological change observed in our analysis.

Conclusions

In addition to testing for evolutionary modularity, the analysis of coincident morphological change used in this study may be useful for examining other cases in which a single developmental process is thought to control morphological change in several features (e.g., testing hypotheses of pleiotropy). Because only changes from the same branch are counted, this technique is best applied to characters that show evidence for mutual developmental or epigenetic influence. Complex sets of morphological change driven by selection on several independent loci or processes will not necessarily be restricted to the same branch, especially in fine-scale (e.g. family-level) phylogenies, and will thus not be detected by the test for coincident morphological change proposed here.

Although the cephalic skin regions of reptiles and birds are similar, the areas of skin they contain are not necessarily homologous. Two lines of evidence suggest that the regions identified in previous studies cannot be considered as independent. First, previous developmental work points to interdependence in the patterning of cephalic skin features, resulting in only two or three developmental modules that can be considered independent. Second, this study's results point to a similar grouping of evolutionary modules, in which regions of skin around the oral margin and regions of skin on the skull roof each show strongly coincident morphological change over the evolutionary history of Sauropsida. The similarity shown in this study provides a basis for considering each module to be homologous across sauropsids, in the sense that the mechanisms that organize these groups of skin features are plesiomorphic. Thus, the similarity that spawned the concept of homology in 'reptilian' or sauropsid cephalic skin features proposed by Cope (1900) and Lönnberg (1904) is not due to homology in the individual features themselves (i.e. topological similarity between labial scales and beak plates), but is instead a result of topographic similarity in the processes that organize these features early in development.

Literature Cited

Alibardi L. 2004. Dermo-epidermal interactions in reptilian scales: Speculations on the evolution of scales, feathers, and hairs. Journal of Experimental Zoology Part B: Molecular and Developmental Evolution 302B(4):365–383.

Boetticher Hv. 1928. Beitrag zur Kenntnis der Morphologie und Phylogenie des hornigen Vogelschnabelüberzuges mit besonderer Berücksichtigung seiner Beziehungen zu den Schnauzenschildern der saurier. Jena: G. Fischer. 451 p.

Brochu CA. 2003. Phylogenetic approaches toward crocodylian history. Annual Review of Earth and Planetary Sciences 31(1):357–397.

Cope ED. 1900. The crocodilians, lizards, and snakes of North America. Annual Report of the United States National Museum for 1898(2):153–1270.

Coues E. 1866. Critical review of the family Procellariidae: Part V; embracing the Diomedeinae and the Halodrominae. With a general supplement. Proceedings of the Academy of Natural Sciences of Philadelphia 18:172–197.

Clark GA. 1961. Occurrence and timing of egg teeth in birds. Wilson Bulletin 73(3):268–278.

Cracraft J, Barker FK, Braun M, Harshman J, Dyke GJ, Feinstein J, Stanley S, Cibois A, Schikler P, Beresford P, Garcia-Moreno J, Sorenson MD, Yuri T, Mindell DP. 2004. Phylogenetic relationships among modern birds (Neornithes): Toward an avian tree of life. Assembling the Tree of Life. p 468–489.

Dufaure JP, Hubert J. 1961. Table de dévelopment du lézard vivipaire: Lacerta (Zootoca) vivipara Jacquin. Archives d'anatomie microscopique et de morphologie expérimentale 50:309–328.

Eames BF, Schneider RA. 2005. Quail-duck chimeras reveal spatiotemporal plasticity in molecular and histogenic programs of cranial feather development. Science 132(7):1499–1509.

Hammer Ø, Harper DAT, Ryan PD. 2001. PAST: Paleontological Statistics Software Package for Education and Data Analysis. Palaeontologica Electronica 4(1):9p.

Harris MP, Fallon JF, Prum RO. 2002. *Shh-Bmp2* signaling module and the evolutionary origin and diversification of feathers. Journal of Experimental Zoology 294(2):160–176.

Jiang TX, Widelitz RB, Shen W-M, Will P, Wu D-Y, Lin C-M, Jung H-S, Chuong C-M. 2004. Integument pattern formation involves genetic and epigenetic controls: feather arrays simulated by digital hormone models. International Journal of Developmental Biology 48:117–136.

Jung H-S, Francis-West PH, Widelitz R, Jiang TX, Ting-Berreth S, Tickle C, Wolpert L, Chuong C-M. 1998. Local inhibitory action of BMPs and their relationships with activators in feather formation: Implications for periodic patterning. Developmental biology 196:11–23.

Kingsbury JW, Allen VG, Rotheram BA. 1953. The histological structure of the beak in the chick. Anatomical Record 116(1):95–115.

Koecke HU, Kuhn O. 1962. Die embryonale pterylose und ihre entwicklungsphysiologischen vorbedingungen bet der hausente (Anas Boschas Domestica). Zoomorphology 50(6):651–686.

Lee MSY, Reeder TW, Slowinski JB, Lawson R. 2004. Resolving reptile relationships: Molecular and morphological markers. Assembling the Tree of Life. p 451–467.

Lönnberg E. 1904. On the homologies of the different pieces of the compound rhamphotheca of birds. Arkiv för Zoologi 1:479–512.

Lucas AM, Stettenheim PR. 1972. Avian anatomy: Integument. Agriculture handbook 362: Agricultural research services. US Department of Agriculture, Washington, DC.

Maddison WP. 1990. A method for testing the correlated evolution of two binary characters: Are gains or losses concentrated on certain branches of a phylogenetic tree? Evolution 44(3):539–557.

Maddison WP, Maddison DR. 2007. Mesquite: a modular system for evolutionary analysis. Version 2.01: http://mesquiteproject.org.

Maderson PFA. 1965. The embryonic development of the squamate integument. Acta Zoologica 46:275–295.

Noramly S, Morgan BA. 1998. BMPs mediate lateral inhibition at successive stages in feather tract development. 125(19):3775–3787.

Patel K, Makarenkova H, Jung H-S. 1999. The role of long range, local and direct signalling molecules during chick feather bud development involving the BMPs, Follistatin and the Eph receptor tyrosine kinase Eph-A4. Mechanisms of Development 86(1–2):51–62.

Prum RO, Brush AH. 2002. The Evolutionary Origin and Diversification of Feathers. The Quarterly Review of Biology 77(3):261–295.

Sawyer RH, Rogers L, Washington L, Glenn TC, Knapp LW. 2005. Evolutionary origin of the feather epidermis. Developmental Dynamics 232(2):256–267.

Schlosser G. 2004. The role of modules in development and evolution. In: Schlosser G, Wagner GP, editors. Modularity in Development and Evolution. Chicago: University of Chicago Press. p 519–582.

Schlosser G, Wagner GP. 2004. Introduction: The modularity concept in developmental and evolutionary biology. In: Schlosser G, Wagner GP, editors. Modularity in Development and Evolution. Chicago: University of Chicago Press. p 1–11.

Sengel P. 1976. Morphogenesis of Skin. Cambridge, UK: Cambridge University Press. 285 p.

Shaffer HB, Meylan P, McKnight ML. 1997. Tests of Turtle Phylogeny: Molecular, Morphological, and Paleontological Approaches. 46(2):235–268.

Sire JY, Arnulf I. 1990. The development of squamation in four teleostean fishes with a survey of the literature. Japanese Journal of Ichthyology 37(2):133–143.

Turing AM. 1952. The Chemical Basis of Morphogenesis. Philosophical Transactions of the Royal Society of London Series B, Biological Sciences 237(641):37–72.

Wagner GP. 1989. The Origin of Morphological Characters and the Biological Basis of Homology. Evolution 43(6):1157–1171.

Wu P, Hou L, Plikus M, Hughes M, Scehnet J, Suksaweang S, Widelitz R, Jiang T-X, Chuong C-M. 2004. Evo-Devo of amniote integuments and appendages. International Journal of Developmental Biology 48(2–3):249–270.

CHAPTER 4: HOMOLOGY AND EVOLUTION OF AVIAN COMPOUND RHAMPHOTHECAE

Abstract

Here we show that the topology of separate elements in avian compound rhamphothecae are strongly similar among different clades, not only in external appearance but in how these elements conform to underlying structures. We conducted a morphological survey of 81 extant bird species, and tested superficial similarities between external beak morphology for substantive similarity in associated skeletal structures and nerve courses. A revised set of morphological characters for compound rhamphothecae was optimized onto two recent phylogenetic trees to assess the relationships of homology and homoplasy in rhamphothecal morphology. Osteological correlates of rhamphothecae from fossil basal ornithurine birds *Hesperornis*, *Parahesperornis*, and *Ichthyornis* show that compound rhamphothecae are the primitive state for living birds (Neornithes). Simple rhamphothecae are the result of the loss of softer keratinous grooves between rhamphothecal components, and there are many examples of transitional forms between compound and simple rhamphothecae in which the grooves remain as shallow depressions without a pronounced edge. Ancestral character state reconstructions of rhamphothecal morphology within Neornithes also show a considerable amount of homoplasy. We suggest that frequent homoplasy in rhamphothecal morphology is the result of underlying similarity in facial development.

Introduction

Rhamphothecae, the horny (keratinous) sheath that covers the jaws in birds, show amazing diversity, and provide some of the most compelling and easily appreciated examples of morphological adaptation in vertebrates (Storer 1960), such as forceps for probing in sandpipers, filters in ducks and flamingos, 'teeth' for gripping fish in mergansers and gannets, and nutcrackers in hawfinches. There is one widely-distributed feature of the rhamphotheca that appears to be unrelated to their adaptive roles in feeding and display that can be seen in birds such as Waved Albatross, *Phoebastria irrorata*, where the skin of the rhamphotheca is separated into several plates (Fig. 4-1). This condition is referred to as a compound rhamphotheca, and contrasts with the continuous cornified sheaths seen in birds such as American Crows, *Corvus brachyrhynchos*, that possess a simple rhamphotheca. Although some adaptive explanations have been suggested for compound rhamphothecae (such as providing a channel for excretions from the nasal salt gland in marine birds; Schmidt-Nielsen and Fänge 1958), the proposed explanations are most often invoked for specific clades (e.g., procellariiform birds), and do not extend to all cases of compound rhamphothecae (e.g., palaeognathous birds).

Birds that have been classically considered to bear compound rhamphothecae (Gadow and Selenka 1891) are scattered throughout most published avian phylogenies. This distribution has led to conflicting views on the nature of compound rhamphothecae and whether the disparate examples are indeed homologous (Lönnberg 1904) or only bear superficially similar convergent structures (Parkes and Clark 1966). Understanding the evolutionary and morphological relationships between compound and simple

rhamphothecae provides insight into the morphology and 'evolvability' of bird beaks, and may ultimately shed light on the early evolution of rhamphothecae from other skin structures in derived coelurosaurian dinosaurs.

Avian compound rhamphothecae have long been used as taxonomic characters. The most prominent system of nomenclature for elements of compound rhamphothecae was first proposed in the context of procellariiform seabird taxonomy (Coues 1866). Coues' (1866) nomenclature will be used throughout this paper with minor changes and additions (Fig. 4-1).

The initial proposal of homology between separate plates in compound rhamphothecae was advanced as part of a hypothesis that rhamphothecal plates were homologous with the facial scales of other reptiles, most notably lizards and snakes (Lönnberg 1904). Although this work provided an extensive review of rhamphothecal morphology, it did not present the observed similarities in phylogenetic context. This omission is understandable, given that the evolutionary relationships of higher-order bird clades were more poorly resolved at the time than they are at present. In addition, Lönnberg's (1904) work only employed data from external rhamphothecal morphology. As such, this hypothesis of similarity between rhamphothecal plates (Fig. 4-2) provides a useful starting point for testing morphological similarity, but not a rigorous test of homology.

A later monograph on avian beak morphology (Boetticher 1928) describes a more thorough test of Lönnberg's (1904) hypothesis, with the inclusion of ontogenetic data and a more explicit phylogenetic context. Boetticher's (1928) work rejected many of the

similarities discussed in Lönnberg (1904) and proposed a more limited hypothesis (Fig. 4-3). Boetticher's (1928) test is still limited by current standards of homology testing, due to a poorly resolved phylogenetic hypothesis and an emphasis on similar development (as opposed to synapomorphy) as the arbiter of homology.

Here we independently test Lönnberg's (1904) and Boetticher's (1928) hypotheses of homology, supplemented with the inclusion of data that have bearing on the topology of structures associated with the rhamphotheca, namely branches of the trigeminal nerve and bony elements of the upper and lower jaws. We employ current phylogenetic hypotheses to reconstruct the ancestral character state of the avian beak at the common ancestor of extant birds (Neornithes), and frame these results within the context of currently accepted tests of homology and the biological basis of homology.

Materials and Methods

Morphological survey

We examined external rhamphothecal morphology in a broad sample of study skins and fixed alcoholic specimens (see Appendix C for list of taxa). This broad survey was complemented by more extensive study on a smaller sample of taxa. Fourteen species were examined by micro-computed tomography (μCT) using a GE eXplore Locus Small Animal μCT Scanner. The resulting volume data (in VFF format) were exported from MicroView 2.1.2 (microview.sourceforge.net) in DICOM format and imported into Amira 3.1.1 and 4.1.1 (Mercury-TGS, Chelmsford, MA) for visualization. Of the fourteen scanned specimens, eight were prepared with radiopaque arterial or venous injections (Microfil® MV series fill compounds, Flow Tech Inc., Carver, MA) to

examine patterns of vascularity in the rostrum. Five of the injected specimens were dissected to directly examine the soft tissues of the dermis beneath the rhamphotheca.

Samples from the five dissected specimens were fixed in neutral phosphate-buffered formalin, dehydrated in a series of ethanol baths, then infiltrated and embedded with polymethylmethacrylate (PMMA) resin using a protocol modified from Sterchi and Eurell (1989). Embedded samples were rough-cut on a high-speed tile saw (D24000®, DeWalt, Baltimore, MD) then serially sectioned using a variable speed diamond wafering saw (Isomet 1000®, Buehler, Lake Bluff, IL) at 800 μm intervals. The resulting sections were mounted on cast acrylic slides with cyanoacrylate glue, then ground and polished to a thickness of approximately 100 μm on a lapidary wheel (Metaserv 2000®, Buehler, Lake Bluff, IL) as semithin sections for histological analysis.

Study skins can sometimes offer a deceptive picture of the rhamphotheca and surrounding skin, as softer skin tends to shrink more as it dries. Study skins may thus show grooves and folds in the rhamphotheca that are not present in living animals. Where possible, study skins were compared to alcoholic specimens, frozen specimens, and/or images of live birds from the Berkeley Natural History Museums' image database (http://calphotos.berkeley.edu).

It is difficult to distinguish the fusion of two rhamphothecal plates from the loss of one rhamphothecal plate in a phylogenetic comparative analysis using morphological data alone. In addition, the morphological differences in this anatomical system between taxa generally involve differences in the depth or extent of the grooves that separate rhamphothecal plates, not necessarily differences in the shapes of the plates themselves.

Thus, it is more useful to consider and describe the structure of the grooves and folds on the rhamphotheca than the areas of homogeneous skin that make up a 'rhamphothecal plate.' We propose a nomenclature for the grooves in compound rhamphothecae and describe these structures in detail below.

The survey of rhamphothecal morphology was complemented by a survey of osteological specimens to establish the bony morphology present beneath rhamphothecae in the study taxa (specimens listed in Appendix C). In those cases in which osteological specimens of the species examined for soft-tissue morphology were not available, skeletons of congeneric specimens were examined as approximations.

Ancestral character state reconstruction

Morphological features for separate regions of the rostrum were coded as multistate characters, using the following character states: (0) single rhamphothecal plate; (1) rhamphothecal plate continuous into adjacent region; (2) cere or apteria; (3) feathered skin (pteryla). This four-state coding scheme was recoded as a binary character set, with state '(0) single rhamphothecal plate' remaining unaltered and states 1–3 combined into a single character state. This recombination separates compound rhamphothecae (as state [0]) from simple rhamphothecae or other skin (as state [1]). Binary recoding is less descriptive, but offers the advantage of reducing the amount of parameter estimation required by some comparative methods.

In addition to the sample of extant taxa, data from fossils representing two close outgroup taxa to living birds (*Ichthyornis* and two genera from the clade Odontoholcae, *Hesperornis* and *Parahesperornis*) were included to polarize rhamphothecal characters

within Neornithes (Martin 1984, 1987; Lamb 1997; Clarke 2004). The correlates between bony morphology and rhamphothecal morphology found in this study were sufficiently robust to allow us to estimate the morphology of the rhamphotheca and other areas of cephalic skin for these fossil birds.

The phylogenetic hypotheses of Cracraft et al. (2004), Livezey and Zusi (2006, 2007), and Hackett et al. (2008) were used for the higher-order topology of Neornithes. Relationships between taxa within terminal clades for these two hypotheses were resolved according to several smaller-scale phylogenetic hypotheses: Cracidae after Pereira et al. (2002) and Pereira and Baker (2004), Anseriformes after Livezey (1996, 1997) and Donne-Goussé et al. (2002), Procellariiformes after Kennedy and Page (2002), Alcidae after Thomas et al. (2004), and Bucerotidae after Kemp (1988). Forty-six of the taxa surveyed above were included in this part of the analysis. Ancestral character states were reconstructed using both a maximum parsimony (MP) algorithm (Maddison et al. 1984) and a maximum likelihood (ML) algorithm (Schluter et al. 1997) in Mesquite 2.5 (Maddison and Maddison 2007). MP ancestral character state reconstruction used the original multistate character set. ML ancestral character state reconstruction used the binary recoded character set to reduce the amount of parameter estimation required in analysis and prevent overfitting. Symmetrical (Mk1) estimated rates of character state change were used for all characters in the ML analysis except for the infralabial groove, which showed significantly greater likelihoods using an asymmetrical two-parameter estimate for rate of character state change.

Branch lengths for the tree topologies used in ML ancestral character state reconstruction were estimated by setting internodes to an age greater than or equal to the age of the oldest known ingroup fossil in millions of years (Benton and Donoghue 2007). Successively older internodes without confidently assigned ingroup fossil taxa for calibration were placed at least 5 ma below calibrated internodes to avoid 'forcing' the uncalibrated nodes into the ancestral state of their closest calibrated daughter node. The problem of 'forcing' is especially relevant with the inclusion of the fossil taxa *Ichthyornis* and *Hesperornis* as outgroups to polarize character states within Neornithes. In addition to the calibrated trees, ML ancestral character state reconstructions were also run on the same topologies with all branch lengths set to one to model punctuational change, and again with branch lengths estimated using the method of Pagel (1992).

Testing homology

Assessment of homology in this study follows Patterson (1982), using the criteria of (1) strong similarity, (2) non-conjunction, and (3) congruence (or synapomorphy) to test the superficial similarities observed by Lönnberg (1904) and Boetticher (1928). The tests of similarity and conjunction directly employ data from the morphological survey. The test of congruence employs the ancestral character state reconstructions of rhamphothecal morphology discussed above. In addition to Patterson's (1982) criteria, the morphological similarities found in this study will be discussed in the context of the biological basis of similarity and homology after Roth (1991) and Hall (2003).

Results

Rhamphothecae show similar topologies among groups

The superficial similarities in rhamphothecal morphology within Neornithes that Lönnberg (1904) and Boetticher (1928) first pointed out are largely borne out by comparative osteological and neurological data. Most of the named components of compound rhamphothecae illustrated above show consistent relationships to specific structures in the rostrum, and these similarities will be described in detail below. Most individual rhamphothecal components thus pass the similarity test of homology proposed by Patterson (1982).

Nearly all examples of avian compound rhamphothecae show a complete groove that extends from the naris (nostril) to the oral margin, here termed the *nasolabial groove* (Fig. 4-4C, D). In taxa with well-defined rhamphothecal plates, such as procellariiform birds, the nasolabial groove separates the latericorn from the culminicorn and the premaxillary nail. Exceptions include some of the anatoid waterfowl (e.g., *Anas clypeata*) which show a premaxillary nail but lack a well-defined nasolabial groove to separate the remaining upper bill into latericorn and culminicorn (Fig. 4-4A). A persistent partial nasolabial groove can sometimes be seen in taxa that are classically considered to bear simple rhamphotheca (e.g., *Butorides striata*, Fig. 4-4E). The nasolabial groove may also extend caudally from the naris to the caudal margin of the rhamphotheca (e.g., *Phoebastria immutabilis*, Fig. 4-4C). *Apteryx* presents an extreme example of this tendency in that nearly all of the nasolabial groove lies caudal to the nostril.

The position of the nasolabial groove at the oral margin is closely approximated by the rostralmost extent of the maxillopremaxillary suture. Taxa with pronounced nasolabial grooves (e.g., *Phoebastria*) often show a bony groove that corresponds to this skin feature (Fig. 4-5C). Bony correlates for the nasolabial groove are clearly visible in the fossil hesperornithiform birds *Hesperornis* and *Parahesperornis* (Martin 1984).

The maxillary process (subnarial bar) of the premaxilla extends caudally beneath the nasolabial groove, usually as far as the caudal extent of the rhamphotheca (Fig. 4-5). Sutures between the subnarial bar and the maxilla are often obscured by bony fusion, but in all birds other than Galliformes, the ventral border of the subnarial bar invariably defines a series of foramina for the lateral branches of the nasopalatine nerve (Fig. 4-5). Galliform beaks are unusual in that the subnarial bar makes up the entire bony support for the edge or tomia of the maxillary rhamphotheca, obscuring the maxilla. Despite the occlusion of the rostral portion of the maxilla from the external surface of the upper jaw, the rostralmost extent of the maxilla corresponds to the position of the nasolabial groove fairly well. Some parts of the dorsal ramus of the medial ophthalmic nerve cross caudally beneath the nasolabial groove to innervate the rostral part of the latericorn (Fig. 4-5), thus the nasolabial groove does not directly correspond to a border between the dermatomes of the medial ophthalmic (CN V_1) and nasopalatine (CN V_2) nerves.

Many taxa, both those with compound rhamphothecae such as procellariiform seabirds and those that have classically been considered to have simple rhamphothecae such as falconiform birds, show a groove that separates the premaxillary nail from the culminicorn, here termed the *culminolabial groove* (Fig. 4-4A, C, D). The culminolabial

groove is often incomplete, in some cases fading out as it approaches the oral margin (e.g., *Fratercula*) and in others forming a shallow, indistinct depression (e.g., *Sula*). The most distinct examples of culminolabial grooves are found in anatoid waterfowl (e.g., *Anas clypeata*; Fig. 4-4A), where the premaxillary nail is pronounced and heavily keratinized compared to the surrounding rhamphotheca.

In nearly all taxa with a compound mandibular rhamphotheca, a complete groove separates the mandibular nail from the ramicorn, here termed the *mentolabial groove*. The position of this groove is variable, but most often approximately matches the position of the nasolabial groove on the oral margin. In palaeognaths, the mentolabial groove is oriented rostrodorsal to caudoventral. In neognaths, the most common orientation of the mentolabial groove is dorsolateral to ventromedial. In both cases, the ventralmost portion of the mentolabial groove sits near the ventral border of the mandibular symphysis. Ibis (e.g., *Plegadis chihi*) are an exception to this pattern, showing a median groove and no well-defined mandibular nail.

An incomplete groove is present on the mandibular nail of Procellariiformes and members of Fregatidae, Phalacrocoracidae, Anhingidae, and Sulidae. The last four Family-level taxa form an unnamed monophyletic clade in the analyses of Cracraft et al. (2004) and Hackett et al. (2008); Livezey and Zusi (2007) place these taxa together with Pelecanidae in Suborder Steganopodes (Chandler 1916). For convenience, the four Family-level taxa that possess an incomplete groove on the mandibular nail will hereafter be referred to as “steganopode pelecaniforms,” as they share this and a number of other rhamphothecal features in common to the exclusion of pelecanids. Where present, the

incomplete groove continues along the line of the median caudal projection of the mandibular nail that Boetticher (1928) termed the pseudomentale, thus this incomplete groove is here termed the *pseudomental fold*.

In *Casuarius,* Anatoidea, and some Procellariiformes, a second complete groove on the mandible mirrors the course of the nasolabial groove, extending from the mandibular malar pteryla to the mentolabial groove, here termed the *infralabial groove*. This groove separates the ramicorn into dorsal and ventral parts. In many taxa, the infralabial groove is absent, but a rostral projection of the mandibular malar pteryla makes a notch in the single ramicorn at a similar position. The position of the infralabial groove in *Casuarius* follows the course of the external mandibular vein, but the independently derived infralabial grooves in procellariiform seabirds and anatoid waterfowl accompany foramina for the intramandibular nerve.

Steganopode pelecaniforms show a novel groove that corresponds to the line of action of the prokinetic hinge in the jugal bar, delineating a separate beak plate termed the jugal operculum (MacDonald 1960). In all of the taxa examined, jugal opercula were accompanied by an accessory ossification, the suprajugal ossiculum (Jollie 1957), that attaches by a short ligament to the jugal as the latter overlaps the jugal process of the maxilla. Many of the osteological specimens examined in this study retained the ligament, holding the suprajugal ossiculum in place in the prepared specimen. Although the suprajugal ossiculum is in close proximity to the caudal extent of the subnarial bar of the premaxilla, there does not appear to be a ligament connecting the two structures, thus the suprajugal ossiculum does not appear to be a separate center of ossification within the

maxillary process of the premaxilla. This finding suggests that the close topological relationship between the caudal extent of the maxillary process of the premaxilla and the caudal end of the rhamphotheca seen in most avian taxa does not occur in steganopode pelecaniforms. It is unclear whether the jugal operculum formed as a sequential addition of a novel, discrete plate of cornified skin caudal to the latericorn or if the existing latericorn extended onto the jugal bar and subsequently divided to accommodate kinesis about the jugal hinge. The relative likelihood of these scenarios cannot be established without a better understanding of the mechanisms that define the caudal boundary of the upper rhamphotheca during development.

Parts of the compound rhamphotheca are primitive for Neornithes

The basal ornithurine birds *Hesperornis*, *Parahesperornis*, and *Ichythyornis* show clear osteological correlates for both nasolabial and mentolabial grooves. The presence of these features in basal Ornithurae and Palaeognathae leads to an unambiguous MP ancestral character state reconstruction of these components of the compound rhamphotheca as primitive for Neornithes (Figs. 4-6 and 4-7). ML ancestral character state reconstructions are somewhat more varied, unambiguously supporting the mentolabial groove as the primitive state for Neornithes and Neognathae, but only showing marginal ML support ($p < 0.2$) for the nasolabial groove as the primitive state for Neornithes (Table 4-1). Thus compound rhamphothecae in a broad sense in basal ornithurine birds (Odontoholcae, *Ichthyornis*, and Palaeognathae) easily pass Patterson's (1982) congruence test of homology, and congruence of these structures into Neognathae and the base of Galloanserae is likely as well (Figs. 4-6 and 4-7).

Table 4-1. Likelihood ratios (expressed as present:absent) and parsimony ancestral character state reconstructions for presence/absence of rhamphothecal grooves at clades shown in Figures 4-6 and 4-7. Superscripts indicate the phylogenetic hypothesis used in reconstruction (H: Hackett et al. 2008; L: Livezey and Zusi 2007; C: Cracraft et al. 2004). *Hesperornis* and *Ichthyornis* emerge as sister taxa in the phylogenetic hypothesis of Livezey and Zusi (2007), resulting in the absence of the clade Carinatae and reduced support for the congruence of nasolabial and culminolabial grooves in Neornithes and neognathous birds. Phylogenetic anlyses that include other basal ornithurine birds, albeit with less extensive data matrices (e.g., Chiappe 2002, You et al. 2006), generally place *Ichthyornis* as closer to neornithine birds than *Hesperornis* in a monophyletic Carinatae. Asterisks indicate significance of ML ancestral character state reconstruction at $p \leq 0.05$. A: absent by MP ancestral character state reconstruction; P: present by MP ancestral character state reconstruction; –: equivocal.

Clade name	Nasolabial groove	Culminolabial groove	Mentolabial groove	Infralabial groove
Ornithurae^{H}	5.81 / P	2.90 / P	53.0* / P	– / A
Ornithurae^{C}	4.93 / P	2.53 / P	36.1* / P	– / A
Ornithurae^{L}	2.93 / P	2.12 / P	26.5* / P	– / A
Carinatae^{H}	8.92* / P	5.41 / P	431* / P	– / A
Carinatae^{C}	7.88* / P	4.87 / P	121* / P	– / A
Neornithes^{H}	4.78 / P	3.34 / P	176* / P	0.24 / A
Neornithes^{C}	4.54 / P	3.08 / P	49.0* / P	0.25 / A
Neornithes^{L}	1.20 / P	1.07 / P	19.1* / P	0.25 / A
Palaeognathae^{H}	50.7* / P	15.3* / P	1010* / P	0.34 / A
Palaeognathae^{C}	41.6* / P	13.2* / P	630* / P	0.44 / A
Palaeognathae^{L}	3.81 / P	2.08 / P	61.9* / P	0.27 / A
Neognathae^{H}	2.58 / A	2.23 / A	57.9* / P	0.25 / A
Neognathae^{C}	2.49 / A	2.12 / A	17.2* / P	0.25 / A

Neognathae^{L}	0.88 / A	0.91 / A	12.8* / P	0.25 / A
Galloanserae^{H}	1.65 / A	1.76 / A	135* / P	0.28 / A
Galloanserae^{C}	1.64 / A	1.67 / A	39.2* / P	0.28 / A
Galloanserae^{L}	0.72 / A	0.95 / A	12.8* / P	0.30 / A
Neoaves^{H}	1.92 / A	1.57 / A	4.01 / –	0.23 / A
Neoaves^{C}	1.84 / A	1.54 / A	1.00 / A	0.23 / A
Neoaves^{L}	0.81 / A	0.83 / A	2.73 / A	0.24 / A

Likelihood ratios for the presence of mentolabial, culminolabial, and/or nasolabial grooves from ML ancestral character state reconstruction are skewed in favor of the presence of these structures in basal neoavians, but fall short of statistical significance. This ambiguity prevents a straightforward assessment of congruence for the compound rhamphothecae observed in Pelecaniformes, Procellariiformes, and Sphenisciformes. The most likely interpretation is that these examples of compound rhamphothecae are congruent with the primitive state observed in palaeognaths, but the alternative hypothesis that they are convergent structures cannot be entirely discounted with the available data. Compound rhamphothecae in basal neoavians thus conditionally pass the congruence test of Patterson (1982), but their marked similarity to compound rhamphotheca in palaeognaths may also be due to an underlying homology or similarity in development (Hall 2003).

The examples of prominent mentolabial, culminolabial, and nasolabial grooves seen in more derived neoavians such as Great Skuas (*Stercorarius skua*) and several

alcids (*Fratercula* spp., *Cerorhinca monocerata*) are more likely to be instances of convergence than the retention of primitive compound rhamphothecae. Although these examples are not congruent, they still pass the similarity and non-conjunctions tests of Patterson (1982), which suggests that they may be the result of similar processes in development.

The remaining examples of rhamphothecal grooves within Coraciiformes and Piciformes are also not congruent, but in some cases they retain strong similarity to grooves in the primitive compound rhamphothecae of Neornithes. Many Piciformes (e.g., *Colaptes auratus*) bear a shallow nasolabial groove (Fig. 4-4G). This feature may be related to nasolabial grooves in other avian taxa in the same manner as the rhamphothecal grooves in alcids: not homologous, but possibly derived from similar development. Other examples of rhamphothecal grooves in Coraciiformes and Piciformes, such as the grooves between lateral and rostral parts of the maxillary rhamphotheca in *Bucorvus* spp. and *Andigena laminirostris*, only show superficial similarity with the nasolabial grooves of basal Neornithes.

Some 'compound' elements are independently derived within Neornithes

The congruent state for rhamphotheca in basal neornithines involves some, but not all, of the separate plates seen in extant birds. The basal neornithine state shows a shallow culminolabial groove between premaxillary nail and culminicorn. Both of these plates are separated from the latericorns by a prominent nasolabial groove. Skin surrounding the nostril is less cornified than the adjacent beak plates, and thus a naricorn, as seen in Procellariiformes, is absent. The mandibular rhamphotheca is divided by a

mentolabial groove into a mandibular nail and a single ramicorn on each side, but an infralabial groove is absent.

Whereas the culminolabial, nasolabial, and mentolabial grooves are primitive for Neornithes, a number of other elements of compound rhamphothecae appear to be independently derived in various Neornithine clades. The separate, heavily cornified naricorns that have led to the name 'tubenoses' for procellariiform seabirds are an apomorphy of the (Gaviiformes + (Pelecaniformes + Ciconiiformes) + (Sphenisciformes + Procellariiformes)) clade of Hackett et al. (2008; Fig. 4-6), and are derived from an area of relatively soft, cereous skin that surrounds the nostril in palaeognaths and galloanserine birds. A separate naricorn is absent in most of the derived 'ground birds' and charadriiforms, although the margin of the nostril is generally cornified in these taxa, in contrast to the softer cereous skin seen in palaeognaths and galloanserines.

An infralabial groove is derived independently in Anatoidea, some Procellariiformes, and *Casuarius* spp. This feature is similar in topology to the infralabial notch present in palaeognaths and some galloanserine birds, but does not appear to be primitive for Neornithes. In anatoids and procellariiforms, the infralabial groove accompanies a series of foramina from the mandibular canal. The anatomical and microanatomical relationships of the nerves and vessels that pass though these foramina are not well understood, but it is possible that the infralabial groove presents a thin-walled area of rhamphotheca allowing for more sensitive mechanoreception along the lateral surface of the mandible.

A pseudomental fold occurs independently in Procellariiformes and steganopode pelecaniforms, but is absent in their commonly recognized outgroups Ciconiiformes, Sphenisciformes, and Gaviiformes. The pseudomental folds of steganopode pelecaniforms and Procellariiformes both cover a thin bony strut that projects caudally from the mandibular symphysis. The factors that contribute to the strong similarity between these convergent morphologies are unknown.

Revised hypothesis of homology for avian rhamphotheca

This study's findings of (a) strong morphological similarity between diverse examples of compound rhamphothecae, (b) congruence of similar rhamphothecal morphologies at the base of Neornithes, and (c) persistent relationships between rhamphothecal morphology and underlying bone and nerve structures, all lead to a revised hypothesis of homology between areas of rhamphotheca in Neornithes (Fig. 4-8). This hypothesis covers rhamphothecal plates found to be primitive for Neornithes, but not plates that are autapomorphic for individual neornithine clades (e.g., the dorsal and ventral ramicorns of Giant Petrels *Macronectes giganteus*). Transition to a simple rhamphotheca occurs with the loss of rhamphothecal grooves, but similarity in the topological relationships of areas of rhamphotheca are retained (Fig. 4-8B). The remaining caudal portions of simple upper rhamphothecae show a topological relationship to the underlying maxillary process of the premaxilla and branches of the nasopalatine nerve that is nearly identical to that seen in compound upper rhamphothecae. These persistent topological relationships would not be expected if

simple rhamphotheca arose instead by the loss of the caudal plates of compound rhamphothecae.

Discussion

Evolution of rhamphothecal morphology within Neornithes

A scenario for the evolutionary history of compound rhamphothecae in neornithine clades can be briefly summarized as a series of trends.

Palaeognaths largely retain the primitive arrangement of plates and grooves in their compound rhamphothecae, but in comparison to *Ichthyornis*, *Parahesperornis*, and *Hesperornis*, the size of the premaxillary and mandibular nails relative to the rest of the rostrum has been reduced. Reduction of the premaxillary and mandibular nails results in a predominantly rostrocaudal orientation of the nasolabial and mentolabial grooves.

Galloanserine birds show a general reduction of the nasolabial groove, with some atavistic exceptions (*Crax rubra*). Whereas the culminolabial groove remains shallow or is lost in most galliform birds, it is exaggerated in many anatoids, such that the division between the premaxillary nail and the rest of the upper rhamphotheca is the most pronounced anatomical feature of the skin of the upper beak. Despite this trend at the base of Anatidae, the culminolabial groove is secondarily reduced in some anseriform taxa (e.g., *Somateria*). The mentolabial groove is reduced in galliform birds and is marked only by the transition from relatively soft skin covering the mandibular rami to cornified skin across the mandibular symphysis. The anatoid mentolabial groove is retained and in some cases exaggerated, resulting in a distinct mandibular nail that matches the premaxillary nail.

Basal neoavians show a trend of increasing cornification of the culminicorn and naricorns. Some basal neoavian clades (e.g., Columbiformes in the topology of Hackett et al. 2008) retain a soft, cereous skin in these areas, and it is unclear if this morphology constitutes a reversal from a cornified state or if cornification of the culminicorn and naricorns occurred several times.

Several basal and derived neoavian clades also show a trend towards a simple conical or crescentic bony rostrum, in contrast to the more complex shapes seen in ratites and procellariiform birds. This contrast can be seen most clearly in comparing closely related taxa such as cormorants (*Phalacrocorax* spp.) and darters (*Anhinga* spp.). Cormorants retain a saddle-shaped culminicorn and a separate, sickle-shaped premaxillary nail on a boxy bony rostrum, while retaining pronounced nasolabial and culminolabial grooves. Darters, on the other hand, show a fused culminicorn and premaxillary nail on a conical bony rostrum, with the nasolabial groove retained only as a shallow fold.

Groove function in compound rhamphothecae

Plates of compound rhamphothecae exhibit different directions of apparent growth. Most plates that make up part of the maxillary and mandibular tomia show a tendency to translate across the surface of the bony rostrum and dermis towards the tomia, rather than growing normal to the surface of the dermis (Fig. 4-9). The cornified epidermis of the rhamphotheca is very stiff (Bonser and Witter 1993), and will only accommodate relatively small strains and deformation during growth (Lüdicke 1933). Although individual plates show clear boundaries of cornification, with softer grooves

intervening, the germinative layer of epidermal cells that underlies these structures is continuous across the entire rostrum. With the assumption that rhamphothecae are similar in growth to sauropsid scales, including avian scutate scales, the cells that feed into both rhamphothecal plates and soft grooves are all tightly linked by desmosomes (Landmann 1986; Sawyer et al. 1986). Lightly cornified grooves between plates may allow the softer skin in the groove to deform as a single generation of desmosomally linked epithelial cells begins to grow in different directions. As the less cornified epidermis of the groove breaks down and wears away, the desmosomes that initially linked separate plates are lost, allowing the heavily cornified plates to continue in their direction of growth as independent units (Fig. 4-9). The trend towards simple rhamphotheca seen in many neoavian clades is interpreted here as a result of the loss of the grooves that define compound rhamphothecae, not the loss of separate rhamphothecal plates. Loss of the softer grooves in a compound rhamphotheca to form a simple rhamphotheca may be dependent upon whether the bony rostrum forms a consistent cross-sectional shape that allows the entire rhamphotheca to translate across its surface as a single unit during growth (Lüdicke 1933).

Potential underlying similarity in compound rhamphotheca

The frequent reversal to compound rhamphothecae among derived neoavians suggests an underlying similarity in beak development. Some elements of this idea have previously been suggested by Olson (1985), who pointed to histological descriptions of ‘labial grooves’ (corresponding to the nasolabial and mentolabial grooves) in developing chickens (Kingsbury et al. 1953).

The hypothesis that the 'labial grooves' of developing chickens are transitory homologs to rhamphothecal grooves in palaeognaths is in accord with other sources of data on rhamphothecal development. Nasolabial and mentolabial grooves develop in *Gallus* and other birds in the early stages of rhamphothecal keratinization (embryonic day [ED] 10, Hamburger and Hamilton stage [HH] 36; Hamburger and Hamilton 1951; Bartels and Flachsbarth 1994) and are lost in *Gallus* by ED 17 (HH 43), whereas they remain prominent in *Larus* and *Columba* (Bartels and Flachsbarth 1994). There is also some correspondence between parts of the compound rhamphotheca and the initial development of centers of ossification in the rostrum. The nasolabial groove corresponds to the initial position of the maxillopremaxillary suture before the subnarial bar of the premaxilla develops (Jollie 1957; Bartels and Flachsbarth 1994). Similarly, the mentolabial groove corresponds to the separation between the mentomeckelian (mentomandibular, predentary) ossification and the more caudal ossification of the dentaries (Jollie 1957) before these centers fuse in later development. It is unclear whether a causal relationship exists between centers of ossification in the rostrum and areas of cornified skin in compound rhamphotheca, but the similar topology of these structures raises the possibility that both are related as an 'underlying homology' (Hall 2003) that may explain the homoplastic occurrence of rhamphothecal grooves in Charadriiformes, Coraciiformes, and Piciformes.

'Egg teeth' and rhamphothecal evolution

Avian 'egg teeth' bear no relationship to typical amniote teeth, and are instead transitory thickened and calcified areas of skin that develop on the tip of the rostrum

during the early stages of skin keratinization. Other terms for these structures (Eischwielen, caruncles) reflect their epidermal origin and distinguish them from the dentinous egg teeth (Eizähne) found in squamates (Röse 1892). Caruncles are a synapomorphy of amniotes, present in monotremes (Hughes and Hall 1998), turtles (Miller 1985), and crocodylians (Ferguson 1985) in addition to birds, and absent only in therian mammals and squamates. Based on the phylogenetic distribution of beaked forms in the fossil record and the congruence of that pattern with the presence or absence of a caruncle, Lee (1997) suggested that the multiple independent origins of rhamphothecae (in birds, turtles, and at least thirteen extinct amniote lineages) are all derived from elaborations of caruncles. The form of this hypothesis as a whole is slightly problematic, because the supporting data from the fossil record are based on an absence of evidence (albeit a very thorough and consistent absence of evidence), but the possible role of caruncles in rhamphothecal evolution in the lineage leading to neornithine birds can be evaluated using additional evidence.

Caruncles in *Gallus* begin to cornify somewhat earlier than the subjacent rhamphotheca (Kingsbury et al. 1953; Tonégawa 1973). The caruncle forms the initial center of rhamphothecal keratinization, which then spreads gradually across the surface of the rostrum (Kingsbury et al 1953). Several avian taxa have been reported to bear caruncles on both the premaxillary nail and the mandibular nail (Clark 1961) in a phylogenetic distribution that ranges from Galloanserae (*Gallus*), through the Metaves of Hackett et al. (2008; several Columbidae), basal Coronaves (*Gavia*, *Gallinula*), Charadriiformes (*Burhinus*, *Haemotopus*, *Chlidonias*), Falconiformes (*Milvus*),

Piciformes and Coraciiformes (*Buceros*, *Colaptes*), to Passeriformes (*Turdus*, *Agelaius*). The broad distribution of this trait suggests that the presence of a caruncle on both the premaxillary nail and the mandibular nail may be plesiomorphic for Neornithes. These data are not enough by themselves to fully test whether avian rhamphotheca are an exaptation or iterative homolog (Roth 1991) of the caruncle, but the origin of avian rhamphotheca as a derivative of the upper and lower caruncles currently stands as the best available hypothesis for rhamphothecal evolution in neornithine birds.

The topology of rhamphothecal grooves is strongly similar across most of Neornithes, even in cases where compound rhamphothecae are clearly homoplastic. Strong similarity in homoplastic examples of rhamphothecal groove morphology, together with the similarity in topology between rhamphothecal plates and centers of ossification in the rostrum, suggests that non-homologous examples of compound rhamphothecae (e.g., Double-crested Cormorant *Phalacrocorax auritus* vs. Rhinoceros Auklet *Cerorhinca monocerata*) may still be linked by 'underlying homology' or homologous developmental similarity.

Compound rhamphothecae as defined by the nasolabial, culminolabial, and mentolabial grooves are a primitive trait for neornithine birds, and are a synapomorphy of the more inclusive clade (Odontoholomorphae + Neornithes, in the sense of Livezey and Zusi 2007). In basal members of this clade such as *Hesperornis*, *Parahesperornis*, and *Ichthyornis*, the premaxillary and mandibular nails were the most heavily cornified parts of the rhamphotheca. Based on evidence from rhamphothecal development, the premaxillary and mandibular nails may be iterative homologs or exaptations of the

caruncle or ‘egg-tooth.’ The presence of teeth in the maxillae and dentaries of *Ichthyornis*, *Parahesperornis*, and *Hesperornis* suggests that tomia may not have been present on the latericorn and ramicorn in these taxa, and that complete tomia on the dorsal and ventral oral margins are a synapomorphy of Neornithes.

Extensive cornification of the naricorn and culminicorn appears to be a recurring trend within Neoaves. The pronounced compound rhamphotheca present in basal neoavians such as Procellariiformes and Pelecaniformes most likely reflect the evolution of heavy cornification across the entire rhamphotheca before the evolution of a morphologically simple bony rostrum, perhaps coupled with a function for the nasolabial groove as a gutter for draining the nasal salt glands. A simple conical or crescentic bony rostrum occurs several times within Neornithes, and this morphology appears to be a prerequisite for the loss of rhamphothecal grooves and the transition to simple rhamphotheca.

The evolution of rhamphothecae in ornithurine birds represents only one of at least seven independent occurrences of rhamphothecae in coelurosaurian dinosaurs, all clustered within a 35 million year span from the Late Jurassic through the Early Cretaceous (Fig. 4-10). This is a striking example of mosaic evolution. Outside of this closely related group of coelurosaurian dinosaurs, there is fossil evidence for only eight other independent occurrences of rhamphothecae in amniotes, and only one of those lineages (turtles) is still extant. Establishing the evolutionary history of rhamphothecae in neornithine birds provides a morphological context for addressing the mosaic evolution of similar structures within Coelurosauria. Comparisons of the morphology and

development of avian rhamphothecae with the bony morphology of the rostrum in coelurosaurian dinosaurs may provide a window into the early evolution of one of the most characteristic features of modern birds.

Literature Cited

Bartels T, Flachsbarth MF. 1994. Rasterelektronenmikroskopische Untersuchungen zur Entwicklung des vogelschnabels. Zoologischer Anzeiger 232:97–110.

Benton MJ, Donoghue PCJ. 2007. Paleontological evidence to date the tree of life. Molecular Biology and Evolution 24:26–53.

Boetticher Hv. 1928. Beitrag zur Kenntnis der Morphologie und Phylogenie des hornigen Vogelschnabelüberzuges mit besonderer Berücksichtigung seiner Beziehungen zu den Schnauzenschildern der saurier. Jena: G. Fischer.

Bonser RHC, Witter MS. 1993. Indentation hardness of the bill keratin of the European Starling. The Condor 95:736–738.

Chiappe LM. 2002. Basal bird phylogeny: Problems and solutions. In: Chiappe LM, Witmer LM, editors. Mesozoic Birds: Above the Heads of Dinosaurs. Berkeley: University of California Press. p 448–472.

Clark GA. 1961. Occurrence and timing of egg teeth in birds. Wilson Bulletin 73:268–278.

Clarke JA. 2004. Morphology, phylogenetic taxonomy, and systematics of *Ichthyornis* and *Apatornis* (Avialae: Ornithurae). Bulletin of the American Museum of Natural History 286:1–179.

Cope ED. 1900. The crocodilians, lizards, and snakes of North America. Annual Report of the United States National Museum for 1898:153–1270.

Coues E. 1866. Critical review of the family Procellariidae: Part V; embracing the Diomedeinae and the Halodrominae. With a general supplement. Proceedings of the Academy of Natural Sciences of Philadelphia 18:172–197.

Cracraft J, Barker FK, Braun M, Harshman J, Dyke GJ, Feinstein J, Stanley S, Cibois A, Schikler P, Beresford P, Garcia-Moreno J, Sorenson MD, Yuri T, Mindell DP. 2004. Phylogenetic relationships among modern birds (Neornithes): Toward an avian tree of life. In: Cracraft J, Donoghue MJ, editors. Assembling the Tree of Life. New York: Oxford University Press. p 468–489.

Donne-Goussé C, Laudet V, Hänni C. 2002. A molecular phylogeny of Anseriformes based on mitochondrial DNA analysis. Molecular Phylogenetics and Evolution 23:339–356.

Ferguson MWJ. 1985. Reproductive biology and embryology of the crocodilians. In: Gans C, Billett F, Maderson PFA, editors. Biology of the Reptilia, vol. 14A. New York : John Wiley & Sons. p 329–492.

Gadow H, Selenka E. 1891. Vogel. I. Anatomischer Theil. In: Bronn HG, editor. Bronn's Klassen und Ordnungen des Thier-Reichs, vol. 6. Leipzig: C. F. Winter. p 1–1008.

Hackett SJ, Kimball ET, Reddy S, Bowie RCK, Braun EL, Braun MJ, Chojnowski JL, Cox WA, Han K-L, Harshman J, Huddleston CJ, Marks BD, Miglia KJ, Moore

WS, Sheldon FH, Steadman DW, Witt CC, Yuri T. 2008. A Phylogenomic Study of Birds Reveals Their Evolutionary History. Science 320:1763–1768.

Hall BK. 2003. Descent with modification: the unity underlying homology and homoplasy as seen through an analysis of development and evolution. Biological Reviews 78:409–433.

Hamburger V, Hamilton HL. 1951. A series of normal stages in the development of the chick embryo. Journal of Morphology 88:49–92.

Holtz TR Jr. 2004. Tyrannosauroidea. In: Weishampel DB, Dodson P, Osmólska H, editors. The Dinosauria. Berkeley: University of California Press. p 111–136.

Holtz TR Jr, Molnar RE, Currie PJ. 2004. Basal Tetanurae. In: Weishampel DB, Dodson P, Osmólska H, editors. The Dinosauria. Berkeley: University of California Press. p 71–110.

Hughes RL, Hall LS. 1998. Early Development and Embryology of the Platypus. Philosophical Transactions of the Royal Society B: Biological Sciences 353:1101–1114.

Jollie MT. 1957. The head skeleton of the chicken and remarks on the anatomy of this region in other birds. Journal of Morphology 100:389–436.

Kemp AC. 1988. The systematics and zoogeography of Oriental and Australasian hornbills (Aves: Bucerotidae). Bonner Zoologische Beitrage 39:315–345.

Kennedy M, Page RDM. 2002. Seabird supertrees: combining partial estimates of procellariiform phylogeny. The Auk 119:88–108.

Kingsbury JW, Allen VG, Rotheram BG. 1953. The histological structure of the beak in the chick. The Anatomical Record 116:95–115.

Lamb JP Jr. 1997. Marsh was right: *Ichthyornis* had a beak. Journal of Vertebrate Paleontology 17:59A.

Landmann L. 1986. The skin of reptiles: Epidermis and dermis. In: Bereiter-Hahn J, Matoltsy AG, Richards KS, editors. Biology of the Integument, Volume 2: Vertebrates. Berlin: Springer-Verlag. p 150–187.

Lee MSY. 1997. The evolution of beaks in reptiles: A proposed evolutionary constraint. Evolutionary Theory and Review 11:249–254.

Livezey BC. 1996. A Phylogenetic Analysis of Geese and Swans (Anseriformes: Anserinae), Including Selected Fossil Species. Systematic Biology 45:415–450.

Livezey BC. 1997. A phylogenetic analysis of basal Anseriformes, the fossil *Presbyornis*, and the interordinal relationships of waterfowl. Zoological Journal of the Linnean Society 121:361–428.

Livezey BC, Zusi RL. 2007. Higher-order phylogeny of modern birds (Theropoda, Aves: Neornithes) based on comparative anatomy. II. Analysis and discussion. Zoological Journal of the Linnean Society. 149:1–95.

Lönnberg E. 1904. On the homologies of the different pieces of the compound rhamphotheca of birds. Arkiv för Zoologi 1:479–512.

Lüdicke M. 1933. Wachstum und Abnutzung des Vogelschnabels. Zoologische Jahrbücher, Abteilung für Anatomie und Ontongenie der Tiere 57:435–564.

MacDonald JD. 1960. Secondary external nares of the gannet. Proceedings of the Zoological Society of London 135:357–363.

Maddison WP, Donoghue MJ, Maddison DR. 1984. Outgroup Analysis and Parsimony. Systematic Zoology 33:83–103.

Maddison WP, Maddison DR. 2007. Mesquite: a modular system for evolutionary analysis. http://mesquiteproject.org.

Makovicky PJ, Kobayashi Y, Currie PJ. 2004. Ornithomimosauria. In: Weishampel DB, Dodson P, Osmólska H, editors. The Dinosauria. Berkeley: University of California Press. p 137–150.

Martin LD. 1984. A new hesperornithid and the relationships of Mesozoic birds. Transactions of the Kansas Academy of Science 87:141–150.

Martin LD. 1987. The beginning of the modern avian radiation. Documents des Labaratoires de Géologie de Lyon 99:9–19.

Miller JD. 1985. Embryology of marine turtles. In: Gans C, Billett F, Maderson PFA, editors. Biology of the Reptilia, vol. 14A. New York: John Wiley & Sons. p 269–328.

Olson SL. 1985. The fossil record of birds. In: Farner DS, King JR, Parkes KC, editors. Avian Biology, vol. 8. New York: Academic Press. p 79–252.

Osmólska H, Currie PJ, Barsbold R. 2004. Oviraptorosauria. In: Weishampel DB, Dodson P, Osmólska H, editors. The Dinosauria. Berkeley: University of California Press. p 165–183.

Parkes KC, Clark GA. 1966. An additional character linking ratites and tinamous, and an interpretation of their monophyly. The Condor 68:459–471.

Patterson C. 1982. Morphological characters and homology. In: Joysey KA, Friday AE, editors. Problems of Phylogenetic Reconstruction. London: Academic Press. p 21–74.

Pereira SL, Baker AJ. 2004. Vicariant speciation of curassows (Aves, Cracidae): a hypothesis based on mitochondrial DNA phylogeny. The Auk 121:682–694.

Pereira SL, Baker AJ, Wajntal A. 2002. Combined Nuclear and Mitochondrial DNA Sequences Resolve Generic Relationships within the Cracidae (Galliformes, Aves). Systematic Biology 51:946–958.

Röse C. 1892. Über die Zahnleiste und die Eischwiele der Sauropsiden. Anatomischer Anzeiger 7:748–758.

Roth VL. 1991. Homology and hierarchies: problems solved and unresolved. Journal of Evolutionary Biology 4:167–194.

Sawyer RH, Knapp LW,O'Guin WM. 1986. The skin of birds: Epidermis, dermis, and appendages. In: Bereiter-Hahn J, Matoltsy AG, Richards KS, editors. Biology of the Integument, Volume 2: Vertebrates. Berlin: Springer-Verlag. p 194–238.

Schluter D, Price T, Mooers AO, Ludwig D. 1997. Likelihood of Ancestor States in Adaptive Radiation. Evolution 51:1699–1711.

Sterchi DL, Eurell JA. 1989. A new method for preparation of undecalcified bone sections. Stain Technology 64:201–205.

Storer RW. 1960. Adaptive radiation in birds. In: Marshall AJ, editor. Biology and Comparative Physiology of Birds, Volume 1. New York: Academic Press. p 15–55.

Thomas GH, Wills MA, Székely T. 2004. A supertree approach to shorebird phylogeny. BMC Evolutionary Biology 4:28.

Tonégawa Y. 1973. Inductive tissue interactions in the beak of a chick embryo. Development, Growth, and Differentiation 15:57–71.

You H, Lamanna MC, Harris JD, Chiappe LM, O'Connor J, Ji S, Lu J , Yuan C, Li D, Zhang X, Lacovara KJ, Dodson P, Ji Q. 2006. A nearly modern amphibious bird from the Early Cretaceous of northwestern China. Science 312: 1640–1643.

CHAPTER 5: THE FACIAL INTEGUMENT OF *PACHYRHINOSAURUS* (CERATOPSIDAE:ORNITHISCHIA): MORPHOLOGICAL AND HISTOLOGICAL CORRELATES OF NOVEL SKIN STRUCTURES.

Abstract

The horned dinosaur *Pachyhinosaurus* possesses rugose bony bosses across the skull roof in lieu of the projecting bony horn cores seen in most ceratopsians. This bizarre elaboration of typical ceratopsian ornaments provides an opportunity to test hypotheses of ceratopsian facial skin morphology and function. We analyzed bone morphology and histology associated with several classes of skin features in extant amniotes, and isolated key osteological and histological correlates for unpreserved skin structures. We then examined dermatocranial elements from *Pachyrhinosaurus* and related centrosaurine dinosaurs for the same osteological and histological correlates. From this comparison we propose that the rugose bosses of *Pachyrhinosaurus* were most likely covered by a thick pad of cornified skin, derived from the caudodorsal side of the primitive horn sheath. A similar relationship between horn sheath and cornified pad is seen in extant muskoxen (*Ovibos*). To assess potential functions associated with our reconstruction of skin morphology for *Pachyrhinosaurus*, we tested extant taxa with similar skin morphologies for consistent adaptive relationships between structure and behavior. High-energy headbutting is consistently associated with the acquisition of thick cornified pads, seen in muskoxen as well as helmeted hornbills (*Buceros* [=*Rhinoplax*] *vigil*) and African buffalo (*Syncerus*). The association of the bizarre ornaments of *Pachyrhinosaurus* with risky agonistic behaviors casts doubt on the role of species recognition as a primary selection

pressure driving the diversity of ceratopsian horns. We suggest that social selection (a broad form of intraspecific competition) is a more appropriate explanation for the explosive diversity of ceratopsian ornaments in the Late Cretaceous.

Introduction

Ceratopsian dinosaurs are well known for the elaborate bony ornaments that adorn their skulls, which include a variety of projecting spikes and flanges, as well as a broad bony frill. The similarity between some of these ornaments and the horns of bovid artiodactyls (goats, sheep, antelope, and cattle) is so striking that one of the first specimens of *Triceratops* to be found was originally classified as a form of bison ("*Bison alticornis*;" Marsh 1887). The strong similarity between the horns of ceratopsians and bovids has led to several interpretations of ceratopsian paleobiology that employ bovids as extant analogs.

In addition to bovid-like horns, some adult centrosaurine ceratopsians show an alternate morphology, in which the horn core is partially or wholly replaced by a rugose boss of bone. For example, the nasal horn cores of adult *Pachyrhinosaurus* spp. (Sternberg 1950; Currie et al. 2008), *Achelousaurus horneri* (Sampson 1995) and Dinosaur Provincial Park pachyrhinosaur (Ryan et al., in press) are preserved as hypertrophied rugose bosses (Fig. 5-1). Whereas there are robust explanations for the evolution and growth of bovid-like horn cores in ceratopsids (Brown and Schlaikjer 1940; Sampson et al. 1997; Goodwin et al. 2006; Horner and Goodwin 2006), explanations for the formation of rugose bosses have been problematic.

This departure from typical ceratopsian horn core morphology seen in derived centrosaurines provides the opportunity to describe broader patterns of evolutionary change in ceratopsian bony ornamentation. Several functions have been proposed for ceratopsian horns, including intraspecific competition (Farlow and Dodson 1975), sexual selection (Sampson et al. 1997), and species recognition (Padian et al. 2004; Goodwin et al. 2006), and each of these functions has a different expected evolutionary pattern (Darwin 1871; West-Eberhard 1983; Padian et al. 2004). The transition between projecting horn cores in *Centrosaurus* and pronounced, rugose bosses in *Pachyrhinosaurus* allows a comparison of expected and observed evolutionary patterns within Neoceratopsia.

Morphological hypotheses for Pachyrhinosaurus *facial skin*

The two most prominent hypotheses for unpreserved skin structures in *Pachyrhinosaurus* spp. both place heavily keratinized (cornified) skin over the rugose surfaces of the skull. Sternberg's (1950) initial assessment of the pitted nasal boss of *Pachyrhinosaurus canadensis* suggested a thin covering of cornified skin (Fig 5-2C). This hypothesis has been retained by later studies (Farlow and Dodson 1975; Sampson et al. 1997), but an appropriate extant analog for this morphology has not been suggested. A second hypothesis places a large, rhinoceros-like keratinous horn on the nasal and supraorbital bosses of *Pachyrhinosaurus* (Fig. 5-2B; Currie 1989; Currie et al. 2008). This hypothesis draws on rhinoceros horn attachment as an extant analog, pointing to similarity between the pitted morphology seen in *Pachyrhinosaurus* and the nasal bosses of extant rhinoceros such as *Ceratotherium* and *Diceros* and the extinct rhinocerotid

Elasmotherium. This morphological similarity was first noted on *Pachyrhinosaurus* cf. *P. canadensis* (Langston 1967; but see also Currie et al. 2008). Aside from these explicitly stated hypotheses of integumentary morphology, a form of anatomical pachyostosis similar to that seen in muskoxen has been suggested for *Pachyrhinosaurus* skulls (Kaiser 1960; Langston 1975), but no skin structures were inferred based on this similarity.

Analogy and the function of centrosaurine cephalic ornaments

The morphological similarity of some ceratopsian ornaments to the horn cores of bovid artiodactyls has been used as a basis for inferring analogous horn-related behaviors, such as horn locking, clashing, and head-butting (Farlow and Dodson 1975; Molnar 1977; Farke 2004). Horn-locking during intraspecific aggression also occurs in species of *Chamaeleo* with pronounced facial horns, such as *Chamaeleo jacksoni* (Bustard 1958). In contrast, the large rugose bosses of *Achelousaurus* and *Pachyrhinosaurus* spp. are open to a broad range of functional interpretations. Sternberg (1950) suggested that the nasal boss of *Pachyrhinosaurus* and its associated skin were used as a battering ram. Farlow and Dodson (1975) suggested a similar function, comparing the nasal boss of *Pachyrhinosaurus* to the enlarged prefrontal and frontal scales of marine iguanas *Amblyrhynchus* which are used in shoving matches (Eibl-Eibesfeldt 1966). These interpretations favor sexual or social selection as driving factors (Darwin 1871; West-Eberhard 1983).

In contrast, Currie et al. (2008) have suggested that the nasal and supraorbital bosses of *Pachyrhinosaurus* may have functioned predominantly as visual display structures. This may be true for either of the two suggested skin reconstructions, but a

tall, rhinoceros-like horn would provide a highly conspicuous visual signal. Horn function in extant rhinoceros varies by species. For example, in black rhinoceros (*Diceros bicornis*), horn size is related to intrasexual dominance, and horns are directly used in male-male aggression (Berger and Cunningham 1998), but similar variation in horn size has no effect on dominance or fight outcome in Indian rhinoceros (*Rhinoceros unicornis*; Dinerstein 1991). Using extant rhinoceros horns as an analog for horns in *Pachyrhinosaurus* would thus not exclusively support either species recognition or sexual selection, but the possibility of tall horns as a visual display, coupled with sexual monomorphism, would favor species recognition as the driving factor in ceratopsian horn evolution (Padian et al. 2004).

Extant analogs and adaptation

Because a bovid or rhinocerotid analogy for ceratopsians horns addresses the function of horns in relation to their morphology, it implicitly addresses adaptation in both systems as well. Specifically, the choice of an extant analog for *Pachyrhinosaurus* implies that in both extant and extinct forms (a) the morphologies were shaped by natural selection, and (b) the process of selection entailed selection for the function of interest, not just selection of a given morphology (Sober 1984). The "fit" of any extant analog, and thus the assessment of function in the extinct taxon, only extends as far as the testable relationship between structure and function in the extant system.

Following Gould and Lewontin's (1979) critique of inductive studies of adaptation, tests of adaptive hypotheses have become increasingly stringent, and most currently accepted tests for adaptive explanations call for data that fossil organisms

simply cannot provide (e.g., Reznick and Travis 1996; Sinervo and Basolo 1996). But even in the absence of data on performance and heritability, the evolutionary history of potentially related morphological traits can be tested for conditions sufficient for adaptive explanations, using the phylogenetic comparative tests proposed by Gould and Vrba (1982), Greene (1986), Coddington (1988), and Baum and Larson (1991). Although these tests cannot be considered comprehensive (Grandcolas and d'Haese 2003; Kluge 2005), they are currently the only objective means to weigh and reject hypotheses of adaptation in extinct taxa.

Hypotheses tested in this study

The two most prominent hypotheses of integumentary structures described above (a flat keratinous pad and a rhinoceros-like horn) are supplemented by several other morphological hypotheses in this study (Fig. 5-3). The additional hypotheses represent combinations of different integumentary tissues. Some of these combinations are represented by structures in extant taxa that have not previously been suggested as analogs for *Pachyrhinosaurus* horns (e.g., hornbill casques), whereas other combinations are not represented by any extant taxa (e.g., thick armor-like dermis with a thin cornified sheath), but still represent plausible morphologies for a novel structure that cannot be ruled out *a priori*.

Materials and Methods

Osteological correlates of known skin structures

Because ceratopsid horn cores and bosses are novel structures and have no direct homologs in extant taxa (an extant phylogenetic bracket [EPB] level III inference per

Witmer 1995), we compared these structures to convergent structures in extant taxa to address structural and functional relationships. A diverse group of extant amniotes was sampled to test relationships between skin structures and underlying bone morphology (list of specimens available from authors upon request). Convergent examples of similar skin structures among extant taxa were sought where available to account for phylogenetic effects.

The degree of relationship between specific types of skin structures and underlying bone morphology in extant taxa was examined by a classification tree analysis. Representative small areas (~4cm^2) of skin from the sampled taxa were grouped into one of eight categories (Table 5-1) using data taken from dissections, preserved specimens, and published accounts. The corresponding bone surface beneath each sampled skin area was identified on a separate skeletal specimen of the same taxon, and the surface morphology of the underlying bone was described by six categorical variables (Fig. 5-4). Using a classification tree technique (recursive partitioning analysis; RPA) available in the JMP 7.0 statistical software package (SAS Institute, Cary, NC), we tested the broad skin categories for strong associations with bone morphology. RPA is a robust analysis that plays a role similar to discriminant function analysis in testing for differences among predefined groups by a set of predictor variables.

Table 5-1. Skin categories for recursive partitioning analysis (RPA).

Skin category	Examples
Villose skin	Typical mammalian pelage (i.e., fur)
Feathered skin	Avian plumage (i.e., feathers)
Glabrous skin	Soft skin with few or no epidermal appendages
Cornified sheaths	Horns of bovid artiodactyls; horny beaks of birds and turtles
Epidermal scales	Scales and cephalic shields of turtles, squamates, and crocodylians
Projecting skin structures	Epidermal horns of rhinoceros; breeding crests of American white pelicans (epidermal) and comb ducks (dermal)
Armor-like dermis	Thickened dermis of rhinoceros, hippopotamus, and swine

JMP's recursive partitioning analysis makes use of logworth ($\log_{10}$ of a weighted *p* value) to select split variables. Logworth values of 1.3 and 0.7 correspond to weighted *p* values of 0.05 and 0.2, respectively, and these values were used as cutoffs to prevent overfitting the RPA to the data. RPA is not intended to function as a hypothesis-testing statistic in this study, but instead provides a relatively objective means of exploring associations in a coded morphological data set. The relationships recovered in RPA at a logworth of greater than 1.3 are used here as robust osteological correlates of specific skin features. Some of the skin categories assigned in this study were represented by relatively few extant taxa (e.g., thickened, armor-like dermis, represented in RPA by only three extant taxa). Although skin structures with poor representation such as these are not likely to be isolated by significant splits in RPA, their osteological correlates are qualitatively different from those of other skin categories, and they will be included as less robust osteological correlates of specific skin features.

Centrosaurine morphology

Osteological correlates of skin structures were examined on specimens of *Pachyrhinosaurus* spp. (Sternberg 1950; Currie et al. 2008), *Achelousaurus horneri*, *Einiosaurus procurvicornis* (Sampson 1995), and *Centrosaurus* spp. (Lambe 1904; Ryan and Russell 2005) for morphological convergence with extant taxa (Appendix D). Specimens of *Chasmosaurus belli* (Lambe 1914), *Anchiceratops ornatus* (Brown 1914), and *Protoceratops andrewsi* (Granger and Gregory 1923) were included as outgroups.

Histological Sampling

Histological samples of bone and corresponding skin were prepared from several extant taxa (see Appendix D for a list of specimens and their preparation protocols). Samples including bone and all adjacent soft tissues were taken from fixed and/or frozen specimens. These samples were dehydrated in ethanol, then infiltrated and embedded with polymethylmethacrylate (PMMA) resin using a protocol modified from Sterchi and Eurell (1989). Additional samples of bone with known skin associations were taken from osteological specimens. Bone samples without adjacent skin were embedded in low-viscosity epoxy resin (Epo-Thin®, Buehler, Lake Bluff, IL). All embedded samples were rough-cut on a high-speed tile saw, then serially sectioned using a variable speed diamond wafering saw (Isomet 1000®, Buehler, Lake Bluff, IL) at 800µm intervals. The resulting sections were mounted on cast acrylic slides with cyanoacrylate glue, then ground and polished to a thickness of approximately 100µm on a lapidary wheel (Metaserv 2000®, Buehler, Lake Bluff, IL).

Several cored samples of *Pachyrhinosaurus lakustai* were available from a previous histological study on this taxon (Edwards and Russell 1994). These samples were subjected to micro-computed tomography (μCT) with a GE eXplore Locus Small Animal μCT Scanner to produce an archival record of their morphology prior to sectioning (see Appendix D for samples). The scan parameters were as follows: slice thickness of 92 μm (isotropic voxels), 80 kV, 450 μA, 100 ms, 720 views. The resulting volume data (in VFF format) were exported from MicroView 2.1.2 (open-source software developed by GE; microview.sourceforge.net) in DICOM format, which were then subsequently imported into Amira 3.1.1 or 4.1.1 (Mercury-TGS, Chelmsford, MA) for viewing, analysis, and visualization. Fossil samples were embedded in Silmar 41 polystyrene resin. Sectioning protocol was nearly identical to that given above for extant specimens, the only exceptions being that the fossil samples were serially sectioned at 1mm intervals and mounted to glass slides using epoxy resin.

Testing hypotheses of adaptation and analogy

After examples of convergent skin morphology between centrosaurines and extant taxa were identified, testing hypotheses of analogy followed in three steps: (1) the strength of any relationships between function and skin morphology was assessed by checking how often similar functions occurred among morphologically convergent extant taxa; (2) extant taxa showing similarity in both function and skin morphology from step 1 were examined in phylogenetic context to test for adaptation in the sense of Gould and Vrba (1982); (3) inferred skin morphologies for centrosaurines were examined in phylogenetic context to test for similarity between the adaptive phylogenetic histories

identified in step 2 and the character transformation history inferred for centrosaurine skin structures.

The first step above, assessing the strength of functional relationships to skin morphology in extant taxa, is ideally carried out as a quantitative character correlation test that accounts for phylogeny, such as the Discrete test found in the BayesTraits software package (Pagel 1994; Pagel and Meade 2006). However, comparing diffuse phylogenetic distributions of convergent morphologies (e.g., comparing horn sheaths on the frontal horns of bovids and the tarsometatarsal spurs of galloanserine birds) can strain the assumptions of these tests, particularly the assumptions of complete representation of a phylogenetic tree and known branch lengths. In cases where phylogenetic comparative tests of character correlation were impractical, contingency table tests such as χ^2 were employed to test relationships between structure and function instead. Both of these approaches test the hypothesis that a specific function co-occurs with a specific skin morphology more often than would be expected by random chance. Significant non-random relationships between structure and function are suggestive of adaptation (although not a complete test for adaptation *per se*; see Kluge 2005), especially if such relationships occur homoplastically in several phylogenetically independent groups (Greene 1986). This first test will hereafter be referred to as the "convergence" test of analogy.

The second step above, examining structure/function relationships in phylogenetic context, was performed by calculating ancestral character state reconstructions of the relevant morphological and functional characters in Mesquite v2.5 (Maddison and

Maddison 2006, 2008). Published phylogenies for extant taxa identified as morphologically convergent with centrosaurines in step 1 above were imported into Mesquite. Morphological and functional (behavioral) traits were coded as categorical characters from osteological data and published descriptions. Both maximum parsimony (MP) and maximum likelihood (ML) methods of ancestral character state reconstruction were used. Branch length information was taken from published phylogenies where available; otherwise, ML ancestral character state reconstructions were run once with all branch lengths equal (modeling punctuated change) and once each with Grafen's (1989) and Pagel's (1992) methods of transforming branch lengths to model gradual change.

Ancestral character state reconstructions for skin morphology and function allowed these characters to be tested against Gould and Vrba's (1982) phylogenetically explicit definition of adaptation, as suggested in Coddington (1988, 1990) and Baum and Larson (1991). Because appropriate fitness or performance data for specific skin morphologies are rarely available, this part of the three-part test for analogy focused on the "historical genesis" of skin morphology in extant taxa (Gould and Vrba 1982), in relationship to the selective regime of specific functions or behaviors. Skin morphology/function relationships identified in step 1 were only considered as appropriate extant analogs if the convergent morphology and a novel function arose on the same branch; i.e., if the structure/selective regime relationship matched a specific subset of Gould and Vrba's (1982) historical definition of adaptation (Fig. 5-5A). Because fitness data were not available for most morphologies considered in this study, more inclusive patterns of "aptation" (i.e., the evolution of novel structure after a change

in selection regime [Fig. 5-5B], or the pattern of exaptation in which a novel selection regime follows the evolution of a novel structure [Fig. 5-5C]) were rejected as analogs, as these patterns could not be distinguished from non-aptation without evidence of current utility. Changes in skin morphology that occurred on the same branch as changes in function in ancestral character state reconstructions were retained as potential extant analogs for centrosaurine morphology. This second test will hereafter be referred to as the "aptation" test of analogy.

The third step, comparing the "historical genesis" of convergent morphology in potential extant analogs to the pattern of horn evolution in centrosaurine dinosaurs, was accomplished by comparing the ancestral character state reconstructions from step 2 with MP and ML ancestral character state reconstructions for centrosaurine horn morphology. Inferred skin morphologies for centrosaurine dinosaurs were coded as categorical characters, using categories similar to those used for the potential extant analogs. The centrosaurine phylogeny of Currie et al. (2008) was imported into Mesquite v2.5. Equal branch lengths (modeling punctuational change) and branch length transformations of Grafen (1989) and Pagel (1992; both modeling gradual change) were included in ML ancestral character state reconstruction analyses.

Similarity in the "historical genesis" of morphological traits among extant and extinct groups, as determined from ancestral character state reconstructions, is the third and final criterion in our test of analogy. Morphological traits in extant taxa were considered to represent analogous structures for centrosaurine morphology only if the sequence of character state changes leading to both extant and extinct morphologies were

similar (Fig. 5-6). Two independent lineages will not necessarily respond to a similar selective regime by producing similar adaptive changes (Kluge 2005); thus this final criterion cannot falsify a potential analog, but may instead be used to rank hypotheses by their relative support. This third and final test will hereafter be referred to as the "correspondence" test of analogy.

Results

Osteological correlates of skin in extant taxa

Cornified sheaths and scales both have osteological correlates that were identified as robust by RPA. Armor-like dermis, projecting skin appendages, and thick pads of papillary epidermis were separated from cornified sheaths in a marginally significant split by RPA ($p \approx 0.06$), and although they were not split further, the osteological correlates for these three taxon-poor skin categories are qualitatively distinctive and consistent among the available samples within each taxon (Table 5-2). Skin morphologies with comparatively soft keratinization and non-specialized dermal architecture (glabrous, villose, and feathered skin) were separated from other skin categories by the absence of specific bony features such as neurovascular grooves or rugose bone.

Table 5-2. Osteological and histological correlates of skin structures.

Skin structure	Example	Osteological correlates	Histological correlates
Cornified sheaths	Bovid horn	Tangentially oriented rugosity Dense neurovascular grooves Oblique neurovascular foramina "Lip" at transition to softer skin	Dense concentrations of extrinsic fibers with low insertion angles and crossed arrays
Epidermal scales	Squamate scales	Shallow hummocky rugosity Osteoderms	Normally-oriented extrinsic fibers
Cornified pads	Muskox horn boss	Pits or elongate grooves Normal neurovascular foramina Raised edge at transition to softer skin	Bone spicules composed of osteonal bone Osteoclast lacunae
Projecting structures	Rhinoceros horn	Projecting rugosity distributed in a ring around the edge of the projecting structure	Bone spicules composed of metaplastically ossified dermis
Armor-like dermis	Hippopotamus facial skin	Evenly-distributed projecting rugosity	Bone spicules composed of metaplastically ossified dermis

Correlates of epidermal morphology: cornified sheath

Cornified sheaths that cover bony cores, such as the horns of bovid artiodactyls and the beaks of birds and turtles, are consistently associated with prominent

neurovascular grooves on bone surfaces, in agreement with the results of Horner and Marshall (2002). Other features that are generally associated with cornified sheaths include a low profile for any rugose bone that may be present, with bone spicules directed tangentially along the bone surface; neurovascular foramina that breach the bone surface at shallow, oblique angles; and the presence of a pronounced "lip" or bony overgrowth at the transition between heavily cornified skin and adjacent soft skin (Fig. 5-7A). The last feature may be absent if the transition between cornified skin and soft skin is gradual, as in the horns of pronghorn antelope (*Antilocapra*). Estimates of type I and II error rates for this correlate in the RPA sample are shown in Table 5-3.

Correlates of epidermal morphology: scales

Epidermal scales show two distinct forms of osteological correlate, coinciding with the difference between intradermal and periosteal ornamentation noted by Vickaryous et al. (2001). The first correlate is formed by intradermal ossifications, generally referred to as osteoderms or osteoscutes. Each separate ossification generally corresponds to a single overlying scale, although in some cases several well-developed osteoderms may sit beneath a single epidermal scale (e.g., *Tiliqua scincoides*; *Tarentola mauretanica*, Lange 1931, p. 418). Osteoderms may co-ossify with subjacent skeletal elements in ontogenetically older individuals, but in most cases osteoderms that have fused with underlying skull bones remain identifiable as discrete elements.

A second form of osteological correlate for scales can be seen in many iguanian lizards, and consists of a regularly arranged, shallow, hummocky rugosity on the bone surface (Fig. 5-7B). These features are not related to intradermal ossification and are

instead derived entirely from apophyseal bone growth beneath individual scales (Fig. 5-8B; Vickaryous et al. 2001). In some iguanian lizards, these features become very pronounced (e.g., the supraorbital and nasal horn cores of *Chamaeleo jacksoni*). Taken together, these two forms of osteological correlate produced a significant split by RPA that isolated most of the scaled specimens included in the analysis, and both of these morphologies are considered robust osteological correlates for epidermal scales in extinct taxa. Estimates of type I and II error rates for these correlates in the RPA sample are shown in Table 5-3.

Table 5-3. Estimates of type I error rate, type II error rate, and accuracy of the two correlates identified by significant splits in recursive partitioning analysis (RPA).

Correlate set	**Type I error rate**	**Type II error rate**	**Accuracy**
Cornified sheath	0.21	0.05	85%
Epidermal scale	0.08	0.39	85%

Correlates of epidermal morphology: cornified pad

Thick, cornified pads of epidermis are comparatively rare and are commonly found in only three of the extant taxa surveyed in this study: helmeted hornbills (*Buceros vigil*), African buffalo (*Syncerus caffer*), and muskoxen (*Ovibos moschatus*). The morphology of the epidermis is slightly different in each case. Adults of both sexes of *Buceros vigil* possess a heavily cornified pad of "hornbill ivory" that covers the rostral end of the casque. The epidermis in this pad grows directly away from the flat face of the casque, and lacks any grossly visible internal structure. Male *Syncerus* possess a

comparatively thin pad of cornified epidermis across a bony frontal boss that is continuous with the horn sheath. The epidermal tissue of both the pad and the horn sheath is organized into discrete bundles, indicating the presence of pronounced dermal papillae at the dermo-epidermal junction. Growth of the cornified pad in *Syncerus* progresses at a very shallow angle with respect to the underlying bone surface, similar to growth of the horn sheath along the bony horn core. The cornified pad of male *Ovibos* is also organized in discrete bundles of papillary epidermis (in the sense of Homberger 2001), but is much thicker than that of *Syncerus*, and grows away from the flat surface of the boss at a much steeper angle.

Adult male *Syncerus* and both sexes of *Buceros vigil* both show very similar bony features beneath the thickened parts of their horns and beaks, respectively. In both cases, the bone that supports the heavily cornified pad of epidermis is highly vascular, and the bone surface itself is pierced by a very dense group of normally-oriented (i.e., oriented more or less perpendicularly to the surface) neurovascular foramina. This correlate contrasts sharply with the oblique neurovascular foramina and neurovascular grooves seen beneath the adjacent horn sheath in *Syncerus* and the adjacent horny beak in *Buceros vigil*.

The frontal bosses of adult male *Ovibos* show a slightly different osteological correlate. In addition to dense concentrations of normally-oriented neurovascular foramina, the bone surface shows a pronounced pitted rugosity, composed of shallow rounded depressions separated by fine projecting bone spicules (Fig. 5-7C). Computed tomographic (CT) scans of an osteological specimen of *Ovibos* with horns in place show

that the rounded depressions and projecting spicules match up with the edges and centers, respectively, of individual bundles of papillary epidermis.

The frontal bosses of adult male *Ovibos* also show a pronounced depression relative to the adjacent horn core, a feature shared by Pleistocene-age woodland muskoxen *Bootherium bombifrons*. A similar depression is found on the nasal boss of atypical individuals of Indian rhinoceros *Rhinoceros unicornis* in which the nasal horn has been worn down to a thin pad (~2cm thick; e.g., USNM 308417). Individuals of *Rhinoceros unicornis* with typical horns (~10–15cm tall) show the distinct osteological correlate for projecting skin structures instead, described below.

Correlates of dermal and epidermal morphology: projecting skin structures

The category of projecting skin structures includes features that are composed predominantly of epidermal tissues (e.g., rhinoceros horns) or dermal tissues (e.g., the crests of male comb ducks, *Sarkidiornis*) that form horns or crests without bony support. Although some examples of projecting skin structures are not associated with bony correlates (e.g., the "warts" of warthogs, *Phacochoerus*), those that are show a surprisingly consistent arrangement of rugose bone, detailed in Hieronymus and Witmer (in review). The outer circumference of the projecting feature is marked by an area of rugosity formed by projecting bone lobules or spicules, which gives way to smooth bone beneath the center of the projecting feature (Fig. 5-7D).

Correlates of dermal morphology: armor-like dermis

The category of armor-like dermis includes several convergent examples of a specific architecture of dermal collagen fibers (Shadwick et al. 1992). This architecture

consists of regular diagonally crossed arrays of thick collagen fiber bundles arranged at oblique angles to the plane of the overlying epidermis. This arrangement contrasts with typical sauropsid dermis, in which smaller fiber bundles are diagonally crossed but lie parallel to overlying epidermis (Landmann 1986; Sawyer et al. 1986), and also differs from typical mammalian dermis, in which smaller fiber bundles are arranged at random but lie parallel to the overlying epidermis (Sokolov 1982). The osteological correlate for armor-like dermis consists of a rugosity formed by large (>2mm in diameter) projecting bone lobules, each composed of metaplastically ossified remnants of collagen fiber bundles from the base of the dermis (Fig. 5-7E). These features are described in more detail in Hieronymus and Witmer (in review).

Histological correlates of cornified sheaths/armor-like dermis

The bony attachments of horn sheaths, horny beaks, and armor-like dermis are characterized by dense concentrations of metaplastically ossified dermal collagen fibers (extrinsic fibers) that meet the bone surface at oblique angles. In some cases (all examples of armor-like dermis, some beaks and horns) these extrinsic fibers are part of an orthogonally crossed array, whereas in others the extrinsic fibers are all oriented along a single shallow chord to the bone surface. Some beak attachments (e.g., *Otus asio*) only show small, restricted patches of extrinsic fibers; others (e.g., *Phalacrocorax auritus*) show a continuous layer of extrinsic fiber bone across the entire attachment (Fig. 5-8A). Although the dermal architecture is similar between cornified sheaths and armor-like dermis, the conformation of bony structures at the periosteal surface is different. Under cornified sheaths, metaplastic ossification of the dermis proceeds along a uniform front,

producing a flat surface (Fig. 5-8A). This differs from the patchy ossification of dermal collagen fiber bundles in armor-like dermis that produces projecting spicules of metaplastic bone (Fig. 5-8E).

Histological correlates of epidermal scales

The bony attachment of epidermal scales is sometimes accompanied by extrinsic fibers, but less often than the attachment of cornified sheaths. The extrinsic fibers that occur beneath the epidermal scales of squamates are generally oriented normal to the periosteal surface of the bone instead of the shallow angles seen with other skin attachment types. The apophyseal ossification that produces scale-associated hummocky rugosity in iguanian squamates (Fig. 5-8B) is not caused by metaplastic ossification of the dermis, and instead appears to be the result of periosteal ossification.

Histological correlates of cornified pads

Of the two gross osteological correlate types associated with thick cornified pads, only the pitted morphology of muskox horn bosses was histologically examined in this study. The bony horn boss is composed of highly vascular plexiform bone, with no evidence of any extrinsic fibers. The spicules on the bone surface are outlined by osteoclast lacunae (Fig. 5-8D), and contain partial remnants of osteons, suggesting that the shape of the spicules is a result of the resorption of existing bone.

Histological correlates of projecting skin structures

The peripherally-distributed rugosity associated with rhinoceros horns is composed of metaplastically ossified dermal collagen fiber bundles that form projecting bone spicules (Fig. 5-8E; Hieronymus and Witmer in review). The comparatively smooth

central region within the peripheral rugosity is composed of periosteally ossified bone with no extrinsic fibers. The size of the projecting bone spicules in this osteological correlate closely matches the size of the large bundles of collagen fibers in the armor-like dermis of rhinoceros. The size difference in individual bone spicules between this osteological correlate in rhinoceros and the correlate for projecting structures in taxa without derived dermal architecture (e.g., *Sarkidiornis*) suggests that the peripheral rugosity in all examples of this correlate is formed by metaplastic ossification of existing dermal collagen fiber bundles.

Osteological correlates of skin in Centrosaurus

Nasal horn cores of *Centrosaurus* generally show prominent neurovascular grooves and obliquely-oriented neurovascular foramina, both of which are robust correlates for the presence of a cornified sheath. Most specimens also show a "lip" or basal sulcus ("bony overgrowth" of Ryan and Russell 2005) that describes a saddle-shaped curve at the base of the nasal horn core (Fig. 5-9A), indicating a transition between more heavily cornified skin on the nasal horn core itself and softer skin across other parts of the nasals.

The dorsal processes of the premaxillae and the premaxillary processes of the nasals also show evidence of a cornified cover that most likely extended ventrally across part of the bony nostril (Fig. 5-9E). Other areas of the nasals are generally smooth, but the combination of sparse neurovascular grooves and a broad convex curve on the caudal edge of the nasals suggests the presence of large epidermal scales.

Supraorbital horn cores of *Centrosaurus* show prominent neurovascular grooves, with a basal sulcus preserved on the medial side of the major horncore in some specimens. The presence of a basal sulcus indicates a sharp transition between a horn sheath covering the horn core and softer skin medially. In some individuals, the supraorbital horn core is marked by one or two pronounced pits on the apex of the horn. The presence of a basal sulcus and pronounced neurovascular grooves associated with these pits (e.g., ROM 12787) indicates that the adjacent areas of the supraorbital horn core were covered by a cornified sheath, and the pits themselves match the correlate for thick cornified pads seen in extant muskoxen. This combination suggests that the apex of the supraorbital horn core was covered by a thickened pad of cornified skin that continued around the base of the horn core as a cornified sheath. A similar arrangement of pitting and neurovascular grooves relating to a thickened distal horn and thinner proximal horn sheath can be found on the horncores of male bighorn sheep (*Ovis canadensis*; Shackleton 1985).

The supraorbital horn core is accompanied by a series of low ridges of bone that closely match the apophyseally derived osteological correlate for scales in iguanian squamates, indicating that the supraorbital horn itself is derived from the third in a series of four scales that line the dorsal rim of the orbit (Fig. 5-9C). This series of scale correlates extends onto the squamosal, where there are another four to five shallow bony prominences in sequence (Fig. 5-9D). In some specimens (ROM 767, AMNH FR 5442) a second row of two scale correlates can be seen rostroventral to the primary row on the

squamosal. A similar row of six bony prominences on the parietal is also interpreted as the correlate for a sequence of scales (Fig. 5-9F).

Osteological correlates of skin in Einiosaurus

The rostrally curved nasal horn cores of adult *Einiosaurus procurvicornis* show prominent bony correlates for the presence of a cornified sheath. A basal sulcus on the nasal horn core defines a saddle-shaped lateral outline for the transition between the heavily cornified horn sheath and softer surrounding skin, similar to that seen in *Centrosaurus* (Fig 5-10A).

Two adult nasal horn cores taken from the Canyon Bonebed site (MOR 456 8-9-6-1 and MOR 456 8-13-7-5) both show a shallow longitudinal groove along their dorsal surfaces (Fig. 5-10B). This groove may have been related to a thickening of the cornified horn sheath on the dorsal surface of the horn core, but the bone surface is weathered and there are no conclusive osteological correlates for such a skin structure. Alternatively, the groove may be a remnant of the internasal suture. The adult nasal horn core taken from the Dino Ridge site (MOR 373 8-20-6-14) lacks a dorsal longitudinal groove.

Supraorbital skin correlates in *Einiosaurus* are similar to those seen in *Centrosaurus*. Some *Einiosaurus* specimens (e.g., MOR 456 8-9-6-1) show a more pronounced apical pit in the position of the supraorbital horn core, but the raised rim of bone surrounding the pit still bears a basal sulcus, indicating a thin cornified sheath at the edge of a thicker cornified pad (Fig. 5-10C). Bony prominences indicative of a row of scales on either side of the supraorbital horn core are also present, although weathering

and cracking in the available *Einiosaurus* material makes it difficult to compare the total number of bony prominences, relative to better-preserved examples from *Centrosaurus*.

Osteological correlates of skin in Achelousaurus

Adult *Achelousaurus horneri* nasal horn cores show a pronounced rostral slant (Fig. 5-11D). This orientation differs from that seen in *Einiosaurus* in that the pitch of the horn core is established at the base and remains straight, instead of curving forward. The caudodorsal surface of the horn core shows the osteological correlate for a thick epidermal pad which grades into the osteological correlate for a cornified sheath laterally. Bone morphology on the dorsal surface of adult *Achelousaurus* nasal horn cores is most similar to the grooved morphology seen at the transition between the boss and the horn core proper in muskoxen, in which thick papillary epidermis grows at a low angle to the underlying bone surface, elongating the characteristic pits into shallow grooves.

The rostral (apical) end of the nasal horn core shows a deep v-shaped notch on the midline (Fig. 5-11B), which may correspond to the dorsal longitudinal groove seen in the Canyon Bonebed *Einiosaurus specimens*. Pitting indicative of a thick pad of rostrally-growing papillary epidermis is superimposed on this midline apical notch.

The rostrally-slanted horn core and rostral pitting seen in *Achelousaurus* can also be seen in another unidentified centrosaurine horn core (ROM 49862; Fig 5-11E). This specimen shows a pronounced basal sulcus, indicating a cornified sheath covering the entire base of the horn core, instead of the development of the caudodorsal side of the horn sheath into a comparatively thick pad as seen in *Achelousaurus*. This may represent

a transitional morph between *Einiosaurus* and *Achelousaurus*, but this specimen lacks locality data and its stratigraphic position relative to these two taxa cannot be established.

The supraorbital bosses of adult *Achelousaurus* specimens show surface morphology that closely resembles the transition between boss and horn core proper in muskoxen, indicating a thick pad of papillary epidermis growing at a shallow angle relative to the bone surface (Fig. 5-11C). The direction of growth of the supraorbital epidermal pad in *Achelousaurus* can be inferred from the orientation of the "fins" of bone in the boss, suggesting a lateral direction of growth similar to that seen on the curved supraorbital horn cores of *Centrosaurus brinkmani* (Ryan and Russell 2005). The large supraorbital boss lacks a basal sulcus, thus the supraorbital horn pad can be inferred to stop at the rostral, caudal, and medial edges of the wrinkled bone of the boss, instead of continuing around the periphery as a thin cornified sheath. This inferred skin morphology can be seen as part of a continuum with the supraorbital horn sheaths inferred for *Einiosaurus* and *Centrosaurus*. Simple apical pitting occurs in cases where a cornified horn sheath remains at the periphery. More complex pitted surfaces such as those of *Achelousaurus* supraorbital bosses resemble epiphyses, and indeed may be constrained to this morphology by a similar need to attach two hardened structures together while maintaining a softer germinative layer between them.

Osteological and histological correlates of skin in Pachyrhinosaurus

Some examples of adult nasal bosses in *Pachyrhinosaurus lakustai* (e.g., TMP 1989.5.427) are very similar to the adult nasal horn core of *Achelousaurus*, with a clearly defined apical notch, rostral pitting, and a gradation from dorsal pitting to lateral

neurovascular grooves (Fig. 5-12E). These correlates indicate skin morphology similar to that inferred for *Achelousaurus*, with a thick pad of papillary epidermis growing rostrally across the dorsal surface of the boss and continuing rostrally from the apical notch. This heavily cornified pad grades laterally into a cornified sheath across the lateral base of the horn core. Further similarities between this morphology and the more derived structures of other specimens of *Pachyrhinosaurus lakustai* and *Pachyrhinosaurus canadensis* provide a basis for identifying homologous regions on the nasal boss in these taxa.

The variable morphology of the dorsal surface of the nasal boss in *Pachyrhinosaurus lakustai* is the result of varying degrees of post-mortem weathering and erosion (Currie et al. 2008). The osteological correlate for a thick cornified pad seen on muskoxen is relatively robust, and remains visible even after considerable weathering, as seen in Pleistocene fossil muskox specimens (e.g., USNM RSFVL 18 S 176; Fig. 5-7C). Thus despite damage to the original bone surface, the pitting and grooving seen on *Pachyrhinosaurus lakustai* can be readily interpreted as a similar osteological correlate.

A histological specimen from the dorsal surface of the nasal boss shows that the bony pitting and grooving is more pronounced than it appears on the prepared surface of the fossil (Fig. 5-12C). The bottoms of the grooves in this specimen lie beneath an additional 3mm of matrix, which preserves several fine bony spicules. Similar bone spicules were reported to have been removed during preparation of the Drumheller *Pachyrhinosaurus* specimen, and it is these bone spicules that were specifically described as potentially similar to the rugose bone of rhinoceros horn attachment (Langston 1967). Comparison of the bone spicules from TMP 1989.55.1038 to histological sections of

rhinoceros horn attachment and muskox horn attachment shows the rugose boss of *Pachyrhinosaurus* to be more similar to the frontal bosses of muskoxen on a histological level. The bone spicules of muskoxen and *Pachyrhinosaurus* are both composed of osteonal bone tissue, whereas the lobules of bone in rhinoceros horn attachment are composed of metaplastically ossified deep dermis that lacks osteonal structure.

An apical notch is absent from most adult nasal bosses, and the corresponding area of horn core instead forms a shallow "step" across the rostral quarter of the nasal boss. In some individuals, a shallow ridge runs across the dorsal surface of the nasal boss and continues as a more pronounced projection in the rostral step. Although this bony morphology differs from *Achelousaurus*, the osteological correlates superimposed on these larger-scale bony structures are identical, indicating similar skin structures.

The lateral surface of nasal bosses in *Pachyrhinosaurus canadensis* shows a series of bony grooves and fins not unlike those seen on the supraorbital bosses of *Achelousaurus*. These structures indicate a thick cornified sheath growing at a low angle to the underlying bone surface; the orientation of the grooves reveals the direction of epidermal growth. The lateral grooves vary from a rostral slant in nasal bosses more similar to that of *Achelousaurus* to nearly vertical in the most derived examples (e.g., the Drumheller specimen of *Pachyrhinosaurus* cf. *P. canadensis*; Langston 1967). Variation in the orientation of lateral grooves within the sample of *Pachyrhinosaurus lakustai* from Pipestone Creek suggests that the direction of growth for the cornified nasal pad was subject to ontogenetic or within-population variation.

The rostral comb (Currie et al. 2008; dorsal processes of the premaxillae and premaxillary processes of the nasals) shows a series of bony prominence not unlike those seen on the squamosals and parietals of centrosaurines in general. These prominences are interpreted as apophyseally ossified osteological correlates for epidermal scales, indicating a midline row of scales between the horny beak and the nasal boss. This differs from the single cornified sheath interpreted for *Centrosaurus*.

Skin correlates for the supraorbital region of adult *Pachyrhinosaurus lakustai* are variable, and similar to those seen both in adult *Einiosaurus* and the holotype of *Achelousaurus*. Some individuals show a single pronounced apical pit with a basal sulcus (e.g., TMP 1989.55.21), indicating a cornified pad with a thinner cornified sheath about the edges. Other individuals show a relatively flattened boss with bony grooves and fins and no basal sulcus, indicating a cornified pad that did not trail out into a thin sheath. Both of these morphs occasionally show perforations in the boss that communicate with underlying parts of the frontal sinus system (Fig. 5-12D). Similar perforations can be seen on the bony frontal bosses of woodland muskoxen *Bootherium bombifrons* (e.g., USNM 2556) that communicate with the paranasal sinuses. These perforations would be well-protected in life by a thick pad of heavily cornified epidermis (Guthrie 1991).

The supraorbital boss forms from the second in a sequence of three scales over the dorsal rim of the orbit, as indicated by shallow bony prominences rostral and caudal to the supraorbital boss itself. Two additional bony prominences on the squamosal indicate the continuation of the supraorbital scale row. Thus the epidermal scales over the orbit in *Pachyrhinosaurus* species are larger and less numerous than those seen in *Centrosaurus*.

A row of bony prominences on the parietal bar is interpreted as a series of scales similar to those of *Centrosaurus*, and in some individuals of *Pachyrhinosaurus lakustai*, one to three of these scales developed into a short horn sheath, supported by a bony horn core (Fig. 5-12G). Similar elaboration of epidermal scales into projecting horns can be seen in extant *Phrynosoma* species. In at least one *Pachyrhinosaurus lakustai* individual (TMP 1987.55.81), the apex of the novel parietal horn core shows the pitted osteological correlate for a cornified pad, similar to the apical resorption seen on the horn cores of other centrosaurines.

Convergence of structure and function in extant taxa

The thick cornified pads inferred to cover the rugose nasal and supraorbital bosses of *Pachyrhinosaurus* species were most similar to the cornified pads on the frontal bosses of adult male muskoxen, as the bony correlate seen in both taxa relates directly to the presence of papillary epidermis growing at comparatively steep angles to the bone surface. Muskoxen are the only extant species that show this particular relationship of strongly papillary epidermis and a bony boss. However, as a single species, muskoxen provide only a single data point for the relationship between this morphology and any putative related function. We have thus broadened our interpretation of "similar" skin structures in extant taxa to include any thickened cornified pad of epidermis that is not directly incorporated into a horn sheath, which includes adult male African buffalo *Syncerus*, adult male banteng *Bos javanicus*, and, among extant dinosaurs, helmeted hornbills *Buceros vigil*.

In three of these four extant examples (*Ovibos*, *Syncerus*, and *Buceros vigil*), the presence of a thickened cornified pad has been noted to co-occur with headbutting behaviors that are more pronounced than those seen in sister taxa (Nowak and Paradiso 1983; Lent 1988; Kemp 1995; Kinniard et al. 2003). No conclusive behavioral data for banteng have been published, leaving this taxon as an unknown as far as this potential structure/function relationship is concerned. The small sample of extant taxa with cornified pads, and their broad phylogenetic distribution (essentially encompassing Amniota), renders phylogenetic tests of character correlation impractical. Correlation between a morphological character with two states (cornified sheath, cornified pad) and a behavioral character with two states (light clashing, headbutting) was examined in a sample of thirty extant taxa (Table 5-4), comprising the three potentially analogous taxa and several of their close outgroup taxa. Skin morphology was scored using a combination of data from this study and published descriptions; behavior was scored using published accounts (citations listed in Table 5-4). The strength of any relationship between skin morphology and behavior was assessed using both Likelihood and Pearson's χ^2 tests in JMP 7. Skin morphology and agonistic behavior are significantly related (p = 0.0142 and 0.0253 by Likelihood χ^2 and Pearson's χ^2, respectively; Table 5-5). Within this sample, the possession of a cornified pad can be seen as a predictor of the associated headbutting behavior. The relationship between cornified pads and headbutting in potentially analogous extant taxa (*Ovibos*, *Syncerus*, and *Buceros vigil*) thus passes the first of the three tests of hypotheses of analogy (convergence) noted above.

Table 5-4. Extant taxa with cornified pads and sister taxa used to asses relationship between skin morphology and agonistic behavior.

Taxon	Cornified skin morphology	Agonistic behavior	Horn shape	Reference
Naemorhedus goral[a]	Sheath	Light clashing	Straight	Mead 1989
Ovibos moschatus[a]	Pad	Headbutting	Ventrally curved	Lent 1988
Oreamnos americanus[a]	Sheath	Light clashing	Straight	Rideout and Hoffman 1975
Ovis dalli[a]	Sheath	Headbutting	Ventrally curved	Bowyer and Leslie 1992
Ovis ammon[a]	Sheath	Headbutting	Ventrally curved	Fedosenko and Blank 2005
Ammotragus lervia[a]	Sheath	Headbutting	Ventrally curved	Gray and Simpson 1980
Capricornis crispus[a]	Sheath	Headbutting	Straight	Jass and Mead 2004
Pseudois nayaur[a]	Sheath	Headbutting	Ventrally curved	Wang and Hoffman 1987
Capra cylindricornis[a]	Sheath	Headbutting	Ventrally curved	Weinberg 2002
Capra sibirica[a]	Sheath	Headbutting	Ventrally curved	Fedosenko and Blank 2001
Budorcas taxicolor[a]	Sheath	Light clashing	Ventrally curved	Neas and Hoffman 1987
Ovis canadensis[a]	Sheath	Headbutting	Ventrally curved	Shackleton 1985
Anthracoceros albirostris[b]	Sheath	Light clashing	Straight	Kemp 1995
Anthracoceros malayanus[b]	Sheath	Light clashing	Straight	Kemp 1995
Buceros bicornis[b]	Sheath	Light clashing	Straight	Kemp 1995
Buceros vigil[b]	Pad	Headbutting	Straight	Kemp 1995
Aceros corrugatus[b]	Sheath	Light clashing	Straight	Kemp 1995
Penelopides panini[b]	Sheath	Light clashing	Straight	Kemp 1995
Buceros hydrocorax[b]	Sheath	Light clashing	Straight	Kemp 1995
Buceros rhinoceros[b]	Sheath	Light clashing	Straight	Kemp 1995
Anthracoceros montani[b]	Sheath	Light clashing	Straight	Kemp 1995
Anthracoceros marchei[b]	Sheath	Light clashing	Straight	Kemp 1995

Anthracoceros coronatus[b]	Sheath	Light clashing	Straight	Kemp 1995
Bison bison[c]	Sheath	Headbutting	Straight	Meagher 1986
Taurotragus oryx[c]	Sheath	Light clashing	Straight	Pappas 2002
Syncerus caffer[c]	Pad	Headbutting	Ventrally curved	Nowak and Paradiso 1983
Tragelaphus angasi[c]	Sheath	Light clashing	Straight	Nowak and Paradiso 1983
Tragelaphus scriptus[c]	Sheath	Light clashing	Straight	Nowak and Paradiso 1983
Tragelaphus strepsiceros[c]	Sheath	Light clashing	Straight	Nowak and Paradiso 1983
Boselaphus tragocamelus[c]	Sheath	Light clashing	Straight	Nowak and Paradiso 1983

[a]Caprinae; [b]Bucerotidae; [c]Bovinae.

Table 5-5. Contingency table test results for Agonistic behavior x Cornified sheath morphology. –Log-Likel.: negative log-likelihood.

N	**DF**	**-Log-Likel.**	**R^2**
30	1	3.005	0.1488

Test	**X^2**	***p***
Likelihood Ratio	6.009	0.0142*
Pearson	5.000	0.0253*

Lundrigan (1996) discussed a functional relationship between robust, ventrally curving horns and headbutting in Bovidae, and thus the possession in *Ovibos* and *Syncerus* of a cornified epidermal pad on the dorsal side of a ventrally curved horn sheath can be seen as an extreme case of this more general phenomenon. When the taxa

considered above are scored instead for ventrally curved horn sheaths vs. other horn curvatures, the relationship between this character and headbutting is even more robust ($p < 0.0001$ by Likelihood χ^2 and Pearson's χ^2; Table 5-6). This broader relationship between ventrally curving horns such as those seen in bighorn sheep (*Ovis canadensis*) and headbutting behavior also passes the test of convergence as a potential analog for the ventrally curving nasal horn of *Einiosaurus*.

Table 5-6. Contingency table test results for Agonistic behavior x Horn shape. –Log-Likel.: negative log-likelihood.

N	DF	-Log-Likel.	R^2
30	1	8.485	0.4203

Test	X^2	*p*
Likelihood Ratio	16.971	<0.0001*
Pearson	15.625	<0.0001*

Tests of adaptation in extant taxa

Ancestral character state reconstructions of the three characters discussed above (cornified pad, robust ventrally curved horns, and headbutting) match an expected pattern for adaptation in all three potentially analogous clades (Caprinae, Bovinae, and Bucerotidae), but the match for adaptive pattern is more robust in Bucerotidae and Caprinae than it is in Bovinae.

The pattern of character state evolution in hornbills (Bucerotidae) is straightforward: helmeted hornbills (*Buceros vigil*) are the only bucerotid taxon that exhibits either of the derived traits of a cornified epidermal pad or headbutting, leading to unequivocal reconstruction of both traits on the same branch (Fig. 5-13). Although other functions have been suggested for the pad of "hornbill ivory" seen in this taxon (Cats-Kuenen 1961), headbutting is the only function that does not also occur in sister taxa (Kemp 1995; Cranbrook and Kemp 1995; Kinniard et al. 2003). The cornified pad of *Buceros vigil* thus passes the second of the three tests of analogy (aptation).

The pattern of character state evolution in cattle (Bovinae) is clouded by a lack of detailed behavioral data for many bovine taxa, and as such does not provide a solid basis for inferring function in extinct taxa. Ancestral character states based on the available information are shown in Figure 5-14, using the published topology and branch lengths of Fernández and Vrba (2005). A majority of reconstructions (six of ten: MP, ML with Grafen branch lengths, and ML with branch lengths of one for both topologies) place headbutting as a primitive character state for Bovini. The most conservative picture that emerges from ancestral character state reconstruction in this system is that the putative selection regime (headbutting) appeared 5–15 Ma before the morphological change (cornified pad). This pattern is still in line with that expected for adaptation (Baum and Larson 1991; Fig. 5-5B), but the inferred time lag between selection regime and adaptation increases the chance that the co-occurrence of these two traits is a false positive. The cornified pad of adult male *Syncerus* thus conditionally fails the aptation

test for analogy, and will not be considered as an appropriate analogous system for assessing function in *Pachyrhinosaurus*.

In contrast, the pattern of character state change in sheep and goats (Caprinae) provides a more compelling case for the relationship between horn shape and headbutting behavior. When the transition to a cornified pad is reconstructed alongside the transition to headbutting, MP and ML analyses of both of the phylogenies used in this study (Fig. 5-15) all place one of three or four unequivocal transitions to headbutting on the branch leading to *Ovibos*, the same branch as the transition to a cornified pad. When horn morphology is scored for either robust, ventrally curving horns or other horn shapes (as shown above for the character correlation test), ML analyses match all of the transitions to headbutting with a transition to robust, ventrally curving horns on the same branch (Fig. 5-15). Cornified pads in *Ovibos* thus pass the aptation test of analogy, and the robust ventrally curved horns of *Ovis*, *Pseudois*, and *Ammotragus* show sufficient evidence of adaptation to be considered as analogous structures in their own right for the ventrally curved nasal horn core of *Einiosaurus*.

Similarity in transformation sequences among extant analogs and centrosaurines

The transition from straight horn core to ventrally curved horncore and flattened boss in Centrosaurinae (Fig. 5-16) is very similar to several morphological transitions seen within Caprinae. The strongest similarity occurs between the pattern of centrosaurine horn evolution and the transition from straight horn cores in goral (*Naemorhedus*) and serow (*Capricornis*) to a rugose boss in muskoxen (*Ovibos*). These examples pass the third test of analogy (correspondence) and stand as the most

appropriate extant analogs for assessing the function of curved horns in *Einiosaurus* and rugose bosses in *Achelousaurus* and *Pachyrhinosaurus*.

The morphological transition seen in Bucerotidae shows a transition from a slightly different starting point (a thin-walled projecting casque, e.g., *Buceros hydrocorax*) to a similar endpoint (the thick cornified casque of *Buceros vigil*). This transition is conditionally accepted in our correspondence test for analogy. The cornified pad of *Buceros vigil* thus provides an appropriate analog for assessing the function of rugose bosses in *Pachyrhinosaurus* and *Achelousaurus*, but carries less weight in this assessment than the cornified pad of muskoxen.

Function of rugose bosses in centrosaurine dinosaurs

Both of the extant analogous systems for the rugose bosses of centrosaurine dinosaurs consist of thick pads of cornified epidermis that function as contact surfaces for butting or ramming. Headbutting is thus the most likely hypothesis of function for the rugose bosses in centrosaurine dinosaurs, in a manner similar to that conceived for the nasal boss of *Pachyrhinosaurus* by Sternberg (1950) and Farlow and Dodson (1975). The curving nasal horn in *Einiosaurus* and the curving supraorbital horns of *Centrosaurus brinkmani* both have extant analogous systems in Caprinae that function in butting or ramming, consistent with the function inferred for the nasal and supraorbital bosses of *Achelousaurus* and *Pachyrhinosaurus*. The change in horn morphology over time within Centrosaurinae is thus entirely consistent with a linear trend of increasing intensity in agonistic behaviors, starting with horn clashing in basal centrosaurines with longer

supraorbital horns (Farke 2004; Farke et al. in press) and ending in high-energy headbutting.

Discussion

Summary of centrosaurine facial skin morphology

Centrosaurine dinosaurs show a diverse array of bony facial morphologies but a comparatively narrow range of osteological correlate for skin structures. Most bony morphology on centrosaurine skulls that can be attributed to skin structures indicates a progression from shallow epidermal scales (generally in the range of 5 to 10cm in diameter in adult skulls), to tall cornified horn sheaths, to thick pads of cornified epidermis that initially develop at the apices of horn sheaths, ending in massive cornified pads across the skull roof (Fig. 5-16). This progression can be seen at different stages in different skull regions. For example, the progression from scales to taller horn sheaths can be seen in the development of the parietal bar scales of basal centrosaurines into short horns in *Pachyrhinosaurus lakustai* (Fig. 5-12G), whereas the progression of taller horn sheaths into massive cornified pads can be seen in the transition between the nasal horn sheath of basal centrosaurines and the nasal pad of *Achelousaurus* (Fig. 5-16). Pronounced scales and short horns are both present on *Pachyrhinosaurus canadensis*, but the majority of the skull roof is occupied by massive cornified pads on the nasal and supraorbital bosses (Fig. 5-12A).

Our reconstruction of thick cornified pads on the nasal and supraorbital bosses of *Pachyrhinosaurus* is not only derived from histological and morphological similarities to the horns of living muskoxen, but also from the ways in which *Pachyrhinosaurus* differs

from the morphology and histology predicted for other hypotheses of skin shape. The tall, rhinoceros-like epidermal horns that constitute the other major competing hypothesis for *Pachyrhinosaurus* horn shape provides a very specific set of morphological and histological predictions: (1) the periphery of both nasal and supraorbital bosses should show a bone surface texture (projecting rugosity) that is distinct from the bone surface texture on the center of the bosses (smooth bone with normal neurovascular foramina), and (2) the projecting rugosity on the boss should be formed entirely of metaplastically ossified dermal collagen fibers. The morphology and histology of the rugose bosses of centrosaurine dinosaurs do not meet either of these predictions. The similarity between the bosses of *Pachyrhinosaurus* and the horn attachments of living rhinoceros is thus only superficial.

Patterns of ossification in centrosaurine ornaments

Some of the scale-related elements on ceratopsian skulls are clearly separate ossification centers (e.g., epinasal and episquamosal ossifications; Hatcher et al. 1907; Horner and Goodwin 2008), while others appear to be direct outgrowths of the dermatocranium (e.g., parietal eminences). The presence of both types of scale correlate on ceratopsian skulls agrees with the pattern found in Ankylosauria by Vickaryous et al. (2001). Unlike extant squamates, where osteoderms and apophyseal scale correlates are largely confined to separate clades, ornithischian dinosaurs had both forms of scale-related bone growth. Thus, while we might expect to find either osteoderms or apophyseal eminences forming ornaments in ornithischian dinosaurs, the critical point is

that both of these features can be directly related to homologous unpreserved skin features.

The similarity between osteodermally and apophyseally demarcated scale correlates opens up several new possibilities for comparing inferred skin structures across ornithischian groups. For example, despite the fact that the bony elements that compose the nasal horn core in centrosaurine and chasmosaurine ceratopsians are non-homologous, the skin structures that induce the growth of the horn core may themselves be homologous, deriving from a single scale in a common ancestor. The Wahweap centrosaurine (Kirkland and Deblieux 2007) may provide more information to test this hypothesis of homology.

In a similar fashion, the supraorbital, postorbital, and squamosal nodes seen on pachycephalosaurian dinosaurs (Maryańska et al., 2004) indicate a pattern of pronounced scales similar to that inferred on the same skull elements of centrosaurine dinosaurs in this study. As noted by Vickaryous et al. (2001) for ankylosaurs, the scale patterns visible on ceratopsians and pachycephalosaurs are strikingly similar in some respects to those seen in extant squamates. Further comparisons of scale correlates in ornithischians may shed more light the cause of this similarity.

Species recognition, sexual selection, and social selection in Centrosaurinae

The bony ornaments of ceratopsian dinosaurs have been suggested to function predominantly in intraspecific communication, but there is ongoing debate as to whether this communication only served the purpose of species recognition or if it was involved in intraspecific sexual selection as well (Farlow and Dodson 1975; Spassov 1979;

Sampson et al. 1997; Padian et al. 2004; Goodwin et al. 2006). Morphological evolution driven by species recognition is expected to show a different pattern of character state change than morphological evolution driven by sexual selection (Padian et al. 2004): (1) Species recognition is expected to occur where the ranges of several closely related species overlap, whereas sexual selection may occur both in sympatry and in isolation. (2) Species recognition is expected to result in non-linear, diverging trends of morphological evolution, whereas sexual selection is expected to result in linear trends. And finally, (3) differences in parental investment between males and females are expected to cause dimorphism in sexually selected characters (Darwin 1871; Emlen and Oring 1977), but no similar tendency to dimorphism has been suggested for species recognition. Sympatry and non-linear trends of divergence both occur frequently in non-avian dinosaur clades, fitting the pattern expected for species recognition. Clear-cut sexual dimorphism in non-avian dinosaurs has been elusive, leading to the current assessment of bony ornaments such those of *Pachyrhinosaurus* as the result of species recognition, not sexual selection (Padian et al. 2004; Goodwin et al. 2006).

Based on the headbutting function inferred for the rugose bosses of *Pachyrhinosaurus*, we suggest that the concept of "social selection" (West-Eberhard 1983) offers a more compatible form of selection to drive the amazing diversity seen in ceratopsian cranial ornaments. Social selection occurs when there is differential success in within-species competition for any limited resource. The limited resource may be mating opportunities, resulting in sexual selection as a subcategory of social selection, or the limited resource may be a feeding or breeding territory, equally contested and

defended by either sex. Some predictions of social selection are similar to those of species recognition (Payne 1983; West-Eberhard 1983), but there are differences that allow the predictions to be tested in fossil taxa such as ceratopsians. Two differences stand out: (1) socially selected traits can function in any phase of courtship or in social interactions outside of mating, whereas species recognition traits are under selection only in the earliest stages of courtship; and (2) socially selected traits may persist and diverge in allopatric isolated populations, whereas species recognition traits are only expected to occur in closely related sympatric species (West-Eberhard 1983, pp. 166-167).

The headbutting behavior inferred for derived centrosaurines would have been comparatively expensive and risky. In the extant caprines that show similar behaviors, headbutting is a late occurrence in intraspecific aggression, generally occurring after a series of visual and auditory displays (Geist 1966; Gray and Simpson 1980; Lent 1988; Weinberg 2002; Fedosenko and Blank 2005). In both caprines and helmeted hornbills, headbutting is a coordinated behavior in which both participants proceed through a series of stereotyped, ritualized behaviors before and after impact (Geist 1966; Kinniard et al. 2003; Fedosenko and Blank 2005). The presence of displays and coordinating behaviors leading up to headbutting in extant taxa suggests that the morphological changes seen in derived centrosaurine horns for headbutting were driven by selection on behaviors that occurred well after early and relatively inexpensive opportunities for species recognition by visual cues. Although they may have been exapted to function in species recognition, the rugose bosses of *Achelousaurus* and *Pachyrhinosaurus* do not match the pattern expected for species recognition without social selection.

Literature Cited

Baum DA, Larson A. 1991. Adaptation reviewed: A phylogenetic methodology for studying character macroevolution. Systematic Zoology 40:1–18.

Berger J, Cunningham C. 1998. Natural variation in horn size and social dominance and their importance to the conservation of black rhinoceros. Conservation Biology 12:708–711.

Bowyer RT, Leslie DM. 1992. *Ovis dalli*. Mammalian Species 393:1–7.

Brown B. 1914. *Anchiceratops*, a new genus of horned dinosaur from the Edmonton Cretaceous of Alberta. With discussion of the origin of the ceratopsian crest and the brain casts of *Anchiceratops* and *Trachodon*. Bulletin of the American Museum of Natural History 33:539–548.

Brown B, Schlaikjer EM. 1940. The origin of ceratopsian horn-cores. American Museum Novitates 1065:1–7.

Bustard HR. 1958. Use of horns by *Chamaeleo jacksoni*. British Journal of Herpetology 2:105–107.

Cats-Kuenen CSWM. 1961. Casque and bill of *Rhinoplax vigil* (Forst.) in connection with the architecture of the skull. Verhandelingen der Koninklijke Nederlandsche Academie van Wetenschappen, Afdeling Natuurkunde 53:1–51.

Coddington JA. 1988. Cladistic tests of adaptational hypotheses. Cladistics 4:3–22.

Coddington JA. 1990. Bridges between evolutionary pattern and process. Cladistics 6:379–386.

Cranbrook E, Kemp AC. 1995. Aerial casque-butting by hornbills (Bucerotidae): A correction and an expansion. Ibis 137:588–589.

Currie PJ. 1989. Long-distance dinosaurs. Natural History 6:60–65.

Currie PJ, Langston W, Jr., Tanke DH. 2008. A new species of *Pachyrhinosaurus* (Dinosauria, Ceratopsidae) from the Upper Cretaceous of Alberta, Canada. In: Currie PJ, Langston W, Jr., Tanke DH, editors. A New Horned Dinosaur From an Upper Cretaceous Bone Bed in Alberta. Ottawa: NRC Research Press. p 1–108.

Darwin C. 1871. The Descent of Man, and Selection in Relation to Sex. London: John Murray.

Dinerstein E. 1991. Sexual dimorphism in the greater one-horned rhinoceros (Rhinoceros unicornis). Journal of Mammalogy 72:450–457.

Edwards SJ, Russell AP. 1994. Bone tissue patterns and the growth of the nasal complex in the horned dinosaur *Pachyrhinosaurus*. Bulletin of the Canadian Society of Zoologists 25:47–48.

Eibl-Eibesfeldt I. 1966. The fighting behaviour of marine iguanas. Philosophical Transactions of the Royal Society, Series B, Biological Sciences 251:475–476.

Emlen ST, Oring LW. 1977. Ecology, Sexual Selection, and the Evolution of Mating Systems. Science 197:215–223.

Farke AA. 2004. Horn use in *Triceratops* (Dinosauria: Ceratopsidae): Testing behavioral hypotheses using scale models. Palaeontologica Electronica 7:10p.

Farlow JO, Dodson P. 1975. The behavioral significance of frill and horn morphology in ceratopsian dinosaurs. Evolution 29:353–361.

Fedosenko AK, Blank DA. 2001. *Capra sibirica*. Mammalian Species 675:1–13.

Fedosenko AK, Blank DA. 2005. *Ovis ammon*. Mammalian Species 773:1–15.

Fernández MH, Vrba ES. 2005. A complete estimate of the phylogenetic relationships in Ruminantia: A dated species-level supertree of the extant ruminants. Biological Reviews 80:269–302.

Geist V. 1966. The evolution of horn-like organs. Behaviour 27:175–214.

Goodwin MB, Clemens WA, Horner JR, Padian K. 2006. The smallest known *Triceratops* skull: New observations on ceratopsid cranial anatomy and ontogeny. Journal of Vertebrate Paleontology 26:103–112.

Gould SJ, Lewontin RC. 1979. The spandrels of San Marco and the Panglossian paradigm: A critique of the adaptationist programme. Proceedings of the Royal Society of London. Series B, Biological Sciences 205:581–598.

Gould SJ, Vrba ES. 1982. Exaptation; a missing term in the science of form. Paleobiology 8:4–15.

Grafen A. 1989. The phylogenetic regression. Philosophical Transactions of the Royal Society of London. Series B, Biological sciences 326:119–157.

Grandcolas P, d'Haese C. 2003. Testing adaptation with phylogeny: How to account for phylogenetic pattern and selective value together. Zoologica Scripta 32:483–490.

Granger WK, Gregory WK. 1923. *Protoceratops andrewsi*, a pre-ceratopsian dinosaur from Mongolia. American Museum Novitates 72:1–9.

Gray GG, Simpson CD. 1980. *Ammotragus lervia*. Mammalian Species 144:1–7.

Greene HW. 1986. Diet and arboreality in the emerald monitor, Varanus prasinus, with comments on the study of adaptation. Fieldiana Zoology 31:1–12.

Hassanin A, Ropiquet A. 2004. Molecular phylogeny of the tribe Bovini (Bovidae, Bovinae) and the taxonomic status of the Kouprey, *Bos sauveli* Urbain 1937. Molecular Phylogenetics and Evolution 33:896–907.

Hatcher JB, Marsh OC, Lull RS. 1907. The Ceratopsia. United States Geological Survey Monograph 49:1–300.

Homberger DG. 2001. The case of the cockatoo bill, horse hoof, rhinoceros horn, whale baleen, and turkey beard: The integument as a model system to explore the concepts of homology and non-homology. In: Dutta HM, Datta Munshi JS, editors. Vertebrate Functional Morphology: Horizon of Research in the 21st Century. Enfield: Science Publishers. p 317–343.

Horner JR, Goodwin MB. 2006. Major cranial changes during Triceratops ontogeny. Proceedings of the Royal Society B: Biological Sciences 273:2757–2761.

Horner JR, Goodwin MB. 2008. Ontogeny of cranial epi-ossifications in *Triceratops*. Journal of Vertebrate Paleontology 28:134–144.

Horner JR, Marshall C 2002. Keratinous covered dinosaur skulls. Journal of Vertebrate Paleontology 22:67A.

Jass CN, Mead JI. 2004. *Capricornis crispus*. Mammalian Species 750:1–10.

Kaiser HE. 1960. Untersuchungen zur vergleichenden Osteologie der fossilen und rezenten Pachyostosen. Palaeontographica Abteilung A 114:113–196.

Kemp AC. 1995. The Hornbills: Bucerotiformes. Oxford: Oxford University Press.

Kinniard MF, Hadiprakarsa Y-Y, Thiensongrusamee P. 2003. Aerial jousting by Helmeted Hornbills *Rhinoplax vigil*: Observations from Indonesia and Thailand. Ibis 145:506–508.

Kirkland J, DeBlieux D. 2007. New centrosaurine ceratopsians from the Wahweap Formation, Grand Staircase-Escalante National Monument, southern Utah. Abstract volume ref

Kluge AG. 2005. Testing lineage and comparative methods for inferring adaptation. Zoologica Scripta 34:653–663.

Lalueza-Fox C, Castresana J, Sampietro L, Marques-Bonet T, Alcover JA, Bertranpetit J. 2005. Molecular dating of caprines using ancient DNA sequences of Myotragus balearicus, an extinct endemic Balearic mammal. BMC Evolutionary Biology 5:70.

Lambe LM. 1904. On the squamoso-parietal crest of two species of horned dinosaurs from the Cretaceous of Alberta. Ottawa Naturalist 8:81–84.

Lambe LM. 1914. On the fore-limb of a carnivorous dinosaur from the Belly River Formation of Alberta, and a new genus of Ceratopsia from the same horizon, with remarks on the integument of some Cretaceous herbivorous dinosaurs. Ottawa Naturalist 27:129–135.

Landmann L. 1986. The skin of reptiles: Epidermis and dermis. In: Bereiter-Hahn J, Matoltsy AG, Richards KS, editors. Biology of the Integument, Volume 2: Vertebrates. Berlin: Springer-Verlag. p 150–187.

Lange B. 1931. Integument der sauropsiden. In: Bolk L, Goppert E, Kallius E, Lubosch W, editors. Handbuch der Vergleichenden Anatomie der Wirbeltiere. Berlin: Urban und Schwarzenberg. p 375–448.

Langston W, Jr. 1967. The thick-headed ceratopsian dinosaur *Pachyrhinosaurus* (Reptilia: Ornithischia), from the Edmonton Formation near Drumheller, Canada. Canadian Journal of Earth Sciences 4:171–186.

Langston W, Jr. 1975. The ceratopsian dinosaurs and associated lower vertebrates from the St. Mary River Formation (Maastrichtian) at Scabby Butte, southern Alberta. Canadian Journal of Earth Sciences 12:1576–1608.

Larson A, Losos JB. 1996. Phylogenetic systematic of adaptation. In: Rose MR, Lauder GV, editors. Adaptation. San Diego: Academic Press. p 187–220.

Lent PC. 1988. Ovibos moschatus. Mammalian Species 302:1–9.

Lundrigan B. 1996. Morphology of horns and fighting behavior in the family Bovidae. Journal of Mammalogy 77:462–475.

Maddison WP, Maddison DR. 2006. StochChar: A package of Mesquite modules for stochastic models of character evolution. v1.1. http://mesquiteproject.org.

Maddison WP, Maddison DR. 2008. Mesquite: A modular system for evolutionary analysis. v2.5. http://www.mesquiteproject.org.

Marsh OC. 1887. Notice of some new fossil mammals. American Journal of Science 34:323–331.

Maryańska T, Chapman RE, Weishampel DB. 2004. Pachycephalosauria. In: Weishampel DB, Dodson P, Osmólska H, editors. The Dinosauria, 2nd ed. Berkeley: University of California Press. p 464–477.

Mead JI. 1989. *Nemorhaedus goral*. Mammalian Species 335:1–5.

Meagher M. 1986. *Bison bison*. Mammalian Species 266:1–8.

Molnar RE. 1977. Analogies in the evolution of combat and display structures in ornithopods and ungulates. Evolutionary Theory 3:165–190.

Neas JF, Hoffman RS. 1987. *Budorcas taxicolor*. Mammalian Species 277:1–7.

Nowak RM, Paradiso JL. 1983. Walker's Mammals of the World, 4th ed. Baltimore: Johns Hopkins University Press.

Padian K, Horner JR, Dhaliwal J. 2004. Species recognition as the principal cause of bizarre structures in dinosaurs. Journal of Vertebrate Paleontology 24:100A.

Pagel M. 1992. A method for the analysis of comparative data. Journal of Theoretical Biology 156:431–442.

Pagel M. 1994. Detecting correlated evolution on phylogenies: A general method for the comparative analysis of discrete characters. Proceedings. Biological sciences 255:37.

Pagel M, Meade A. 2006. Bayesian analysis of correlated evolution of discrete characters by reversible-jump Markov chain Monte Carlo. The American Naturalist 167:808–825.

Pappas LA. 2002. *Taurotragus oryx*. Mammalian Species 689:1-–5.

Payne RB. 1983. Bird songs, sexual selection, and female mating strategies. In: Waser S, editor. Social Behavior of Female Vertebrates. New York: Academic Press. p 55–90.

Reznick D, Travis J. 1996. The empirical study of adaptation in natural populations. In: Rose MR, Lauder GV, editors. Adaptation. San Diego: Academic Press. p 243–289.

Rideout CB, Hoffman RS. 1975. *Oreamnos americanus*. Mammalian Species 63:1–6.

Ropiquet A, Hassanin A. 2005. Molecular phylogeny of caprines (Bovidae, Antilopinae): The question of their origin and diversification during the Miocene. Journal of Zoological Systematics and Evolutionary Research 43:49–60.

Ryan MJ, Russell AP. 2005. A new centrosaurine ceratopsid from the Oldman Formation of Alberta and its implications for centrosaurine taxonomy and systematics. Canadian Journal of Earth Sciences 42:1369–1387.

Ryan et al., in press. New Ceratopsian book. Indiana University Press: Bloomington.

Sampson SD. 1995. Two horned dinosaurs from the Upper Cretaceous Two Medicine Formation of Montana; with a phylogenetic analysis of the Centrosaurinae (Ornithischia: Ceratopsidae). Journal of Vertebrate Paleontology 15:743–760.

Sampson SD, Ryan MJ, Tanke DH. 1997. Craniofacial ontogeny in centrosaurine dinosaurs (Ornithischia: Ceratopsidae): Taxonomic and behavioral implications. Zoological Journal of the Linnean Society 121:293–337.

Sawyer RH, Knapp LW, O'Guin WM. 1986. The skin of birds: Epidermis, dermis, and appendages. In: Bereiter-Hahn J, Matoltsy AG, Richards KS, editors. Biology of the Integument, Volume 2: Vertebrates. Berlin: Springer-Verlag. p 194–238.

Shackleton DM. 1985. *Ovis canadensis*. Mammalian Species 230:1–9.

Shadwick RE, Russell AP, Lauff RF. 1992. The structure and mechanical design of rhinoceros dermal armour. Philosophical transactions of the Royal Society of London. Series B, Biological sciences 337:419–428.

Sinervo B, Basolo AL. 1996. Testing adaptation using phenotypic manipulations. In: Rose MR, Lauder GV, editors. Adaptation. San Diego: Academic Press. p 149–185.

Sober E. 1984. The Nature of Selection. Cambridge: MIT Press.

Sokolov VE. 1982. Mammal skin. Berkeley: University of California Press.

Spassov NB. 1979. Sexual selection and the evolution of horn-like structures of ceratopsian dinosaurs. Paleontology Stratigraphy Lithology 11:37–48.

Sterchi DL, Eurell JA. 1989. A new method for preparation of undecalcified bone sections. Stain Technology 64:201–205.

Sternberg CM. 1950. *Pachyrhinosaurus canadensis*, representing a new family of the Ceratopsia, from southern Alberta. Bulletin of the National Museum of Canada 118:109–120.

Vickaryous MK, Russell AP, Currie PJ. 2001. Cranial ornamentation of ankylosaurs (Ornithischia:Thyreophora): Reappraisal of developmental hypotheses. In:

Carpenter K, editor. The Armored Dinosaurs. Bloomington: Indiana University Press.

Wang X, Hoffman RS. 1987. *Pseudois nayaur* and *Pseudois schaeferi*. Mammalian Species 278:1–6.

Weinberg PJ. 2002. *Capra cylindricornis*. Mammalian Species 695:1–9.

West-Eberhard MJ. 1983. Sexual selection, social competition, and speciation. The Quarterly Review of Biology 58:155–183.

Witmer LM. 1995. The extant phylogenetic bracket and the importance of reconstructing soft tissues in fossils. In: Thomason J, editor. Functional Morphology in Vertebrate Paleontology. Cambridge: Cambridge University Press. p 19–33.

CHAPTER 6: EVIDENCE FOR DERMAL ARMOUR AND FACE BITING BEHAVIOUR IN PREDATORY ABELISAURID DINOSAURS

Abstract

Dinosaurs show many striking examples of bizarre bony ornaments. In most cases, these bony features are thought to have functioned as visual displays, but whether the evolution of these structures was driven by sexual selection or by species recognition is a current point of contentio (Sampson et al. 1997; Padian et al. 2004; Goodwin et al. 2006). The bony ornaments of abelisaurid theropod dinosaurs such as *Majungasaurus crenatissimus* include gnarled, rugose bone across the skull roof and deeply incised neurovascular grooves across the lateral aspect of the skull. Similar features in other abelisaurid theropods have been tentatively interpreted as evidence of a continuous sheath of horny skin on the head (Sereno and Brusatte 2008). Evaluation of the fine-structural details of these bony ornaments provides tests of such hypotheses and allows assessment of the significance of these features for the form and function of the overlying skin. Here we show that the rugose bony ornamentation on the skull roof of *Majungasaurus* is causally related to a skin architecture that functions as body armour in many extant amniotes (Shadwick et al. 1992). Histological sections show the rugose bone of the skull roof to be composed of ossified remnants of the dermis that preserve large (~50–200 μm in diameter) collagen fiber bundles in crossed arrays. This form of bone tissue is only found in conjunction with thick, armour-like dermis (e.g., rhinoceros hide) in living amniotes, where it is consistently associated with violent agonistic behaviours. Head-biting is suggested as the most conservative inference for agonistic behaviour in

Majungasaurus. The bony ornaments of *Majungasaurus* do not match predictions for structures involved in sexual display (Darwin 1871), but the risk of the inferred agonistic behaviours associated with these structures is also incongruent with species recognition (West-Eberhard 1983). We suggest that strong intraspecific competition over limited resources (Rogers et al. 2007) drove the diversification of bony ornaments in abelisaurid theropods by the process of social selection (West-Eberhard 1983).

Introduction

Gnarled, rugose skull bones are characteristic features of abelisaurid theropod dinosaurs (Fig. 6-1). The prominent grooving and pitting that makes up much of this rugosity has been linked to the presence of heavily keratinized skin structures in life (Sereno and Brusatte 2008), as these bony features in abelisaurids are similar to the bony supports of bird beaks, bovid horns, and other examples of heavily keratinized skin in extant vertebrates (Chapter 5; Fig. 6-1).

Although grooving and pitting on abelisaurid skulls is indeed extensive, a separate form of rugose bone, formed by projecting bone spicules, is also present across the skull roof of *Majungasaurus*. The difference in bone surface texture between the skull roof and lateral surfaces of the skull has previously been noted (Hieronymus and Witmer 2004; Sampson and Witmer 2007), but the relationship between this bone morphology and the structure of overlying skin has not been assessed. In this study we examined the gross morphology and osteohistology of the projecting bone spicules of *Majungasaurus* in comparison with a broad synoptic sample of cephalic skin-to-bone contacts in living amniotes. Strong similarities in both gross morphology and histology between

Majungasaurus and living animals allow us to draw a series of robust inferences about skin structure in *Majungasaurus*, which in turn provide tests of functional hypotheses relating to these structures.

Results and Discussion

Bone spicules on *Majungasaurus* are generally subcircular in cross-section and range from 1–2 mm in diameter and height. Several adjacent spicules may occasionally fuse to form a larger area of tuberculate rugosity. The morphology and size range of projecting bone spicules on *Majungasaurus* is very similar to that seen on adult skulls of several large-bodied extant mammals, including *Hippopotamus*, the African suids *Hylochoerus* and *Potamochoerus*, and most extant species of rhinoceros (Fig. 6-2).

Projecting bone spicules on the skull roof of *Majungasaurus* are arranged in discrete fields. A median field covers the dorsal surfaces of the premaxillae, nasals, frontals, and parts of the postorbitals; two smaller lateral fields cover the auricular processes of the nasals and the dorsolateral surfaces of the lacrimals and postorbitals (Fig. 6-1). Fields of projecting rugosity are thus placed at the 'edges' of the skull roof, on areas that stand out from the general shape of the head. This distribution is again similar to the distribution of projecting bone spicules seen on *Hippopotamus*, suids, and rhinoceros (Fig. 6-2).

Paleohistological analysis of the projecting bone spicules of *Majungasaurus* shows these features to be composed of metaplastic bone (Haines and Mohuiddin 1968) with large (~50–200 μm) bundles of extrinsic fibers derived from the overlying dermis. These extrinsic fiber bundles are oriented at alternating oblique angles to the underlying

dermatocranium (Fig. 6-3). Projecting bone spicules on the skulls of white rhinoceros (*Ceratotherium simum*) show a similar organization of metaplastic bone, which forms as a result of ossification of the deep dermis and superficial fascia of the skin. The alternating oblique angles of extrinsic fiber bundles in *Majungasaurus* projecting bone spicules indicate that the deep dermis of these dinosaurs showed crossed-array dermal architecture (CADA), a trait that has evolved convergently in rhinoceros (Shadwick et al. 1992), *Hippopotamus* (Schumacher 1931), suids (Fradrich 1974; Sokolov 1982), and several other extant mammals (Dubost and Terrade 1970). In mammalian taxa with CADA, the random feltwork of collagen fiber bundles typical of mammalian skin is replaced by dense, highly organized arrays of thick collagen fiber bundles (Chapter 2). CADA greatly increases the stiffness of the skin, resulting in a compressive modulus similar to that of hyaline cartilage (Shadwick et al. 1992). The increased stiffness of CADA allows the dermis to function as body armour, protecting areas that are prone to injury (Shadwick et al. 1992).

Character correlation tests (supplementary material/Chapter 2) show that CADA is consistently associated with the use of specialized, sharpened, mesial teeth in violent agonistic behaviours in extant mammals. Many of the taxa with CADA included in the character correlation test use sharpened tusks as their primary weapons in agonistic encounters (e.g., Indian rhinoceros, elephant seals, rock hyrax; Nowak and Paradiso 1983; Dinerstein 1991). The areal extent of CADA in the skin of these taxa closely matches the areas that are most often injured in fighting, such as the face, shoulders, or haunches (Dubost and Terrade 1970; Sokolov 1982; Shadwick et al 1992). Thus, the

presence of CADA across the skull roof in *Majungasaurus* indicates that this region was prone to injury or a common target during fighting. Head-biting has been suggested as a common behaviour for theropod dinosaurs in general based on paleopathological evidence including tooth marks on the skulls and mandibles of several theropod taxa (Tanke and Currie 1998). Given that *Majungasaurus* has no other obvious weapons, head-biting stands as the most conservative inference for violent agonistic behaviour in these animals.

The osteological correlates for CADA are not unique to *Majungasaurus*, but are instead part of a suite of bone "sculpturing" that is a synapomorphy of Abelisauridae (Sereno and Brusatte 2008). Some other abelisaurid taxa (*Abelisaurus*, *Carnotaurus*) show projecting rugosity on the nasals and frontals alongside pitting and grooving on the maxillae (Bonaparte and Novas 1985, Bonaparte et al. 1990). Projecting rugosity may also be present in other abelisaurids (Coria and Salgado 1998; Coria et al. 2002; Wilson et al 2003; Calvo et al. 2004; Sereno et al. 2004) Applying the character correlation between CADA and violent agonistic behaviour from extant taxa to abelisauroid theropods yields a range of possible scenarios for the transition to more violent agonistic behaviours within Abelisauridae (Fig. 6-4), either as a general trait of abelisaurids that arises in the Early Cretaceous, or as convergent occurrences in *Abelisaurus*, *Carnotaurus*, and *Majungasaurus* in the Late Cretaceous.

The convergent evolution of CADA in abelisaurids and extant taxa provides the strongest, most direct evidence for the inference of violent agonistic behaviours, but several other novel features also provide *post hoc* support for increasing intraspecific

aggression within Abelisauridae relative to other ceratosaurs (Fig. 6-4). For example, several bony outgrowths that appear to be the result of additional metaplastic bone growth in dermal tissue cover parts of the lateral aspect of the skull (e.g., the suborbital flange [Carrano and Sampson 2008]). The pitting and grooving of the maxillae and dentaries characteristic of Abelisauridae is a robust osteological correlate for the presence of a thick sheet of heavily keratinized skin, providing an additional resistant covering for the face. This pitting and grooving extends into the oral cavity on the interdental plates, indicating that abelisaurid oral cavities also bore a resistant, heavily keratinized epithelium. Adult *Hippopotamus* show a similar extension of projecting rugose bone from the maxillae and premaxillae onto the hard palate.

Sexual selection and species recognition have been suggested as two prominent selection regimes that drove morphological variation in the bony ornaments seen on many dinosaurs (Sampson et al. 1997; Goodwin et al. 2006). The predictions of both hypotheses are similar in many respects, but salient differences allow each alternative to be tested separately. Morphological change driven by sexual selection is expected to result in sexual dimorphism (Darwin 1871; Emlen and Oring 1977), whereas change driven by species recognition is more likely to result in monomorphism (Goodwin et al. 2006). Although there is considerable morphological variation in rugose bone on skull roof elements referred to *Majungasaurus*, there is currently no evidence for the bimodal pattern of morphological variation that would be expected if these ornaments were sexually dimorphic (Sampson and Witmer 2007). Thus, there is no justification to assert

that CADA and violent agonistic behaviours in abelisaurid theropods are the products of sexual selection.

Morphological change driven by species recognition is expected to result in features that function in the early phases of courtship or confrontation (West-Eberhard 1983; Goodwin et al. 2006). Species recognition features provide an energetically inexpensive 'first approximation' for recognizing conspecifics before committing to more costly courtship or territoriality displays. The violent agonistic behaviours associated with CADA are risky (Dinerstein 1991), and are only seen after an escalating series of cheaper visual and vocal displays in extant taxa (Kingdon 1988). CADA is thus not likely to be subject to selection for species recognition.

We propose that violent intraspecific agonistic behaviours in *Majungasaurus* and other abelisaurid theropods, together with associated morphological changes in the facial skin and skull, were driven by intense intraspecific competition for limited resources in a pattern known as "social selection" (West-Eberhard 1983). Paleoenvironmental analyses of sediments in the late Campanian to Maastrichtian Maeverano Formation beds that preserve *Majungasaurus* indicate a highly seasonal environment (Rogers et al. 2007). Strong seasonality, and the accompanying changes in resource availability, may have maintained social selection pressure in *Majungasaurus* by creating a temporally patchy distribution of resources that could have been monopolized by dominant individuals. Social selection is expected to produce patterns of morphological divergence similar to those driven by sexual selection, but if both sexes compete equally for a limited resource

(e.g., a temporally patchy food resource), the resulting morphological changes are expected to be sexually monomorphic (West-Eberhard 1983).

Identifiable tooth marks on the ribs and vertebrae of several specimens of *Majungasaurus* have indicated that these animals engaged in cannibalism (Rogers et al 2003), adding another independent line of evidence that leads to a picture of *Majungasaurus* as a large predator that may have frequently been as aggressive towards conspecifics as it was towards potential prey. With the morphological (Fig. 6-3) and evolutionary (Fig. 6-4) evidence from this study complementing existing paleoenvironmental (Rogers et al. 2007), taphonomic (Rogers et al 2003), and morphological data (Sampson and Witmer 2007), *Majungasaurus* stands as one of the best-understood examples of agonistic behaviour in theropod dinosaurs, and provides a "model taxon" for testing paleobiological and paleoecological hypotheses for theropod dinosaurs in general.

Methods Summary

Osteological survey

Gross morphology of bony ornamentation on *Majungasaurus* specimens was compared to a broad sample of amniote skeletal material. Relationships between bony features and overlying skin in a subsample of extant taxa were explored by means of a recursive partitioning analysis (RPA) using the JMP 7.0 statistical software package (Hieronymus et al in review /Chapter 5). A synthesis of the resulting quantitatively-defined osteological correlates and traditional anatomically-defined osteological

correlates provided the first line of evidence to interpret unpreserved skin structures in *Majungasaurus*.

Histological Survey

A left lacrimal of *Majungasaurus crenatissimus* (UA 8718) provided a sample of rugose bone surface. This sample was μCT scanned to produce an archival record of morphology with a GE eXplore Locus Small Animal μCT Scanner. Scan parameters were as follows: slice thickness of 45 μm (isotropic voxels), 80 kV, 500 μA, 800 ms, 3600 views. The resulting volume data (in VFF format) were exported from MicroView 2.1.2 (open-source software developed by GE; microview.sourceforge.net) in DICOM format, which were then subsequently imported into Amira 3.1.1 or 4.1.1 (Mercury-TGS, Chelmsford, MA) for viewing, analysis, and visualization. The bone sample was molded and cast to produce a physical replica, then processed for paleohistological sectioning using standard protocols (Wilson 1994). A synoptic sample of histological sections from extant amniote skin and calcified bone tissues was prepared using a modified hard-plastic embedding protocol (Sterchi and Eurell 1989) to allow the visualization of semithin sectioned bone tissue with known skin structures *in situ* (see Chapter 5 for details of paleohistological and histological protocols). Qualitatively defined histological correlates provided the second line of evidence to interpret unpreserved skin structures in *Majungasaurus*.

Comparative Analyses

To assess the relationship between CADA and agonistic behaviour, categorical character states for skin (Sokolov 1982) and agonistic behaviour (Nowak and Paradiso

1983) in extant mammals were placed in the context of a composite phylogeny (Arnason and Janke 2002; Fernandez and Vrba 2005; Kriegs et al 2006) and analyzed with Pagel's Omnibus Test of character correlation (Pagel 1994) in Mesquite 2.5 (Maddison and Maddison 2008), using 10 likelihood searches and 1000 Markov chain Monte Carlo replicates. See Chapter 2 for a more thorough discussion of this analysis.

Literature Cited

Arnason U, Janke A. 2002. Mitogenomic analyses of eutherian relationships. Cytogenetic and Genome Research 96(1-4):20.

Bonaparte JF, Novas FE. 1985. Abelisaurus comahuensis, n. gen., n. sp., Carnosauria del Cretacio tarido de Patagonia. Ameghiniana 21:259-265.

Bonaparte JF, Novas FE, Coria RA. 1990. Carnotaurus sastrei Bonaparte, the horned, lightly built carnosaur from the middle Cretaceous of Patagonia. Contributions to Science, Natural History Museum of Los Angeles County 416:1-42.

Calvo JO, Rubilar-Rogers D, Moreno K. 2004. A new Abelisauridae (Dinosauria: Theropoda) from northwest Patagonia. Ameghiniana 41:555-563.

Carrano MT, Sampson SD. 2008. The phylogeny of Ceratosauria (Dinosauria: Theropoda). Journal of Systematic Palaeontology 6:183-236.

Coria RA, Chiappe LM, Dingus L. 2002. A new close relative of Carnotaurus sastrei Bonaparte 1985 (Theropoda: Abelisauridae) from the Late Cretaceous of Patagonia. Journal of Vertebrate Paleontology 22(2):460-465.

Coria RA, Salgado L. 1998. A basal Abelisauria Novas 1992 (Theropoda-Ceratosauria) from the Cretaceous of Patagonia, Argentina. GAIA 15:89-102.

Darwin C. 1871. The Descent of Man, and Selection in Relation to Sex. London: John Murray.

Dinerstein E. 1991. Sexual dimorphism in the greater one-horned rhinoceros (Rhinoceros unicornis). Journal of Mammalogy 72(3):450-457.

Dubost G, Terrade R. 1970. La transformation de la peau des Tragulidae en bouclier protecteur. Mammalia 34:505-513.

Emlen ST, Oring LW. 1977. Ecology, Sexual Selection, and the Evolution of Mating Systems. Science 197(4300):215-223.

Fernández MH, Vrba ES. 2005. A complete estimate of the phylogenetic relationships in Ruminantia: a dated species-level supertree of the extant ruminants. Biological Reviews 80(2):269-302.

Fradrich H. 1974. A comparison of behaviour in the Suidae. In: Geist V, Walther F, editors. The Behavior of Ungulates and its Relation to Management: I.U.C.N. Publication, New Series. p 133-143.

Goodwin MB, Clemens WA, Horner JR, Padian K. 2006. The smallest known Triceratops skull: new observations on ceratopsid cranial anatomy and ontogeny. Journal of Vertebrate Paleontology 26(1):103-112.

Haines RW, Mohuiddin A. 1968. Metaplastic bone. Journal of anatomy 103(3):527-538.

Hieronymus TL, Witmer LM. 2004. Cranial rugosity and dinosaur "horns:" Rhino and giraffe as model systems for skin reconstruction in fossil taxa. Journal of Vertebrate Paleontology 24(3, suppl.):70A.

Kingdon J. 1988. East African Mammals: An Atlas of Evolution in Africa, Volume 3, Part B (Large Mammals). Chicago: University of Chicago Press. 450 p.

Kriegs JO, Churakov G, Kiefmann M, Jordan U, Brosius J, Schmitz J. 2006. Retroposed elements as archives for the evolutionary history of placental mammals. PLoS biology 4(4):e91.

Maddison WP, Maddison DR. 2008. Mesquite: a modular system for evolutionary analysis. Version 2.5: http://www.mesquiteproject.org.

Nowak RM, Paradiso JL. 1983. Walker's Mammals of the World. Nowak RM, Paradiso JL, editors. Baltimore: Johns Hopkins University Press. 2 v. (xliv, 1362, xxv p.) : p.

Padian K, Horner JR, Dhaliwal J. 2004. Species recognition as the principal cause of bizarre structures in dinosaurs. Journal of Vertebrate Paleontology 24(3(suppl.)):100A.

Pagel M. 1994. Detecting Correlated Evolution on Phylogenies: A General Method for the Comparative Analysis of Discrete Characters. Proceedings Biological sciences 255(1342):37.

Rogers RR, Krause DW, Curry Rogers K. 2003. Cannibalism in the Madagascan dinosaur Majungatholus atopus. Nature 422:515-518.

Rogers RR, Krause DW, Rogers KC, Rasoamiaramanana AH, Rahantarisoa L. 2007. Paleoenvironment and paleoecology of Majungasaurus crenatissimus (Theropoda: Abelisauridae) from the Late Cretaceous of Madagascar. Journal of Vertebrate Paleontology 27(sp8):21-31.

Sampson SD, Ryan MJ, Tanke DH. 1997. Craniofacial ontogeny in centrosaurine dinosaurs (Ornithischia: Ceratopsidae): Taxonomic and behavioral implications. Zoological Journal of the Linnean Society 121:293-337.

Sampson SD, Witmer LM. 2007. Craniofacial anatomy of Majungasaurus crenatissimus (Theropoda: Abelisauridae) from the Late Cretaceous of Madagascar. Journal of Vertebrate Paleontology 27(sp8):32-102.

Schumacher Sv. 1931. Integument der Mammalier. In: L. Bolk EG, E. Kallius, W. Lubosch, editor. Handbuch der Vergleichenden Anatomie der Wirbeltiere. Berlin: Urban und Schwarzenburg. p 449-504.

Sereno PC, Brusatte SL. 2008. Basal abelisaurid and carcharodontosaurid theropods from the Lower Cretaceous Elrhaz Formation of Niger. Acta Palaeontologica Polonica 53(1):15-46.

Sereno PC, Wilson JA, Conrad JL. 2004. New dinosaurs link southern landmasses in the Mid-Cretaceous. Proceedings of the Royal Society B: Biological Sciences 271(1546):1325-1330.

Shadwick RE, Russell AP, Lauff RF. 1992. The structure and mechanical design of rhinoceros dermal armour. Philosophical transactions of the Royal Society of London Series B, Biological sciences 337(1282):419-428.

Sokolov VE. 1982. Mammal skin. Berkeley: University of California Press. vii, 695 p. : p.

Sterchi DL, Eurell JA. 1989. A new method for preparation of undecalcified bone sections. Stain Technology 64:201-205.

Tanke DH, Currie PJ. 1998. Head-biting behavior in theropod dinosaurs: Paleopathological evidence. Gaia 15:167-184.

West-Eberhard MJ. 1983. Sexual Selection, Social Competition, and Speciation. The Quarterly Review of Biology 58(2):155-183.

Wilson J. 1994. Histological techniques. In: Leiggi P, May P, editors. Vertebrate Paleontological Techniques. Cambridge: Cambridge University Press. p 205-234.

Wilson JA, Sereno PC, Srivastava S, Bhatt DK, Khosla A, Sahni A. 2003. A new abelisaurid (Dinosauria, Theropoda) from the Lameta Formation (Cretaceous, Maastrichtian) of India. Contributions for the Museum of Paleontology, University of Michigan 31:1-42.

FIGURES AND FIGURE CAPTIONS

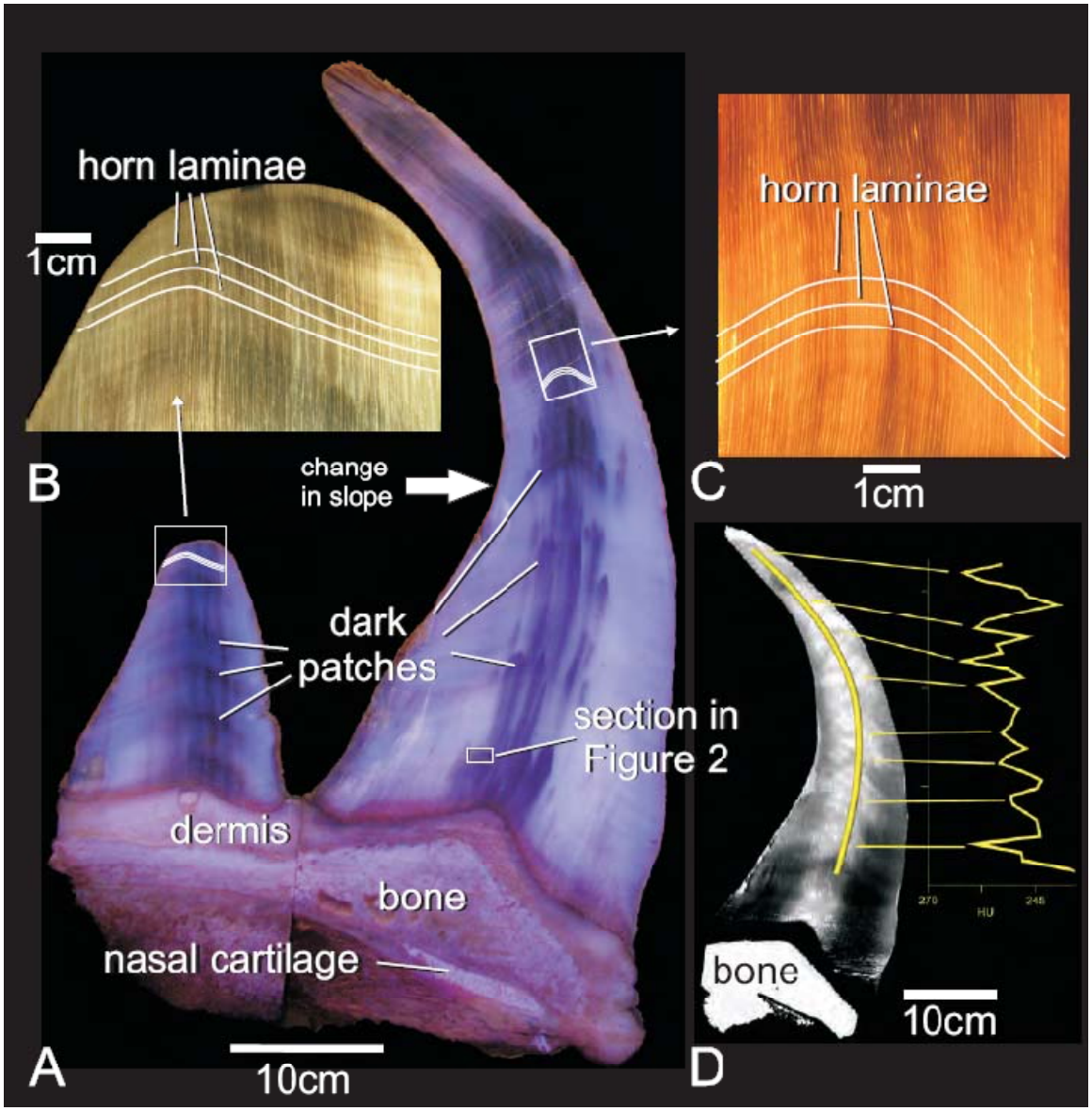

Figure 1-1. Nasal and frontal horns of white rhinoceros (*Ceratotherium simum*, OUVC 9541) in sagittal section, as viewed under fluorescent light (A), white light (B, C), and by CT (D). Note the fine horn lamellae (B, C) as well as the periodic alternation of dark patches (A). Small box in A shows area sampled for histological section in Figure 1-2. Arrow in A shows a break in the curvature of the nasal horn, most likely related to a decreased rate of wear of the more calcified and melanized horn. Strong overlap exists between the melanized dark patches (A) and radiodense patches in CT scan (D). The line probe next to the CT scout in D shows this change in radiodensity in Hounsfield units.

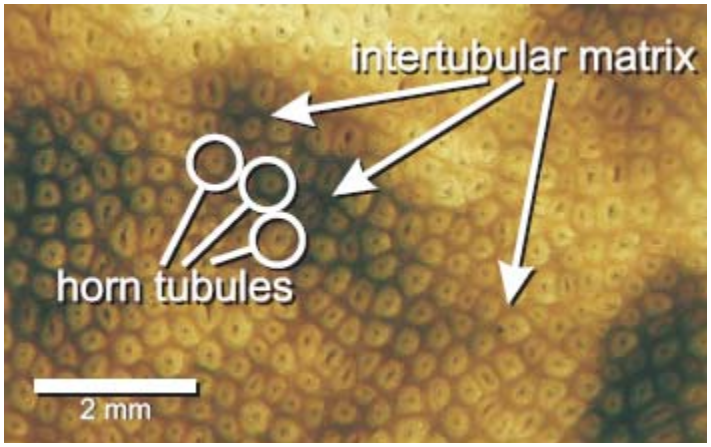

Figure 1-2. Transmitted light view of a thick section (200µm) of white rhinoceros horn from the center of a dark patch, showing areas of melanized intertubular matrix surrounding lighter horn tubules. *Ceratotherium simum*, OUVC 9541.

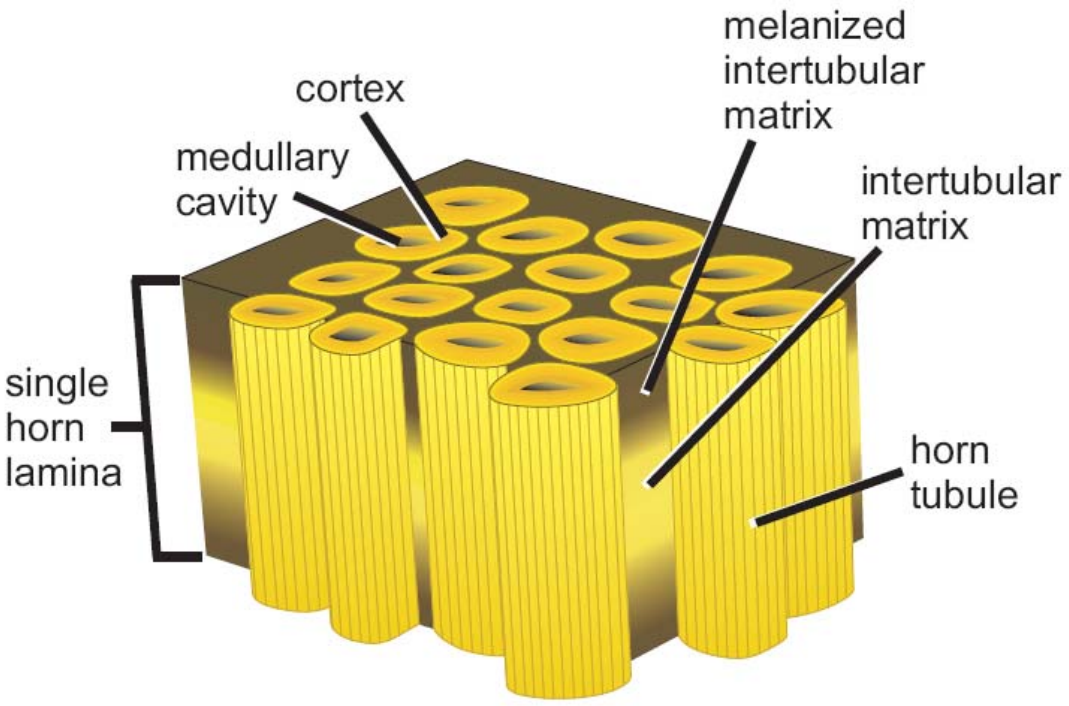

Figure 1-3. Schematic of white rhinoceros horn showing horn tubules, each with cortex and medullary cavity, as well as melanized and non-melanized intertubular matrix, together composing one horn lamina.

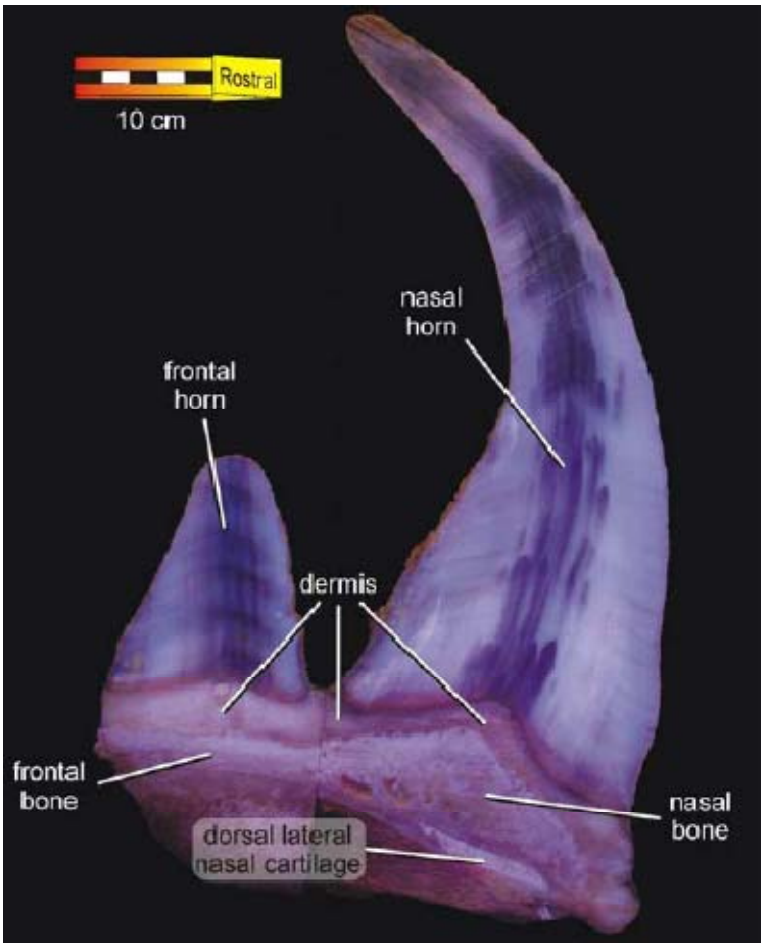

Figure 2-1. Sagittal section of white rhinoceros rostrum (Ceratotherium simum, OUVC 9541).The dermis that attaches the horns to the skull retains the thickness seen in other regions. For details of horn structure and growth, see Hieronymus et al. (2006).

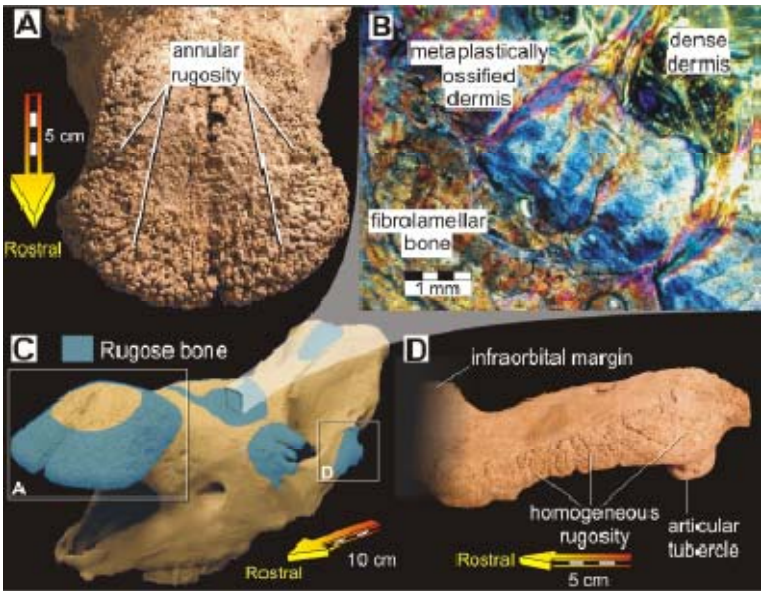

Figure 2-2. Anatomy and histology of rhinoceros horn attachment. (A) Nasal rugosity of white rhinoceros (United States National Museum [USNM] 164598), showing annular rugosity prominent near the edge of the overlying nasal horn. (B) Histological section of the bone-dermis border beneath white rhinoceros frontal horn (Ohio University Vertebrate Collections [OUVC] 9541) illuminated in plane polarized light, showing underlying fibrolamellar bone of the frontal, metaplastically ossified dermis forming the rugose bone of an annular rugosity, and the overlying fibers of the dense dermis. (C) Areas of rugose bone on white rhinoceros skull. (D) Position of homogeneous rugosity on an Indian rhino squamosal (USNM 545848), relative to articular tubercle and infraorbital margin.

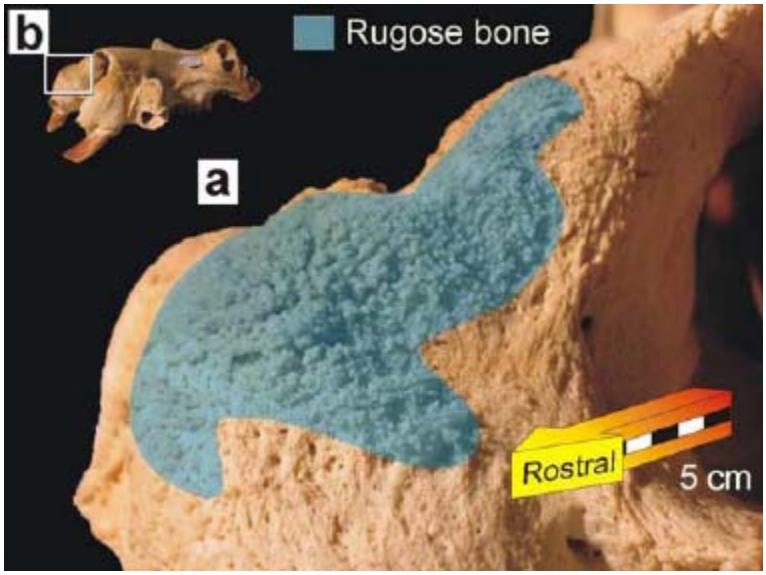

Figure 2-3. Rugose bone on the premaxilla of *Hippopotamus amphibius*, United States National Museum of Natural History (USNM) 313712. (A) The area of bone marked in blue shows a pronounced rugose surface, very similar in form to the rugosities on extant and extinct rhinocerotids. *Hippopotamus* and its sister taxon *Hexaprotodon* display an area of rugose bone distal to the canine fossa of the maxilla in addition to the area shown here, both areas that are in close contact with aggressors during agonistic behaviors (Kingdon 1979). (B**)** Inset box shows the location of A on the skull.

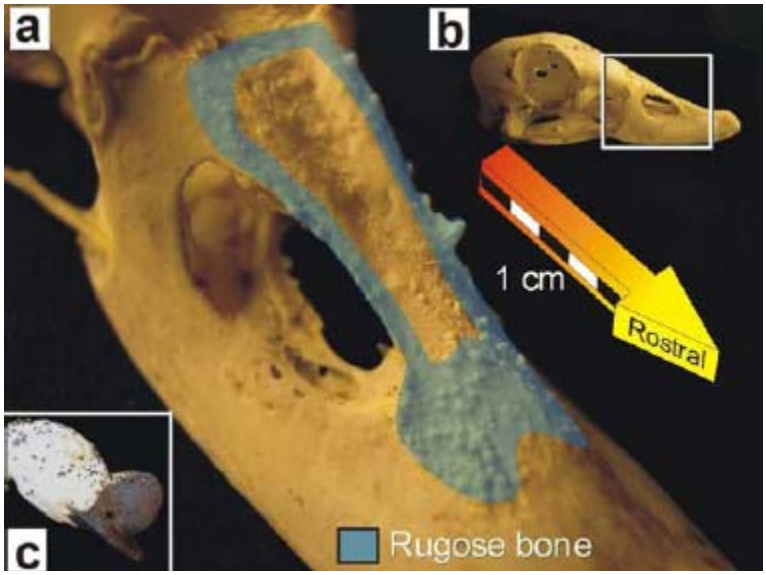

Figure 2-4. Rugose bone on the nasals and premaxillae of the comb duck *Sarkidiornis melanotos*. (A) The area of bone marked in blue constitutes an annular rugosity, similar in morphology to those seen beneath rhinoceros horns, but at a smaller scale (Royal Ontario Museum [ROM] 120525). (B) Inset box shows the location of a on the skull. (C) Study skin (ROM 91881) showing the 'comb,' a solid fleshy appendage composed primarily of elaborated dermis.

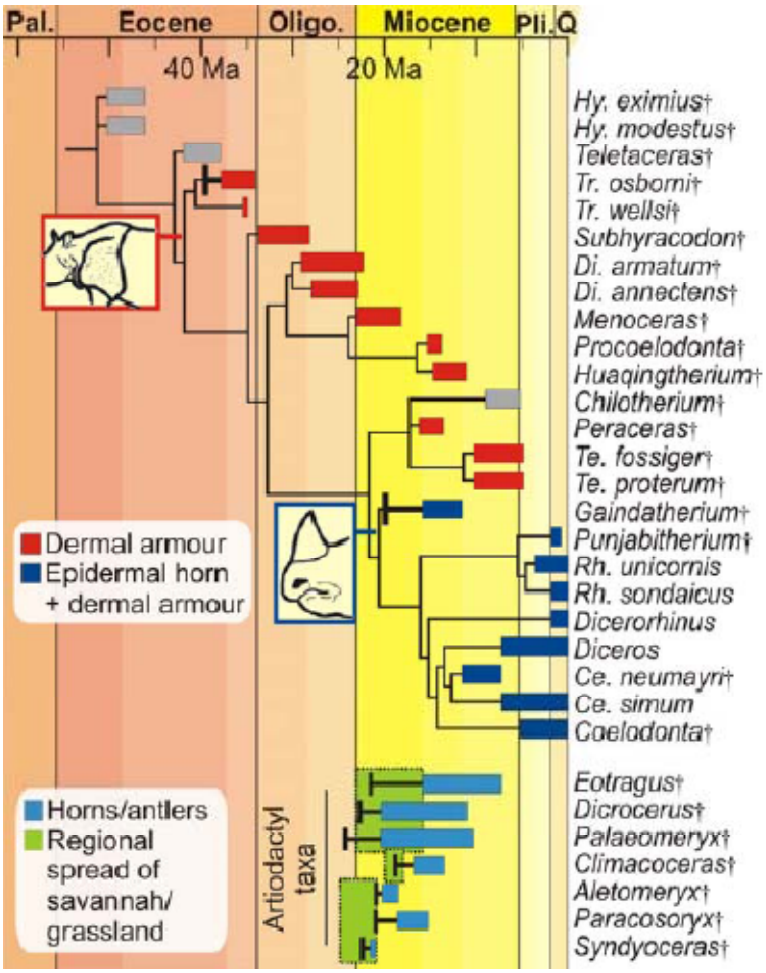

Figure 2-5. Schematic of rhinocerotid dermal body armor and horn evolution. Solid bars show time range of known fossil occurrences; whiskers show Strauss and Sadler stratigraphic 95% confidence intervals (Strauss and Sadler 1989) on first appearances of indicated taxa. Dermal body armor characterizes rhinocerotids more derived than Teletaceras, with first recorded appearance in *Trigonias osborni* (38–40 Ma). Epidermal horns characterize crown rhinocerotids + *Gaindatherium*, with first recorded appearance in *Gaindatherium* (16–20 Ma). First appearance of epidermal horns in rhinocerotids is congruent with grassland spread and the first appearance of cranial appendages in *Eotragus*, *Dicrocerus*, and *Palaeomeryx* (Eurasia); *Climacoceras* (Africa); and *Aletomeryx*, *Paracosoryx*, and *Syndyoceras* (North America). Genus name abbreviations: (Hy) *Hyrachyus*, (Tr) *Trigonias*, (Di) *Diceratherium*, (Te) *Teleoceras*, (Rh) *Rhinoceros*, (Ce) *Ceratotherium*.

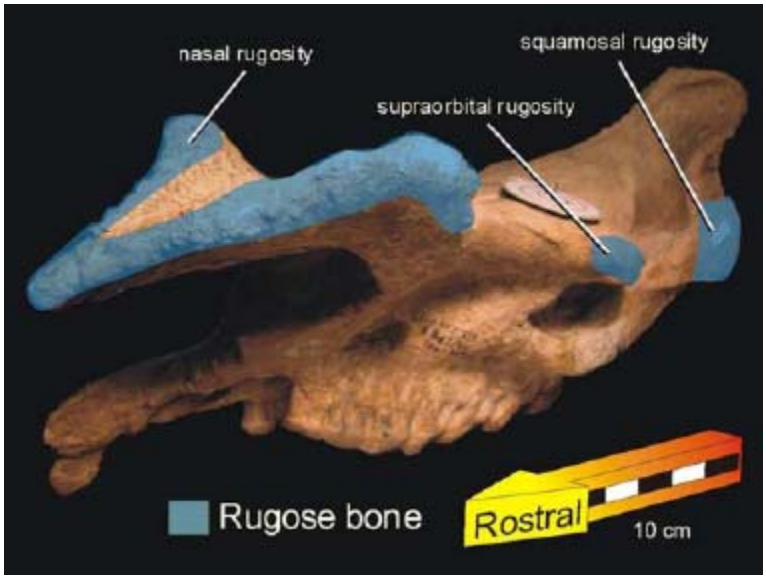

Figure 2-6. Skull of *Diceratherium armatum* (American Museum of Natural History Fossil Mammals [AMNH FM] 112176), showing the distribution of rugose bone surfaces. Pronounced rugosities occur on projecting surfaces of the skull. The long arch of the nasal rugosity has been previously reconstructed as bearing short laterally paired horns. The nasal rugosities sampled from this taxon were homogeneous, and did not show the annular structure associated with epidermal horns.

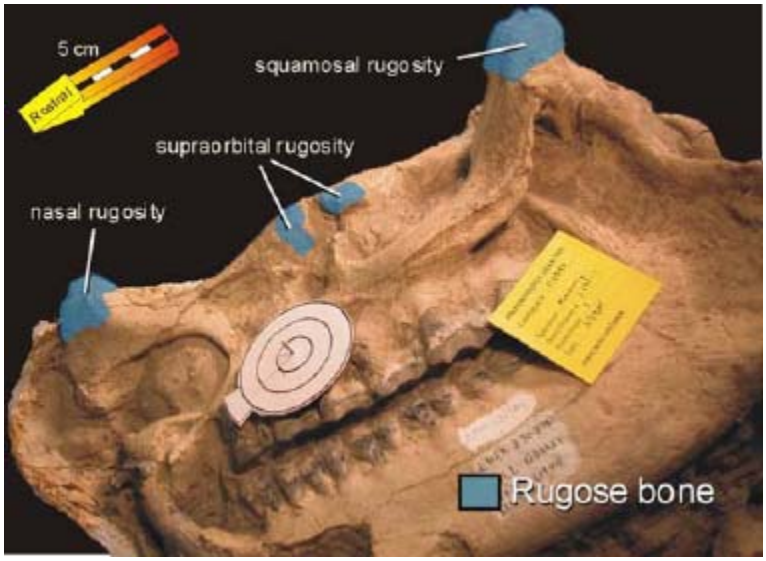

Figure 2-7. Skull of *Menoceras arikarense* (AMNH FM 112246), showing the distribution of rugose bone surfaces. As in *Diceratherium*, rugosities are associated with projecting bone surfaces, most notable on the squamosal rugosity, and are homogeneous. Rugose bone on the squamosal is prominent in many rhinocerotids, including the extant basal rhinocerotids (*Rhinoceros* and *Dicerorhinus*) and the elasmotherine lineage (e.g. *Iranotherium*; 14).

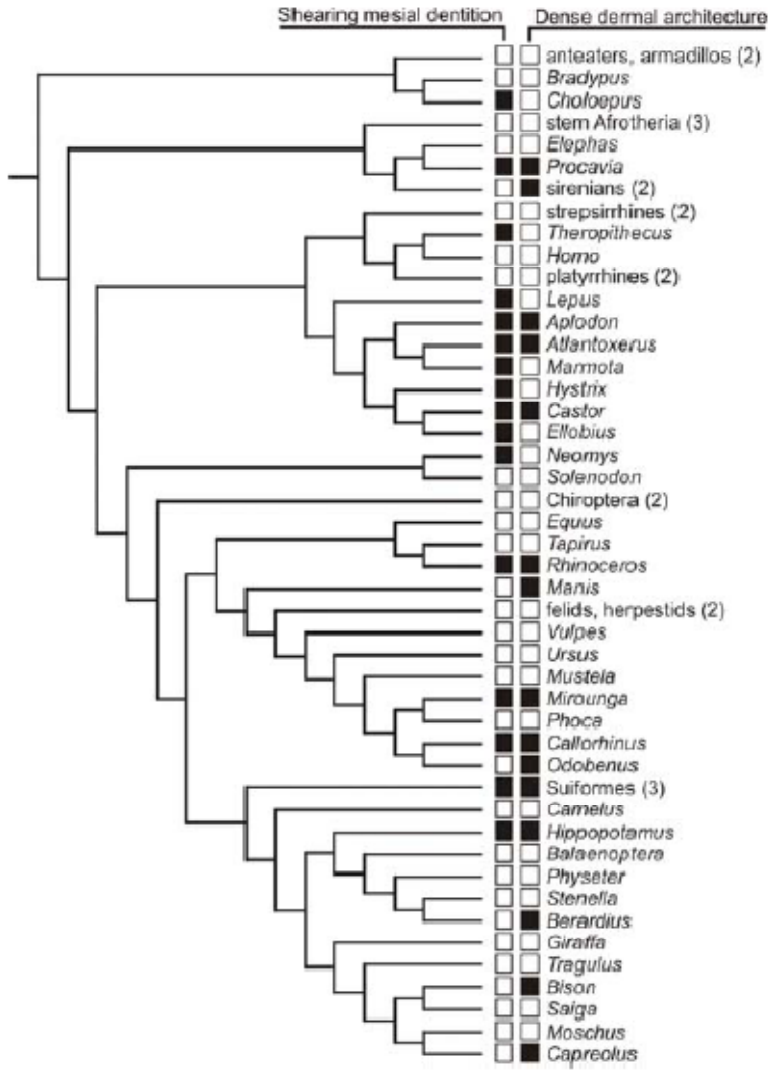

Figure 2-8. Convergent evolution among mammals of shearing mesial dentition and dermal morphology similar to rhinocerotid body armor. Taxa were scored for shearing mesial dentition if they possessed prominent oblique wear facets on enlarged incisors or canines, and dense dermal architecture if they possessed densely packed and obliquely oriented dermal fibers in a crossed array.

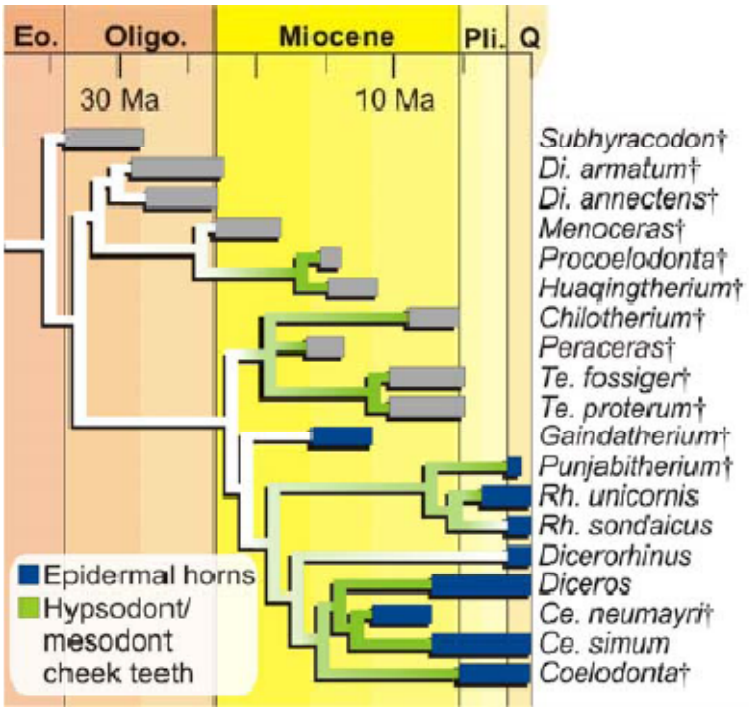

Figure 2-9. Cheek tooth height and epidermal horns in Rhinocerotidae. Ancestral character state reconstructions of low vs. high cheek tooth crown height are shown here in white (low crown) and green (high crown), based on a joint reconstruction from the full rhinocerotid supertree. Variation in color corresponds to the likelihood ratio for each state in a given branch—darkest green branches have likelihood ratios greater than 9:1 for high:low crowned cheek tooth states. Epidermal horns appear shortly before the most likely times of occurrence for tall cheek teeth in the lineage leading to extant rhinoceros. Genus name abbreviations: (Di) *Diceratherium*, (Te) *Teleoceras*, (Rh) *Rhinoceros*, (Ce) *Ceratotherium*.

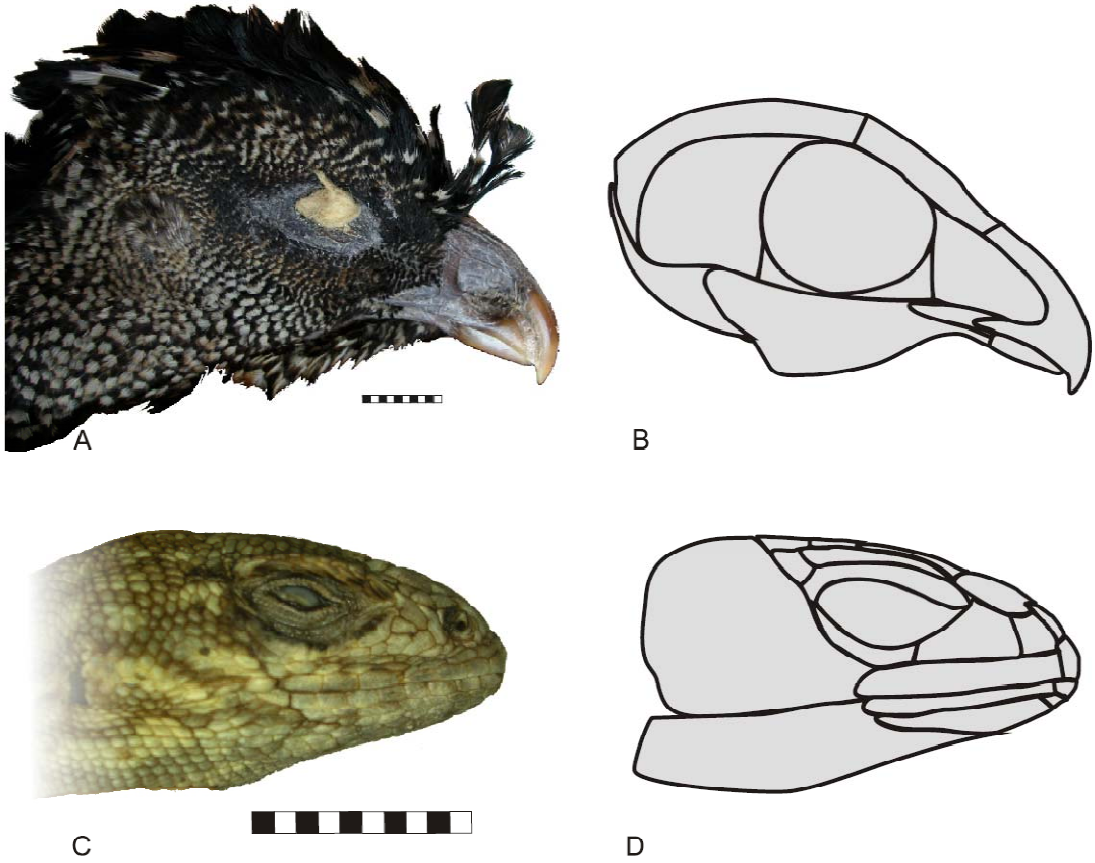

Figure 3-1. Previous classification schemes for cephalic skin. A: Greater curassow (*Crax rubra*) in lateral view. B: Capital feather tract boundaries for *Crax rubra* after Lucas and Stettenheim (1972). Many of the boundaries shown are based on underlying skeletal structures (e.g., the bony rim of the orbit) and cannot be readily discerned in the pattern of feathers. C: Collared iguana (*Oplurus cuvieri*) in lateral view. D: Scale groups for *Oplurus cuvieri* after Cope (1900). Although scales can generally be sorted into topographically connected scale groups with relative ease, there are no diagnostic criteria for placing the boundaries between groups in this classification scheme. Scale bars are 1 cm.

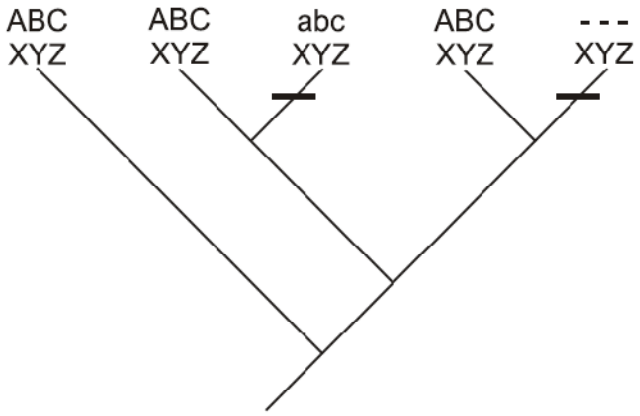

Figure 3-2. Phylogenetic pattern expected for evolutionary modules, after Schlosser (2004). Characters A, B, & C form a module independent of characters X, Y, & Z. Change in any part of the ABC module (e.g., A→a) is accompanied by change in other elements of the module (B→b, C→c), but is dissociated from change in elements outside the module.

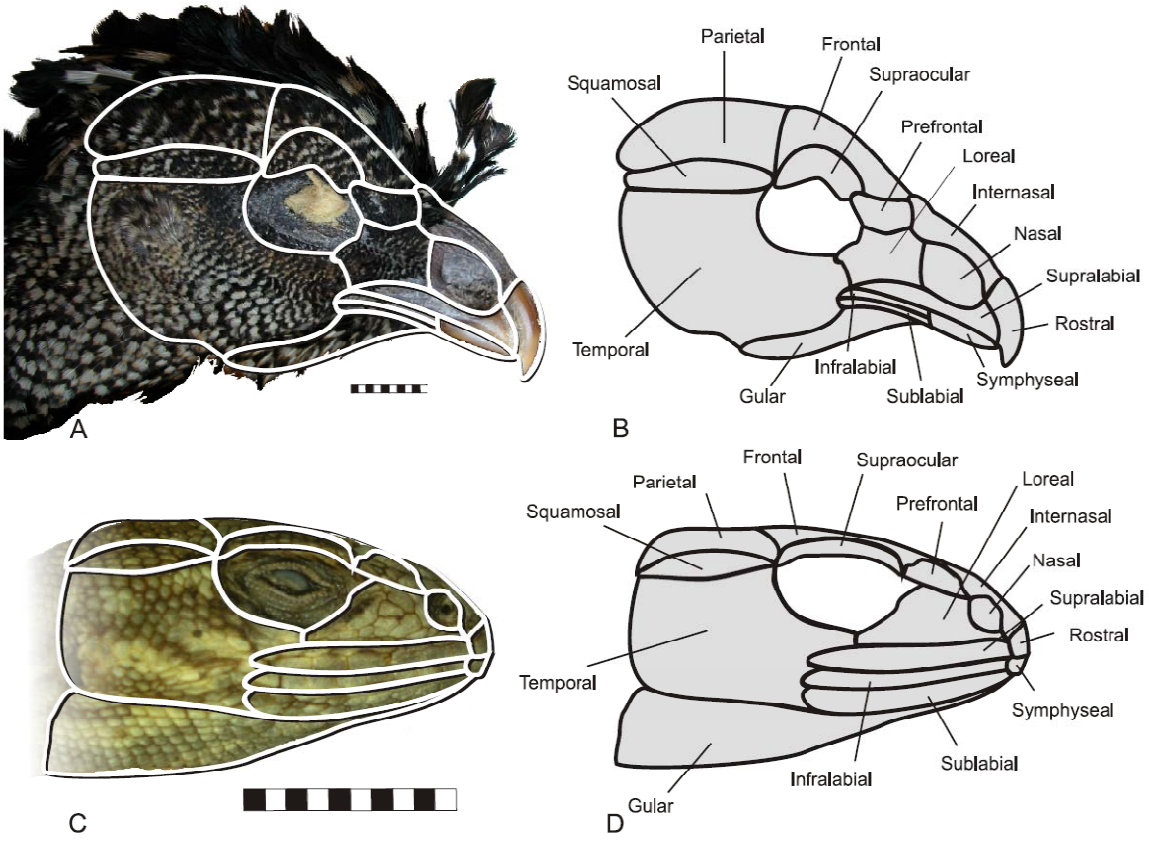

Figure 3-3. Topographic anatomy of sauropsid cephalic skin used in this study, shown on (A) *Crax rubra* and (C) *Oplurus cuvieri*. (B) and (D) show the nomenclature used in this study. The boundaries shown here represent a composite of areas of skin that were morphologically distinct from adjacent regions in a majority of the sauropsid taxa in our sample. Scale bars are 1 cm.

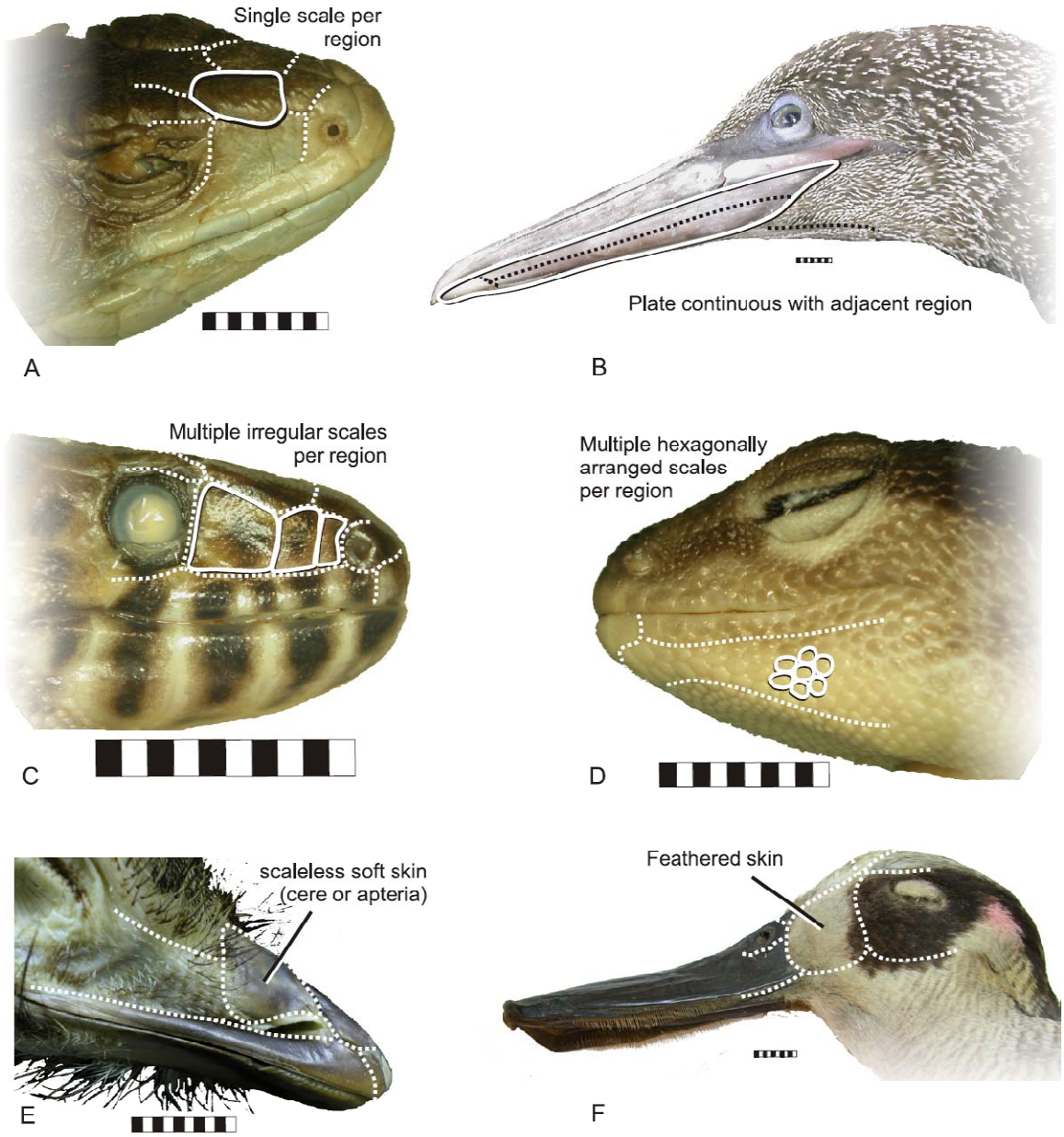

Figure 3-4. Character state scores for this analysis. Skin features are shown by solid lines; topographic regions are shown by dashed lines. A: State 0, a single scale per topographic region, shown for the prefrontal scale of *Gerrhosaurus major*. B: State 1, a scale or plate continuing into adjacent topographic regions, shown for the mandibular part of the horny beak of *Sula bassana* which continues across the symphyseal, infralabial, and sublabial regions. C: State 2, multiple irregular scales within a single topographic region, shown for the loreal region of *Lepidophyma maculatus*. D: State 3, multiple hexagonally arranged scales within a topographic region, shown for the sublabial region of *Hemitheconyx caudicinctus*. E: State 4, scaleless or soft skin lacking a

distinct break between topographic regions, shown for the nasal region of *Dromaius novaehollandiae*. F: State 5, feathered skin, shown for the loreal region of *Malacorhynchus membranaceus*. Scale bars are 1 cm.

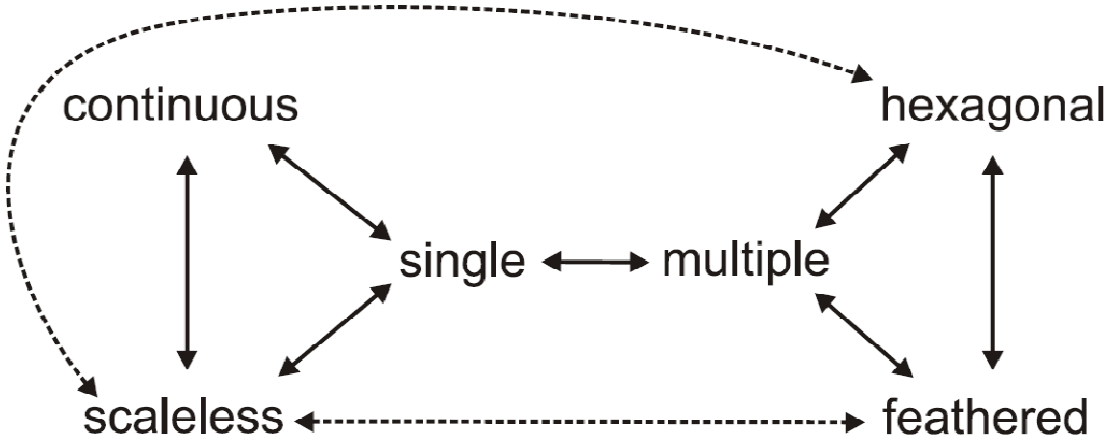

Figure 3-5. Simplified model of evolutionary change between character states used to generate the cost matrix for parsimony ancestral character state reconstruction. Solid lines indicate a cost of one step, dashed lines indicate a cost of two steps. In general, transitions between the states on the left side of the diagram and states on the right side involve increasing the number of scale primordia per topographic region. Feathered skin was considered to be a transformational homolog of skin with several small scale primordia (Harris et al. 2002; Prum and Brush 2002; Wu et al. 2004; Sawyer et al. 2005), modeled by equivalent transition costs to hexagonal scales or multiple irregular scales. Scaleless skin was considered to be either the result of the loss of keratinization in an existing broad plate or scale (modeled by a transition cost of one from single scale/plate or scale/plate continuing into adjacent regions) or the failure of scale or feather primordia to form during development (Maderson 1965; Sengel 1976; modeled by a transition cost of two from all other states).

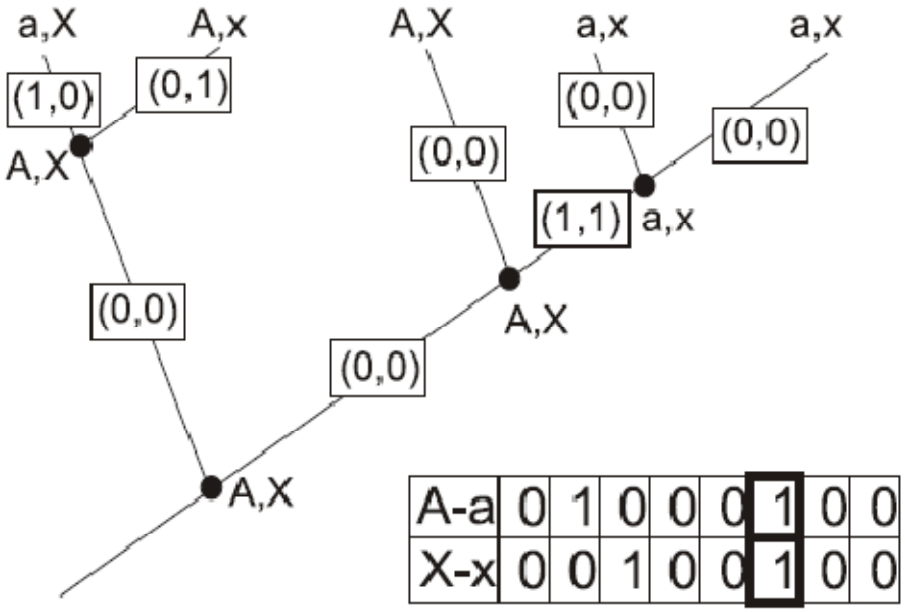

Figure 3-6. Schematic of the test for coincident change in two characters. States for two characters (A/a and X/x) are shown at the tips, along with parsimony ancestral character state reconstructions at the nodes. Change or stasis along a branch is shown by 1 or 0, respectively. The matrix of characters (rows) by change along branches (columns) at lower right shows the parameters before they are analyzed by a similarity index. Although each character shows a parsimony reconstruction of two episodes of state change on this tree, only one episode of change is linked between the two characters (bold boxes).

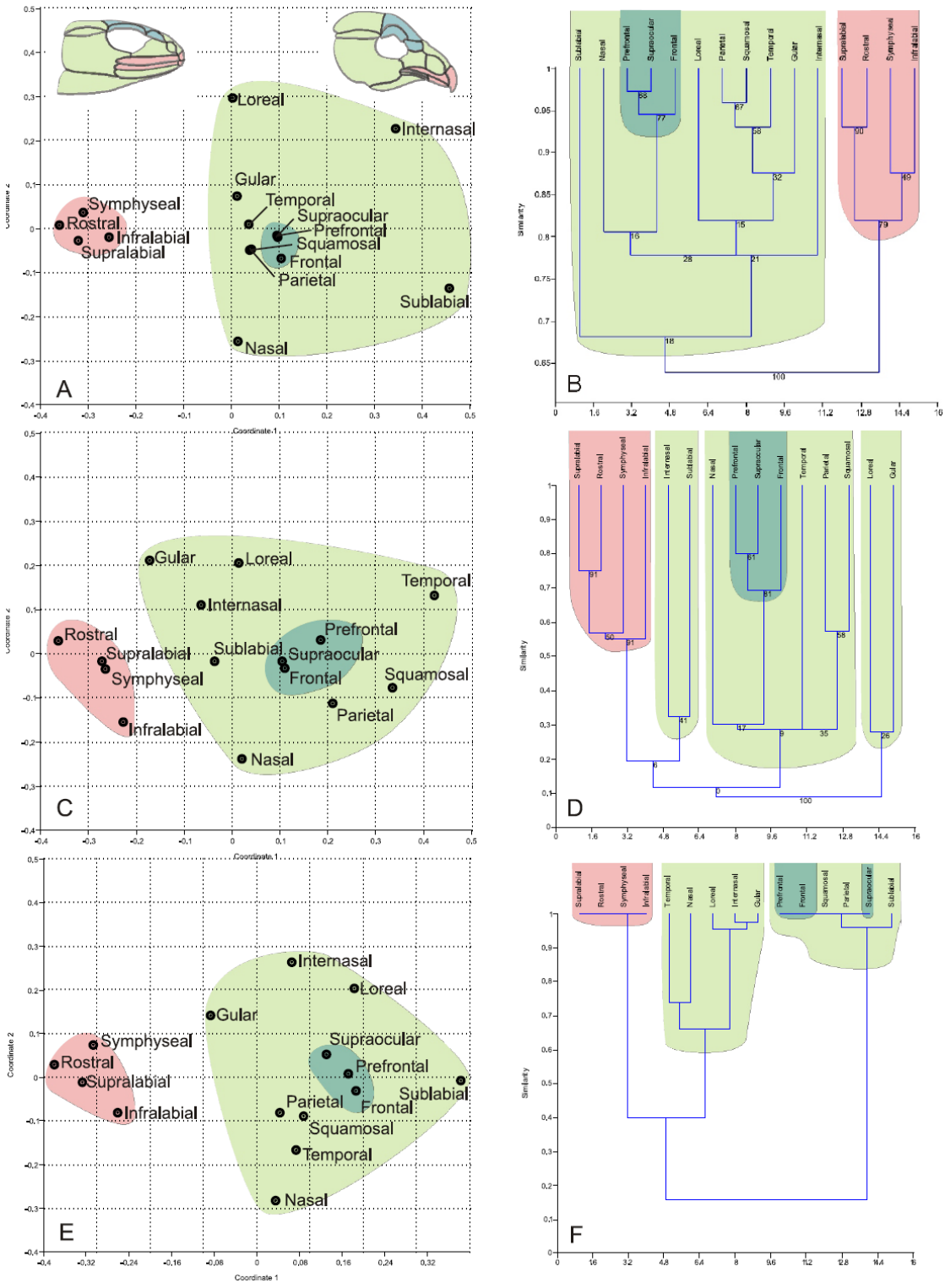
A
Loreal
Internasal
Gular
Temporal
Supraocular
Prefrontal
Squamosal
Frontal
Parietal
Symphyseal
Rostral
Infralabial
Supralabial
Sublabial
Nasal
B
C
Gular
Loreal
Temporal
Internasal
Prefrontal
Rostral
Supralabial
Sublabial
Supraocular
Frontal
Squamosal
Symphyseal
Parietal
Infralabial
Nasal
D
E
Internasal
Loreal
Gular
Symphyseal
Supraocular
Rostral
Prefrontal
Supralabial
Sublabial
Parietal
Frontal
Infralabial
Squamosal
Temporal
Nasal
F
Coordinate 1
Coordinate 2
Similarity

Figure 3-7. NMDS plots and UPGMA trees showing degrees of coincident change in cephalic skin regions. Colored shapes are hand-drawn to highlight consistent associations. Perioral module shown in red; cranial module shown in light green, with tightly clustered components of the cranial module shown in dark green. The insets at top map the two modules by region on outlines of *Oplurus cuvieri* and *Crax rubra*. A and B: NMDS plot and UPGMA tree using Hamming similarity, which groups regions on the basis of both coincident change and coincident stasis. C and D: NMDS plot and UPGMA tree using Jaccard similarity, which groups only by coincident change. E and F: NMDS plot and UPGMA tree using Raup-Crick similarity, which groups only by coincident change and assigns similarity by comparison to a 200-replicate bootstrapped distribution of matrices. Randomly associated features are expected to have a Raup-Crick similarity of 0.5.

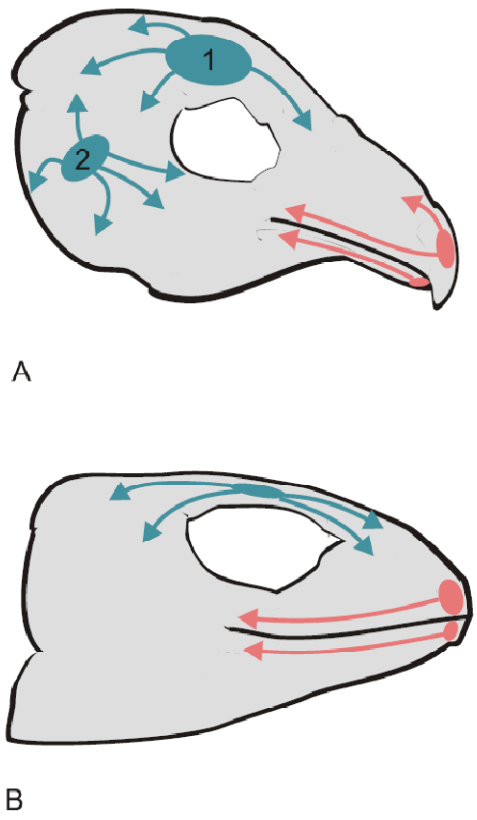

Figure 3-8. Outlines of (A) *Crax rubra* and (B) *Oplurus cuvieri* showing sites for the initiation of primordium formation reported from published studies. A: Neornithine birds are reported to have two or more centers of feather primordium development on the head (shown in dark green); (1) a patch dorsal to the orbit, and (2) a patch dorsal to the external auditory meatus (Koecke and Kuhn 1962). The keratinization of the horny beak (shown in red) begins around the caruncle or "egg tooth" (Kingsbury et al. 1953), which occurs on both the upper and lower beak in many taxa (Clark 1961). B: Lepidosaurs are reported to have three major centers of scale primordium development on the head (Dufaure and Hubert 1961); one between the orbits over the frontals (shown in dark green) and two more at the tips of the rostrum and the mandible (red).

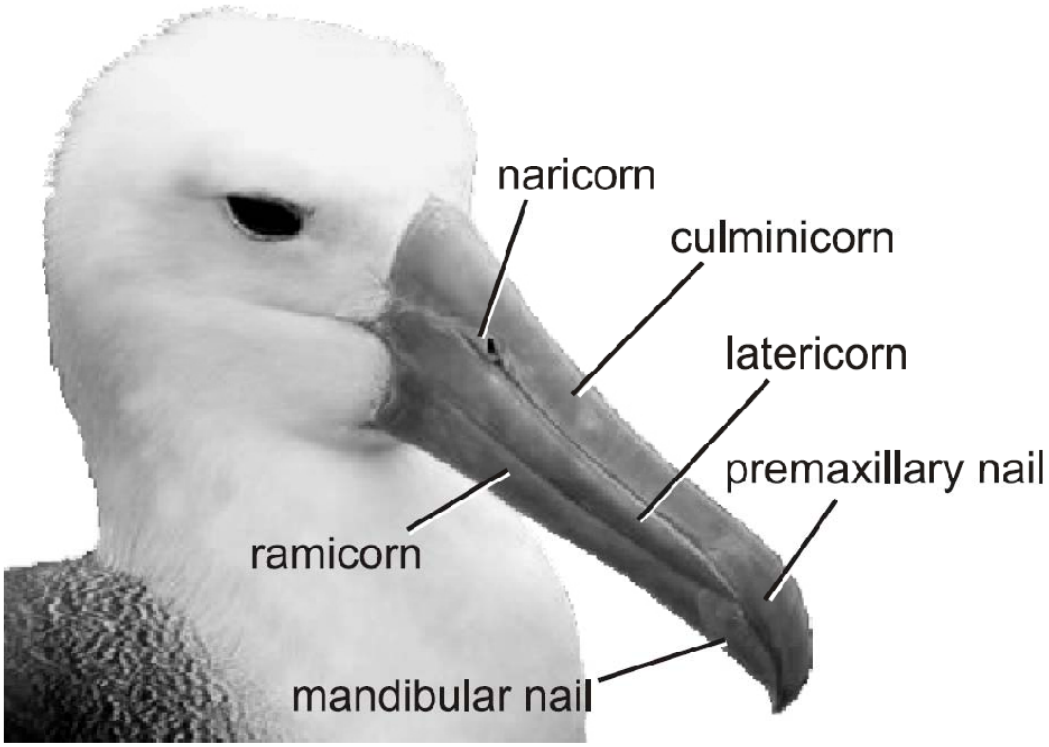

Figure 4-1. Compound rhamphotheca, shown in a Waved Albatross (*Phoebastria irrorata*). Nomenclature for separate plates of the compound rhamphotheca used here is largely derived from the nomenclature used by Coues (1866) to describe beak plates in Procellariiformes. Coues' 'maxillary nail' has been changed to 'premaxillary nail' to reflect the topological relationship between premaxilla and maxilla in the bony upper jaw. Image licensed to James Preston under Creative Commons Attribution 2.0.

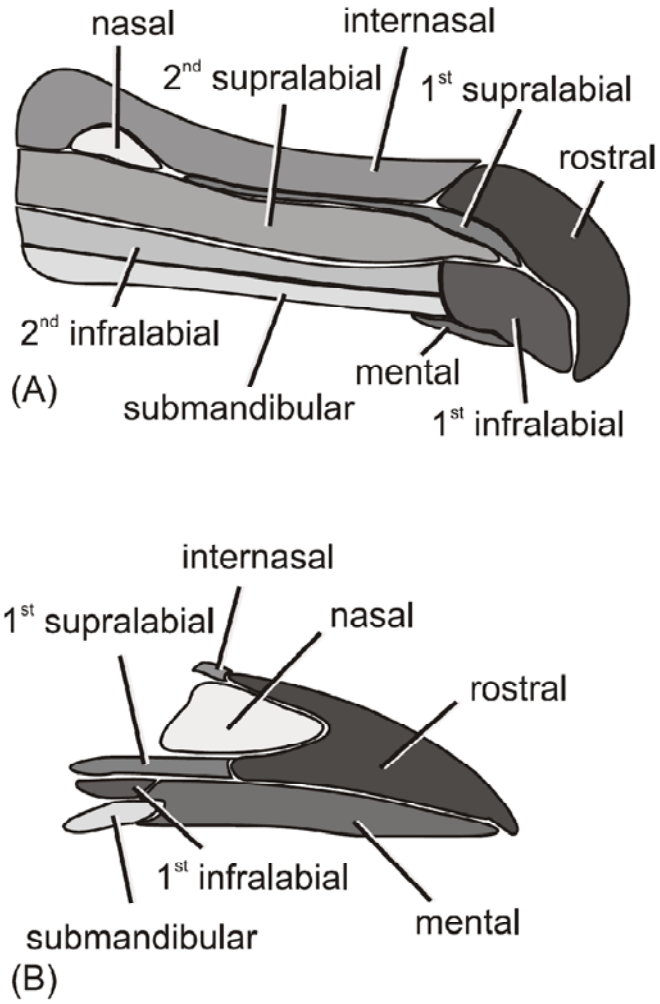

Figure 4-2. Hypothesis of homology between areas of rhamphotheca proposed by Lönnberg (1904), shown on the outlines of (A) Laysan Albatross (*Phoebastria immutabilis*) and (B) American Crow (*Corvus brachyrhynchos*). This hypothesis was heavily influenced by contemporary hypotheses of homology for the cephalic scales of reptiles (Cope 1900); the terms chosen for individual plates match Cope's (1900) scale nomenclature. The latericorn of Coues (1866) is divided into two supralabial plates, and the ramicorn and most of the mandibular nail are listed as infralabial plates. Lönnberg's (1904) hypothesis represents these elements as the result of fusion or reduction of the labial scales of squamates. Separation of the ramicorn into infralabial and submandibular plates is based on the presence of a shallow groove in *Casuarius* spp., anatoids, and some Procellariiformes.

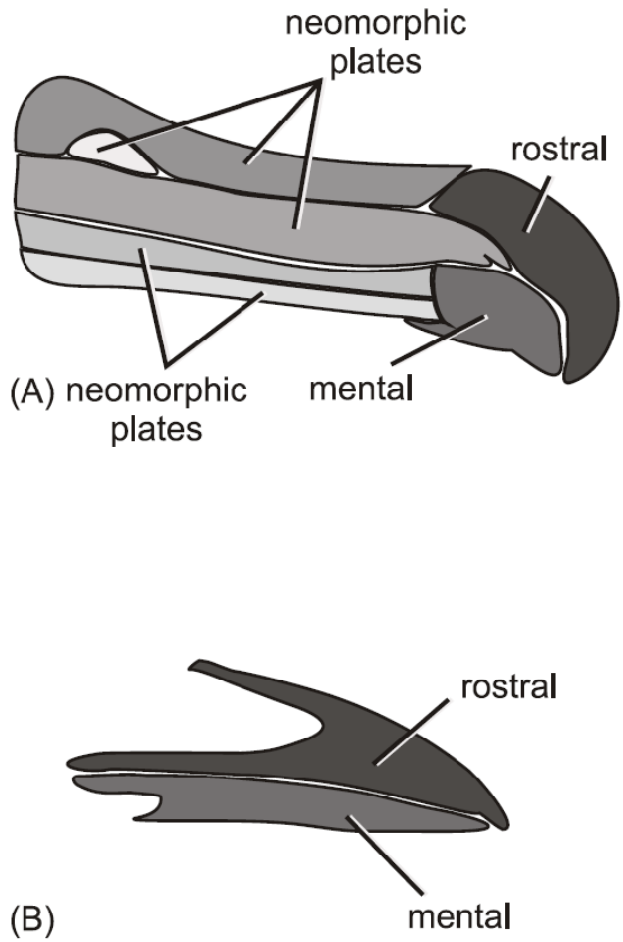

Figure 4-3. Boetticher's (1928) hypothesis of homology between rhamphothecal plates, shown on outlines of (A) Laysan Albatross (*Phoebastria immutabilis*) and (B) American Crow (*Corvus brachyrhynchos*). The phylogeny included in Boetticher (1928) shows a polytomy at the base of Neornithes. This polytomy prevented a clear polarization of compound vs. simple rhamphothecae as primitive for Neornithes. Boetticher (1928) used the sequence of development in rhamphothecal plates to resolve this ambiguity, selecting a simple rhamphotheca with only rostral and mental plates as primitive for Neornithes, as these plates are the first to appear during development. Although Boetticher (1928) recognized strong similarity between different examples of compound rhamphothecae, these similarities were cast as independent, convergent examples of additional beak plates.

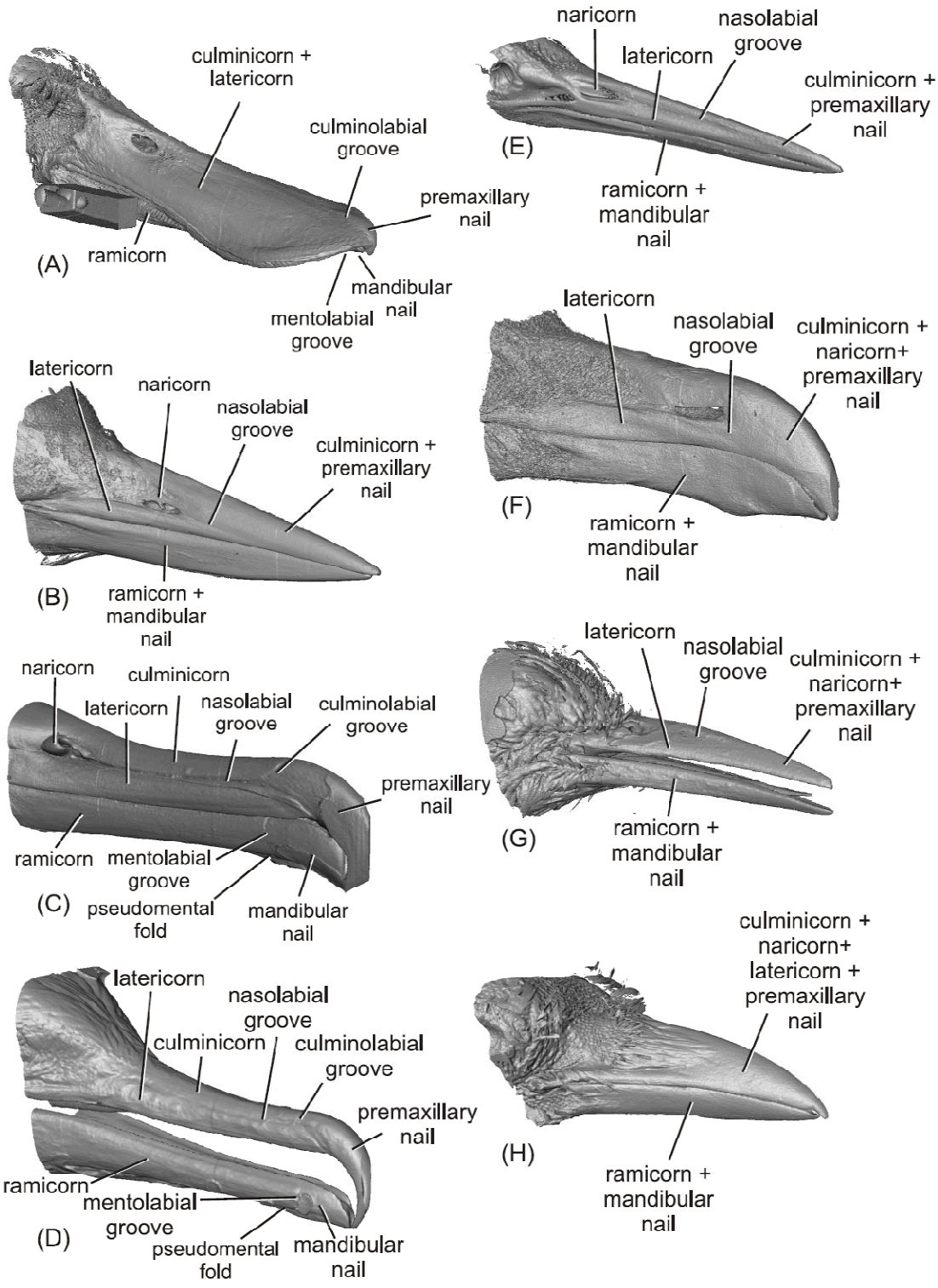
culminicorn + latericorn
culminolabial groove
premaxillary nail
ramicorn
(A)
mandibular nail
mentolabial groove
naricorn
nasolabial groove
latericorn
culminicorn + premaxillary nail
(E)
ramicorn + mandibular nail
latericorn
naricorn
nasolabial groove
culminicorn + premaxillary nail
(B)
ramicorn + mandibular nail
latericorn
nasolabial groove
culminicorn + naricorn+ premaxillary nail
(F)
ramicorn + mandibular nail
naricorn
culminicorn
latericorn
nasolabial groove
culminolabial groove
premaxillary nail
ramicorn
mentolabial groove
(C)
pseudomental fold
mandibular nail
latericorn
nasolabial groove
culminicorn + naricorn+ premaxillary nail
(G)
ramicorn + mandibular nail
latericorn
nasolabial groove
culminicorn
culminolabial groove
premaxillary nail
ramicorn
mentolabial groove
(D)
pseudomental fold
mandibular nail
culminicorn + naricorn+ latericorn + premaxillary nail
(H)
ramicorn + mandibular nail

Figure 4-4. Topographic anatomy of rhamphotheca, showing rhamphothecal plates as well as nasolabial, culminolabial, and mentolabial grooves, in (A) Northern Shoveler (*Anas clypeata*), (B) Common Loon (*Gavia immer*), (C) Laysan Albatross (*Phoebastria immutabilis*), (D) Double-crested Cormorant (*Phalacrocorax auritus*), (E) Striated Heron (*Butorides striata*), (F) Ring-billed Gull (*Larus delawarensis*), (G) Northern Flicker (*Colaptes auratus*), and (H) American Crow (*Corvus brachyrhynchos*). Where the loss of a rhamphothecal groove results in fusion of plates, those plates are identified as composites (e.g., culminicorn + latericorn in *Anas clypeata*).

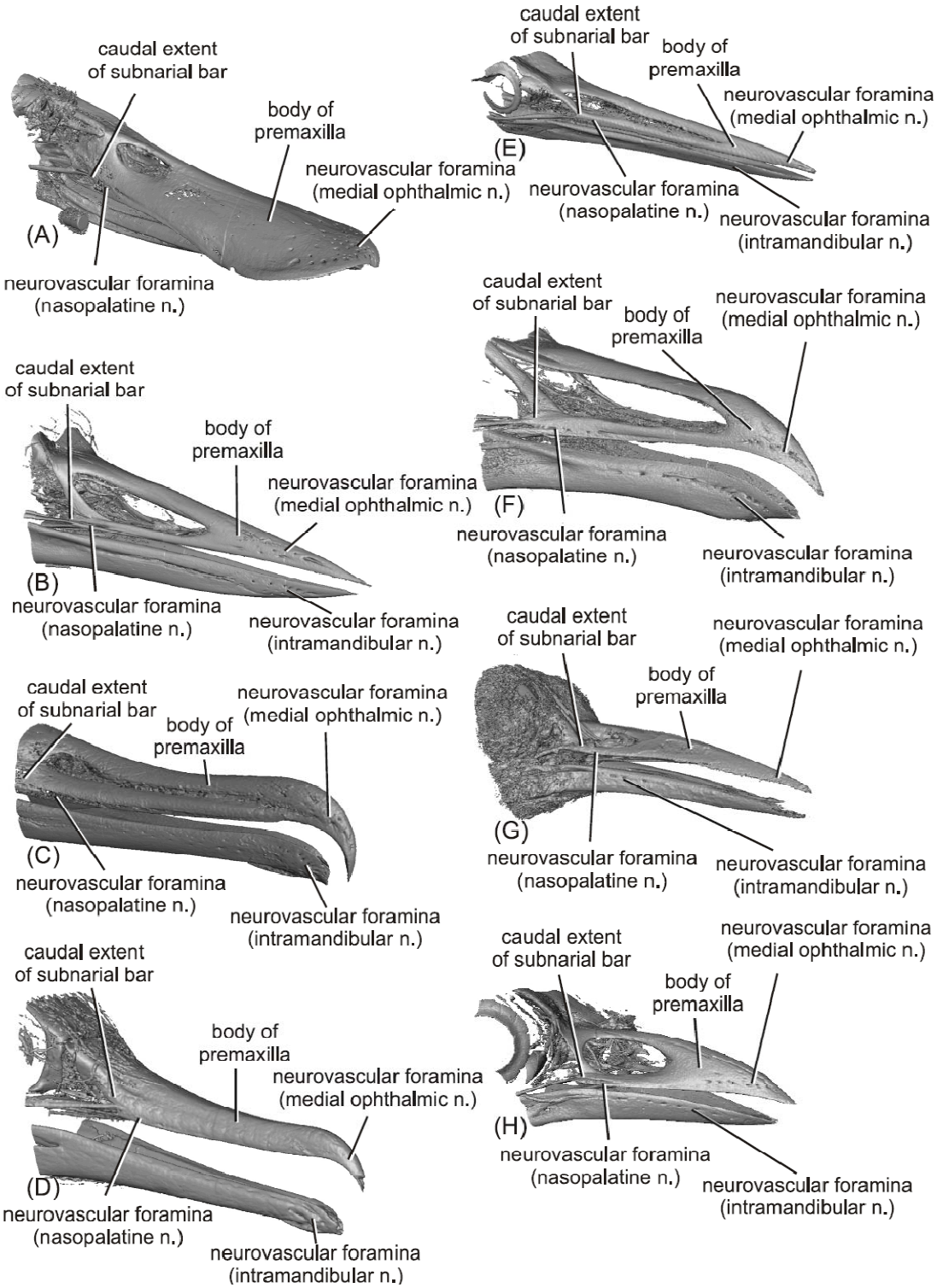
caudal extent of subnarial bar
body of premaxilla
neurovascular foramina (medial ophthalmic n.)
(A)
neurovascular foramina (nasopalatine n.)
caudal extent of subnarial bar
body of premaxilla
neurovascular foramina (medial ophthalmic n.)
(E)
neurovascular foramina (nasopalatine n.)
neurovascular foramina (intramandibular n.)
caudal extent of subnarial bar
body of premaxilla
neurovascular foramina (medial ophthalmic n.)
(B)
neurovascular foramina (nasopalatine n.)
neurovascular foramina (intramandibular n.)
caudal extent of subnarial bar
body of premaxilla
neurovascular foramina (medial ophthalmic n.)
(F)
neurovascular foramina (nasopalatine n.)
neurovascular foramina (intramandibular n.)
caudal extent of subnarial bar
body of premaxilla
neurovascular foramina (medial ophthalmic n.)
(C)
neurovascular foramina (nasopalatine n.)
neurovascular foramina (intramandibular n.)
caudal extent of subnarial bar
body of premaxilla
neurovascular foramina (medial ophthalmic n.)
(G)
neurovascular foramina (nasopalatine n.)
neurovascular foramina (intramandibular n.)
caudal extent of subnarial bar
body of premaxilla
neurovascular foramina (medial ophthalmic n.)
(D)
neurovascular foramina (nasopalatine n.)
neurovascular foramina (intramandibular n.)
caudal extent of subnarial bar
body of premaxilla
neurovascular foramina (medial ophthalmic n.)
(H)
neurovascular foramina (nasopalatine n.)
neurovascular foramina (intramandibular n.)

Figure 4-5. Anatomy of the bony rostrum for individuals portrayed in Figure 4-4. Note that the subnarial bar of the premaxilla closely corresponds to the caudal extent of the latericorn in most taxa. Steganopode pelecaniforms, represented here by *Phalacrocorax auritus* (D), are the only exception to this general rule. The neurovascular bundles that emerge from the caudalmost neurovascular foramina for the medial ophthalmic nerve generally continue under the rostral portion of the latericorn; in palaeognaths and galloanserine birds, the latericorn overlaps several of these neurovascular foramina (e.g., *Anas clypeata,* A).

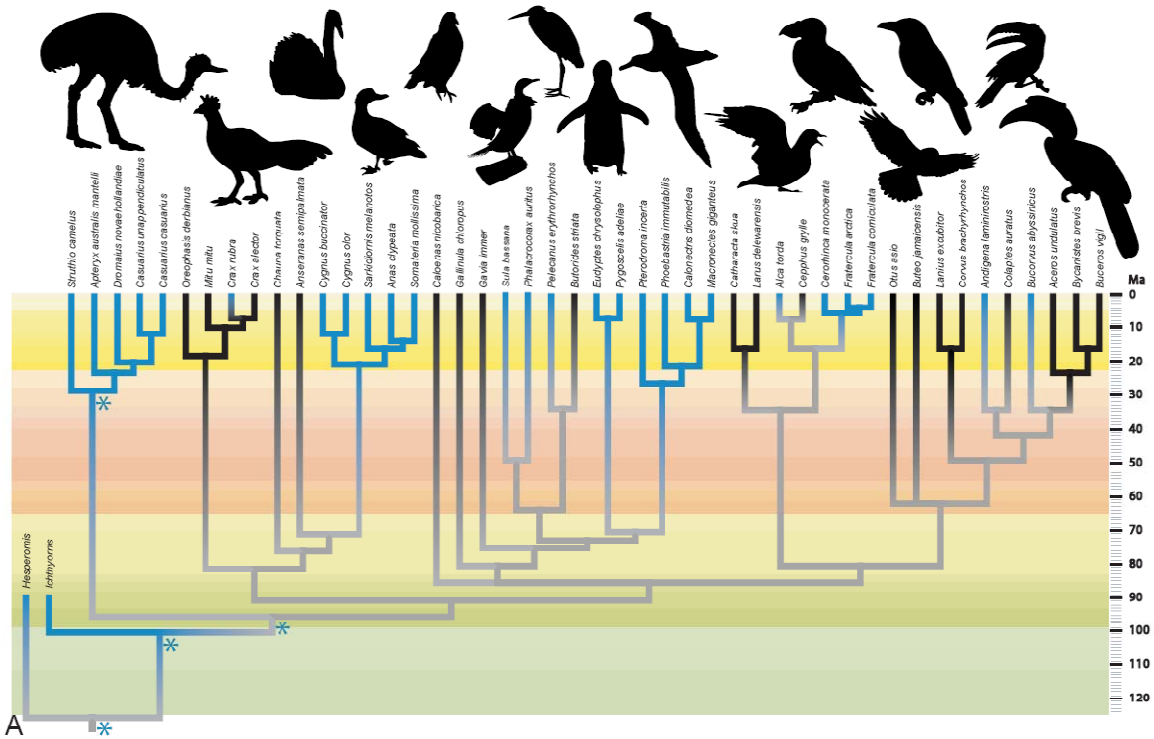
Struthio camelus
Apteryx australis mantelli
Dromaius novaehollandiae
Casuarius unappendiculatus
Casuarius casuarius
Oreophasis derbianus
Mitu mitu
Crax rubra
Crax alector
Chauna torquata
Anseranas semipalmata
Cygnus buccinator
Cygnus olor
Sarkidiornis melanotos
Anas dypeata
Somateria mollissima
Calonas nicobarica
Gallinula chloropus
Gavia immer
Sula bassana
Phalacrocorax auritus
Pelecanus erythrorhynchos
Butorides striata
Eudyptes chrysolophus
Pygoscelis adeliae
Pterodroma incerta
Phoebastria immutabilis
Calonectris diomedea
Macronectes giganteus
Cathartacta aura
Larus delawarensis
Alca torda
Cepphus grylle
Cerorhinca monocerata
Fratercula arctica
Fratercula corniculata
Otus asio
Buteo jamaicensis
Larius excubitor
Corvus brachyrhynchos
Andigena laminirostris
Colaptes auratus
Bucorvus abyssinicus
Aceros undulatus
Bycanistes brevis
Buceros vigil
Hesperornis
Ichthyornis
Ma
0
10
20
30
40
50
60
70
80
90
100
110
120
A

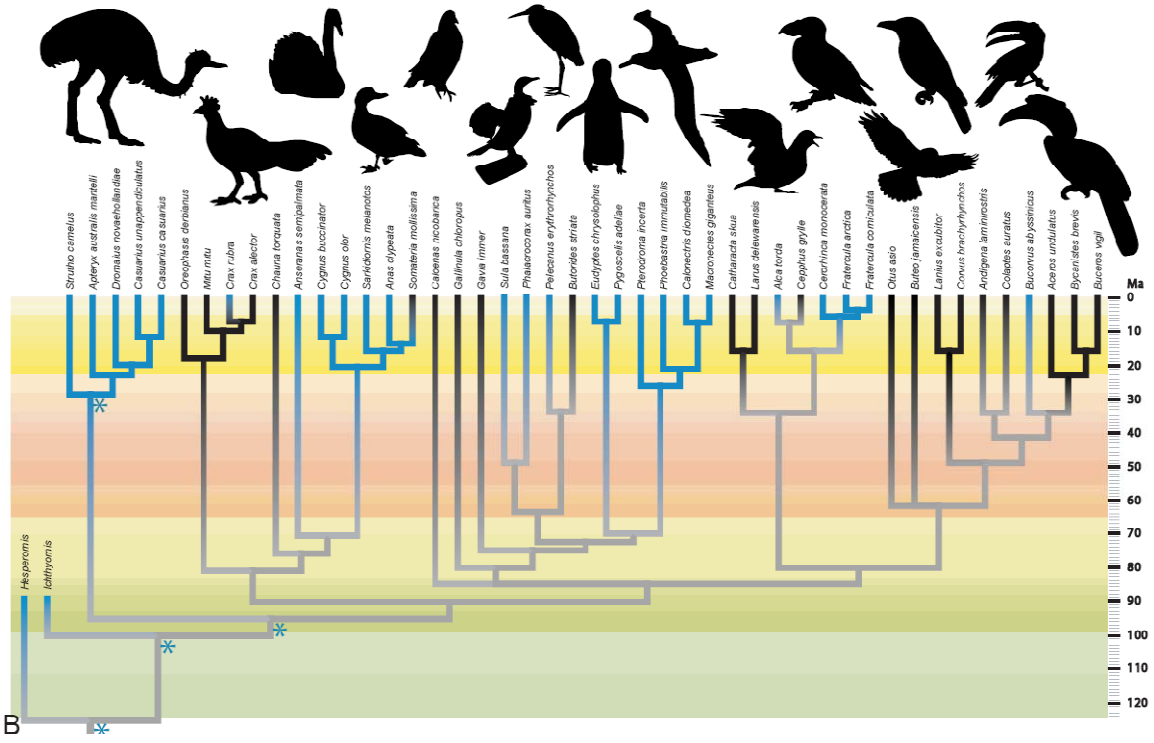
Struthio camelus
Apteryx australis mantelli
Dromaius novaehollandiae
Casuarius unappendiculatus
Casuarius casuarius
Oreophasis derbianus
Mitu mitu
Crax rubra
Crax alector
Chauna torquata
Anseranas semipalmata
Cygnus buccinator
Cygnus olor
Sarkidiornis melanotos
Anas dypeata
Somateria mollissima
Calonas nicobarica
Gallinula chloropus
Gavia immer
Sula bassana
Phalacrocorax auritus
Pelecanus erythrorhynchos
Butorides striata
Eudyptes chrysolophus
Pygoscelis adeliae
Pterodroma incerta
Phoebastria immutabilis
Calonectris diomedea
Macronectes giganteus
Cathartacta aura
Larus delawarensis
Alca torda
Cepphus grylle
Cerorhinca monocerata
Fratercula arctica
Fratercula corniculata
Otus asio
Buteo jamaicensis
Larius excubitor
Corvus brachyrhynchos
Andigena laminirostris
Colaptes auratus
Bucorvus abyssinicus
Aceros undulatus
Bycanistes brevis
Buceros vigil
Hesperornis
Ichthyornis
Ma
0
10
20
30
40
50
60
70
80
90
100
110
120
B

Figure 4-6. Parsimony (MP) and maximum likelihood (ML) ancestral character state reconstructions for (A) distinct nasolabial grooves and (B) distinct culminolabial grooves. Blue branches show the presence of grooves by significant ML ancestral character state reconstruction; blue asterisks at basal nodes show the presence of grooves by MP ancestral character state reconstruction. The rates of character state change fitted by the ML ancestral character state reconstruction lead to uncertainty at the root of the tree (Ornithurae) in both of these characters, in contrast to the positive assessment of congruence by maximum parsimony (asterisks). Although the character state for both sets of grooves is uncertain for Neognathae and Neoaves by both ML and MP, the likelihood ratios for these nodes favor the presence of grooves as a primitive state (Table 4-1). Some of the taxa on this tree retain a pronounced furrow between the nostril and the oral margin which we interpret as a remnant of the nasolabial groove, (e.g., *Colaptes auratus*, *Butorides striata*), and in some cases a similar furrow is accompanied by a second, indistinct furrow that we interpret as the remnant of the culminolabial groove (e.g., *Catharacta skua*, *Caloenas nicobarica*). Higher-order topology after Hackett et al. (2008).

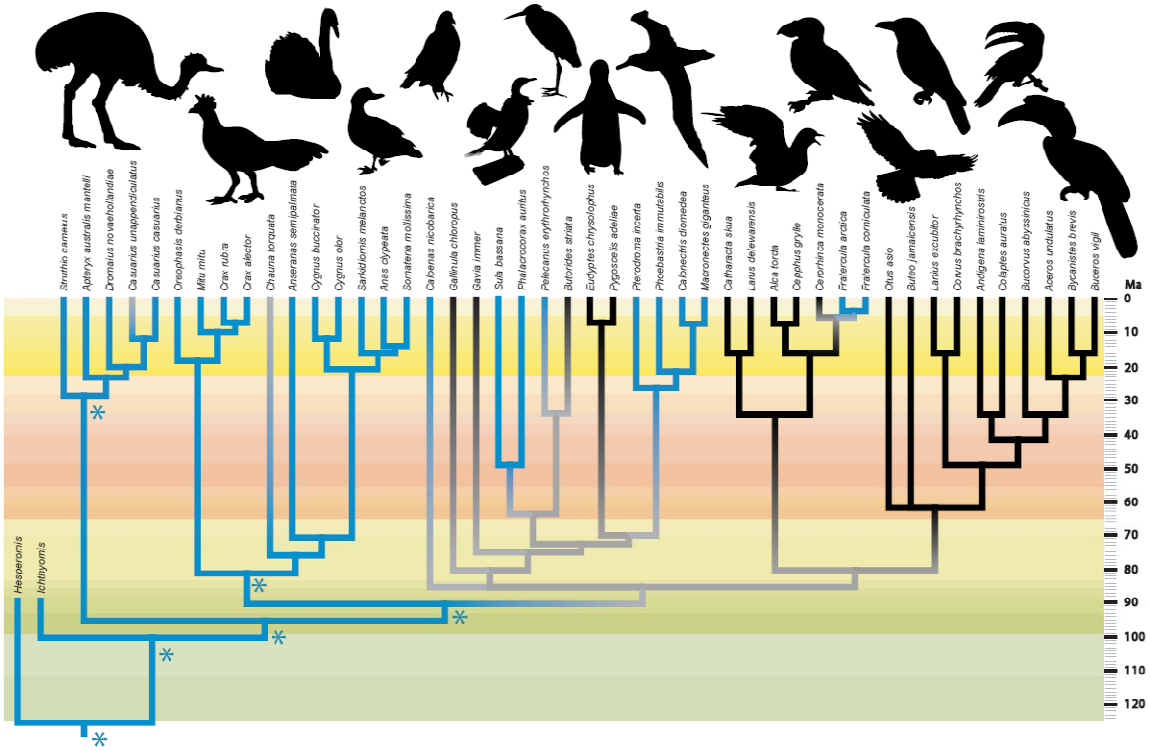

Figure 4-7. Parsimony (MP) and maximum likelihood (ML) ancestral character state reconstructions for mentolabial grooves. Blue branches show the presence of grooves by significant ML ancestral character state reconstruction; blue asterisks at basal nodes show the presence of grooves by MP ancestral character state reconstruction. In contrast to the uncertainty seen in the ancestral character state reconstructions for grooves in the upper jaw (Fig. 4-6), both MP and ML reconstructions of the mentolabial groove show congruence of to the base of Neognathae and into Galloanserae. Higher-order topology after Hackett et al. (2008).

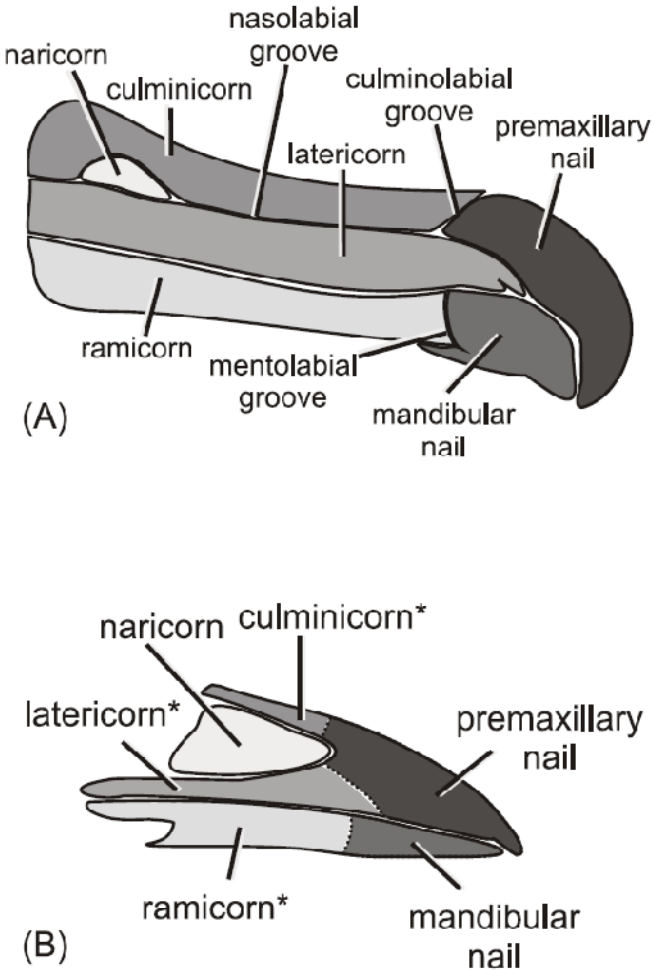

Figure 4-8. Hypothesis of homology for areas of rhamphotheca proposed in this study, shown on (A) Laysan Albatross (*Phoebastria immutabilis*) and (B) American Crow (*Corvus brachyrhynchos*). Regions marked by asterisks in (B) are fused with other plates that share a common direction of growth, and are delineated on the basis of topological relationships to underlying bones and nerves.

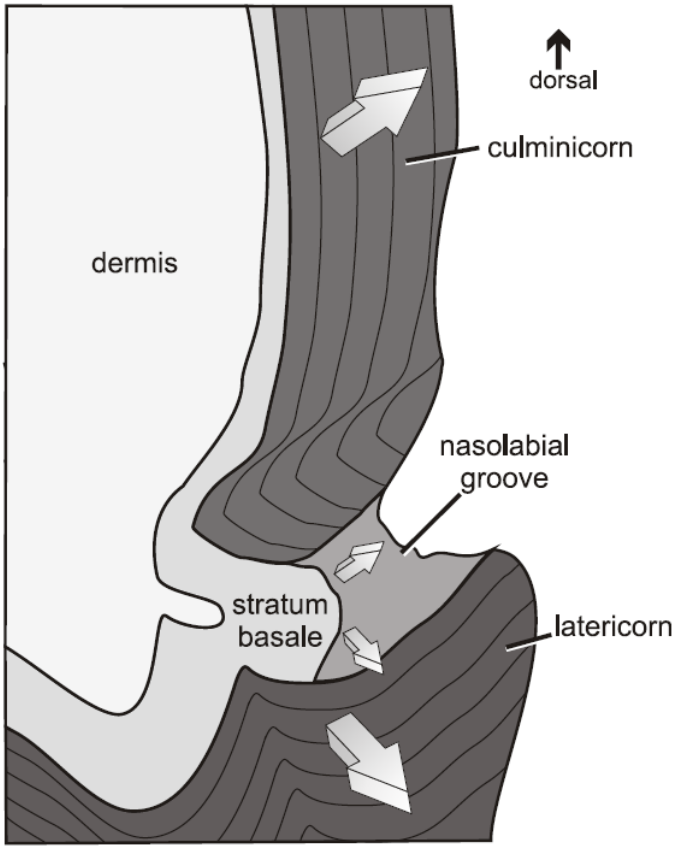

Figure 4-9. Schematic cross-section of the nasolabial groove illustrating the possible function of rhamphothecal grooves in growth and maintenance of adult rhamphothecal shape, drawn from a histological section of a Double-crested Cormorant (*Phalacrocorax auritus,* OUVC 10401). White arrows indicate the direction of growth of the culminicorn and latericorn, including growth out of the plane of the section. The strain that results from cornified plates growing in different directions is taken up by the softer, less cornified tissue in the nasolabial groove, which wears and falls apart more quickly than the surrounding cornified plates.

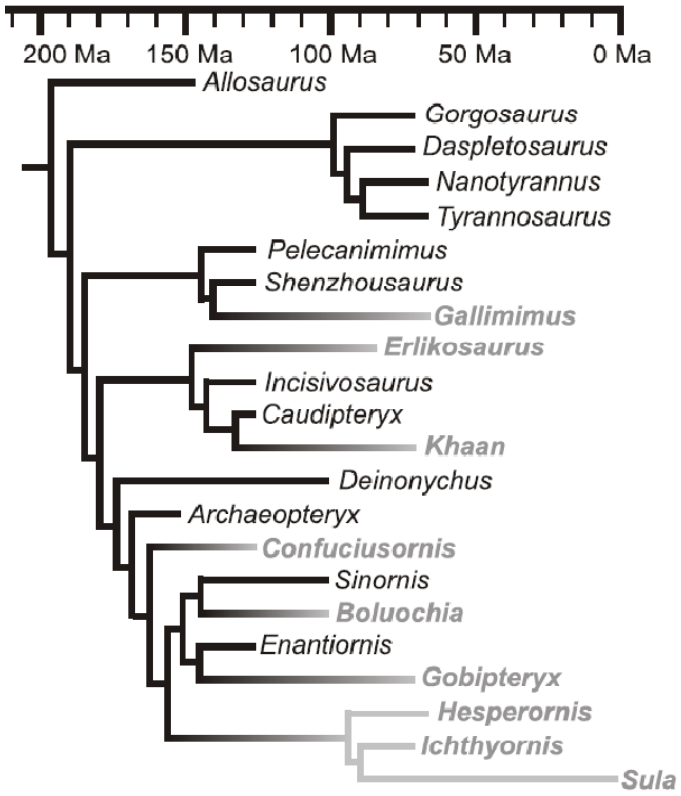

Figure 4-10. Representative phylogeny of derived coelurosaurian dinosaurs, showing the mosaic evolution of rhamphothecae within this clade (gray branches and genus names). The density of convergent occurrences of rhamphothecae in Coelurosauria stands in contrast to the relative rarity of the evolution of similar structures in other amniotes. Topology after Chiappe (2002), Holtz et al. (2004), Holtz (2004), Makovicky et al, (2004), and Osmólska et al. (2004).

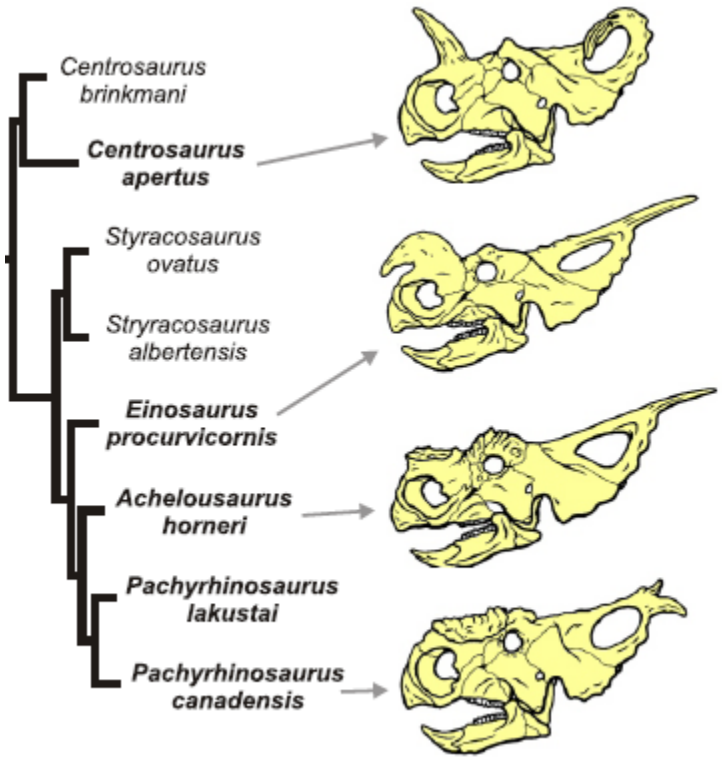

Figure 5-1. Skull morphology and phylogenetic relationships of centrosaurine dinosaurs. Topology after Currie et al. (2008). Taxa included in this study are marked in bold.

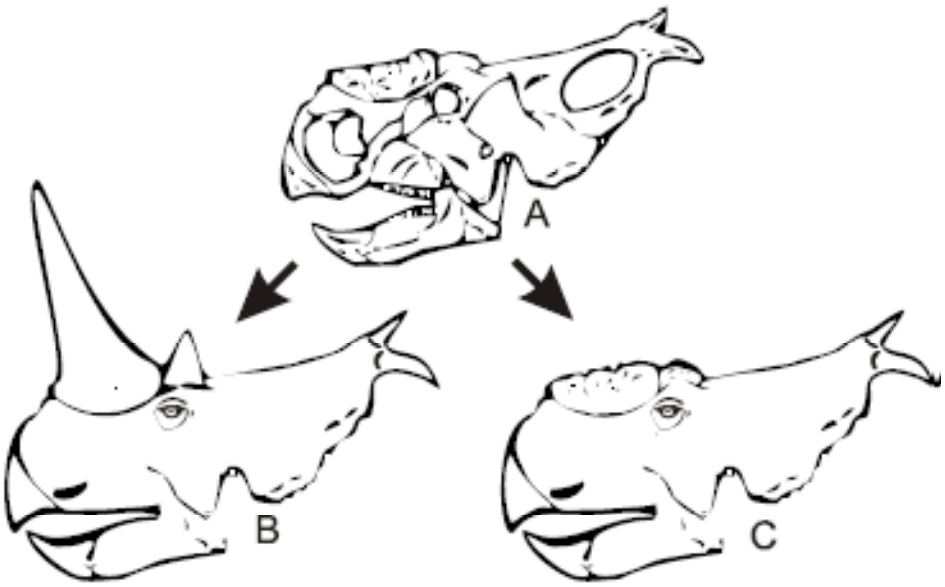

Figure 5-2. The two most prominent hypotheses proposed for skin structures associated with the rugose nasal and supraorbital bosses of *Pachyrhinosaurus* (A). One hypothesis (B) places tall epidermal horns, similar to those of living rhinoceros, on the rugose patches of bone. The second hypothesis (C) places a comparatively thin covering of cornified skin on the same structures.

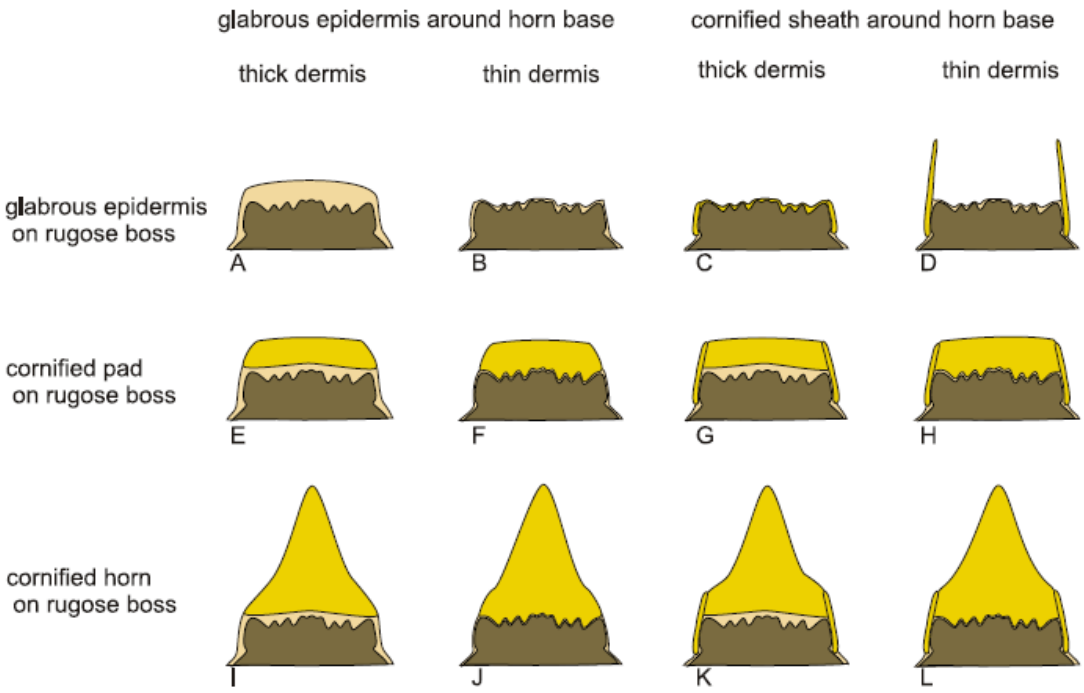

Figure 5-3. Multiple working hypotheses of centrosaurine facial skin structure, using a schematic cross-section of the nasal boss of *Pachyrhinosaurus* as an example. The twelve hypotheses shown here are permutations of possible skin morphologies. The two most prominent hypotheses are shown by (H) and (I), and are similar to skin features on extant muskoxen (H) and rhinoceros (I), respectively. Other hypotheses are similar to skin features found in extant taxa, such as suids (A) and hornbills (C, D), while some of the hypotheses (J) do not have extant equivalents.

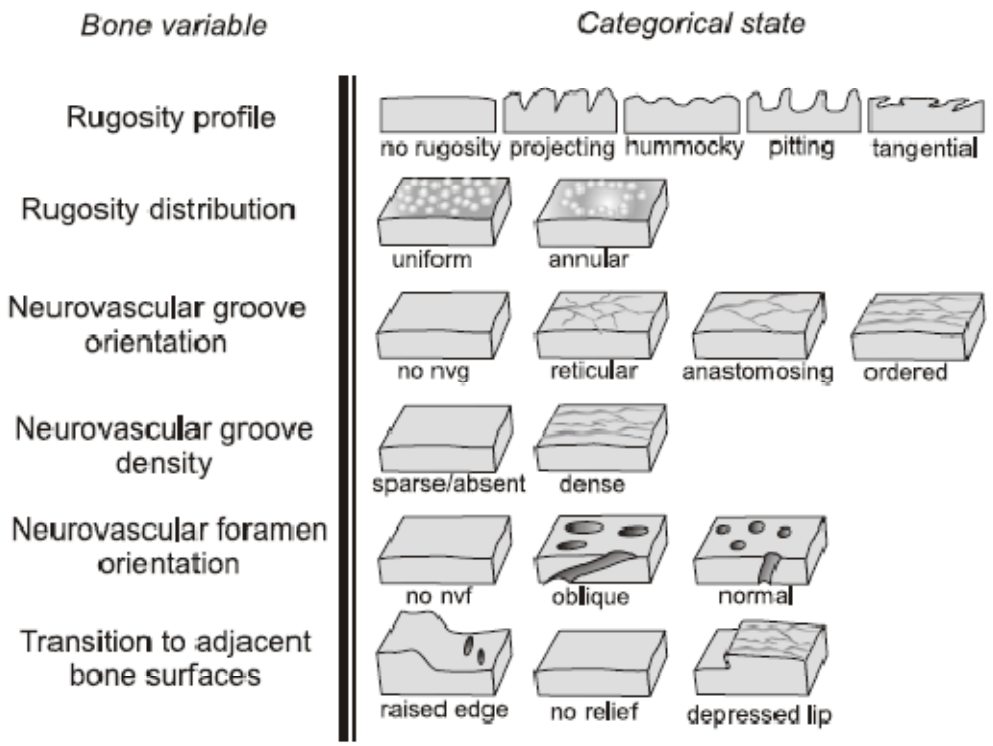

Figure 5-4. Schematics for categorical variables used to describe bone surfaces in this study (rows), with examples of the states for each variable. Schematics for rugosity type show the surface profile in cross-section; other schematics show the surface and profile of a small (2x2 cm) sample area. Nvf: neurovascular foramina; nvg: neurovascular grooves.

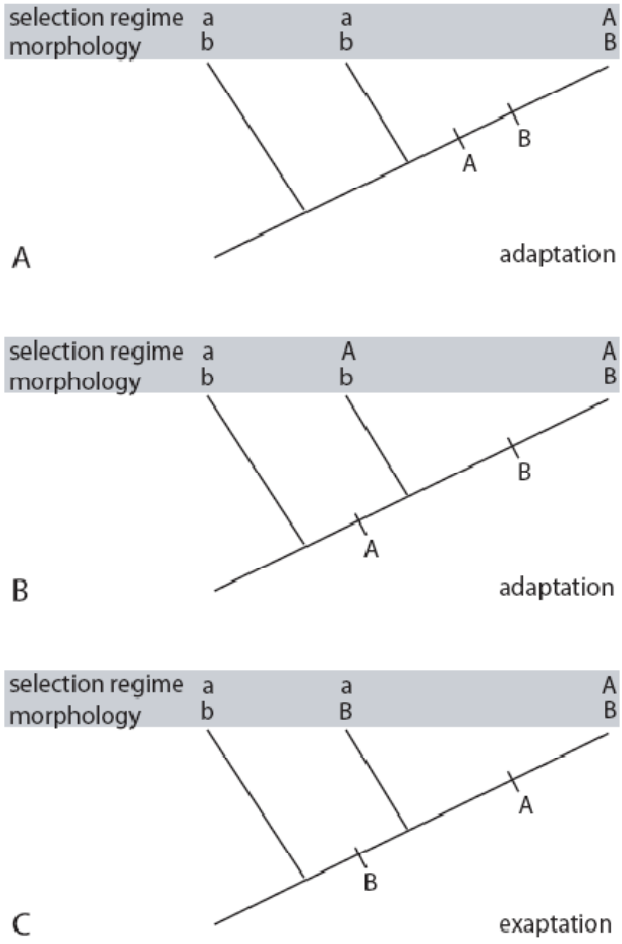

Figure 5-5. Phylogenetic patterns of character state change and selection regime. (A) Character state and selection regime change on the same branch. This pattern is one of two patterns that falls under Gould and Vrba's (1982) definition of adaptation, and the only pattern that we consider sufficient evidence for analogy in the absence of fitness data. (B) Character state changes after change in selection regime. While this pattern also falls under Gould and Vrba's (1982) definition of adaptation, it permits varying degrees of separation between character state change and the change in selection regime. This pattern is thus more likely to occur by random chance than pattern (A), although it is unclear which pattern is more common among known examples of adaptation (viz. Larson and Losos 1996, p. 203). (C) Character state change before change in selection regime. This pattern fits Gould and Vrba's (1982) definition of exaptation, and may represent a biologically meaningful relationship between structure and function, but is also expected to occur more often by random chance than pattern (A). In the absence of data on current utility, such as performance or fitness, pattern (A) provides a more stringent criterion of analogy than patterns (B) or (C).

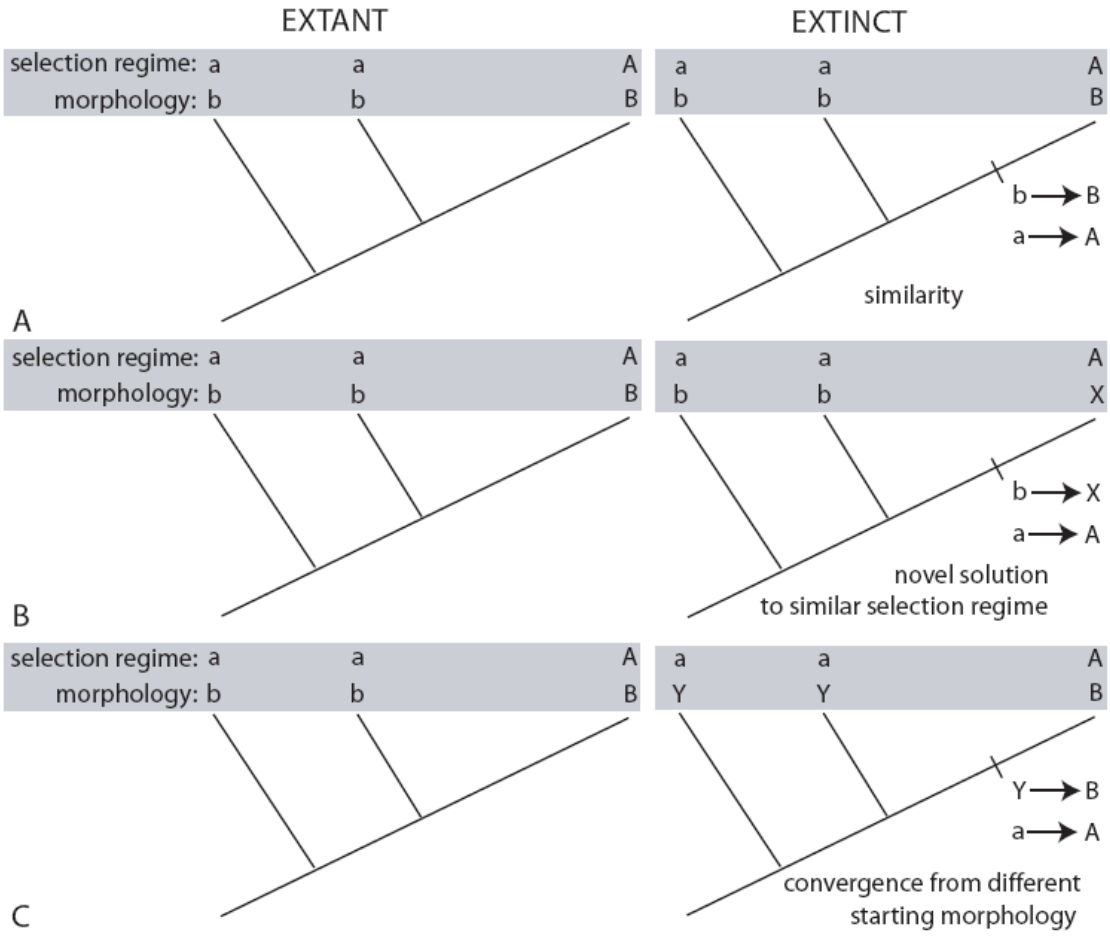

Figure 5-6. Patterns of similar and dissimilar character state transformation among potential analogs. (A) Similar transition sequences among extant and extinct taxa. This is the preferred pattern for hypotheses of analogy. (B) Different "solutions" to similar selection regimes. This pattern leads to a false negative in assessing function (Kluge 2003). (C) Convergence from different primitive morphologies. This pattern cannot falsify a hypothesis of analogy, but leads to a lower rank of preference than pattern (A).

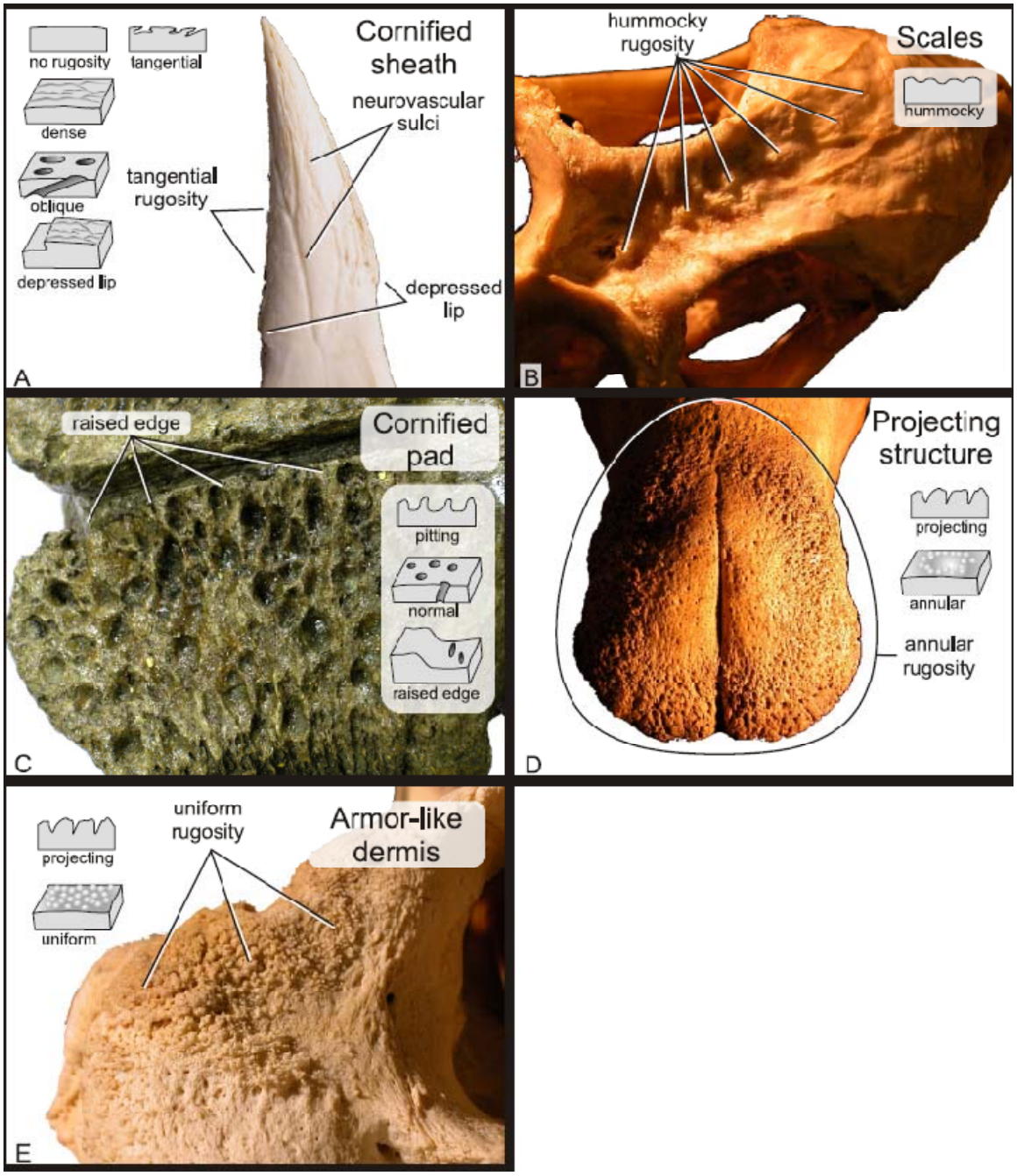
no rugosity
tangential
dense
oblique
depressed lip
Cornified sheath
neurovascular sulci
tangential rugosity
depressed lip
A
hummocky rugosity
Scales
hummocky
B
raised edge
Cornified pad
pitting
normal
raised edge
C
Projecting structure
projecting
annular
annular rugosity
D
uniform rugosity
Armor-like dermis
projecting
uniform
E

Figure 5-7. Osteological correlates for categories of skin structures used in this study, represented by an example of the associated bone surface and schematics of the associated bone variable scores: (A) cornified sheath, shown on the metacarpophalangeal spur of a crested creamer (*Chauna torquata*, UMMZ 156989); (B) scales, shown on the skull roof of a green iguana (*Iguana iguana*, UMMZ 149093); (C) cornified pad, shown on the frontal boss of a fossil specimen of muskox (*Ovibos moschatus*, USNM RSFVL # 18 S. #176); (D) projecting skin structure, shown on the nasal boss of white rhinoceros (*Ceratotherium simum*, AMNH 81815); and (E) armor-like dermis, shown on the premaxilla of hippopotamus (*Hippopotamus amphibius*, USNM 313712). Villose skin, feathered skin, and glabrous skin are not associated with bony correlates.

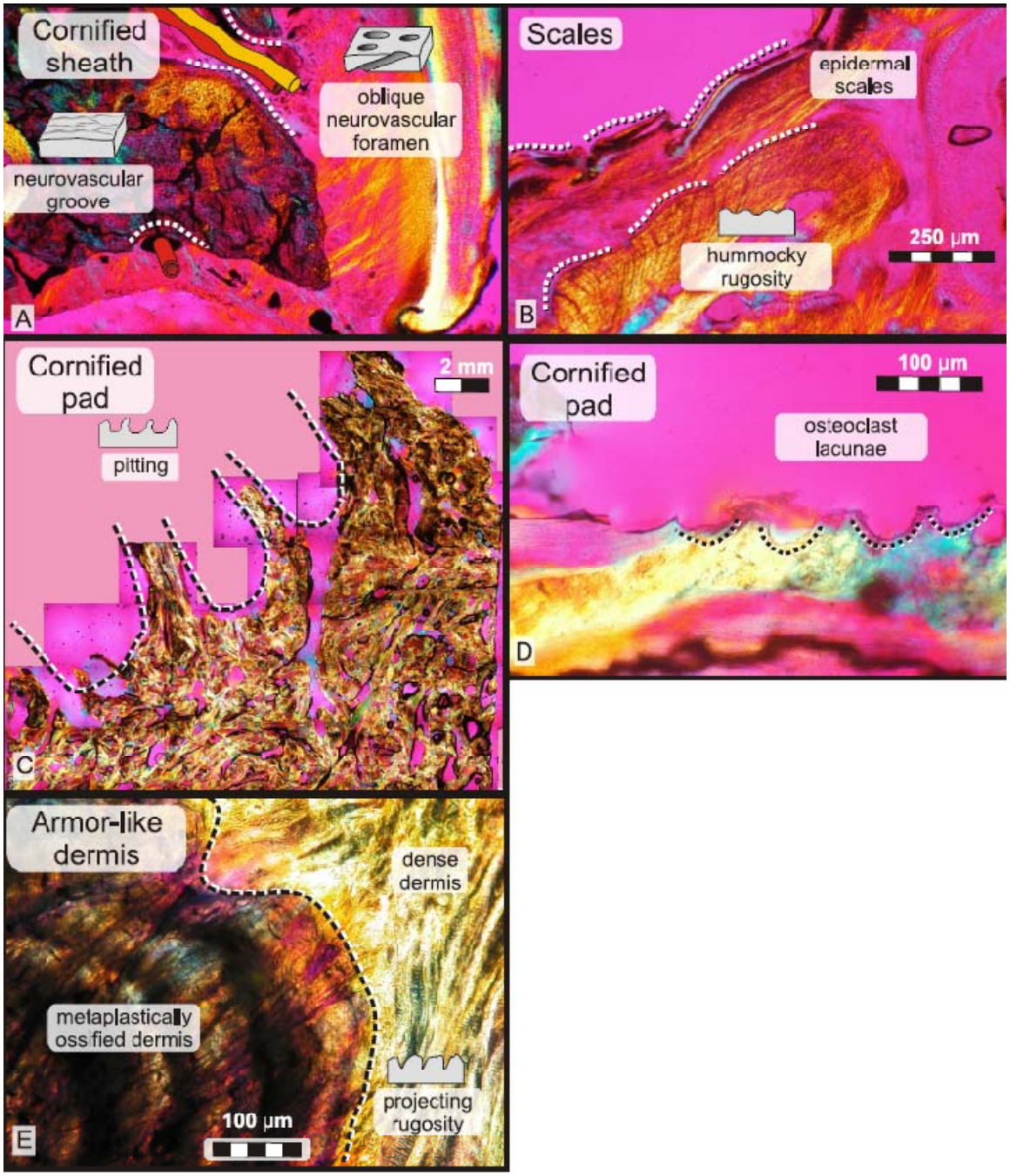
Cornified sheath
oblique neurovascular foramen
neurovascular groove
A
Scales
epidermal scales
hummocky rugosity
250 µm
B
Cornified pad
2 mm
pitting
C
Cornified pad
100 µm
osteoclast lacunae
D
Armor-like dermis
dense dermis
metaplastically ossified dermis
projecting rugosity
100 µm
E

Figure 5-8. Histological correlates for categories of skin structures used in this study, represented by an example histological section: (A) cornified sheath, shown on a coronal section from the rostrum of a double-crested cormorant (*Phalacrocorax auritus*, OUVC 10401); (B) scales, shown on a longitudinal section from the nasals of a Madagascar spiny-tailed iguana (*Oplurus cuvieri*, OUVC 10419); (C) and (D) cornified pads, shown on coronal sections from the frontal boss of a muskox (*Ovibos moschatus*, UAM 86916); and (E) armor-like dermis, shown on a coronal section from the frontal of a white rhinoceros (*Ceratotherium simum*, OUVC 9541).

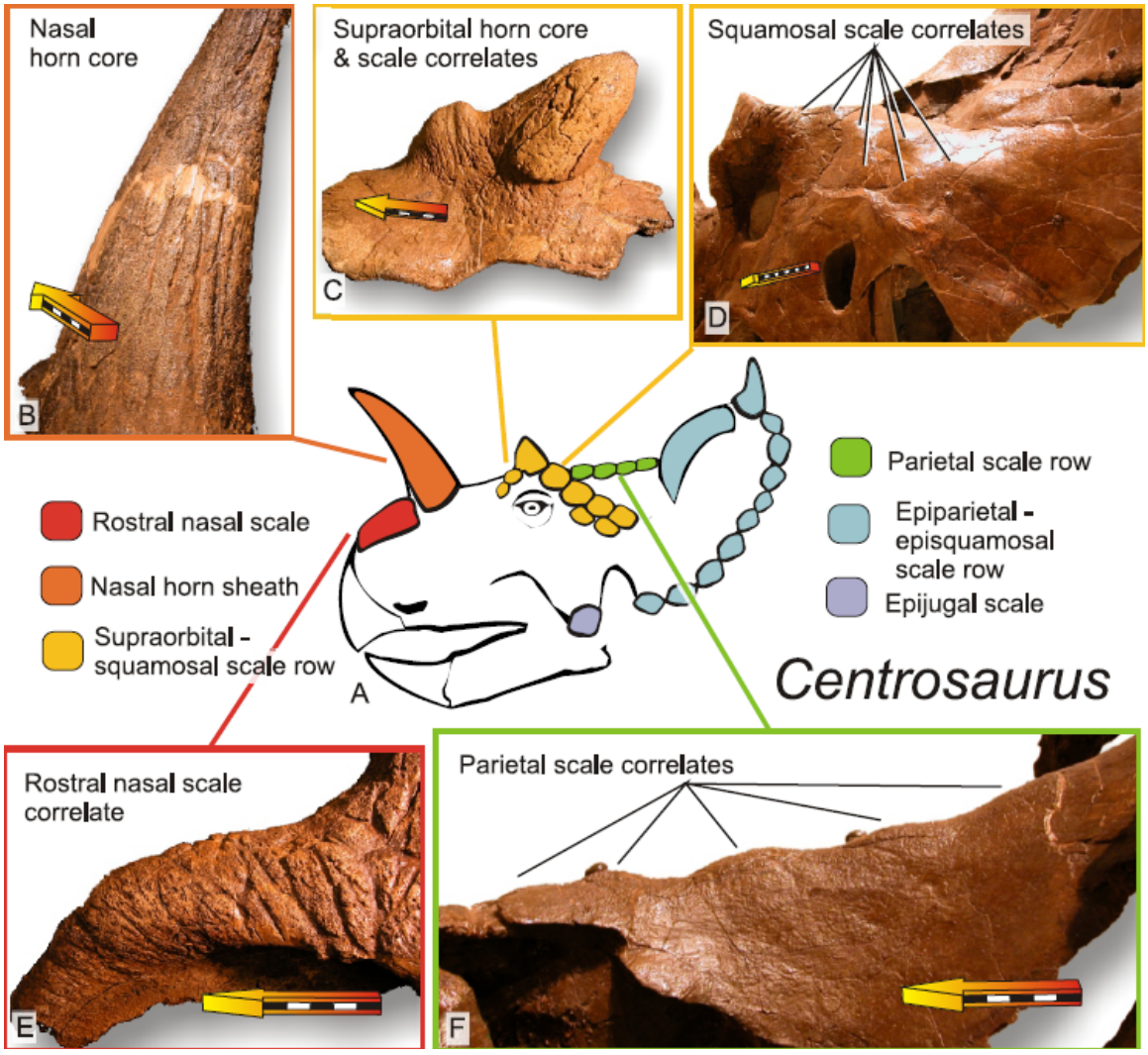

Figure 5-9. (A) Skin structures inferred for *Centrosaurus*, based on osteological correlates visible in insets (B-F). Scale bars are 5 cm with arrowhead pointing rostrally, unless otherwise noted. (B) Neurovascular grooves on the nasal horn core, shown on ROM 49863 cf. *Centrosaurus*. (C) Basal sulcus on supraorbital horn core, caudal to a raised scale correlate, shown on ROM 12782 cf. *Centrosaurus*. (D) A row of shallow scale correlates on the squamosal, shown on ROM 767 *Centrosaurus apertus*. Scale bar is 10 cm. (E) Neurovascular sulci and faint basal sulcus on the nasal rostral to the nasal horn core, shown on ROM 831 *Centrosaurus*. (F) A median row of shallow scale correlates on the parietal bar, shown in ROM 767 *Centrosaurus apertus*.

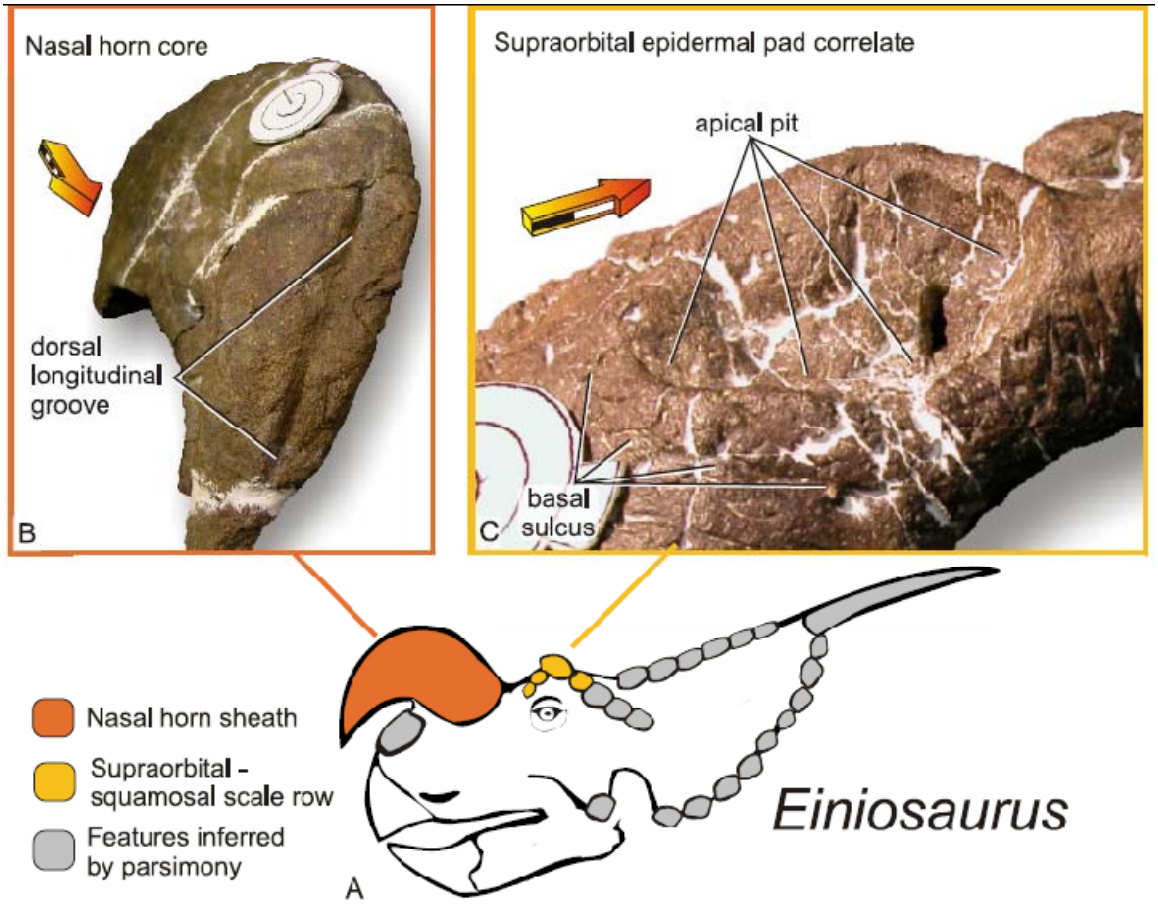

Figure 5-10. (A) Skin structures inferred for *Einiosaurus*. Shaded elements were not represented by skeletal specimens in this study, and are inferred from the presence of similar structures in other centrosaurine taxa. (B) Nasal horn core, showing dorsal longitudinal groove present in Canyon Bonebed specimens, shown on MOR 456 8-13-7-5 *Einiosaurus procurvicornis*. Scale bar is 5 cm, with arrowhead pointing rostrally. (C) Apical pit in the place of supraorbital horncore, with a basal sulcus indicating the extent of the cornified sheath, shown on MOR 456 8-9-6-1 *Einiosaurus procurvicornis*. Scale bar is 2 cm.

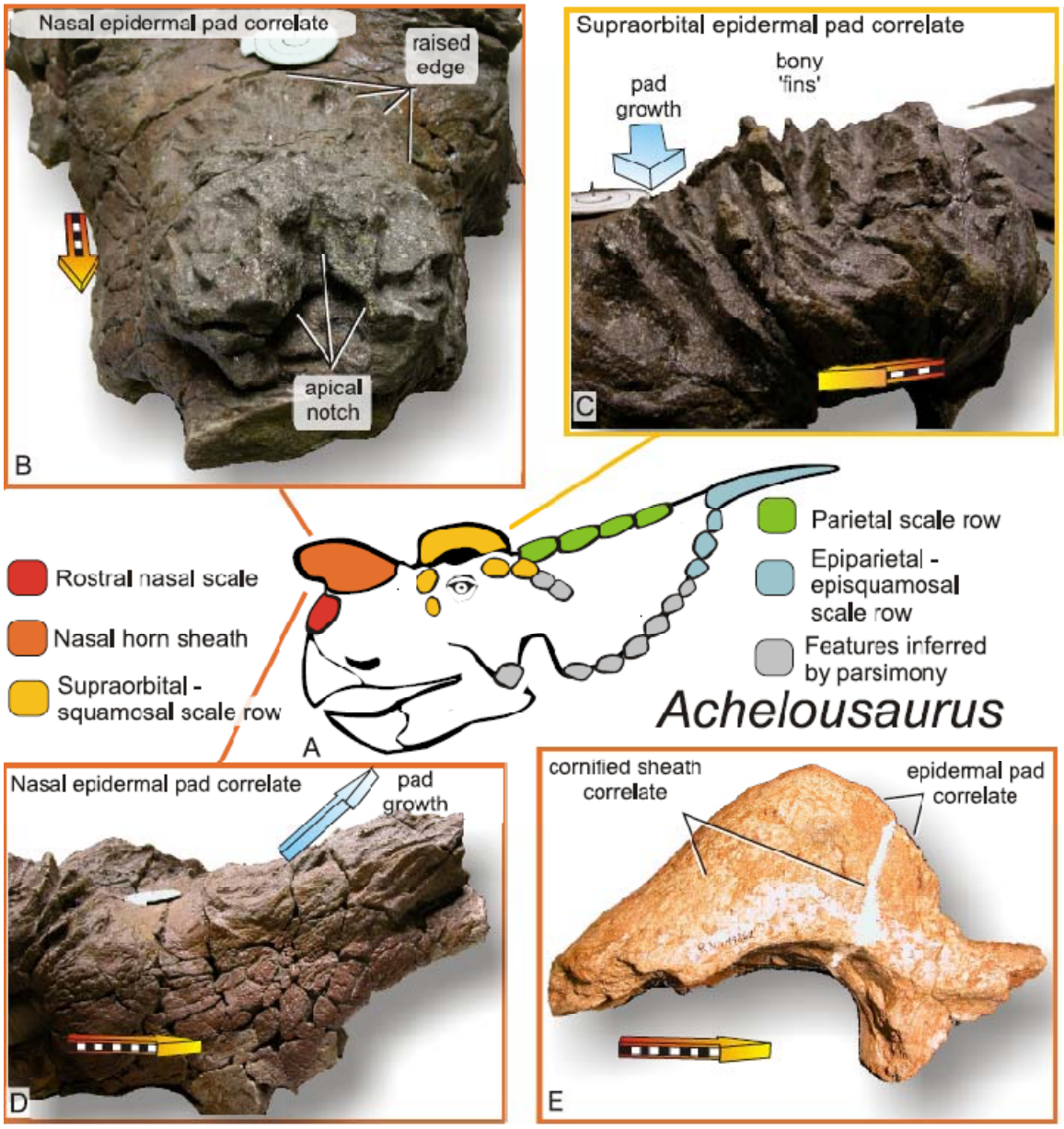

Figure 5-11. (A) Skin structures inferred for *Achelousaurus.* Shaded elements as in Figure 5-10. Scale bars are 5 cm with arrowhead pointing rostrally, unless otherwise noted. (B) Rostral view of the nasal boss, showing the apical notch with superimposed pitting on MOR 485 *Achelousaurus horneri*. Raised edge indicates the caudal extent of the cornified nasal pad. (C) Rostrolateral view of the supraorbital region, showing bony "fins" similar to those seen on extant muskoxen on MOR 485 *Achelousaurus horneri*. Blue arrow indicates inferred growth direction, towards the viewer. (D) Lateral view of nasal boss, with inferred growth direction for the cornified nasal pad, shown on MOR 485 *Achelousaurus horneri*. Compare with Figure 5-12E. Scale bar is 10cm. (E) Unidentified centrosaurine nasal horn core (ROM 49862) with the osteological correlate for a cornified pad at the rostral apex. Morphology is transitional between that of *Einiosaurus/Centrosaurus* and *Achelousaurus*. Scale bar is 10 cm.

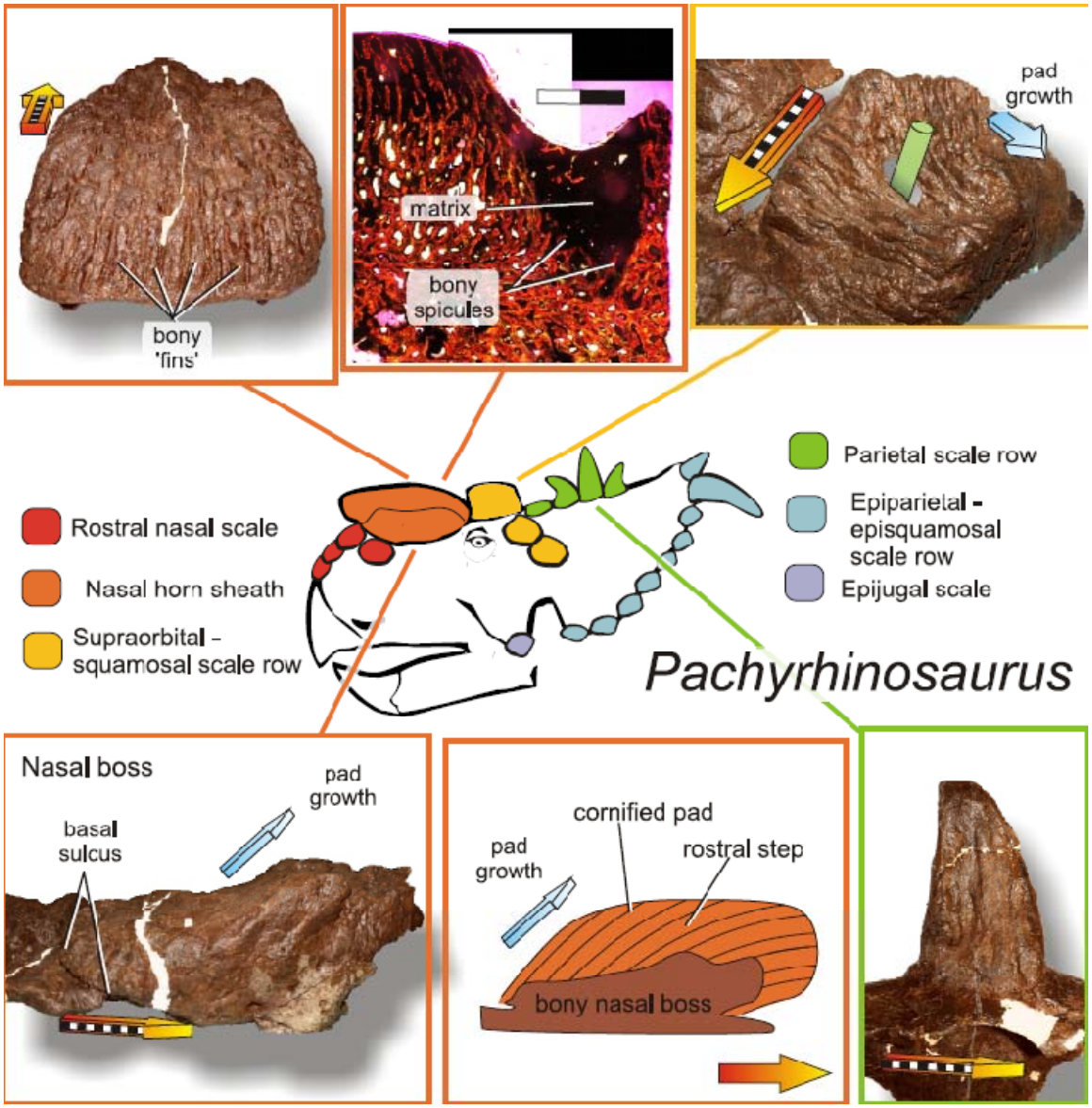

Figure 5-12. (A) Skin structures inferred for *Pachyrhinosaurus*. Scale bars are 10 cm with arrowhead pointing rostrally, unless otherwise noted. (B) Caudal view of the nasal boss of TMP 86.55.206 *P. lakustai*, showing bony "fins" indicative of a cornified pad growing at a low angle to the bone surface. (C) Histological section of a bony "fin" and sulcus from the nasal boss of *P. lakustai*, showing infill of matrix and fine bone spicules; compare to Figure 5-8C. Scale bar is 2mm. (D) Supraorbital boss of TMP 89.55.427 *P. lakustai*, showing bony "fins" and communication with frontal sinus (green bar). Blue arrow shows inferred growth direction for the overlying cornified pad. (E) Nasal boss of TMP 89.55.427 *P. lakustai*, showing basal sulcus and bony "fins" at the caudal end of the boss. The nasal boss of this specimen is very similar to an adult *Achelousaurus* nasal boss (Fig. 5-11D). (F) Schematic of inferred cornified tissue on the bony nasal boss of *Pachyrhinosaurus* spp. (G) Parietal horn of TMP 86.55.258 *P. lakustai*.

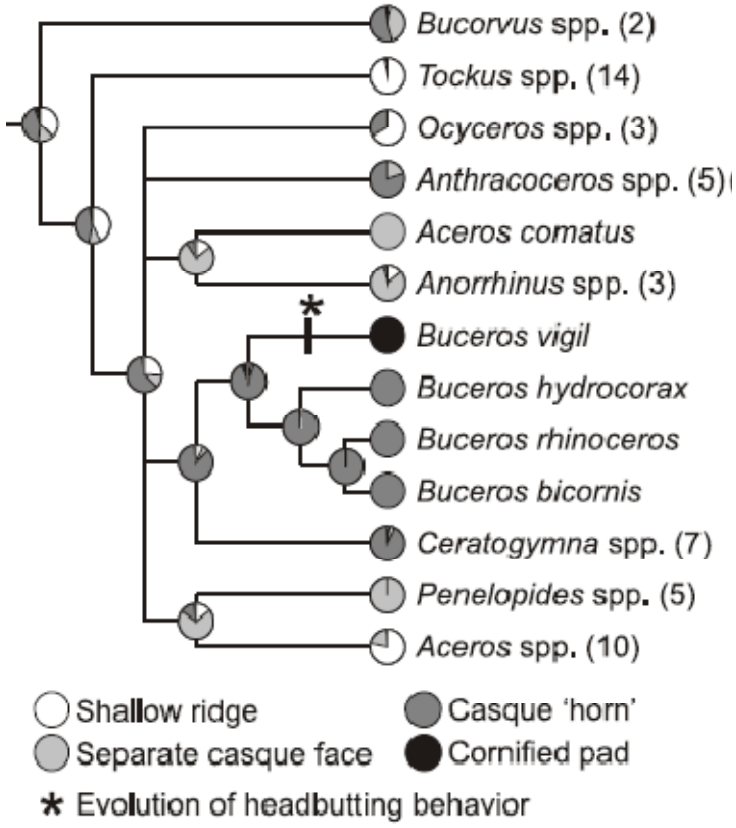

Figure 5-13. Ancestral character state reconstructions of casque morphology and headbutting behavior in Bucerotidae (hornbills). A casque with a projecting "horn" is unequivocally reconstructed for *Ceratogymna+Buceros*, and the transition to a cornified pad in *Buceros vigil* is accompanied by a transition from light bill clashing to headbutting behaviors (asterisk). Nodes show proportional likelihoods for each morphological character state with Pagel (1992) transformed branch lengths. Topology after Kemp (1995).

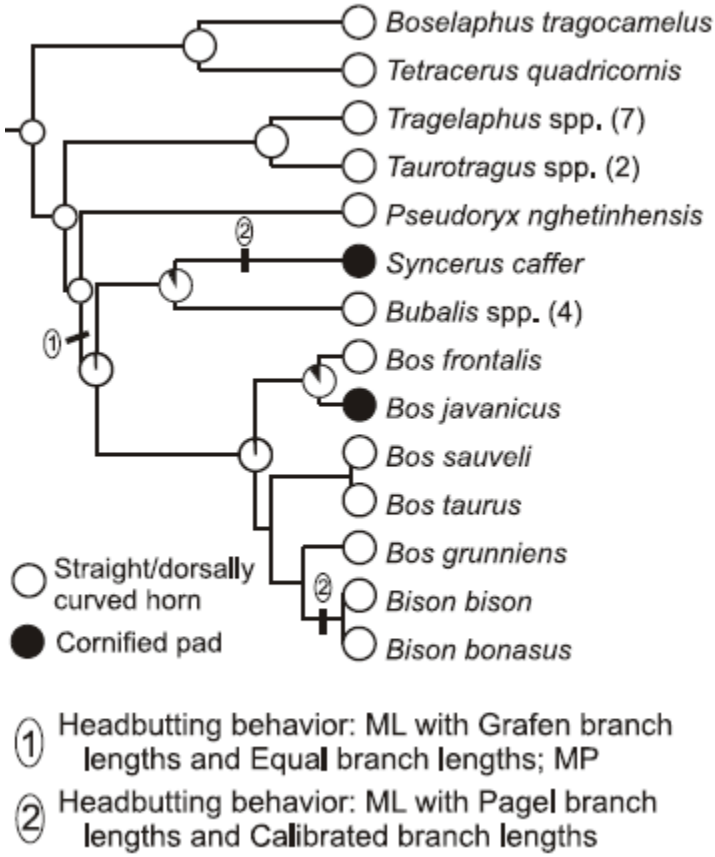

Figure 5-14. Ancestral character state reconstructions of horn morphology and headbutting behavior in Bovinae (cattle and allies). The transition to a cornified pad in *Syncerus* is associated with an increase in the intensity of headbutting and charging behavior compared to related taxa, but the domestication of some forms of *Bubalis* and *Bos* and a paucity of behavioral data for the remaining members of Bovini contribute to a low-resolution picture of the relationship between horn morphology and agonistic behavior in this clade. Nodes show proportional likelihoods for each morphological character state with the published topology and branch lengths of Fernández and Vrba (2005). The topology of Hassanin and Ropiquet (2004) was also used for this test.

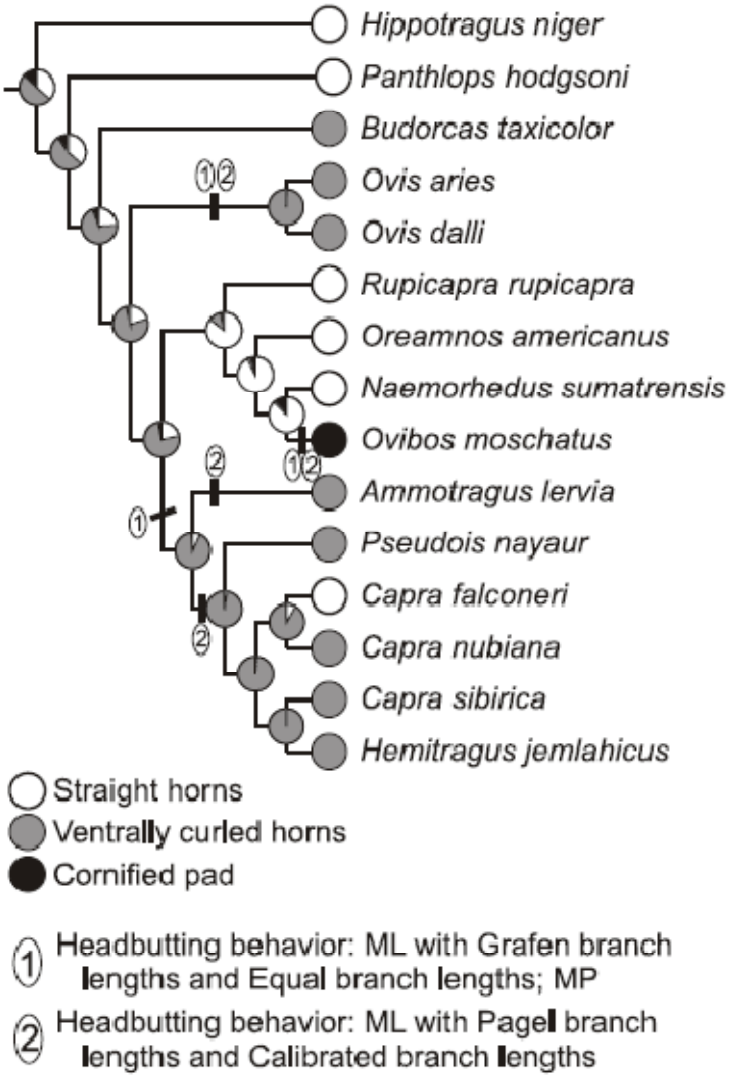

Figure 5-15. Ancestral character state reconstructions of horn morphology and headbutting behavior in Caprinae (goats and sheep) and outgroups. Most unequivocal reconstructions of ventrally curved horns (*Ovis*, *Ammotragus*, and *Capra*+*Pseudois* in this example) are matched by unequivocal reconstructions of headbutting behavior, as is the transition from straight horns to cornified pads in *Ovibos*. Node show proportional likelihoods for each morphological character state with Pagel (1992) transformed branch lengths and the topology of Ropiquet and Hassanin (2005). The topology of Lalueza-Fox et al. (2005) was also used for this test.

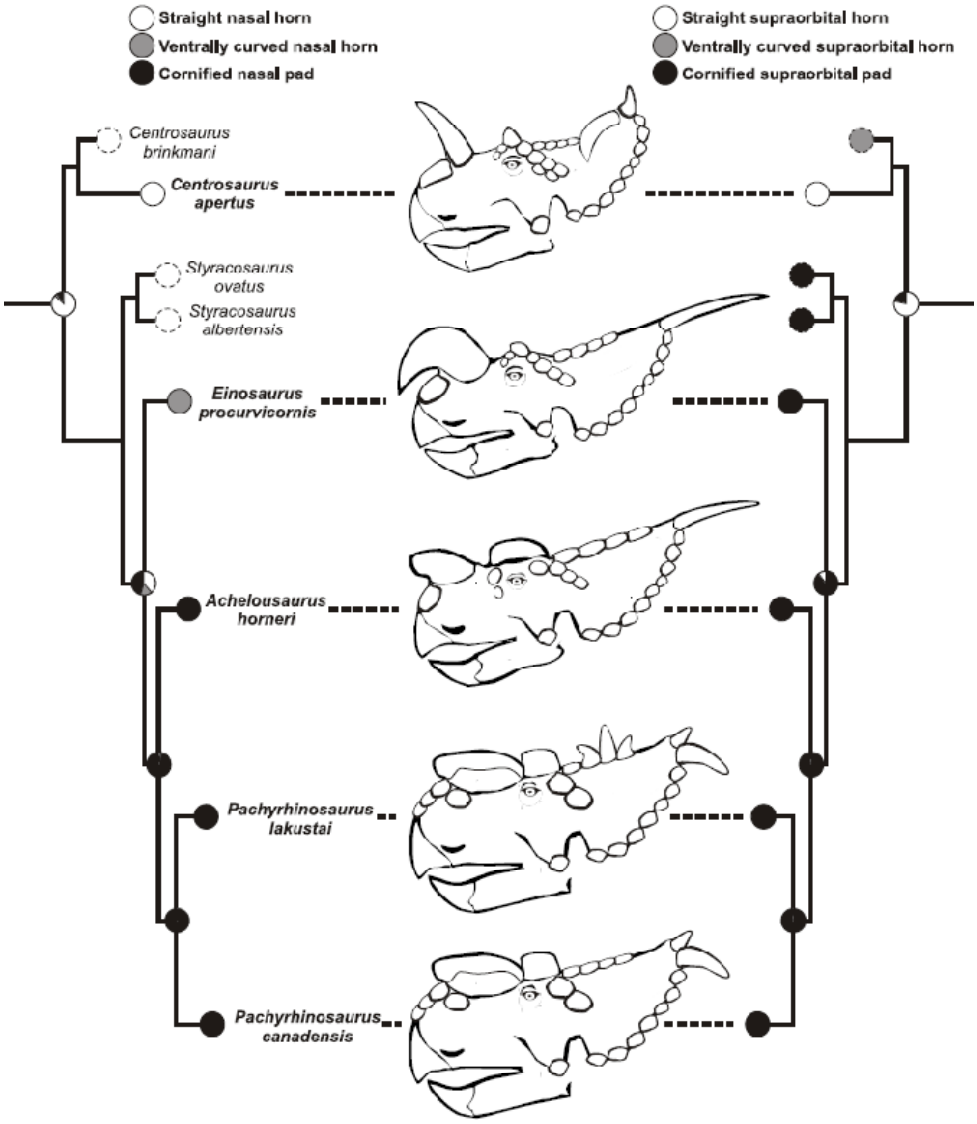

Figure 5-16. ML Ancestral character state reconstructions of nasal (A) and supraorbital (B) horn morphology in centrosaurine dinosaurs. The transition from straight horns in basal centrosaurines to ventrally curved nasal horns and cornified pads in derived centrosaurines is very similar to the morphological transitions associated with headbutting behavior in extant caprines. The primitive polymorphism of supraorbital horn cores in *Centrosaurus* (Sampson et al. 1997) is canalized in more derived centrosaurines, and this development is followed by the progression of ventrally curved nasal horns and cornified pads in *Einiosaurus*, *Achelousaurus*, and *Pachyrhinosaurus*. Character states for *Centrosaurus brinkmani*, *Styracosaurus ovatus*, and *Styracosaurus albertensis* were taken from published descriptions, and were not included in ancestral character state reconstructions.

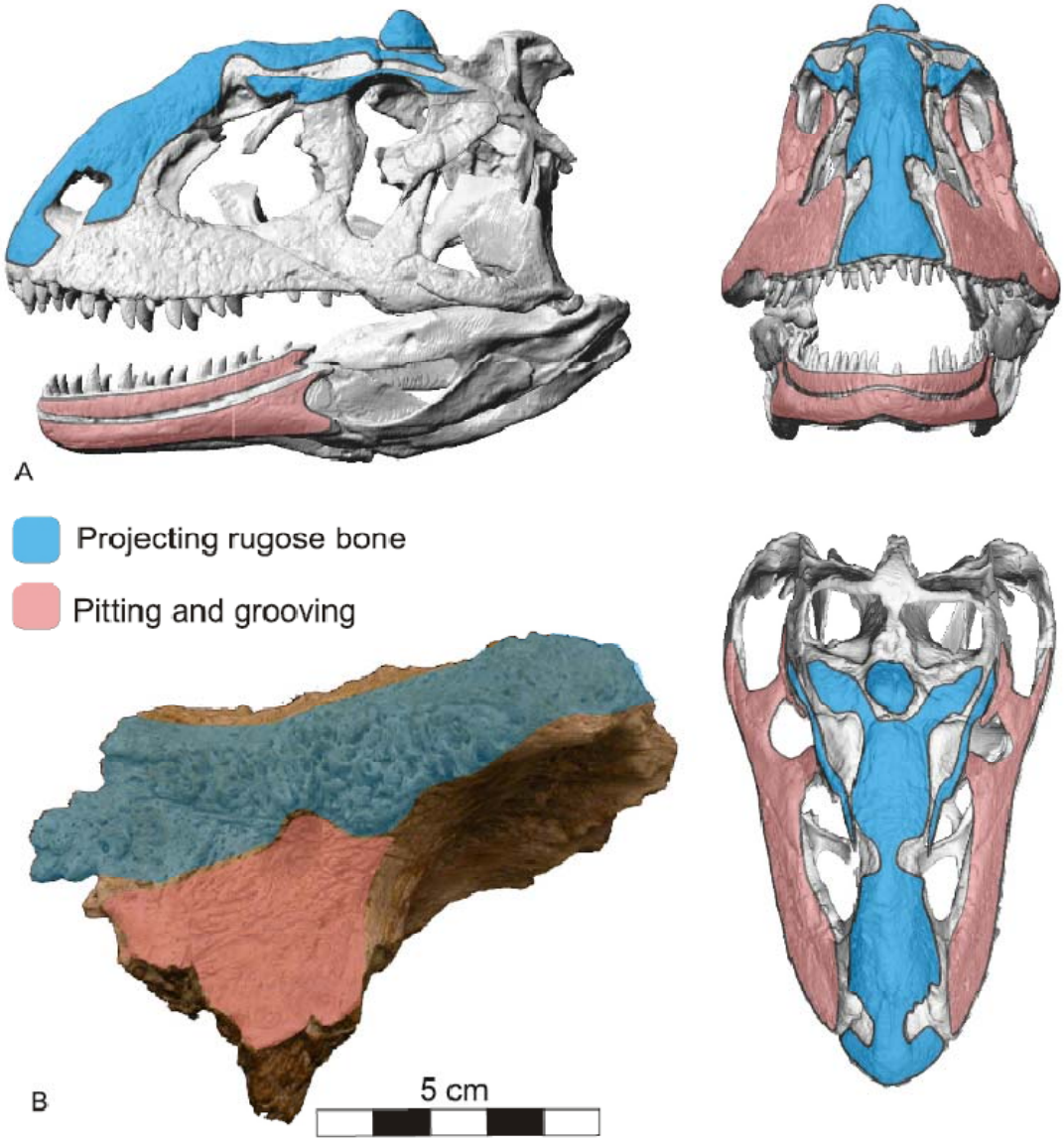

Figure 6-1. Surface rendering of the skull of *Majungasaurus crenatissimus* (FMNH PR 2100), showing (A) areas of pitting and grooving on the lateral surface of the face (red) as distinguished from projecting rugose bone across the skull roof (blue). Inset in (B) shows projecting rugose bone texture on the dorsal part of the lacrimal in UA 8718.

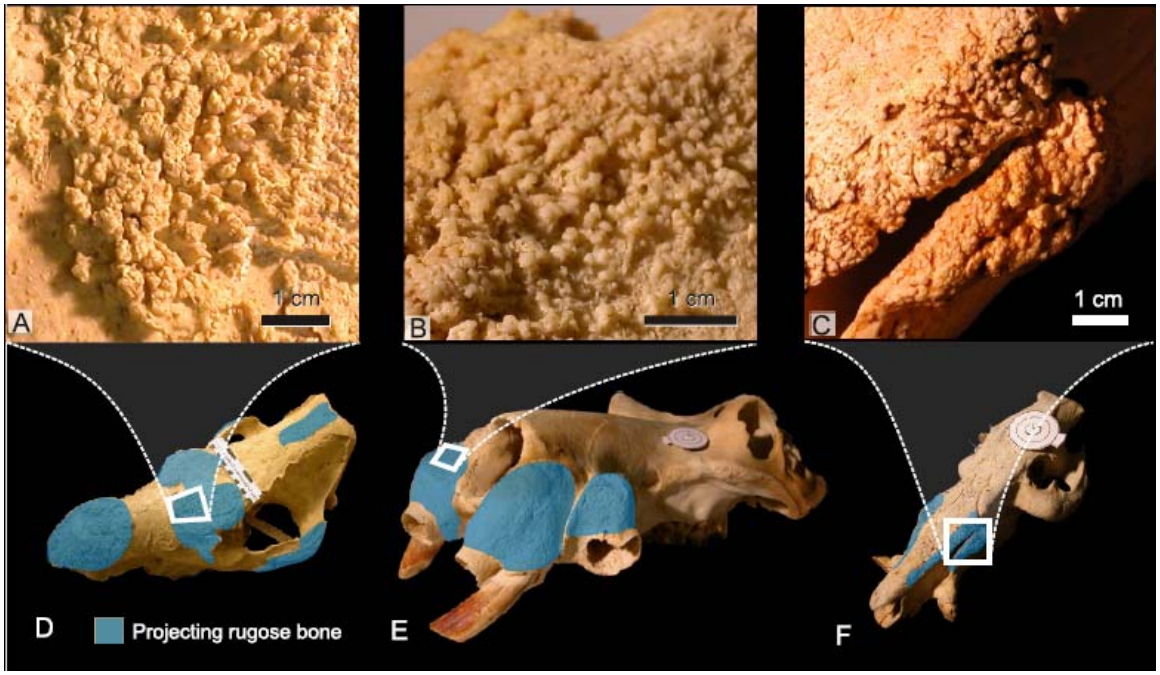

Figure 6-2. Skulls of *Dicerorhinus* (Sumatran rhino; A, D), *Hippopotamus* (B, E), and *Potamochoerus* (red river hog; C, F), all in oblique left rostrolateral view, showing projecting rugose bone (A–C) and its distribution (D–F). Scale bar on D is 14 cm; round scale bars on E and F are 6 cm in diameter.

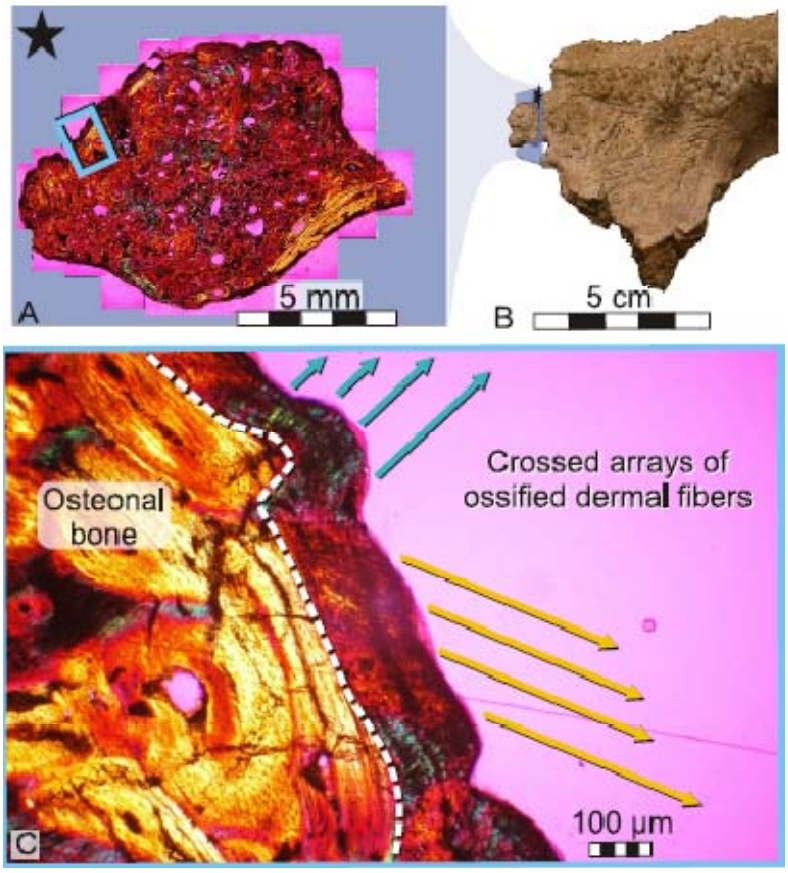

Figure 6-3. Paleohistology of projecting rugose bone in *Majungasaurus crenatissimus* (UA 8718). A lateral view of the left lacrimal (B) shows the plane of section (A), with the star in the upper left marking the dorsolateral corner of the section. Inset at bottom (C) shows an external "rind" of dermal ossification (dashed line) composed of crossed arrays of ossified dermal collagen fiber bundles ranging from 50–200 µm in diameter. Yellow and blue arrows show bundle orientations.

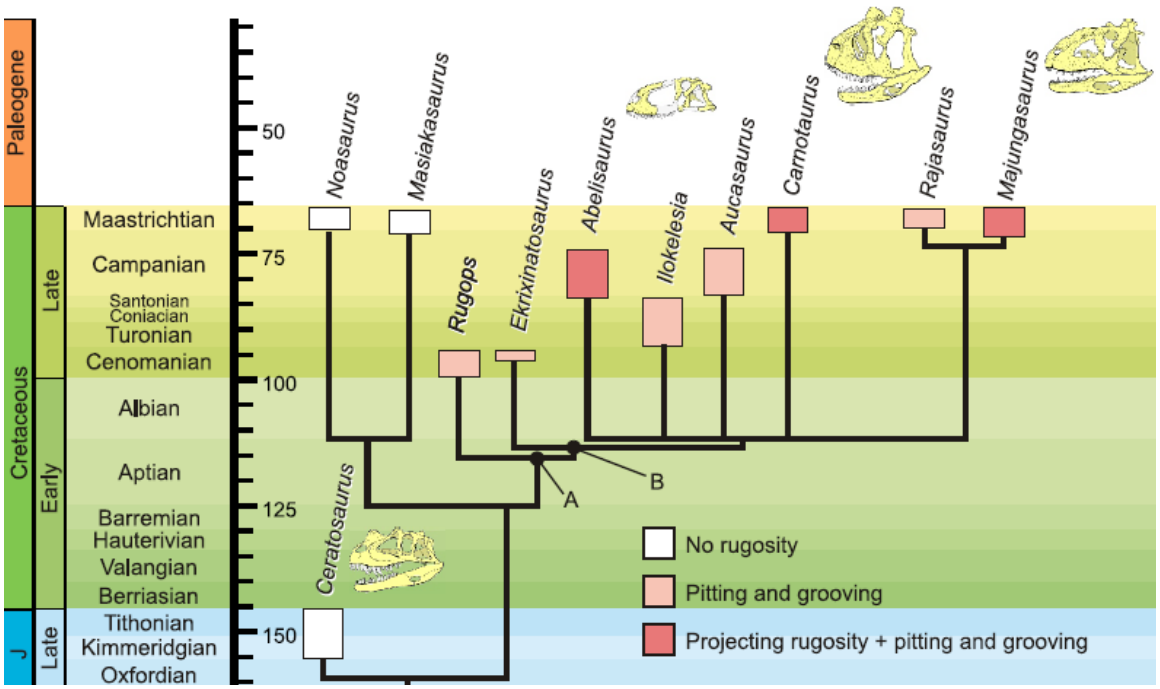

Figure 6-4. Phylogenetic and stratigraphic context for the evolution of CADA in *Majungasaurus* and other abelisaurids. Placement of the ancestral state for several cephalic characters that may also reflect more violent agonistic behaviors are shown as reconstructed by parsimony: (A) retreat of the antorbital fossa from the dorsolateral margin of the maxilla; presence of dermal bone covering the lacrimal fossa; grooving on interdental plates. (B) Presence of suborbital flange of the postorbital bone; presence of dermal bone covering the squamosal-postorbital contact. Topology, divergence dates, and character states in A and B after Carrano and Sampson (2008).

APPENDIX A: SUPPLEMENTARY INFORMATION FOR CHAPTER 2

Data for comparative analyses were downloaded from the Paleobiology Database (www.paleodb.org) on 24 February, using the following parameters: output data = occurrence matrix; taxa to include = trigonias, gaindatherium, aletomeryx, climacoceras, syndyoceras, dicrocerus, eotragus, paleomeryx, paracosoryx; timescale = Gradstein 7: stages; include preservation categories = regular taxon, form taxon.

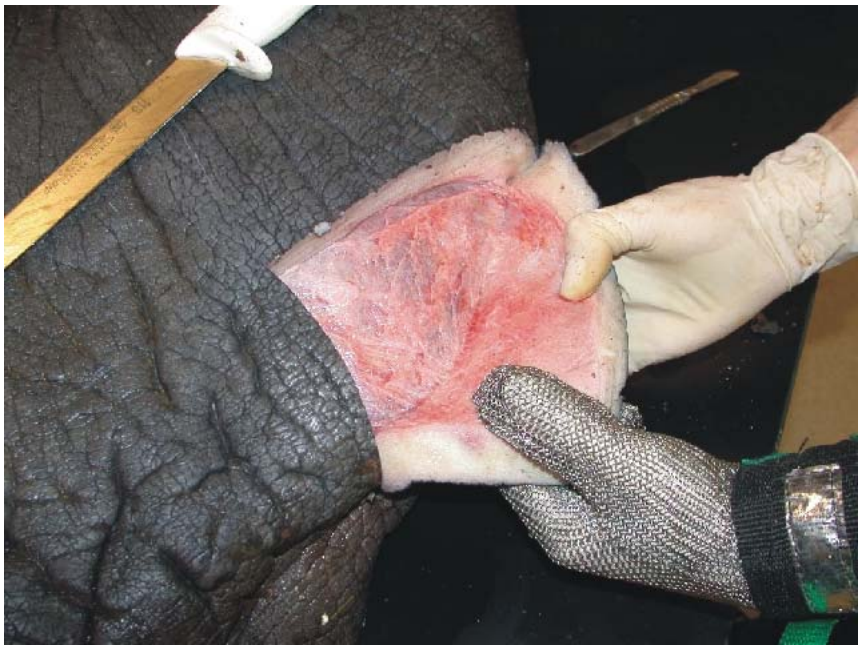

Figure A-1. A portion of skin overlying the left cheek region of a white rhinoceros (*Ceratotherium simum*, Ohio University Vertebrate Collections [OUVC] 9541). This sample is representative of skin thickness across the rest of the head and much of the body for extant rhinoceros taxa. In addition to the marked difference in thickness when compared to the dermis of other mammals, rhinoceros dermis is composed of crossed arrays of large-diameter collagen fibers, imparting increased stiffness and strength to the tissue (Shadwick et al. 1992).

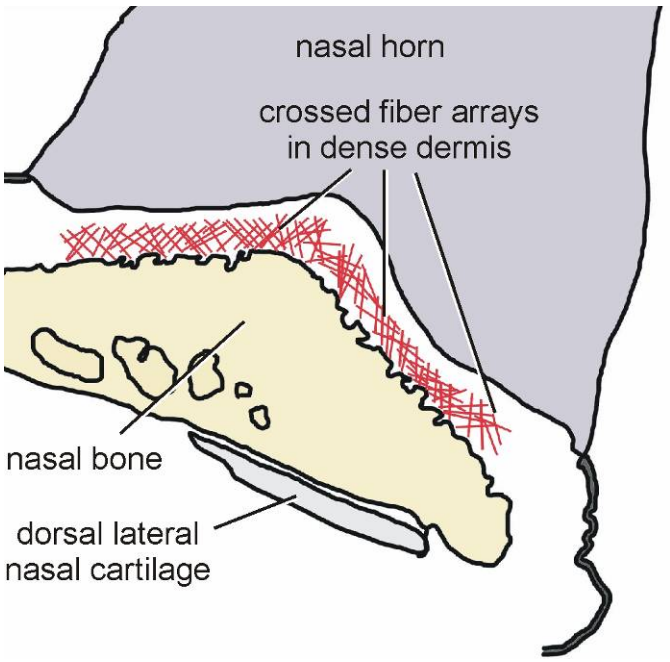

Figure A-2. Schematic representation of dermal fiber bundle orientations at the midline beneath the nasal horn of white rhinoceros (*Ceratotherium simum*, OUVC 9541), showing crossed fiber arrays. Fiber bundles along the midline are predominantly oriented along the sagittal plane.

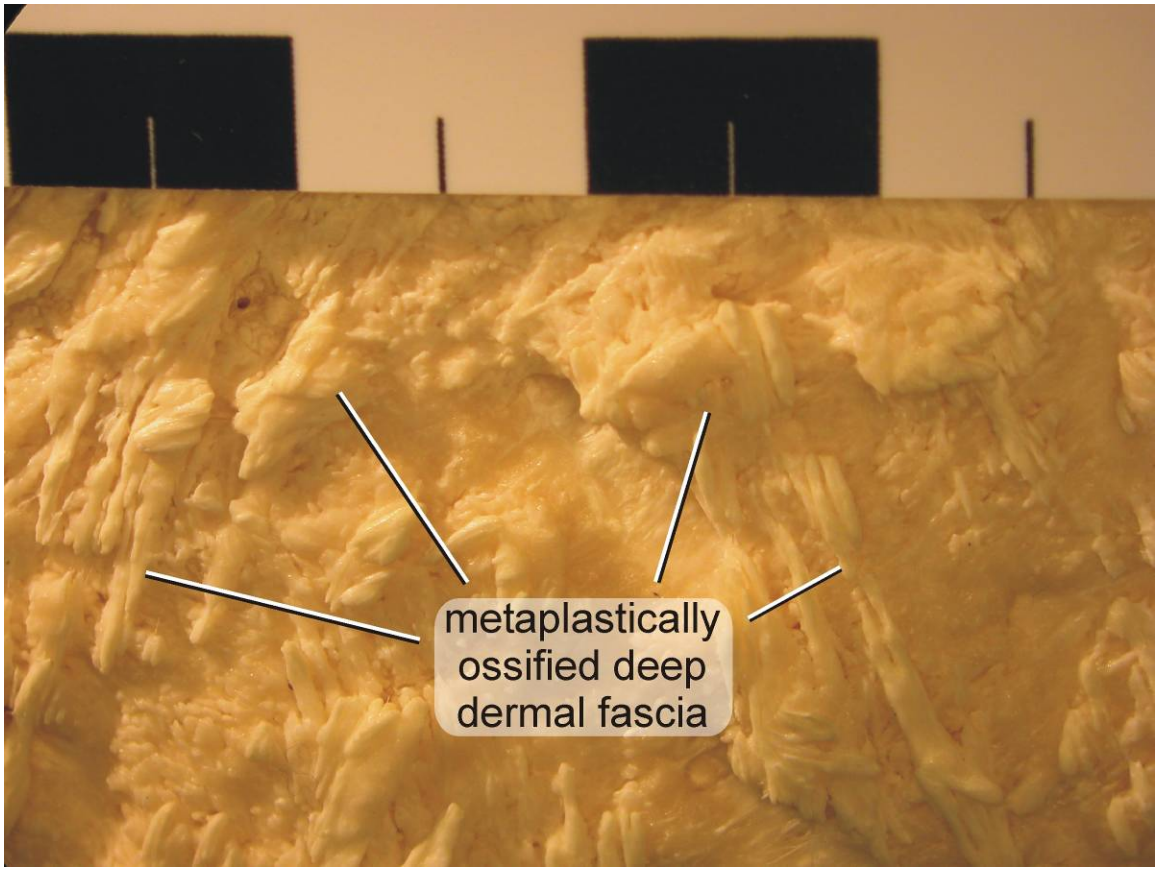

Figure A-3. Cleaned bone surface from beneath frontal horn of white rhinoceros (*Ceratotherium simum*, OUVC 9541). Much of the rugose texture visible on the bone surface is the result of metaplastic ossification, or bone growth within existing connective tissue (Haines and Mohuiddin 1968) of the deep dermal fascia (= superficial fascia of human anatomy). Scale bar increments equal 1 cm.

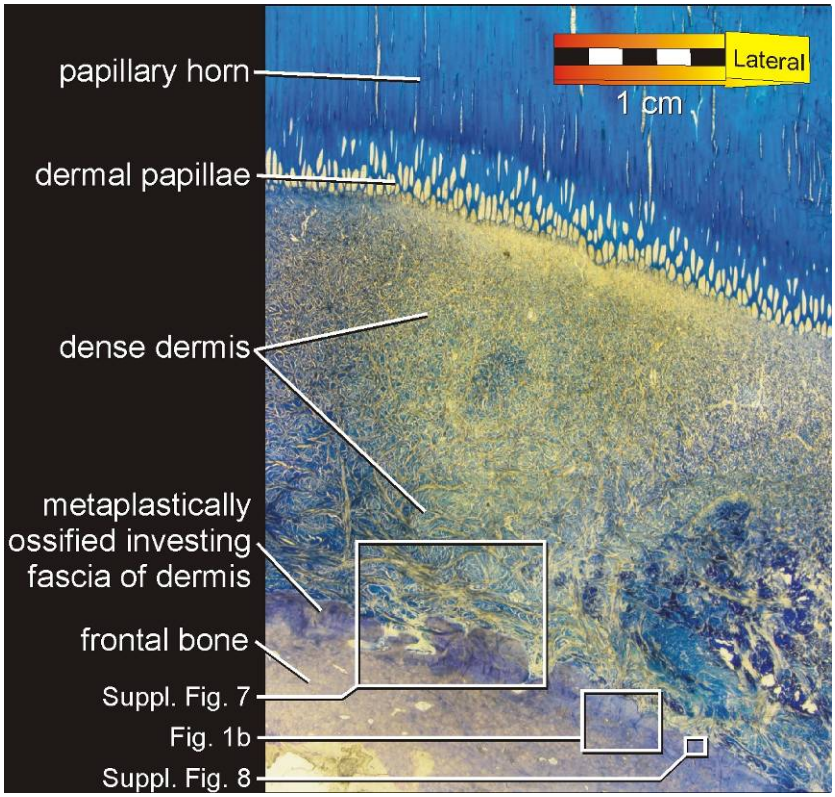

Figure A-4. Plan view of transverse cross-sectional histology beneath the frontal horn of a white rhinoceros (*Ceratotherium simum*, OUVC 9541). Histological sections for this study were cut from polymethylmethacrylate (PMMA) plastic embedded tissue blocks, polished, and surface stained with Toluidine Blue O. Illumination for this image was provided by unaltered white light. The individual tubules of cornified epidermis that make up the horn (Ryder 1962) are clearly visible, especially at the base of the horn where they surround dermal papillae. The reticular or dense dermis beneath the horn shows a gradient in collagen fiber bundle size between approximately 50 μm near the horn and approximately 700 μm near the underlying bony attachment. Inset boxes show the areas displayed in other figures.

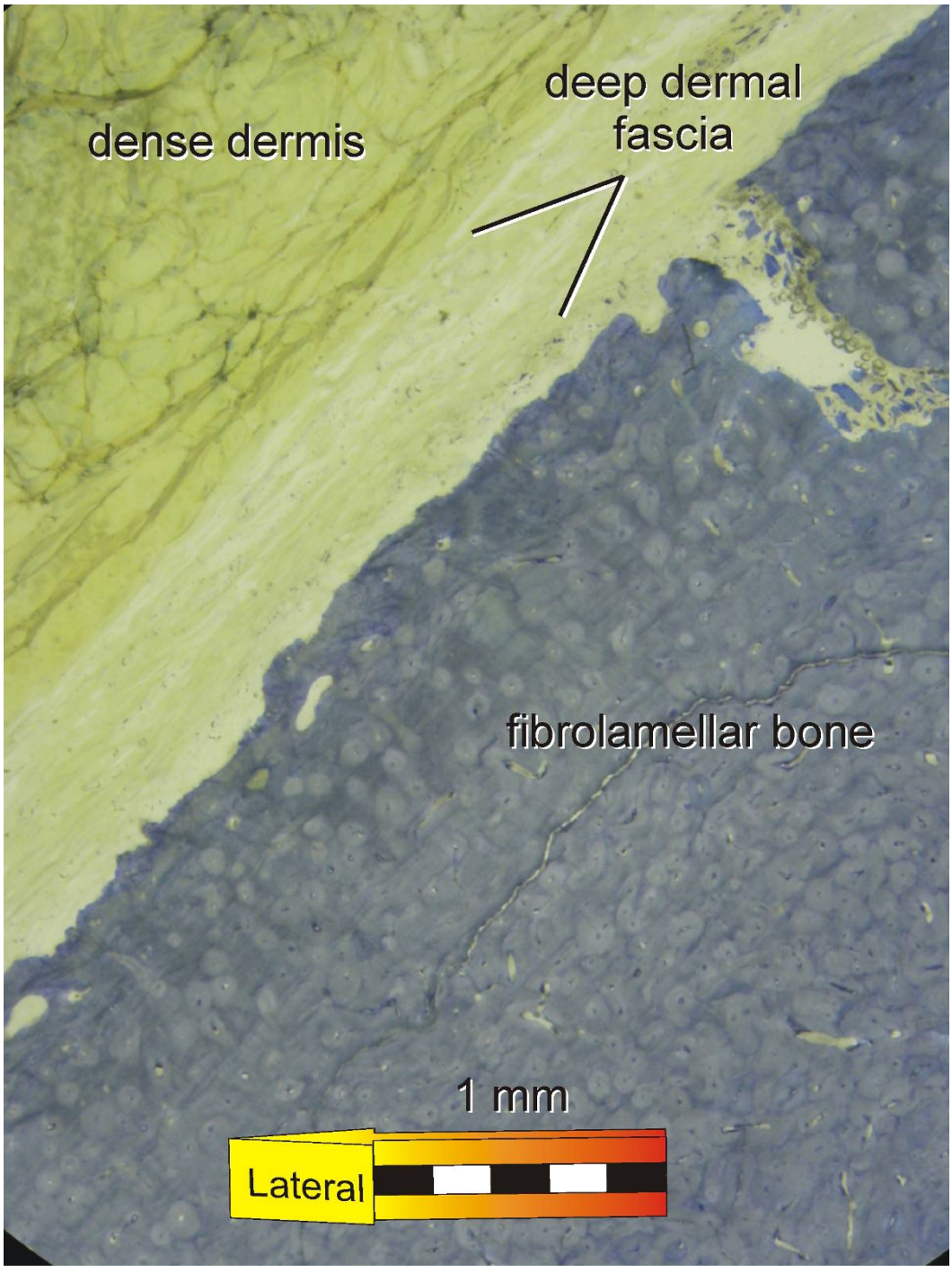

Figure A-5. Bone-dermis border from behind the frontal horn, illuminated with unaltered white light. This section was taken approximately 4 cm caudal to the edge of the frontal horn, and shows fibrolamellar bone extending to the periosteal surface, with the absence of metaplastically ossified dermis. A thick deep dermal fascia merges with the periosteum here. In other locations of the skull, as over the origin of *M. levator nasolabialis*, the deep dermal fascia leaves the bone surface and continues over the epimysium.

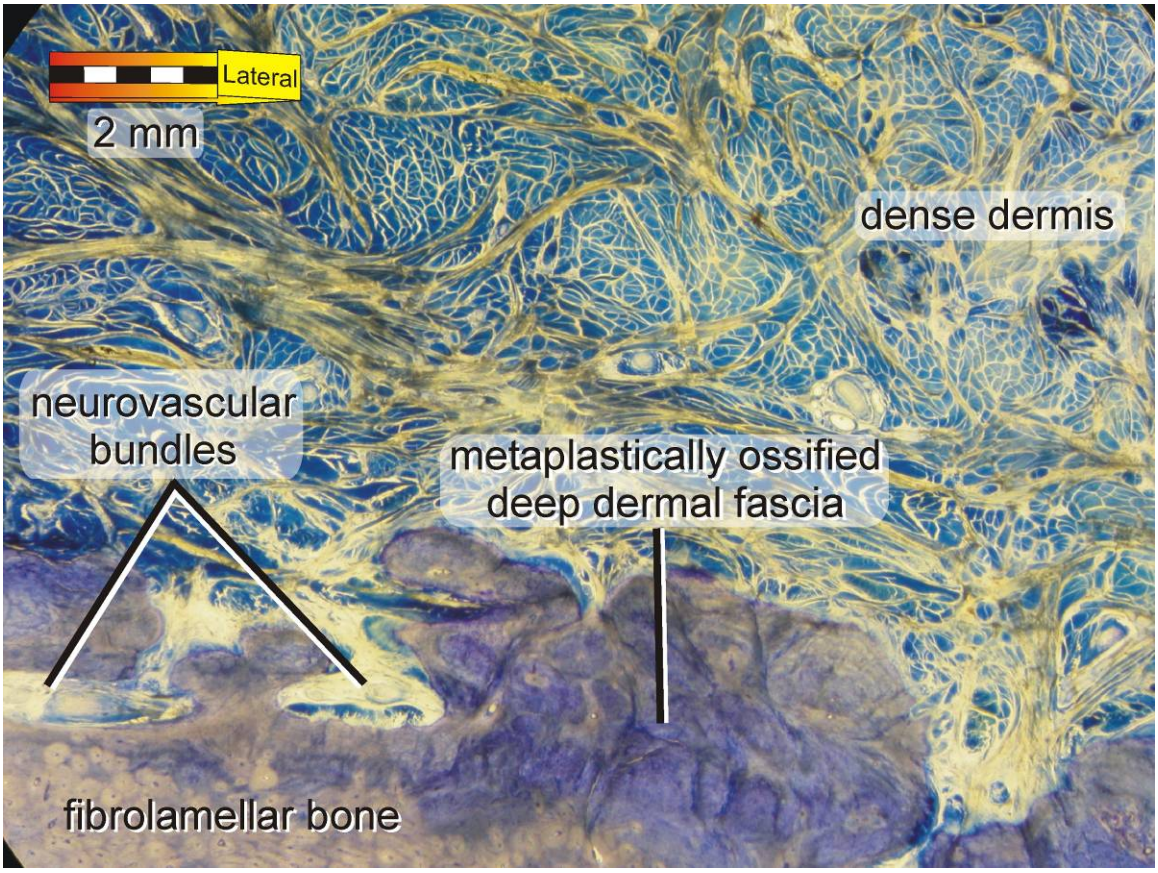

Figure A-6. Detail of the transverse section in Fig. 54, illuminated by unaltered white light. The rugose border between ossified tissues (purple) and soft tissues (blue) can be seen clearly in this image. Appositional growth around neurovascular bundles creates some of the rugosity associated with rhinoceros horn attachment. Other rugose areas (dark purple) are the result of uneven metaplastic ossification of the deep dermal fascia.

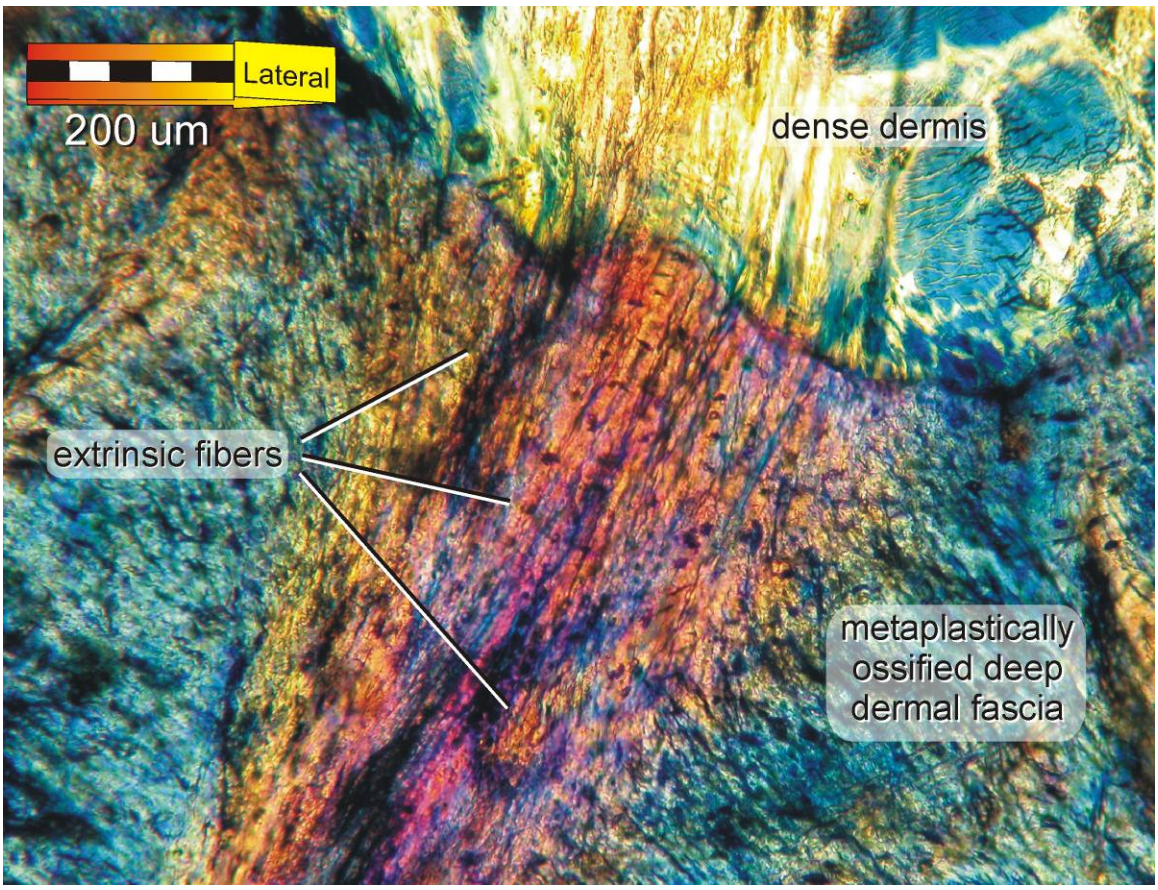

Figure A-7. Detail of the transverse section in Fig. 54, viewed under crossed polarizers with a ¼ wave plate. In this image, different fiber orientations have resulted in different interference colors, allowing normally-oriented extrinsic fibers from the dense dermis (purple-red) to be differentiated from the tangentially-oriented fibers of the metaplastically ossified deep dermal fascia. This arrangement of tissue is similar to the fibrous entheses found at some muscle and ligament attachments (Benjamin et al. 2002).

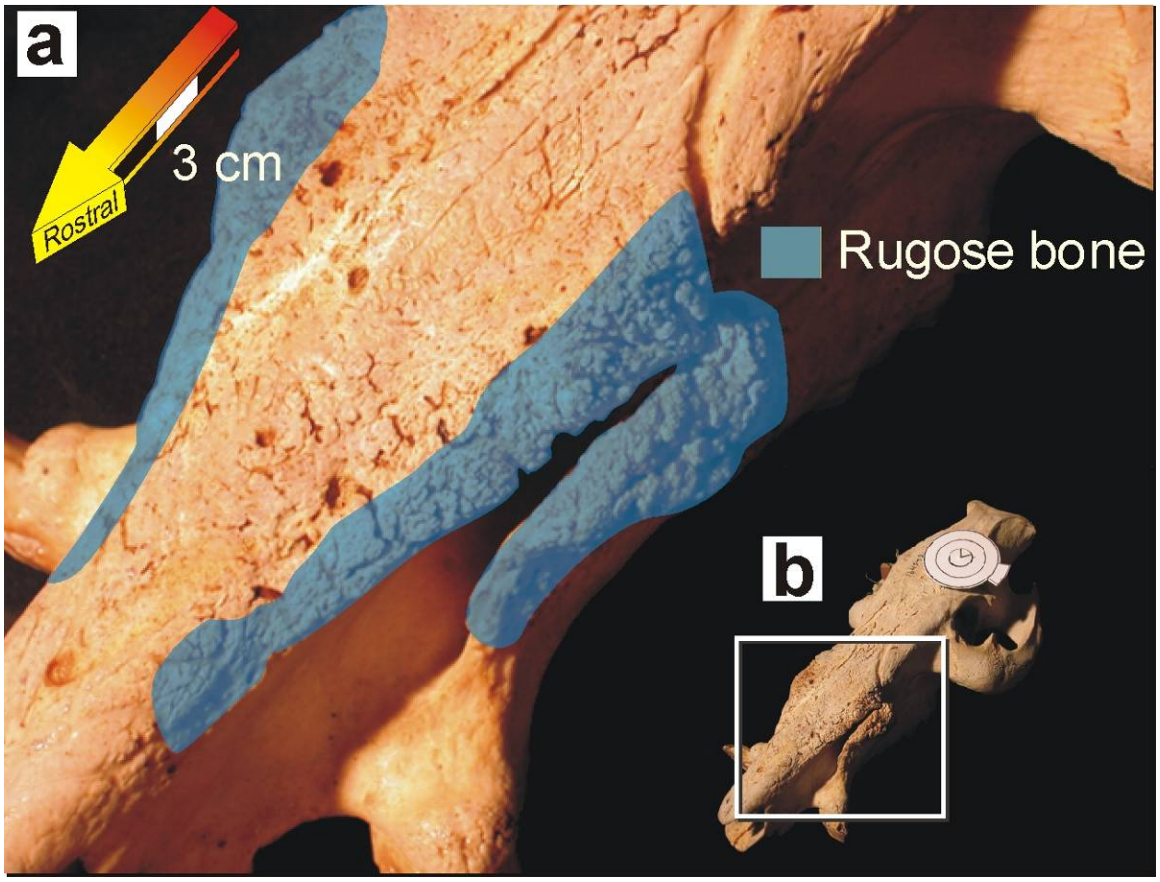

Figure A-8. Rugose bone on the maxillae and nasals of the red river hog *Potamochoerus porcus*, USNM 164542. **a.** As in *Hippopotamus*, *Potamochoerus* displays patches of rugose bone around the canine fossa of the maxilla. The extent of rugose bone closely matches the area of skin that is most often in contact with aggressors during agonistic behaviors (Kingdon 1979). In addition to the gross similarity of these rugose patches to those seen on extant and extinct rhinocerotids, the histological structure of the overlying dermis in hippopotamids and suiforms is also similar to that in extant rhinocerotids, showing prominent crossed fiber arrays (Schumacher 1931;Sokolov 1982; Shadwick et al. 1992). Although the dermal and bony morphologies of these animals are very similar, they have very different degrees of epidermal elaboration (massive horns vs. thin pliable epidermis), suggesting that dermal metaplasia is not a sufficient bony indicator for horns, but instead provides a clear bony indicator for dermal body armor. **b.** Inset box shows the location of **a** on the skull.

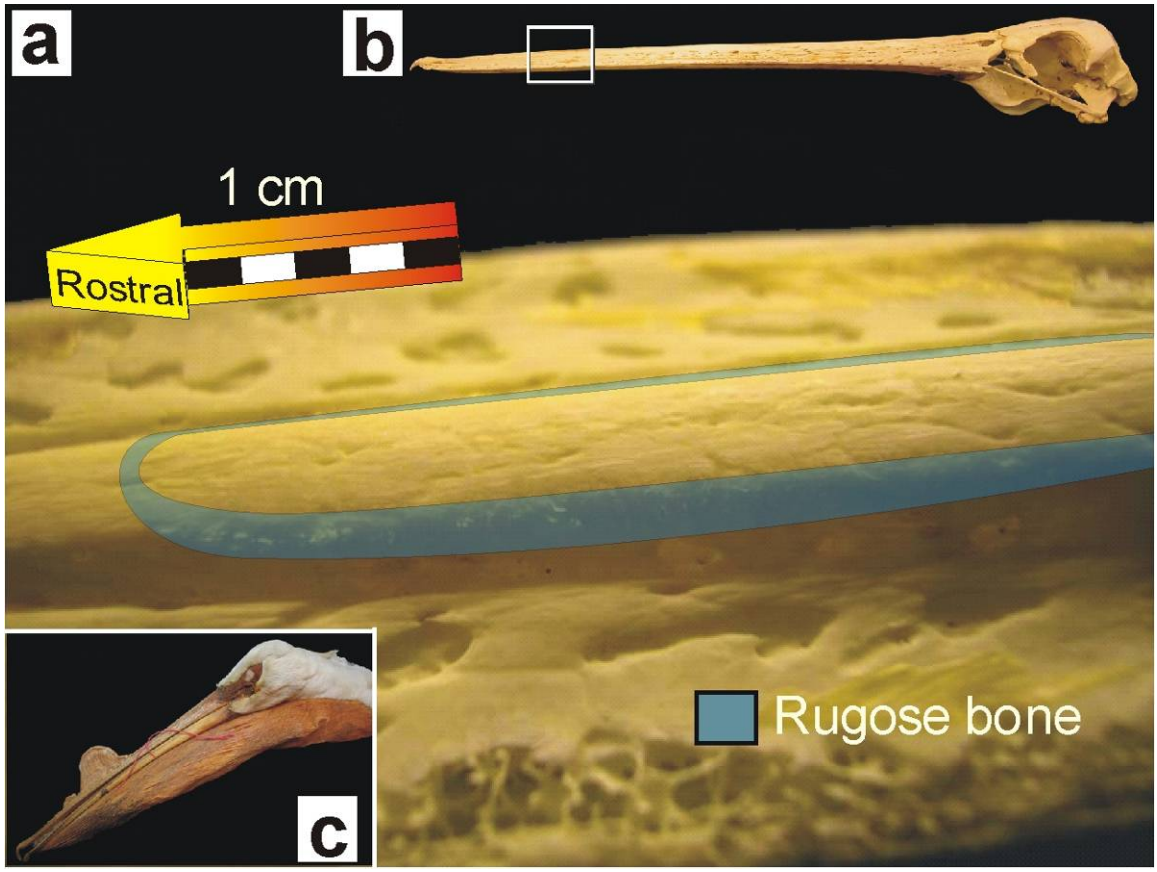

Figure A-9. Rugose bone on the premaxillae of the American white pelican *Pelecanus erythrorhynchos*. **a.** American white pelicans grow short crests of keratinous tissue for display in breeding that are shed at the end of the breeding season (May–July). Skeletal specimens from individuals that have died during this period show a faint annular rugosity at the location of the crest (ROM 151169). The annular rugosities of *P. erythrorhynchos* and *Sarkidiornis* are finer than the annular rugosities of extant rhinocerotids, most likely due to the difference in collagen fiber bundle size in metaplastically ossifying dermis. Nevertheless, the similarity in overall pattern, coupled with the similarity in skin elaborations in these taxa, suggests that annular rugosity provides a positive bony indicator for the presence of skin-derived horns and crests. **b.** Inset box shows the location of **a** on the skull. **c.** Study skin (ROM 34371) showing the size and location of the breeding crest.

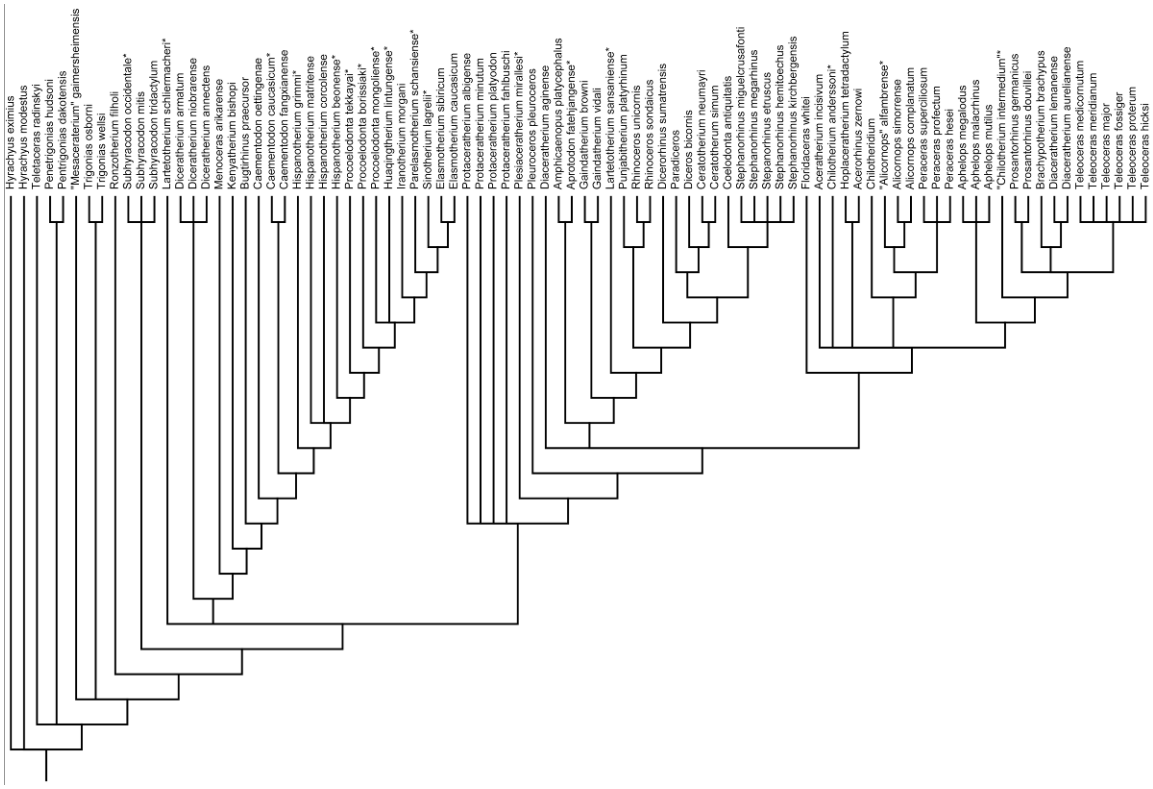

Figure A-10. Adams consensus supertree of extant and extinct Rhinocerotidae. Three morphologically based trees including extinct rhinocerotid taxa (Cerdeño 1995; Antoine 2002; Antoine et al. 2003) and three molecular trees of extant rhinocerotids (Morales and Melnick 1994; Tougard et al. 2001; Orlando et al. 2003) were coded using matrix representation with parsimony (MRP; Ragan 1992) in Mesquite 1.12 (Maddison and Maddison 2006). The tree matrix was then analyzed by a heuristic search in PAUP*4.10b (Swofford 2001). Analysis was stopped when the heuristic search returned 1000 equally parsimonious trees. The resulting trees were combined in an Adams consensus tree in PAUP*4.10b. Source code for MRP matrix, heuristic search trees, and other consensus trees are available from the authors by request.

Table A-1. Extant ingroup skeletal specimens. Institutional abbreviations: American Museum of Natural History (AMNH); Carnegie Museum of Natural History (CM); Muséum national d'Histoire naturelle (MNHN, MNHNA); Ohio University Vertebrate Collections (OUVC); United States National Museum of Natural History (USNM).

Specimen #	**Taxon**	**Common Name**
AMNH 90131	*Ceratotherium simum*	white rhinoceros
MNHN1928-310	*Ceratotherium simum*	white rhinoceros
MNHNA.2274	*Ceratotherium simum*	white rhinoceros
USNM 164598	*Ceratotherium simum*	white rhinoceros
AMNH 51854	*Ceratotherium simum*	white rhinoceros
OUVC 9541	*Ceratotherium simum*	white rhinoceros
AMNH 51855	*Ceratotherium simum cottoni*	northern white rhinoceros
AMNH 51856	*Ceratotherium simum cottoni*	northern white rhinoceros
AMNH 51857	*Ceratotherium simum cottoni*	northern white rhinoceros
AMNH 51858	*Ceratotherium simum cottoni*	northern white rhinoceros
AMNH 51859	*Ceratotherium simum cottoni*	northern white rhinoceros
AMNH 51860	*Ceratotherium simum cottoni*	northern white rhinoceros
AMNH 51861	*Ceratotherium simum cottoni*	northern white rhinoceros
AMNH 51862	*Ceratotherium simum cottoni*	northern white rhinoceros
AMNH 51864	*Ceratotherium simum cottoni*	northern white rhinoceros
AMNH 51865	*Ceratotherium simum cottoni*	northern white rhinoceros
AMNH 51870	*Ceratotherium simum cottoni*	northern white rhinoceros
AMNH 51872	*Ceratotherium simum cottoni*	northern white rhinoceros
AMNH 51881	*Ceratotherium simum cottoni*	northern white rhinoceros
AMNH 51882	*Ceratotherium simum cottoni*	northern white rhinoceros
AMNH 51883	*Ceratotherium simum cottoni*	northern white rhinoceros
AMNH 51889	*Ceratotherium simum cottoni*	northern white rhinoceros
AMNH 51890	*Ceratotherium simum cottoni*	northern white rhinoceros
AMNH 51891	*Ceratotherium simum cottoni*	northern white rhinoceros
AMNH 51897	*Ceratotherium simum cottoni*	northern white rhinoceros
AMNH 51912	*Ceratotherium simum cottoni*	northern white rhinoceros
AMNH 51913	*Ceratotherium simum cottoni*	northern white rhinoceros

AMNH 51917	*Ceratotherium simum cottoni*	northern white rhinoceros
AMNH 54125	*Ceratotherium simum cottoni*	northern white rhinoceros
AMNH 81815	*Ceratotherium simum simum*	southern white rhinoceros
AMNH 81816	*Ceratotherium simum simum*	southern white rhinoceros
AMNH 173576	*Dicerorhinus sumatrensis*	Sumatran rhinoceros
AMNH 54763	*Dicerorhinus sumatrensis*	Sumatran rhinoceros
AMNH 81892	*Dicerorhinus sumatrensis*	Sumatran rhinoceros
MNHNA.7965	*Dicerorhinus sumatrensis*	Sumatran rhinoceros
USNM 19885	*Dicerorhinus sumatrensis*	Sumatran rhinoceros
USNM 199551	*Dicerorhinus sumatrensis*	Sumatran rhinoceros
USNM 49561	*Dicerorhinus sumatrensis*	Sumatran rhinoceros
AMNH 113776	*Diceros bicornis*	black rhinoceros
AMNH 113777	*Diceros bicornis*	black rhinoceros
AMNH 113778	*Diceros bicornis*	black rhinoceros
AMNH 120448	*Diceros bicornis*	black rhinoceros
AMNH 13692	*Diceros bicornis*	black rhinoceros
AMNH 13693	*Diceros bicornis*	black rhinoceros
AMNH 13694	*Diceros bicornis*	black rhinoceros
AMNH 14136	*Diceros bicornis*	black rhinoceros
AMNH 187802	*Diceros bicornis*	black rhinoceros
AMNH 245690	*Diceros bicornis*	black rhinoceros
AMNH 27756	*Diceros bicornis*	black rhinoceros
AMNH 277578	*Diceros bicornis*	black rhinoceros
AMNH 30055	*Diceros bicornis*	black rhinoceros
AMNH 35740	*Diceros bicornis*	black rhinoceros
AMNH 54034	*Diceros bicornis*	black rhinoceros
AMNH 54283	*Diceros bicornis*	black rhinoceros
AMNH 54284	*Diceros bicornis*	black rhinoceros
AMNH 54383	*Diceros bicornis*	black rhinoceros
AMNH 80210	*Diceros bicornis*	black rhinoceros
AMNH 85174	*Diceros bicornis*	black rhinoceros

AMNH 85175	*Diceros bicornis*	black rhinoceros
AMNH 85176	*Diceros bicornis*	black rhinoceros
AMNH 85178	*Diceros bicornis*	black rhinoceros
AMNH 85179	*Diceros bicornis*	black rhinoceros
AMNH 85180	*Diceros bicornis*	black rhinoceros
AMNH 85181	*Diceros bicornis*	black rhinoceros
AMNH 85181[b]	*Diceros bicornis*	black rhinoceros
AMNH 85182	*Diceros bicornis*	black rhinoceros
AMNH 90204	*Diceros bicornis*	black rhinoceros
CM 1763	*Diceros bicornis*	black rhinoceros
CM 40561	*Diceros bicornis*	black rhinoceros
MNHN1931-581	*Diceros bicornis*	black rhinoceros
MNHN1944-278	*Diceros bicornis*	black rhinoceros
MNHN1974-124	*Diceros bicornis*	black rhinoceros
AMNH 34741	*Diceros bicornis somaliensis*	black rhinoceros
AMNH 34742	*Diceros bicornis somaliensis*	black rhinoceros
AMNH 202594	*Diceros* sp.	black rhinoceros
AMNH 204214	*Equus caballus*	domestic horse
AMNH 14096	*Equus quagga burchelli*	common zebra
AMNH 146717	*Rhinoceros sondaicus*	Javan rhinoceros
AMNH 146718	*Rhinoceros sondaicus*	Javan rhinoceros
AMNH 43	*Rhinoceros sondaicus*	Javan rhinoceros
MNHN1932-48	*Rhinoceros sondaicus*	Javan rhinoceros
MNHN1932-42	*Rhinoceros sondaicus*	Javan rhinoceros
MNHN1940-483	*Rhinoceros sondaicus*	Javan rhinoceros
MNHNA.2277	*Rhinoceros sondaicus*	Javan rhinoceros
MNHNA.7966	*Rhinoceros sondaicus*	Javan rhinoceros
MNHNA.7970B	*Rhinoceros sondaicus*	Javan rhinoceros
MNHNA.7971	*Rhinoceros sondaicus*	Javan rhinoceros
USNM 156507	*Rhinoceros sondaicus*	Javan rhinoceros
USNM 269392	*Rhinoceros sondaicus*	Javan rhinoceros

AMNH 119475	*Rhinoceros unicornis*	Indian rhinoceros
AMNH 171290	*Rhinoceros unicornis*	Indian rhinoceros
AMNH 245543	*Rhinoceros unicornis*	Indian rhinoceros
AMNH 274636	*Rhinoceros unicornis*	Indian rhinoceros
AMNH 35759	*Rhinoceros unicornis*	Indian rhinoceros
AMNH 54454	*Rhinoceros unicornis*	Indian rhinoceros
AMNH 54455	*Rhinoceros unicornis*	Indian rhinoceros
AMNH 54456	*Rhinoceros unicornis*	Indian rhinoceros
AMNH 70445	*Rhinoceros unicornis*	Indian rhinoceros
MNHN1932-49	*Rhinoceros unicornis*	Indian rhinoceros
MNHN1960-59	*Rhinoceros unicornis*	Indian rhinoceros
USNM 336953	*Rhinoceros unicornis*	Indian rhinoceros
USNM 398417	*Rhinoceros unicornis*	Indian rhinoceros
USNM 464963	*Rhinoceros unicornis*	Indian rhinoceros
USNM 540042	*Rhinoceros unicornis*	Indian rhinoceros
USNM 545847	*Rhinoceros unicornis*	Indian rhinoceros
USNM 545848	*Rhinoceros unicornis*	Indian rhinoceros
MNHNA.12.344	*Tapirus bairdii*	Baird's tapir
MNHN1906-550	*Tapirus indicus*	Asian tapir
MNHN1944-267	*Tapirus indicus*	Asian tapir
MNHN1982-034	*Tapirus pinchaque*	mountain tapir
MNHN1939-225	*Tapirus terrestris*	Brazilian tapir

Table A-2. Outgroup comparison specimens. Institutional abbreviations: American Museum of Natural History (AMNH); Carnegie Museum of Natural History (CM); Museum of the Rockies (MOR OST); Muséum national d'Histoire naturelle (MNHN, MNHNAE); Ohio University Vertebrate Collections (OUVC); Royal Ontario Museum (ROM); Senckenberg Museum (SMF); United States National Museum of Natural History (USNM); University of Michigan Museum of Zoology (UMMZ).

Specimen #	Taxon	Common Name
CM1557	*Antilocapra americana*	pronghorn
MNHNAE.685	*Cephalophus dorsalis*	bay duiker
MNHNAE.710	*Cephalophus* sp.	duiker
MOR OST 320	*Choloepus* sp.	two-toed sloth
AMNH 27675	*Giraffa camelopardalis*	giraffe
AMNH 81820	*Giraffa camelopardalis*	giraffe
AMNH 82001	*Giraffa camelopardalis*	giraffe
CM 5834	*Giraffa camelopardalis*	giraffe
CM10445	*Giraffa camelopardalis*	giraffe
CM2071	*Giraffa camelopardalis*	giraffe
CM2112	*Giraffa camelopardalis*	giraffe
CM30461	*Giraffa camelopardalis*	giraffe
CM59645 DC1559	*Giraffa camelopardalis*	giraffe
MNHNAE.806	*Giraffa camelopardalis*	giraffe
USNM 270902	*Hexaprotodon liberiensis*	pygmy hippopotamus
USNM 302054	*Hexaprotodon liberiensis*	pygmy hippopotamus
USNM 314046	*Hexaprotodon liberiensis*	pygmy hippopotamus
USNM 477361	*Hexaprotodon liberiensis*	pygmy hippopotamus
USNM 538815	*Hexaprotodon liberiensis*	pygmy hippopotamus
USNM 549277	*Hexaprotodon liberiensis*	pygmy hippopotamus
CM 1757	*Hippopotamus amphibius*	hippopotamus
CM 2033	*Hippopotamus amphibius*	hippopotamus
MNHN1943-27	*Hippopotamus amphibius*	hippopotamus
MNHN1944-999	*Hippopotamus amphibius*	hippopotamus
MNHN1959-131	*Hippopotamus amphibius*	hippopotamus

USNM 313712	*Hippopotamus amphibius*	hippopotamus
USNM 336648	*Hippopotamus amphibius*	hippopotamus
USNM 3883	*Hippopotamus amphibius*	hippopotamus
USNM 178701	*Hippopotamus amphibius amphibius*	hippopotamus
USNM 268091	*Hippopotamus amphibius amphibius*	hippopotamus
USNM 123387	*Hippopotamus amphibius capensis*	hippopotamus
USNM 36871	*Hippopotamus amphibius capensis*	hippopotamus
USNM 3882	*Hippopotamus amphibius capensis*	hippopotamus
USNM 162981	*Hippopotamus amphibius kiboko*	hippopotamus
USNM 182395	*Hippopotamus amphibius kiboko*	hippopotamus
USNM 182396	*Hippopotamus amphibius kiboko*	hippopotamus
USNM 182397	*Hippopotamus amphibius kiboko*	hippopotamus
USNM 254978	*Hippopotamus amphibius kiboko*	hippopotamus
USNM 161942	*Hippopotamus amphibius kiboko*	hippopotamus
USNM 162980	*Hippopotamus amphibius kiboko*	hippopotamus
CM 20960	*Hylochoerus meinertzhageni*	giant forest hog
CM 57916	*Hylochoerus meinertzhageni*	giant forest hog
USNM 163250	*Hylochoerus meinertzhageni*	giant forest hog
USNM 164627	*Hylochoerus meinertzhageni*	giant forest hog
USNM 308851	*Hylochoerus meinertzhageni*	giant forest hog
USNM 270155	*Hyemoschus aquaticus*	water chevrotain
USNM 482001	*Hyemoschus aquaticus*	water chevrotain
MNHNAE.696	*Madoqua* sp.	dik-dik
MNHNAE.676	*Neotragus pygmaeus*	royal antelope
AMNH 51200	*Okapia johnstoni*	okapi
MNHN159-262	*Okapia johnstoni*	okapi
MNHN1961-131	*Okapia johnstoni*	okapi
MNHN1996-102	*Okapia johnstoni*	okapi
USNM 308877	*Okapia johnstoni*	okapi
USNM 399337	*Okapia johnstoni*	okapi
CM20947	*Ovibos moschatus*	musk-ox

CM20955	*Ovibos moschatus*	musk-ox
CM21047	*Ovibos moschatus*	musk-ox
ROM CN 1148	*Ovibos moschatus*	musk-ox
CM 5154	*Potamochoerus porcus*	red river hog
USNM 164542	*Potamochoerus porcus*	red river hog
USNM 259174	*Potamochoerus porcus*	red river hog
MNHNAE.682	*Sylvicapra grimmae*	gray duiker
MNHN1927-18	*Tetracerus quadricornis*	chousingha
MNHN1983-122	*Tetracerus quadricornis*	chousingha
MNHN1995-148	*Tetracerus quadricornis*	chousingha
MNHN2004-295	*Tetracerus quadricornis*	chousingha
USNM 49692	*Tragulus napu*	greater Oriental chevrotain
USNM 578462	*Tragulus napu*	greater Oriental chevrotain
USNM 151800	*Tragulus napu borneanus*	greater Oriental chevrotain
USNM 151801	*Tragulus napu borneanus*	greater Oriental chevrotain
USNM 49772	*Tragulus napu borneanus*	greater Oriental chevrotain
USNM 49871	*Tragulus napu napu*	greater Oriental chevrotain
USNM 267335	*Tragulus napu perflavus*	greater Oriental chevrotain
USNM 49605	*Tragulus napu pretiosus*	greater Oriental chevrotain
UMMZ 152361	*Anhima cornuta*	horned screamer
ROM 91698	*Caloenas nicobarica*	Nicobar pigeon
ROM 126617	*Caloenas nicobarica*	Nicobar pigeon
CM 8126	*Cerorhinca monocerata*	rhinoceros auklet
CM 8125	*Cerorhinca monocerata*	rhinoceros auklet
CM 5119	*Cerorhinca monocerata*	rhinoceros auklet
ROM 39934	*Cerorhinca monocerata*	rhinoceros auklet
UMMZ 156989	*Chauna torquata*	crested screamer
UMMZ 149033	*Cyclura cornuta*	horned ground iguana
UMMZ 174428	*Cyclura cornuta*	horned ground iguana
UMMZ 128581	*Cyclura cornuta*	horned ground iguana
UMMZ 149036	*Cyclura ricordi*	Ricord's iguana

UMMZ 149096	*Iguana iguana*	green iguana
UMMZ 149093	*Iguana iguana*	green iguana
UMMZ 128103	*Iguana iguana*	green iguana
UMMZ 45409	*Iguana iguana*	green iguana
UMMZ 210529	*Moloch horridus*	thorny devil
ROM 0151169	*Pelecanus erythrorhynchos*	American white pelican
ROM 123578	*Pelecanus erythrorhynchos*	American white pelican
ROM 159651	*Pelecanus erythrorhynchos*	American white pelican
ROM 159650	*Pelecanus erythrorhynchos*	American white pelican
ROM 159653	*Pelecanus erythrorhynchos*	American white pelican
ROM 159652	*Pelecanus erythrorhynchos*	American white pelican
ROM 159649	*Pelecanus erythrorhynchos*	American white pelican
SMF2099	*Pelecanus occidentalis*	brown pelican
SMF2098	*Pelecanus occidentalis*	brown pelican
ROM 120525	*Sarkidiornis melanotos*	comb duck

Table A-3. Extinct ingroup fossil specimens. Institutional abbreviations: American Museum of Natural History Fossil Mammals Collection (AMNH FM); United States National Museum of Natural History (USNM); University of California Museum of Paleontology (UCMP).

Specimen #	Taxon	Age
AMNH FM 26091	*Amynodontopsis* sp. *("large sp.")*	E. "Sannoisan"
AMNH FM 21599	*Amynodontopsis* sp. *("small sp.")*	E. Oligocene
AMNH FM 104189	*Aphelops* cf. *Aphelops malacorhinus*	E. Hemphillian
AMNH FM Hig 29-436	*Aphelops* sp.	E. Hemphillian
UCMP 21802	*Ceratotherium neumayri*	Tortonian
AMNH FM 26342	*Chilotherium anderssoni*	E. Turolian
AMNH FM 26338	*Chilotherium habereri var laticeps*	-
AMNH China 30-L289	*Chilotherium sp.*	E. Turolian
AMNH China 46-387	*Chilotherium sp.*	E. Turolian
AMNH China 80-L619	*Chilotherium sp.*	E. Turolian
AMNH FM 7324	*Diceratherium annectens*	Oligocene
AMNH FM 112176	*Diceratherium armatum*	E. Lt Arikareean
USNM 11682	*Diceratherium armatum*	Arikareean
AMNH FM 112171	*Diceratherium sp.*	E. Arikareean?
AMNH FM 111948	*Diceratherium sp.*	E. Barstovian
AMNH FM 112185	*Diceratherium sp.*	E. Arikareean
AMNH FM 112187	*Diceratherium sp.*	E. Lt Arikareean
AMNH FM 112195	*Diceratherium sp.*	E. Lt Arikareean
AMNH FM 26660	*Forstercooperia confluens*	M. "Bartonian"
AMNH FM 26643	*Forstercooperia sp.*	M. "Bartonian"
AMNH FM 26531	*Huaqingtherium lintungense*	Lt. Vindobonian
AMNH FM 26521	*Huaqingtherium lintungense*	Lt. Vindobonian
AMNH FM 12364	*Hyrachyus eximius*	Bridgerian
AMNH FM 13756	*Hyrachyus modestus*	Bridgerian
AMNH FM 12296	*Hyracodon nebraskensis*	
AMNH FM 14229	*Menoceras arikarense*	Late Arikareean
AMNH FM 22458	*Menoceras arikarense*	Late Arikareean

AMNH FM 26892	*Menoceras arikarense*	Late Arikareean
AMNH FM 39358	*Menoceras arikarense*	-
AMNH FM 86114	*Menoceras arikarense*	Late Arikareean
AMNH FM 86115	*Menoceras arikarense*	Late Arikareean
AMNH FM 86116	*Menoceras arikarense*	Late Arikareean
AMNH FM 86223	*Menoceras arikarense*	Late Arikareean
AMNH FM 86227	*Menoceras arikarense*	Late Arikareean
AMNH FM 86229	*Menoceras arikarense*	Late Arikareean
AMNH FM 112245	*Menoceras arikarense*	Late Arikareean
USNM 10297	*Menoceras arikarense*	Arikareean
AMNH FM 82849	*Menoceras barbouri*	E. Hemingfordian
AMNH FM 112246	*Menoceras sp.*	Lt. Lt Arikareean
AMNH FM 112250	*Menoceras sp.*	Lt. Lt Arikareean
AMNH FM 1496	*Metamynodon planifrons*	E. Orellan
AMNH FM 547	*Metamynodon planifrons*	-
AMNH FM 114923	*Peraceras hesei*	Lt. Lt. Barstovian
AMNH FM 19185	*Procoelodonta mongoliense*	E. ? Vindobonian
AMNH FM 21601	*Sharamynodon mongoliensis*	M. "Ludian"
AMNH 8088	*Subhyracodon sp.*	E. Whitneyan
AMNH FM 1126	*Subhyracodon sp.*	M. Whitneyan
AMNH FM 1127	*Subhyracodon sp.*	M. Whitneyan
AMNH FM 541	*Subhyracodon sp.*	M. Whitneyan
AMNH FM Lusk 0-151-4114	*Subhyracodon sp.*	Chadronian/Orellan
AMNH FM 109618	*Teleoceras* cf. *Teleoceras minor*	E. E. Valentinian
USNM Fla. 147-2452	*Teleoceras proterum*	E. Hemphillian
USNM Fla. 29-522	*Teleoceras proterum*	E. Hemphillian
AMNH FM 115853	*Teleoceras sp.*	E. Hemphillian
AMNH FM 8404	*Teleoceras sp.*	Clar. - Hemp.
UCMP 129000	*Teletaceras radinskyi*	
AMNH FM 12389	*Trigonias osborni*	E. Chadronian

AMNH B.H. 12-512	*Trigonias wellsi*	M. Chadronian
AMNH FM 26034	*Zaisamynodon borizovi*	E. "Sannoisan"

Literature Cited

Antoine P-O 2002. *Phylogénie et évolution des Elasmotheriina (Mammalia, Rhinocerotidae.)* Paris: Publications scientifiques du Muséum.

Antoine P-O, Duranthon F, Wellcome J-L. 2003. *Alicornops* (Mammalia, Rhinocerotidae) dans le Miocene superieur des Collines Bugti (Balouchistan, Pakistan): implications phylogenetiques. GEODIVERSITAS 25:575–603.

Benjamin M, Kumai T, Milz S, Boszczyk BM, Boszczyk AA, Ralphs JR. 2002. The skeletal attachment of tendons—tendon 'entheses'. Comparative Biochemistry and Physiology Part A 133:931–945.

Cerdeño E. 1995. Cladistic analysis of the family Rhinocerotidae (Perissodactyla). American Museum Novitates 3143:1–25.

Haines RW, Mohuiddin A. 1968. Metaplastic bone. Journal of Anatomy 103:96–98.

Hieronymus TL, Witmer LM, Ridgely RC. 2006. Structure of white rhinoceros (*Ceratotherium simum*) horn investigated by X-ray computed tomography and histology with implications for growth and external form. Journal of Morphology 267:1172–1176.

Kingdon J. 1979. East African mammals: An atlas of evolution in Africa. Vol.3. Part B, Large mammals London: Academic Press.

Maddison WP, Maddison DR. 2006. Mesquite: a modular system for evolutionary analysis, v1.12 (http://mesquiteproject.org).

Morales JC, Melnick DJ. 1994. Molecular systematics of the living rhinoceros. Molecular Phylogenetics and Evolution 3:128–134.

Orlando L, Leonard JA, Thenot A, Laudet V, Guerin C, Hänni C. 2003. Ancient DNA analysis reveals woolly rhino evolutionary relationships. Molecular Phylogenetics and Evolution 28:485–499.

Ragan MA. 1992. Phylogenetic inference based on matrix representation of trees. Molecular Phylogenetics and Evolution 1:53–58.

Ryder ML. 1962. Structure of rhinoceros horn. Nature 193:1199–1201.

Schumacher Sv. 1931. Integument der Mammalier. In: Bolk L, Goppert E, Kallius E, Lubosch W, editors. Handbuch der Vergleichenden Anatomie der Wirbeltiere. Berlin: Urban und Schwarzenburg. p. 449–504.

Shadwick RE, Russell AP, Lauff RF. 1992. The structure and mechanical design of rhinoceros dermal armour. Philosophical Transactions of the Royal Society of London. Series B, Biological sciences 337:419–428.

Sokolov VE. 1982. Mammal skin. Berkeley: University of California Press.

Swofford DL. 2001. PAUP*: phylogenetic analysis using parsimony (*and other methods), v4.10b. Sunderland: Sinauer Associates.

Tougard C, Delefosse T, Hänni C, Montelgard C. 2001. Phylogenetic relationships of the five extant rhinoceros species (Rhinocerotidae, Perissodactyla) based on mitochondrial cytochrome b and 12S rRNA genes. Molecular Phylogenetics & Evolution 19:34–44.

APPENDIX B: SUPPLEMENTARY INFORMATION FOR CHAPTER 3

Table B-1. Character scores for taxa by region. Ros: rostral; Int: internasal; Nas: nasal; Lor: loreal; Pre: prefrontal; Spl: supralabial; Fro: frontal; Par: parietal; Squ: squamosal; Tem: temporal; Spo: Supraocular; Sym: symphyseal; Inf: infralabial; Sub: sublabial; Gul: gular. Character codes: 0: single plate or scale; 1: plate or scale continuous with adjacent region; 2: multiple irregular scales; 3: multiple hexagonal scales; 4: scaleless soft skin; 5: feathered skin. Figure 9 shows the phylogenetic hypothesis used for this study.

Taxon	Ros	Int	Nas	Lor	Pre	Spl	Fro	Par	Squ	Tem	Spo	Sym	Inf	Sub	Gul
Basiliscus basiliscus	0	3	0	3	3	2	3	3	3	3	3	0	2	3	3
Basiliscus vittatus	0	3	0	3	3	2	3	3	3	3	3	0	2	3	3
Chamaeleo calyptratus	3	3	2	3	3	3	3	3	3	3	3	3	3	3	3
Chamaeleo jacksoni	3	3	2	3	3	3	3	3	3	3	3	3	3	3	3
Chlamydosaurus kingii	2	3	2	3	3	3	3	3	3	3	3	2	3	3	3
Cordylus giganteus	0	0	0	2	0	2	0	2	3	3	2	0	2	2	3
Corytophanes cristatus	0	3	0	3	3	2	3	3	3	3	3	0	2	3	3
Cyclura cornuta	0	2	0	3	3	2	3	3	3	3	3	0	2	2	3
Cyclura ricordi	0	3	0	3	3	2	3	3	3	3	3	0	2	3	3
Elgaria multicarinata	0	2	0	2	2	2	0	3	3	3	2	0	2	2	2
Enyalioides laticeps	2	3	2	3	3	2	3	3	3	3	3	2	2	3	3
Gekko gecko	0	3	2	3	3	2	3	3	3	3	3	0	2	3	3
Gerrhonotus liocephalus	0	2	0	2	2	2	0	3	3	3	2	0	2	2	2
Gerrhosaurus major	0	0	0	2	0	2	0	2	2	3	2	0	2	2	2
Heloderma horridum	0	3	2	3	3	2	3	3	3	3	3	0	2	3	?
Hemitheconyx caudicinctus	0	3	2	3	3	3	3	3	3	3	3	0	3	3	3
Iguana iguana	0	3	0	2	2	2	2	3	3	3	3	0	2	2	2
Laemanctus serratus	0	3	0	3	3	2	3	3	3	3	3	?	2	3	3
Lamprolepis smaragdina	0	0	2	2	0	2	0	2	2	3	2	0	2	2	?
Lepidophyma flavimaculatus	0	2	2	2	2	2	0	2	2	2	0	0	1	1	?
Moloch horridus	3	3	2	3	3	3	3	3	3	3	3	3	3	3	3
Oplurus cuvieri	0	3	2	3	2	2	2	3	3	3	3	2	2	3	3
Phrynosoma cornuta	2	3	2	2	3	3	3	3	2	3	3	2	3	2	3
Sceloporus poinsetti	0	3	2	2	2	2	2	2	2	3	2	0	2	2	3
Tiliqua rugosa	0	0	0	2	0	2	2	2	3	3	2	0	2	2	?
Tiliqua scincoides	0	0	0	2	0	2	2	2	3	3	2	0	2	2	3
Uromastyx aegypticus	2	3	2	3	3	3	3	3	3	3	3	3	3	3	3
Varanus beccari	3	3	3	3	3	3	3	3	3	3	3	3	3	3	3
Varanus exanthematicus	2	3	3	3	3	3	3	3	3	3	3	2	3	3	3
Sphenodon punctatus	2	3	3	3	3	2	3	3	3	3	3	3	2	3	3
cf. *Geochelone*	0	2	2	1	0	1	0	?	?	?	3	1	1	2	3
Chelonia mydas	1	2	1	1	2	1	2	2	2	2	2	1	1	?	?
Chelydra serpentina	1	2	2	1	2	1	2	2	2	3	2	1	1	1	3
Malaclemys terrapin	1	4	1	1	4	1	4	1	1	4	4	1	1	?	?
Sternotherus minor	1	4	4	1	4	1	4	4	4	4	?	1	1	1	?
Alligator mississippiensis	2	2	2	3	2	3	1	1	2	3	0	3	3	3	3
Crocodylus novaeguiniae	2	2	2	2	2	3	1	1	2	2	1	3	3	3	3
Crocodylus porosus	2	2	2	2	2	2	1	1	2	2	0	2	2	0	3

Aceros undulatus	1	0	1	1	5	1	5	5	5	5	5	1	1	1	4
Alca torda	0	5	0	5	5	0	5	5	5	5	5	1	1	5	5
Anas clypeata	0	4	4	4	5	0	5	5	5	5	5	0	4	4	4
Andigena laminirostris	1	1	5	4	5	0	5	5	5	5	5	1	1	1	5
Anseranas semipalmata	0	0	4	4	4	0	5	5	5	5	5	0	0	4	4
Apteryx australis mantelli	0	1	1	5	5	0	5	5	5	5	5	0	1	1	?
Buceros vigil	1	2	5	1	5	1	5	5	5	5	5	1	1	1	4
Bucorvus abyssinicus	0	0	5	4	5	0	5	5	5	5	5	1	1	1	4
Buteo jamaicensis	1	1	1	5	5	1	5	5	5	5	5	1	1	5	5
Butorides striatus	1	1	0	4	5	1	5	5	5	5	5	1	1	1	5
Bycanistes brevis	1	0	1	1	5	1	5	5	5	5	5	1	1	1	4
Caloenas nicobarica	0	4	4	5	5	4	5	5	5	5	5	0	4	4	5
Calonectris diomedea	1	1	0	5	5	0	5	5	5	5	5	0	0	0	?
Casuarius casuarius	0	0	4	4	1	0	1	4	4	4	5	0	0	0	4
Catharacta skua	1	0	1	5	5	1	5	5	5	5	5	1	1	1	?
Cepphus grylle	1	5	1	5	5	1	5	5	5	5	5	1	1	?	1
Cerorhinca monocerata	0	1	1	5	5	0	5	5	5	5	5	1	1	5	5
Colaptes auratus	1	1	1	5	5	1	5	5	5	5	5	1	1	1	5
Corvus brachyrhynchos	1	1	5	5	5	1	5	5	5	5	5	1	1	1	5
Crax alector	1	4	4	4	5	1	5	5	5	5	5	0	0	0	5
Crax rubra	0	4	4	5	5	0	5	5	5	5	5	0	4	4	?
Cygnus buccinator	0	4	4	4	5	0	5	5	5	5	5	0	4	4	4
Cygnus olor	0	4	4	4	4	0	5	5	5	5	5	0	0	4	5
Dromaius novaehollandiae	0	0	4	4	5	0	5	5	5	4	5	0	0	0	5
Eudyptes chrysolophus	1	1	5	5	5	0	5	5	5	5	5	1	1	5	5
Fratercula arctica	0	0	0	5	5	0	5	5	5	5	0	0	1	1	1
Fratercula corniculata	0	0	0	5	5	0	5	5	5	5	5	0	1	1	1
Gallinula chloropus	1	1	1	0	1	1	5	5	5	5	5	1	1	1	5
Gavia immer	1	1	0	5	5	1	5	5	5	5	5	1	1	1	5
Lanius excubitor	1	1	1	5	5	1	5	5	5	5	5	1	1	1	?
Larus delewarensis	1	1	1	5	5	1	5	5	5	5	5	1	1	1	5
Macronectes giganteus	0	0	0	5	5	0	5	5	5	5	5	0	0	0	?
Malacorhynchos membranaceus	0	4	4	5	5	0	5	5	5	5	5	0	0	4	4
Mitu mitu	1	1	4	5	5	1	5	5	5	5	5	1	1	5	5
Oreophasis derbianus	1	5	5	5	5	1	4	5	5	5	4	1	1	5	5
Otus asio	1	1	1	5	5	1	5	5	5	5	5	1	1	5	5
Pelecanus erythrorhynchos	0	0	1	4	5	0	5	5	5	5	5	0	1	1	4
Phalacrocorax auritus	0	0	-	5	5	0	5	5	5	5	5	0	1	1	4
Phoebastria immutabilis	0	0	0	5	5	0	5	5	5	5	5	0	1	1	5
Pterodroma incerta	1	1	0	5	5	0	5	5	5	5	5	0	0	0	?
Pygoscelis adeliae	1	1	1	0	5	0	5	5	5	5	5	1	1	1	5
Sarkidiornis melanotos	0	4	4	5	5	0	5	5	5	5	5	0	0	4	4
Somateria mollissima	1	1	4	5	4	0	5	5	5	5	5	0	0	4	?
Struthio camelus	0	4	4	5	5	0	5	5	5	5	5	0	1	1	5
Sula bassana	0	0	-	4	5	0	5	5	5	5	5	0	1	1	4

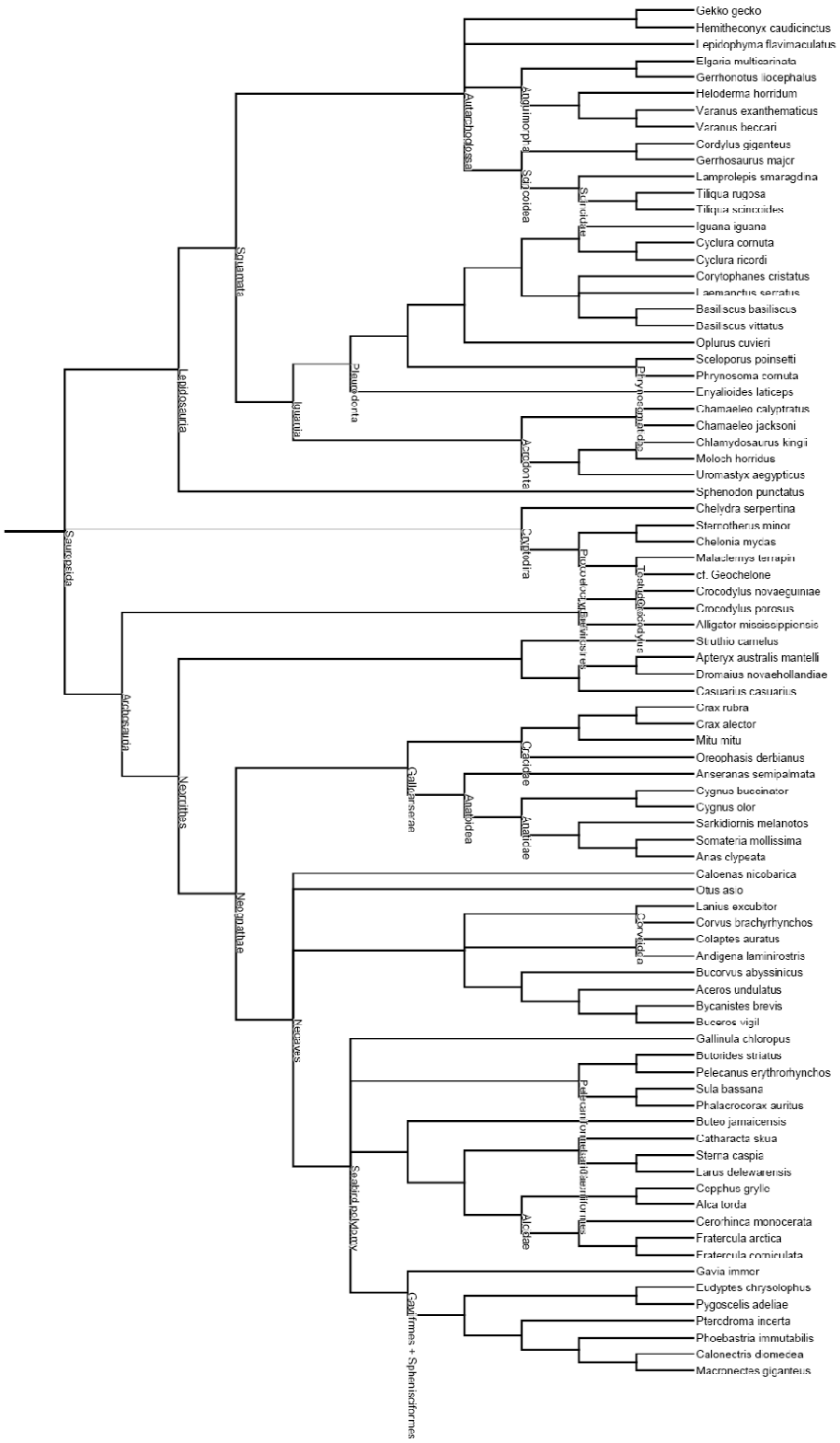

Figure B-1. Composite phylogenetic tree of Sauropsida used in this study.

APPENDIX C: SUPPLEMENTARY INFORMATION FOR CHAPTER 4

Table C-1. Taxa included in this study. Taxa in bold were included in ancestral character state reconstructions. Material examined is coded as: O, osteological material; S, study skin (whole or partial preservation); P, verification in Calphotos archive for partial study skins; F, fresh, frozen, or formalin-fixed; μCT, MicroCT scanned; VI, MicroCT with vascular injection; H, histological preparation of rhamphotheca.

Taxon	**Material examined**
Aceros undulatus	O, S, P
Aethia cristatella	S
Alca torda	O, S
Anas clypeata	O, F, VI
Anastomus lamelligerus	O, S
Andigena laminirostris	S
Anhima cornuta	O
Anhinga melanogaster	O
Anseranas semipalmata	O, S
Anthracoceros malabaricus	O
Aptenodytes forsteri	O
Apteryx australis	O, S
Apteryx owenii	O
Aramus guarana	O
Ardea cinerea	O
Ardeotis kori	O
Argusianus argus	O

Balaeniceps rex	O
Buceros bicornis	O
Buceros hydrocorax	O
Buceros vigil	O, S
Bucorvus abyssinicus	O, S
Bucorvus leadbetteri	O
Buteo jamaicensis	O, F, μCT
Butorides striatus	O, F, μCT
Bycanistes brevis	O, S, P
Bycanistes bucinator	O
Caloenas nicobarica	O, S
Calonectris diomedea	O, S, P
Casuarius casuarius	O, S
Casuarius unappendiculatus	O, S, P
Catharacta skua	O, S, P
Cepphus grylle	O
Ceratogymna fistulator	O
Cerorhinca monocerata	O, S
Chauna torquata	O, S, P
Chionis alba	O
Colaptes auratus	O, F, VI, H
Corvus brachyrhynchos	O, F, VI, H

Crax alector	O, S
Crax rubra	O, S
Cygnus buccinator	O, F
Cygnus olor	O, S
Daption capense	O
Didunculus strigirostris	S
Diomedea antipodensis	O
Diomedea melanophrys	O
Dromaius novaehollandiae	O, F
Dryocopus pileatus	O
Egretta garzeta	O
Eudyptes chrysolophus	O, S
Eudyptula minor	O
Eurypyga helias	O
Falco rusticolus	O
Fratercula arctica	O, S
Fratercula cirrhata	O, S
Fratercula corniculata	O, S
Fregata minor	O
Fregata sp.	O
Fulmarus glacialis	O
Gallinula chloropus	O, F, μCT

Gavia immer	O, F, VI
Gavia stellata	O
Halobaena caerulea	O
Lanius excubitor	O, S, P
Larus argentatus	O
Larus delewarensis	O, F, VI, H
Macronectes giganteus	O, S, P
Macronectes sp.	O
Malacorhynchus membranaceus	O
Mergus cucullatus	O
Mergus merganser	O
Mitu mitu	S
Nyctibius grandis	O
Oceanites oceanicus	O
Oreophasis derbianus	S
Otus asio	O, F, VI, H
Pachyptila desolata	O
Pachyptila turtur	O
Pachyptila vittata	O
Pelecanoides urinatrix	O
Pelecanus erythrorhynchos	O, S, F
Pelecanus onocrotalus	O

Penelopides panini	O
Phaethon lepturus	O
Phalacrocorax aristotelis	O
Phalacrocorax auritus	O, F, VI, H
Phalacrocorax carbo	O
Phobastria immutabilis	O, F, μCT
Pinguinus impinnis	O
Podiceps cristatus	O
Psophia leucoptera	O
Pterodroma hypoleuca	O
Pterodroma incerta	O, S, P
Pteroglossus aracan	O
Pygoscelis adeliae	O, S, P
Rhynchops flavirostris	O
Rhynchops niger	O
Rhynchotus rufescens	O
Sarkidiornis melanotos	O, S
Somateria mollissima	O, S
Somateria spectabilis	O
Spheniscus humboldti	O
Sterna caspia	O
Struthio camelus	O

Sula bassana	O, F
Sula dactylatra	O
Tinamus major	O
Tockus erythrorhynchus	O
Tockus flavirostris	F, μCT
Turdus merula	O
Uria lomvia	O
Xema sabini	O

APPENDIX D: SUPPLEMENTARY INFORMATION FOR CHAPTER 5

List of centrosaurine specimens and outgroups examined for gross osteological correlates. Museum abbreviations: AMNH FR, American Museum of Natural History Fossil Reptiles; MOR, Museum of the Rockies; ROM, Royal Ontario Museum; TMP, Royal Tyrrell Museum of Palaeontology; UCMP, University of California Museum of Paleontology.

Achelousaurus horneri—MOR 485, MOR 571, MOR 591; *Anchiceratops ornatus*—ROM 802; *Anchiceratops* sp.—AMNH FR 5251; Centrosaurinae indet. —ROM 49862; *Centrosaurus apertus*—ROM 12776, ROM 767, TMP 1966.33.17; *Centrosaurus* sp.—ROM 831; cf. *Centrosaurus*—AMNH FR 5442, ROM 12782, ROM 12787, ROM 43214, ROM 49863, ROM 636, ROM 641, ROM 728, TMP 1992.36.224; *Centrosaurus* cf. *C. apertus*—TMP 1987.18.20, TMP 1989.18.148; *Chasmosaurus brevirostris*—ROM 839; *Einiosaurus procurvicornis*—MOR 373a, MOR 373b, MOR 373c, MOR 456a, MOR 456b, MOR 456c, MOR 456d, MOR 456e; *Pachyrhinosaurus* cf. *P. canadensis*—Drumheller skull[1], UCMP 88H8-4-4; *Pachyrhinosaurus lakustai*—TMP 1985.112.1, TMP 1985.112.28, TMP 1986.55.102, TMP 1986.55.155, TMP 1986.55.206, TMP 1986.55.258, TMP 1987.55.110, TMP 1987.55.156, TMP 1987.55.228, TMP 1987.55.304, TMP 1987.55.320, TMP 1987.55.323, TMP 1987.55.81, TMP 1989.55.1009, TMP 1989.55.1111, TMP 1989.55.1112, TMP 1989.55.1125, TMP 1989.55.1131, TMP 1989.55.1185, TMP 1989.55.1234, TMP 1989.55.1396, TMP 1989.55.1524, TMP 1989.55.172, TMP 1989.55.172, TMP 1989.55.188, TMP 1989.55.21, TMP 1989.55.203, TMP 1989.55.207, TMP 1989.55.256, TMP 1989.55.367,

TMP 1989.55.427, TMP 1989.55.467, TMP 1989.55.561, TMP 1989.55.566, TMP 1989.55.566, TMP 1989.55.72, TMP 1989.55.781, TMP 1989.55.918, TMP 1989.55.927; TMP 1989.55.931, TMP 1989.55.958; Protoceratops andrewsi—AMNH FR 6429.

[1]This specimen, described in Langston (1967), was studied from a cast housed in the collections of the Royal Tyrrell Museum of Palaeontology.

Table D-1. Extant histological specimens.

Taxon	Specimen #	Location	Tissues sampled
Colaptes auratus	OUVC 10400	premaxilla and rictus	Bone and soft tissue
Corvus brachyrhynchos	OUVC 10403	premaxilla and rictus	Bone and soft tissue
Gerrhosaurus major	OUVC 10410	premaxilla and maxilla	Bone and soft tissue
Hemitheconyx caudicinctus	OUVC 10411	premaxilla and maxilla	Bone and soft tissue
Larus delewarensis	OUVC 10399	premaxilla and rictus	Bone and soft tissue
Lepidophyma flavimaculatus	OUVC 10418	premaxilla and maxilla	Bone and soft tissue
Oplurus cuvieri	OUVC 10419	premaxilla and maxilla	Bone and soft tissue
Otus asio	OUVC 10402	maxillary rostrum	Bone and soft tissue
Phalacrocorax auritus	OUVC 10401	premaxilla and rictus	Bone and soft tissue
Varanus exanthematicus	OUVC 10414	premaxilla, maxilla, dentary	Bone and soft tissue
Ceratotherium simum	OUVC 9541	nasal horn, frontal horn	Bone and soft tissue
Giraffa camelopardalis	OUVC ?	median ossicone	Bone and soft tissue
Ovibos moschatus	UAM 86916	frontal horn boss	Bone and horn sheath
Crocodylus porosus	OUVC 10576	maxilla	Bone
Alligator mississippiensis	OUVC 9633	maxilla	Bone
Chrysemys picta	OUVC unnumbered	maxilla	Bone and horny beak

Table D-2. Paleohistological specimens.

Specimen #	Source specimen #	Description
TMP 1993.55.2	TMP 1989.55.894	Border of bony nostril
TMP 1993.55.8	TMP 1989.55.1038	Caudal nasal boss
TMP 1993.55.9	TMP 1989.55.894	Tip of developing nasal horn core
TMP 1993.55.10	TMP 1989.55.894	Lateral surface of developing nasal horn core
TMP 1993.55.11	TMP 1989.55.174	Lateral surface of developing nasal horn core
TMP 1993.55.12	TMP 1986.55.48	Lateral surface of developing nasal horn core
TMP 1993.55.13	TMP 1987.55.161	Lateral surface of developing nasal horn core
TMP 1993.55.16	TMP 1989.55.1342	Basal sulcus of nasal boss
TMP 1993.55.17	TMP 1989.55.1342	Lateral surface of nasal boss
TMP 1993.55.18	TMP 1989.55.1342	Lateral surface of nasal adjacent to boss
TMP 1993.55.20	TMP 1989.55.1342	Basal sulcus of nasal boss